US Army Corps of Engineers



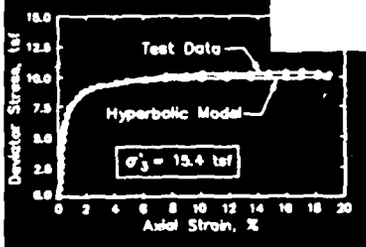



TECHNICAL REPORT ITL

# SOIL STRUCTURE INTERACTI
# FOR SILTS

by

Timothy D. Stark
Department of Civil Engin
University of Illinois
Urbana, Illinois 618

Joseph J. Vettel, Steven M. F
Department of Civil Engin
San Diego State Univer
San Diego, California 9

and

Robert M. Ebeling

Information Technology Lab

DEPARTMENT OF THE A
Waterways Experiment Station, Cor
3909 Halls Ferry Road, Vicksburg, Missi


June 1991

Final Report



Prepared for DEPARTMENT OF
US Army Corps of Engine
Washington, DC 20314-

Under Contract No. DACW39-9

Destroy this report when no longer needed. Do not return it to the originator.

The findings in this report are not to be construed as an official Department of the Army position unless so designated by other authorized documents.

The contents of this report are not to be used for advertising, publication, or promotional purposes. Citation of trade names does not constitute an official endorsement or approval of the use of such commercial products.

# REPORT DOCUMENTATION PAGE

Form Approved
OMB No. 0704-0188



| 1. AGENCY USE ONLY (Leave blank) | 2. REPORT DATE | 3. REPORT TYPE AND DATES COVERED |
|---|---|---|
| | June 1991 | Final Report |

**4. TITLE AND SUBTITLE**

Soil-Structure Interaction Parameters for Silts

**5. FUNDING NUMBERS**

DACW39-90-M-2087

**6. AUTHOR(S)**

Timothy D. Stark  Steven M. Fitzwilliam
Joseph J. Vettel  Robert M. Ebeling

**7. PERFORMING ORGANIZATION NAME(S) AND ADDRESS(ES)**

See reverse

**8. PERFORMING ORGANIZATION REPORT NUMBER**

Technical Report
ITL-91-2

**9. SPONSORING / MONITORING AGENCY NAME(S) AND ADDRESS(ES)**

US Army Corps of Engineers
Washington, DC 20314-1000

**10. SPONSORING / MONITORING AGENCY REPORT NUMBER**

**11. SUPPLEMENTARY NOTES**

Available from National Technical Information Service, 5285 Port Royal Road, Springfield, VA 22161.

**12a. DISTRIBUTION / AVAILABILITY STATEMENT**

Approved for public release; distribution is unlimited

**12b. DISTRIBUTION CODE**

**13. ABSTRACT** *(Maximum 200 words)*

This report describes the work completed under the research project entitled "Soil-Structure Interaction Parameters for Silts." The main objective of this research was to characterize the drained and undrained stress-strain behavior of normally consolidated silts and clayey-silts. The results of this research were also used to develop a database of hyperbolic stress-strain and Mohr-Coulomb strength parameters for silts and clayey-silts. This research involved extensive drained and undrained triaxial tests on silt specimens with varying clay contents. The percentages of clay used in the silt mixtures were 0, 10, 30, and 50%. The effect of density was investigated by compacting the triaxial test specimens at Standard Proctor relative compactions of 85, 90, 95, and 100%. This report summarizes the test results and the resulting hyperbolic stress-strain and Mohr-Coulomb strength parameters for the various silt mixtures considered.



**14. SUBJECT TERMS**

**15. NUMBER OF PAGES**
204

**16. PRICE CODE**

| 17. SECURITY CLASSIFICATION OF REPORT | 18. SECURITY CLASSIFICATION OF THIS PAGE | 19. SECURITY CLASSIFICATION OF ABSTRACT | 20. LIMITATION OF ABSTRACT |
|---|---|---|---|
| UNCLASSIFIED | UNCLASSIFIED | | |

7. (Concluded).

University of Illinois, Department of Civil Engineering, Urbana, IL 61801; San Diego State University, Department of Civil Engineering, San Diego, CA 92182; USAE Waterways Experiment Station, Information Technology Laboratory, Vicksburg, MS 39180-6199.

# PREFACE

This report was prepared by Dr. Timothy D. Stark, Assistant Professor of Civil Engineering at the University of Illinois at Urbana-Champaign. The research was conducted at San Diego State University (SDSU) under Contract No. DACW39-90-M-2087 with the US Army Engineer Waterways Experiment Station (WES) during Dr. Stark's tenure at SDSU. Mr. Joseph J. Vettel and Mr. Steven M. Fitzwilliam, Research Assistants at San Diego State University, performed the triaxial tests described in this report under the supervision of Dr. Stark. Dr. Robert M. Ebeling, Research Civil Engineer, Computer-Aided Engineering Division, Information Technology Laboratory (ITL), WES, supervised and monitored the research. Dr. Ebeling and Dr. John F. Peters, Research Civil Engineer, Geotechnical Laboratory, WES, also provided technical guidance and review on the project under the general supervision of Mr. Reed Mosher, Research Civil Engineer, Computer-Aided Engineering Division, ITL, and Dr. N. Radhakrishnan, Chief, ITL.

The Commander and Director of WES was COL Larry B. Fulton, EN. Technical Director was Dr. Robert W. Whalin.



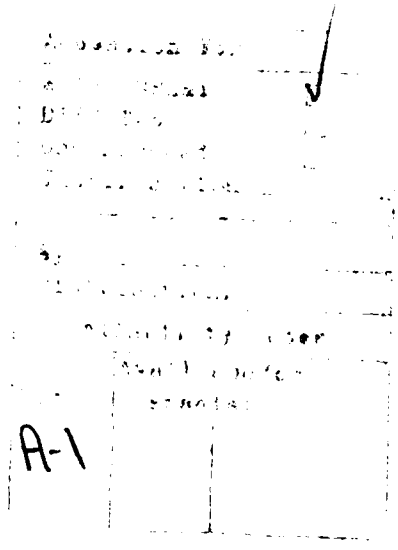

# TABLE OF CONTENTS

## CONVERSION FACTORS, NON-SI TO SI (METRIC) UNITS OF MEASUREMENT

Non-SI units of measurement used in this report can be converted to SI (metric) units as follows:

| Multiply | By | To Obtain |
|---|---|---|
| feet | 0.3048 | metres |
| inches | 2.54 | centimetres |
| inches | 0.0254 | metres |
| pounds | 4.4822 | newtons |
| tons | 8.896 | kilonewtons |
| pounds per square foot | 47.8803 | pascals |
| pounds per square foot | 0.04788 | kilopascals |
| pounds per square inch | 6.8948 | kilopascals |
| tons per square foot | 95.76 | kilopascals |
| tons per square foot | 0.976 | $kg/cm^2$ |

# PART I: INTRODUCTION

## Background

1. The finite element method provides a powerful technique for the analysis of stresses and movements in earth masses, and it has been applied to a variety of soil-structure interaction problems. The results of soil stress-deformation analyses are controlled by the stress-strain characteristics of the soil being modeled. Modeling the stress-strain characteristics of soils is extremely complex, because the behavior of soil is nonlinear, inelastic, and highly dependent on the magnitudes of the stresses in the soil.

2. The hyperbolic stress-strain relationships, developed by Duncan and Chang, (1970), provide a simple model which encompasses the most important characteristics of soil stress-strain behavior, using data from conventional laboratory tests. Due to its simplicity, applicability to drained and undrained problems, and the availability of a database of hyperbolic stress-strain parameters, the hyperbolic model is frequently used in soil-structure interaction problems. The model has been successfully applied to embankment dams (Duncan et al. 1982), open excavations (Chang 1969), retaining walls (Duncan, Clough and Ebeling 1990), braced excavations (Mana and Clough 1981), lock and dam structures (Clough and Duncan 1969), and a variety of soil-structure interaction problems, such as compaction induced earth pressures (Seed and Duncan 1986).

3. The database of drained and undrained hyperbolic parameters for approximately 135 different soils was assembled by Duncan et al. (1978 and 1980) and has been extremely useful for:

a.) judging the reliability of parameter values determined from laboratory test data,

b.) determining the effects of various factors which influence the values of the parameters, and

c.) estimating values of the parameters when insufficient data are available for their determination.

4. The soil types included in the database range from clays to gravels. However, hyperbolic parameters and shear strength parameters for silts and clayey-silts have not been adequately defined in the database or the professional literature. As a result, the summary table presented by Duncan et al., (1978), see Table 1, does not include hyperbolic or shear strength parameters for silts or clayey-silts.

Table 1 - Summary of Hyperbolic Stress-Strain Parameters (from Duncan et al., 1978)

| Unified Soil Classification | RC Stand. AASHTO | $\gamma_m$ k/ft$^3$ | $\phi_o$ ($\Delta\phi$) degrees | c k/ft$^2$ | k | n | $R_f$ | $k_b$ | m |
|---|---|---|---|---|---|---|---|---|---|
| GW, GP SW & SP | 105% | 0.150 | 42 (9) | 0 | 600 | 0.4 | 0.7 | 175 | 0.2 |
| | 100 | 0.145 | 39 (7) | 0 | 450 | 0.4 | 0.7 | 125 | 0.2 |
| | 95 | 0.140 | 36 (5) | 0 | 300 | 0.4 | 0.7 | 75 | 0.2 |
| | 90 | 0.135 | 33 (3) | 0 | 200 | 0.4 | 0.7 | 50 | 0.2 |
| SM | 100% | 0.135 | 36 (8) | 0 | 600 | 0.25 | 0.7 | 450 | 0.0 |
| | 95 | 0.130 | 34 (6) | 0 | 450 | 0.25 | 0.7 | 350 | 0.0 |
| | 90 | 0.125 | 32 (4) | 0 | 300 | 0.25 | 0.7 | 250 | 0.0 |
| | 85 | 0.120 | 30 (2) | 0 | 150 | 0.25 | 0.7 | 150 | 0.0 |
| SM-SC | 100% | 0.135 | 33 (0) | 0.5 | 400 | 0.6 | 0.7 | 200 | 0.5 |
| | 95 | 0.130 | 33 (0) | 0.5 | 200 | 0.6 | 0.7 | 100 | 0.5 |
| | 90 | 0.125 | 33 (0) | 0.3 | 150 | 0.6 | 0.7 | 75 | 0.5 |
| | 85 | 0.120 | 33 (0) | 0.2 | 100 | 0.6 | 0.7 | 50 | 0.5 |
| CL | 100% | 0.135 | 30 (0) | 0.4 | 150 | 0.45 | 0.7 | 140 | 0.2 |
| | 95 | 0.130 | 30 (0) | 0.3 | 120 | 0.45 | 0.7 | 110 | 0.2 |
| | 90 | 0.125 | 30 (0) | 0.2 | 90 | 0.45 | 0.7 | 80 | 0.2 |
| | 85 | 0.120 | 30 (0) | 0.1 | 60 | 0.45 | 0.7 | 50 | 0.2 |

## Purpose and Scope

5. Due to the limited information available on the hyperbolic and shear strength parameters of silts, the main objectives of this research are to:

a.) characterize the drained and undrained stress-strain behavior of normally consolidated silts and clayey-silts at various densities or relative compactions,

b.) characterize the drained and undrained shear behavior of normally consolidated silts with varying percentages of clay,

c.) determine the appropriate hyperbolic stress-strain and Mohr-Coulomb strength parameters for normally consolidated silts with varying percentages of clay, and

d.) evaluate the effect of clay mineralogy on the drained stress-strain behavior of normally consolidated silts and clayey-silts.

6. The resulting information on the behavior of normally consolidated silts was used to develop a database of hyperbolic stress-strain and Mohr-Coulomb strength parameters for silts and clayey-silts. The database contains both drained and undrained parameters for a variety of initial densities and water contents. Table 2 presents a summary of the 116 triaxial tests that were performed to achieve these objectives.

# PART II: HYPERBOLIC STRESS-STRAIN MODEL

## Stiffness Parameters

7. Duncan et al. (1980) provide an extensive derivation of the hyperbolic model and a detailed procedure for determining the values of the hyperbolic stress-strain parameters from conventional triaxial tests. As a result, only the major features of the model will be described in this introduction in order to define the various hyperbolic stress-strain parameters.

8. The hyperbolic model represents the nonlinear stress-strain curve of soils using a hyperbola as shown in Figure 1. It can be seen that transforming the hyperbolic equation results in a linear relationship between $\epsilon/(\sigma'_1 - \sigma'_3)$ and $\epsilon$, where $\epsilon$ is the axial strain and $(\sigma'_1 - \sigma'_3)$ is the effective deviator stress. The stress dependent stress-strain behavior of soil is represented by varying the initial tangent modulus, $E_i$, and the ultimate deviator stress, $(\sigma'_1 - \sigma'_3)_{ult}$, with the effective confining pressure, $\sigma'_3$. It can be seen from Figure 1 that the ultimate deviator stress is the asymptotic value of the deviator stress and is related to the compressive strength of the soil. The variation of the initial tangent modulus with confining pressure is represented by an empirical equation proposed by Janbu (1963):

$$E_i = K p_a \left( \frac{\sigma'_3}{p_a} \right)^n \qquad (1)$$

where K is the modulus number, n is the modulus exponent, and $p_a$ is the atmospheric pressure in the same units as $\sigma'_3$ and $E_i$.

9. The variation of $E_i$ with $\sigma'_3$ is linear when the logarithm of $(E_i/p_a)$ and $(\sigma'_3/p_a)$ are plotted against each other. The modulus number equals $(E_i/p_a)$ at a value of $(\sigma'_3/p_a)$ equal to one and n is the slope of the resulting line.

10. The variation of ultimate deviator stress with $\sigma'_3$ is accounted for by relating $(\sigma'_1 - \sigma'_3)_{ult}$ to the stress difference at failure, $(\sigma'_1 - \sigma'_3)_f$, and using the Mohr-Coulomb strength equation to relate $(\sigma'_1 - \sigma'_3)_f$ to $\sigma'_3$. The criteria used to define $(\sigma'_1 - \sigma'_3)_f$ is usually the maximum deviator stress. However, the criteria which results in the best approximation of the actual stress-strain curve should be used. The values of $(\sigma'_1 - \sigma'_3)_{ult}$ and $(\sigma'_1 - \sigma'_3)_f$ are related by:

Table 2. Triaxial Testing Performed on Kaolinite and Montmorillonite-Silt Mixtures

| Objective(s) | Type of Triaxial Test Required | Test Variables | Total Number of Triaxial Tests | Comments |
|---|---|---|---|---|
| Drained Stress-Strain & Strength, Parameters at Various Relative Compactions and Define Sand-Clay Transition Point. | S, i.e. Consolidated-Drained | % Clay = 0, 10, 30 & 50<br>RC = 85, 90, 95 & 100%<br>W = optimum | 3-4 test per failure envelope => 56 | Samples fabricated using modified Chan cyclic compactor and Kaolinite. |
| Undrained & Drained Strength Parameters & Vector Curve Behavior at Various Relative Compactions | R, i.e. Consolidated-Undrained | % Clay = 0, 10, 30, & 50<br>RC = 85, 90, 95 & 100%<br>W = optimum | 3-4 tests per failure envelope => 50 | Samples fabricated using modified Chan cyclic compactor and Kaolinite. |
| Effect of Clay Mineralogy on Define Sand-Clay Transition Point, Drained Stress-Strain & Strength Parameters at Relative Compaction=100% | S, i.e. Consolidated-Drained | % Clay = 0, 10, 30, & 50<br>RC = 100%<br>W = optimum | 3-4 tests per failure envelope => 10 | Samples fabricated using modified Chan cyclic compactor and Montmorillonite. |
| | Total Number of Triaxial Tests Performed | = | 116 | |

NOTES:
1.) Samples fabricated using dry mixing
2.) RC = Relative Compaction based on Standard Proctor for consistency with Table 1
3.) w = Compaction Water Content
4.) All Triaxial Test Specimens Isotropically Consolidated

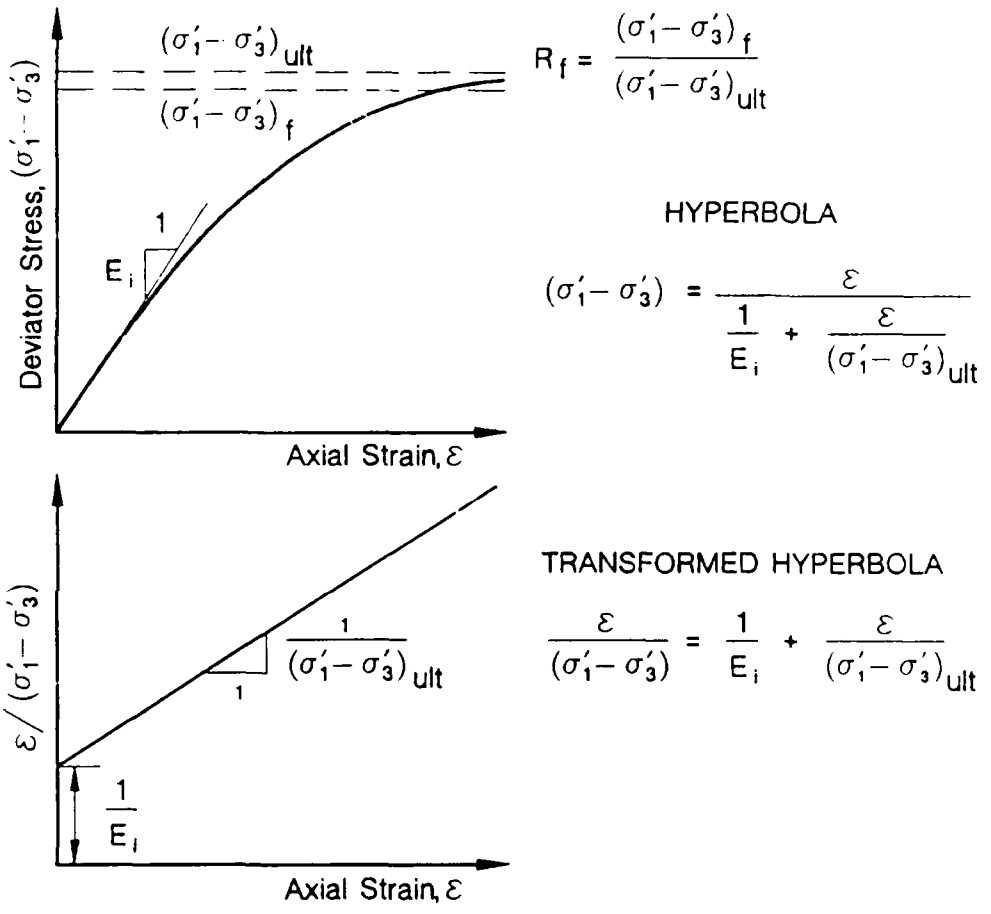


Figure 1. Hyperbolic Representation of a Stress-Strain Curve (from Duncan et al. 1980)

$$(\sigma'_1 - \sigma'_3)_f = R_f(\sigma'_1 - \sigma'_3)_{ult} \quad (2)$$

in which $R_f$ is the failure ratio as shown in Figure 1. The value of $R_f$ is always less than or equal to 1.0, and varies from 0.5 to 0.9 for most soils. The variation of $(\sigma'_1 - \sigma'_3)_f$ with $\sigma'_3$ can be expressed as follows using the Mohr-Coulomb strength equation:

$$(\sigma'_1 - \sigma'_3)_f = \frac{2c'\cos\phi' + 2\sigma'_3 \sin\phi'}{1 - \sin\phi'} \quad (3)$$

in which c' and $\phi'$ are the effective stress Mohr-Coulomb cohesion intercept and friction angle, respectively.

11. By differentiating the equation of a hyperbola shown in Figure 1 with respect to the axial strain and substituting the expression into Equations (1), (2) and (3), an expression for the tangent modulus, $E_t$, can be obtained:

$$E_t = \left[1 - \frac{R_f(1 - \sin\phi')(\sigma'_1 - \sigma'_3)}{2c'\cos\phi' + 2\sigma'_3 \sin\phi'}\right]^2 K p_a \left(\frac{\sigma'_3}{p_a}\right)^n \quad (4)$$

12. This equation can be used to calculate the value of $E_t$ for any stress condition if the hyperbolic parameters K, n, and $R_f$ and the Mohr-Coulomb shear strength parameters, c' and $\phi'$, are known.

## Volume Change Parameters

13. The hyperbolic stress-strain model accounts for the nonlinear volume change behavior of soils by assuming that the bulk modulus is independent of stress level, $(\sigma'_1 - \sigma'_3)$, and that it varies with confining pressure. The variation of bulk modulus, B, with confining pressure is approximated by the following equation:

$$B = K_b p_a \left(\frac{\sigma'_3}{p_a}\right)^m \quad (5)$$

where $K_b$ is the bulk modulus number and m is the bulk modulus exponent. The variation of B is linear when the logarithm of $(B/p_a)$ and $(\sigma'_3/p_a)$ are plotted against each other. The bulk modulus number equals $(B/p_a)$ at a value of $(\sigma'_3/p_a)$ equal to one and m is the slope of the resulting line.

# PART III: LABORATORY TESTING PROGRAM

## Silt Origin

14. The main objective of this research was to characterize the drained and undrained stress-strain behavior of normally consolidated silts and clayey-silts. To achieve this objective, extensive drained and undrained triaxial tests had to be conducted on silt with varying clay contents. As a result, a borrow area containing pure silt or a silt with a very low clay content needed to be located.

15. A bluff containing Mississippi loess was located at the U.S. Army Engineers Waterways Experiment Station (WES) in Vicksburg, Mississippi. The location of the bluff is shown on the information map of WES in Figure 2. The loess comprising this bluff contained approximately 9 to 22% clay and 78 to 91% silt. The percentage of clay is defined as the material finer than 0.002 mm. It was anticipated that the clay content could be removed from the loess using a sedimentation process and the remaining silt could be used as the base soil for the proposed testing.

16. The Mississippi loess belt is approximately 70 to 120 miles wide, extending eastward from the bluffs along the Mississippi River. Generally the loess is less than 10 feet thick except at the bluffs where it is up to 100 feet thick. The bluff at WES where the loess samples were obtained is approximately 40 feet high.

17. The Mississippi loess deposits were created by westerly winds carrying fine particles from the Mississippi River alluvial valley to its eastern uplands where it was deposited. This deposition occurred during the late Pleistocene and early Recent times.

18. Mississippi loess contains mainly silt and clay size particles. It can be seen from the scanning electron microscope photograph in Figure 3 that the silt particles are subangular to subrounded. The loess is a highly structured and/or cemented material. In its natural state, the cementation allows the loess to stand at a vertical slope. The mechanism for the cementation is not known. However, the clay particles, the capillary pore pressure, and the carbonates in the loess are believed to contribute to the cementation process.

## Silt Sampling

19. In mid-October, 1989, Dr. T.D. Stark of San Diego State University (SDSU) and Dr. R.M. Ebeling of WES excavated a four-gallon bucket of the loess from the bluff at

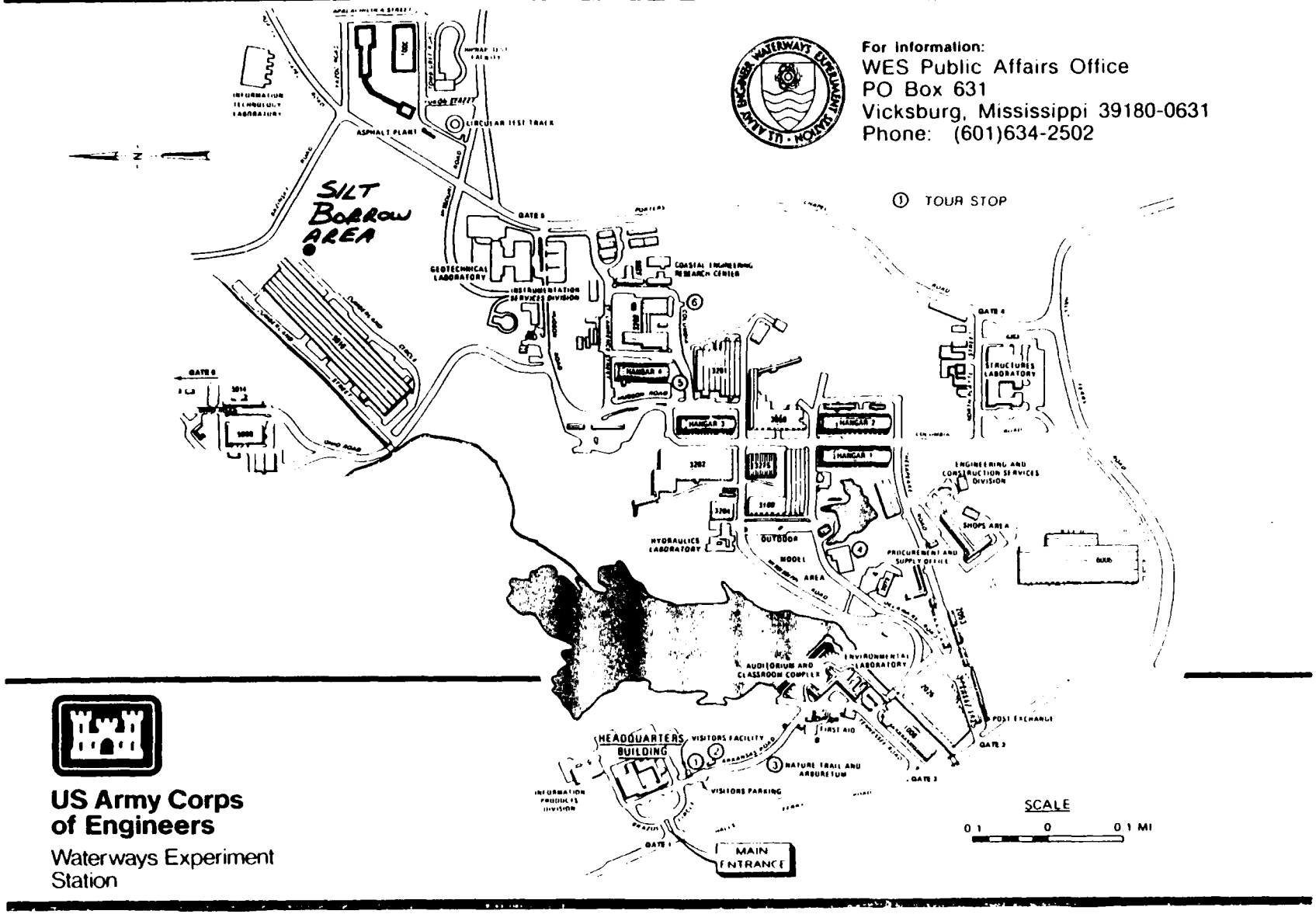


Figure 2. Location Map of Silt Borrow Area

Figure 3. Scanning Electron Microscope Photograph of Silt Particles

WES using a hand-held shovel. This bucket was flown back to San Diego State University by Dr. Stark to investigate the feasibility of using this deposit of Mississippi loess as the source of the silt material.

20. Hydrometer analyses revealed that the clay content of the light-brown loess was approximately 9 to 11%. Approximately 2 to 3% of the loess was fine sand, shells, and organics particles which did not pass the No. 200 ASTM sieve. It was anticipated that the 9 to 11% clay fraction could be removed using a sedimentation process which is described subsequently. As a result, thirty-three additional four-gallon buckets of silt were shipped to SDSU by WES. However, eighteen of the buckets contained loess with a clay content of 16 to 22% and were not used during this study. Only loess containing a clay fraction of 9 to 11% were used to facilitate the sedimentation process. Therefore, a total of sixteen buckets or approximately 800 lbs. of Mississippi loess containing 9 to 11% silt was delivered to SDSU and used during this study.

## Silt Processing

21. The main objective of the processing was to remove most, if not all, of the clay particles naturally present in the Mississippi loess. An extensive study was conducted to determine the optimal sedimentation time and ratio of soil to water which resulted in the maximum removal of the clay particles and the minimum removal of the silt. It was found that 8 pounds of soil and 4 gallons of water resulted in the optimal mix for the sedimentation process. After vigorous hand agitation each mix was allowed to sediment for 10 minutes. Shorter settling times were found to remove more clay, however there was also a greater loss of silt. After 10 minutes the water was poured or decanted from the bucket. Each 8 pound sample underwent this agitation, sedimentation, and decanting process four times.

22. The entire processing of the 800 pounds of silt required 100 - eight pound samples undergoing 400 sedimentation/decant cycles and approximately 1600 gallons of deionized water. It was found that regular tap water caused the clay particles to flocculate and settle very quickly. Therefore, deionized water was used because it did not flocculate the clay particles which allowed the clay to remain suspended during the sedimentation process. The processing of the 800 lbs of the loess took approximately ten days.

23. After four sedimentation/decant cycles the clay fraction of the loess was reduced to approximately 1.0% while 55 to 60% of the silt was retained. After the

sedimentation process was completed, the silt was air-dried. As the silt dried, it was sieved through the No. 200 ASTM sieve to remove the fine sand, shells and organics present in the natural loess. After sieving, approximately 450 lbs (56%) of the original 800 lbs of the Mississippi loess remained. All of the processed silt was combined in a large pile and thoroughly mixed to insure a uniform sample. Hydrometer tests were performed, in accordance with ASTM Standard D422 (ASTM 1990), on ten test specimens which were obtained from various locations in the pile. The clay fraction of these ten specimens content ranged from 0.8 to 1.2%. This was determined to be an acceptable level of clay for the proposed triaxial tests. During the addition of the various amounts of kaolinite and montmorillonite, this 1% of natural clay was neglected.

Sample Preparation and Mixing

24. Sample preparation usually affects the stress-strain and strength behavior of soils and thus was a key element of this investigation. Based on research by Lupini et al. (1981), Mulilis et al. (1977), Seed et al. (1964), and Skempton, (1985), the silt mixtures were fabricated using a dry mixing technique. The samples were composed of the processed silt and the following clay percentages: 0, 10, 30, and 50. These percentages were based on the dry weight of the silt and clay.

25. The dry mixing process involved carefully weighing out the proper amounts of silt and clay, thoroughly mixing the silt and clay by hand in a four-gallon bucket, and then adding the appropriate amount of water. The dry mixing process usually involved mixing approximately 10 to 15 pounds of silt and clay at one time. This resulted in small samples which could be controlled fairly accurately. The deionized water was applied to the sample using a hand-operated spray bottle. This allowed small amounts of water to be carefully added to the mixture. The mixture was thoroughly mixed after each addition or spray of water. Any clumps of soil which developed during mixing were forced through a No. 10 ASTM sieve to facilitate compaction and to increase the uniformity of the mix. This somewhat tedious mixing process resulted in a homogeneous mixture.

26. To characterize the effect of clay mineralogy on the stress-strain and strength behavior of silt, two different clay minerals were combined with the processed silt. Manufactured kaolinite and montmorillonite were mixed with the silt to obtain samples representative of low and high plasticity silt. The manufactured kaolinite and montmorillonite were first passed through a No. 200 ASTM sieve and then mixed with the silt to obtain the clayey-silt samples. The kaolinite was manufactured by NL Products of

Edgar, Florida and is shipped in 50 pound bags. The montmorillonite is a product of M-1 Drilling Company of Houston, Texas. It is a Wyoming bentonite and is shipped in 100 pound bags. Approximately 5% of both the kaolinite and montmorillonite were retained on the No. 200 ASTM sieve and removed. During mixing the fact that the natural water content of both products was approximately 6% was taken into account.

# PART IV: INDEX TESTING

## Classification and Compositional Data

27. The index properties of the various silt mixtures are shown in Table 3. It can be seen from Table 3 that the Unified Soil Classification System (USCS) Symbol for the various kaolinite-silt mixtures ranged from ML to CL. The gradation curves for the various kaolinite-silt mixtures are shown in Figure 4. It can be seen from Figure 4 that the 0% kaolinite sample, i.e. 100% processed silt, contained approximately 1% finer than 0.002mm. The 10, 30, and 50% kaolinite mixtures contained a clay fraction (% < 0.002 mm) of 9, 19, and 33%, respectively. The index properties of the 40% kaolinite mixture were used to confirm the properties of the 30 and 50% mixtures. However, triaxial tests were not performed on the 40% kaolinite mixture.

28. The addition of montmorillonite instead of kaolinite resulted in a high plasticity clay with a USCS symbol of CH for all mixtures (Table 3). It can be seen from Figure 5 that the 10, 30, and 50% montmorillonite mixtures contained a clay fraction of 11, 21, 39%, respectively. The specific gravity and plasticity tests for the kaolinite and montmorillonite mixtures were performed in accordance with ASTM (1990) Standard D854-83 and D4318-84, respectively. The grain size analyses were performed using hydrometer analyses in accordance with ASTM (1990) Standard D422-63.

## Proctor Compaction Tests

29. To study the effect of density on the stress-strain behavior and the Mohr-Coulomb strength parameters, the silt mixtures were tested at a range of dry densities. The dry densities correspond to Standard Proctor relative compactions of 85, 90, 95, and 100%. The triaxial test specimens were compacted at the optimum water content for each of these dry densities or relative compactions. The effect of density could also have been studied by varying the water content and keeping the relative compaction constant. From Figure 6 it can be seen that a dry density corresponding to 95% of the maximum Standard Proctor dry density can be obtained using a compaction water content of $w_1$ or $w_2$. However, compacting soils at water contents dry of optimum, i.e. $w_1$, will result in a flocculated soil fabric while a compaction water content wet of optimum, i.e. $w_2$, will result in a disperse soil structure. Therefore, a decision would have to be made regarding which soil fabric, flocculated or disperse, should be used if the relative compaction was held constant. To simplify the effect of the compaction water content, and thus the soil fabric, on the triaxial test results, it was decided to compact the test specimens at the optimum water content for

Table 3. Index Properties of the Silt-Clay Mixtures

| Silt-Clay Mixture | Specific Gravity | Liquid Limit | Plastic Limit | Plasticity Index | USCS Symbol |
|---|---|---|---|---|---|
| 0% Kaolinite | 2.7 | 27 | NP | NP | ML |
| 10% Kaolinite | 2.69 | 29 | 23 | 6 | CL-ML |
| 30% Kaolinite | 2.67 | 30 | 20 | 10 | CL |
| 40% Kaolinite | 2.63 | 31 | 22 | 9 | CL |
| 50% Kaolinite | 2.62 | 38 | 22 | 16 | CL |
| 10% Montmorillonite | 2.71 | 55 | 29 | 26 | CH |
| 30% Montmorillonite | 2.71 | 152 | 26 | 26 | CH |
| 50% Montmorillonite | 2.72 | 186 | 53 | 133 | CH |

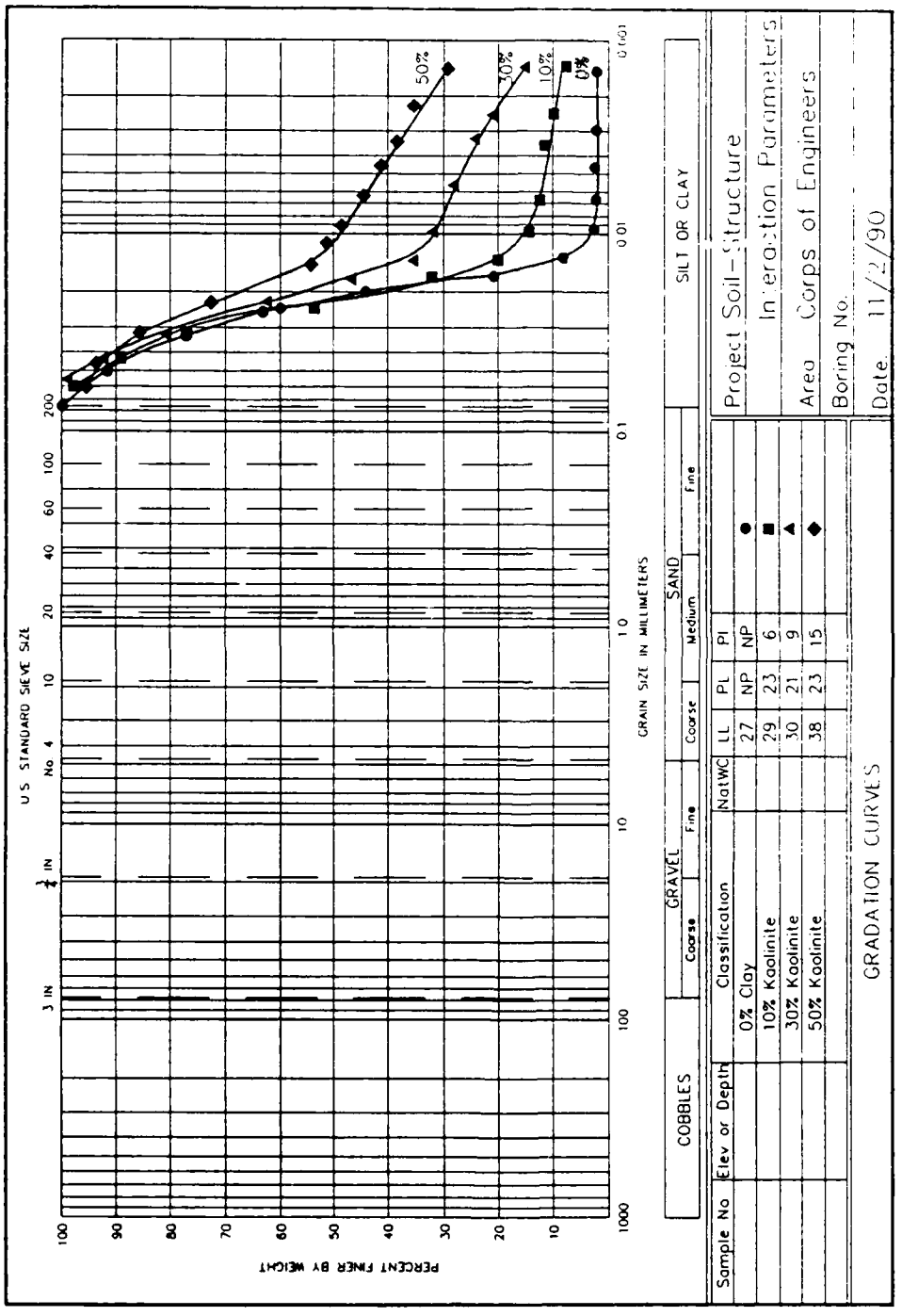


Figure 4. Gradation Curves for Kaolinite-Silt Mixtures

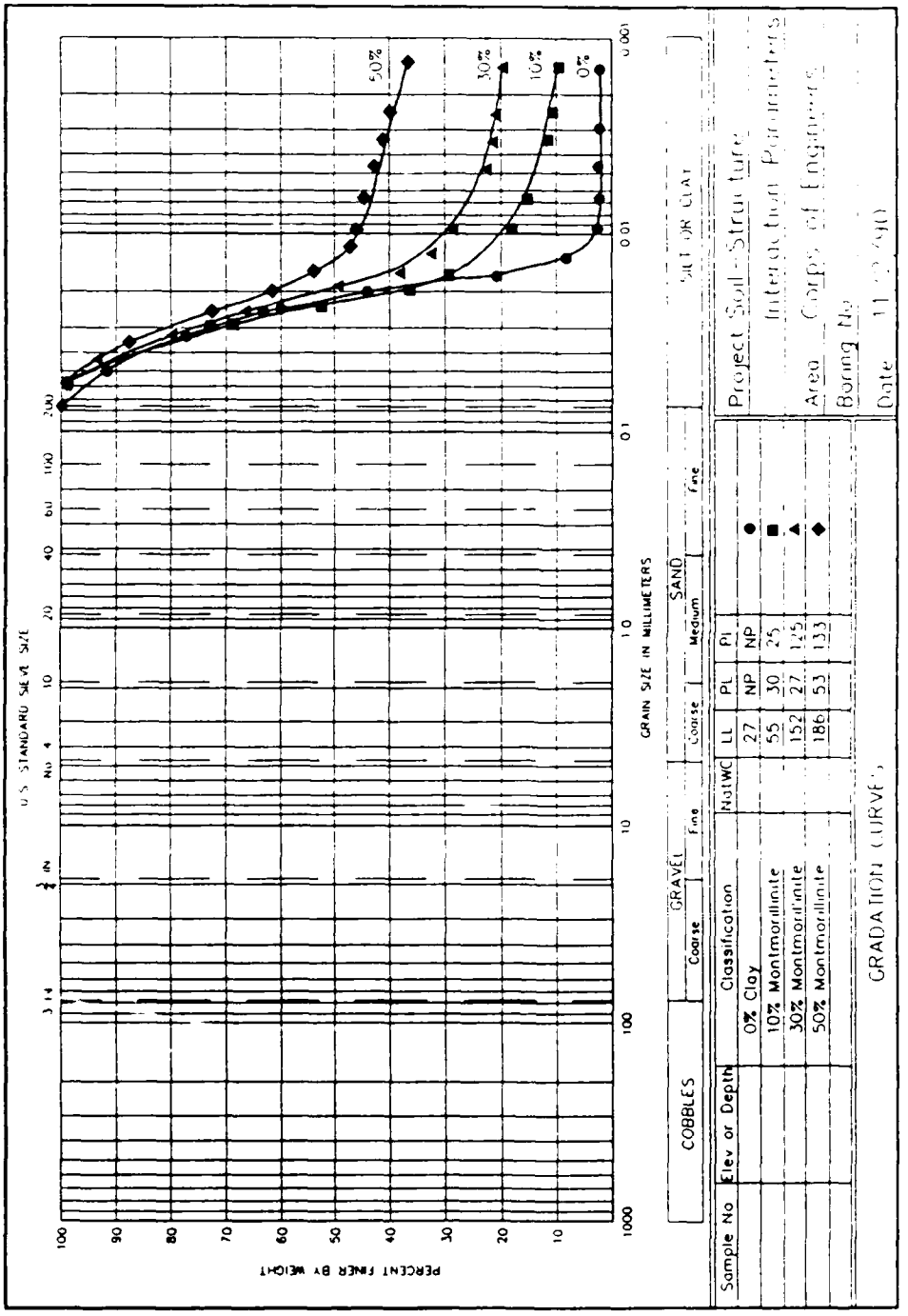


Figure 5. Gradation Curves for Montmorillonite-Silt Mixtures

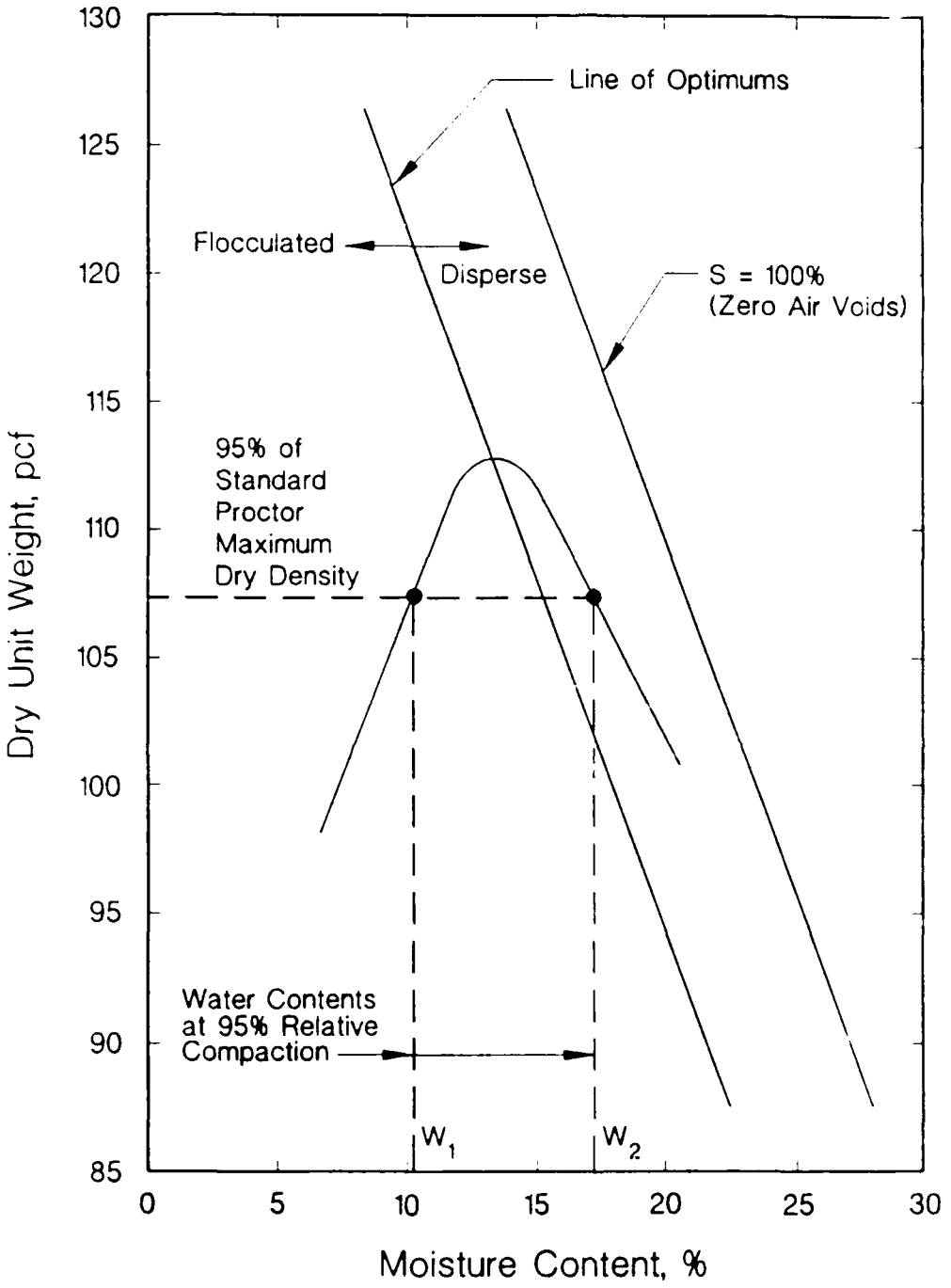


Figure 6. Effect of Compaction Water Content on Soil Fabric

each relative compaction. It was anticipated that the optimal water content would also produce triaxial test results which would be more applicable to natural silt deposits. Therefore, the hyperbolic stress-strain and Mohr-Coulomb strength parameters for natural silt deposits can be estimated from these test results using the insitu dry density and water content.

30. To determine the optimum water content for each relative compaction, the line of optimums for each silt mixture had to be developed. The line of optimums for each kaolinite-silt mixture was obtained from the results of Modified Proctor and Standard Proctor compaction tests which were performed in accordance with ASTM (1990) Standards D1557 and D698.

31. Figure 7 illustrates the technique used to obtain the optimum water content for each relative compaction. For example, the dry density and water content used to obtain a Standard Proctor relative compaction of 100% is obtained from the peak of the Standard Proctor compaction curve. It can be seen from Figure 7 that the dry density and water content for this condition is approximately 106.3 pcf and 15.5%, respectively. The dry density and water content for a Standard Proctor relative compaction of 95% is obtained by moving down the line of optimums curve to a dry density that corresponds to 95% of the maximum dry density or 101.0 pcf. The optimum water content for 95% is approximately 17%. It can be seen from Figure 7 that the dry density and water content for relative compactions of 90 and 85% are obtained in a similar fashion. The triaxial test specimens were then compacted to these dry densities and water contents to investigate the effect of dry density and water content on the measured hyperbolic stress-strain parameters and the Mohr-Coulomb strength parameters. Table 4 presents the compaction water contents and dry densities used for the kaolinite and montmorillonite-silt mixtures.

32. Figures 8 through 11 show the Modified Proctor and Standard Proctor compaction curves, and the line of optimums for the 0, 10, 30 and 50% kaolinite-silt mixtures, respectively. Figure 12 shows the Standard Proctor compaction curves for the 10, 30 and 50% montmorillonite-silt mixtures. Consolidated-Drained (S) triaxial tests were only performed on montmorillonite-silt mixtures at a Standard Proctor relative compaction of 100%. Therefore, it was not necessary to determine a line of optimums or perform Modified Proctor compaction tests for these mixtures.

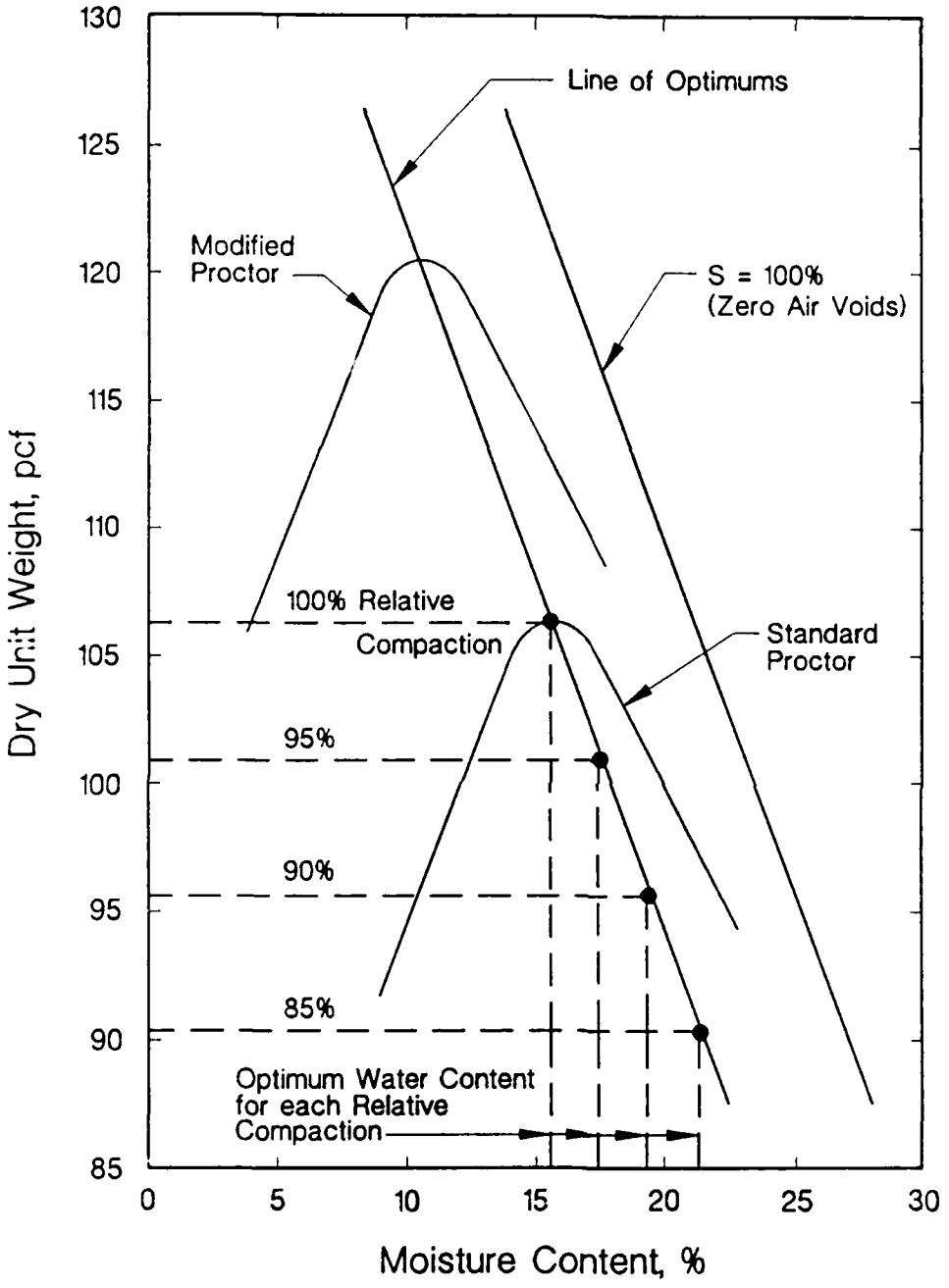


Figure 7. Line of Optimums and Compaction Criteria

Table 4 - Compaction Water Contents and Dry Densities for the Kaolinite and Montmorillonite-Silt Mixtures

| % Clay | Standard Proctor Relative Compaction | Compacted Dry Density (pcf) | Compacted Water Content (%) | Compacted Wet Density (pcf) |
|---|---|---|---|---|
| 0% Kao | 100 | 98.0 | 21.0 | 118.6 |
| 0% Kao | 95 | 93.1 | 23.5 | 115.0 |
| 0% Kao | 90 | 88.2 | 26.2 | 111.3 |
| 0% Kao | 85 | 83.3 | 28.7 | 107.2 |
| 10% Kao | 100 | 104.8 | 17.3 | 122.9 |
| 10% Kao | 95 | 99.6 | 19.2 | 118.7 |
| 10% Kao | 90 | 94.3 | 21.3 | 114.4 |
| 10% Kao | 85 | 89.1 | 23.2 | 110.0 |
| 30% Kao | 100 | 106.6 | 15.5 | 123.1 |
| 30% Kao | 95 | 101.3 | 16.8 | 118.3 |
| 30% Kao | 90 | 95.9 | 18.1 | 113.3 |
| 30% Kao | 85 | 90.6 | 19.4 | 108.2 |
| 50% Kao | 100 | 102.0 | 18.7 | 121.1 |
| 50% Kao | 95 | 96.9 | 20.0 | 116.3 |
| 50% Kao | 90 | 91.8 | 21.1 | 111.2 |
| 50% Kao | 85 | 86.7 | 21.9 | 105.7 |
| 10% Mont | 100 | 100.6 | 21.8 | 122.5 |
| 30% Mont | 100 | 95.2 | 24.5 | 118.5 |
| 50% Mont | 100 | 88.8 | 27.5 | 113.2 |

NOTES:
1.) Kao = Kaolinite
2.) Mont = Montmorillonite

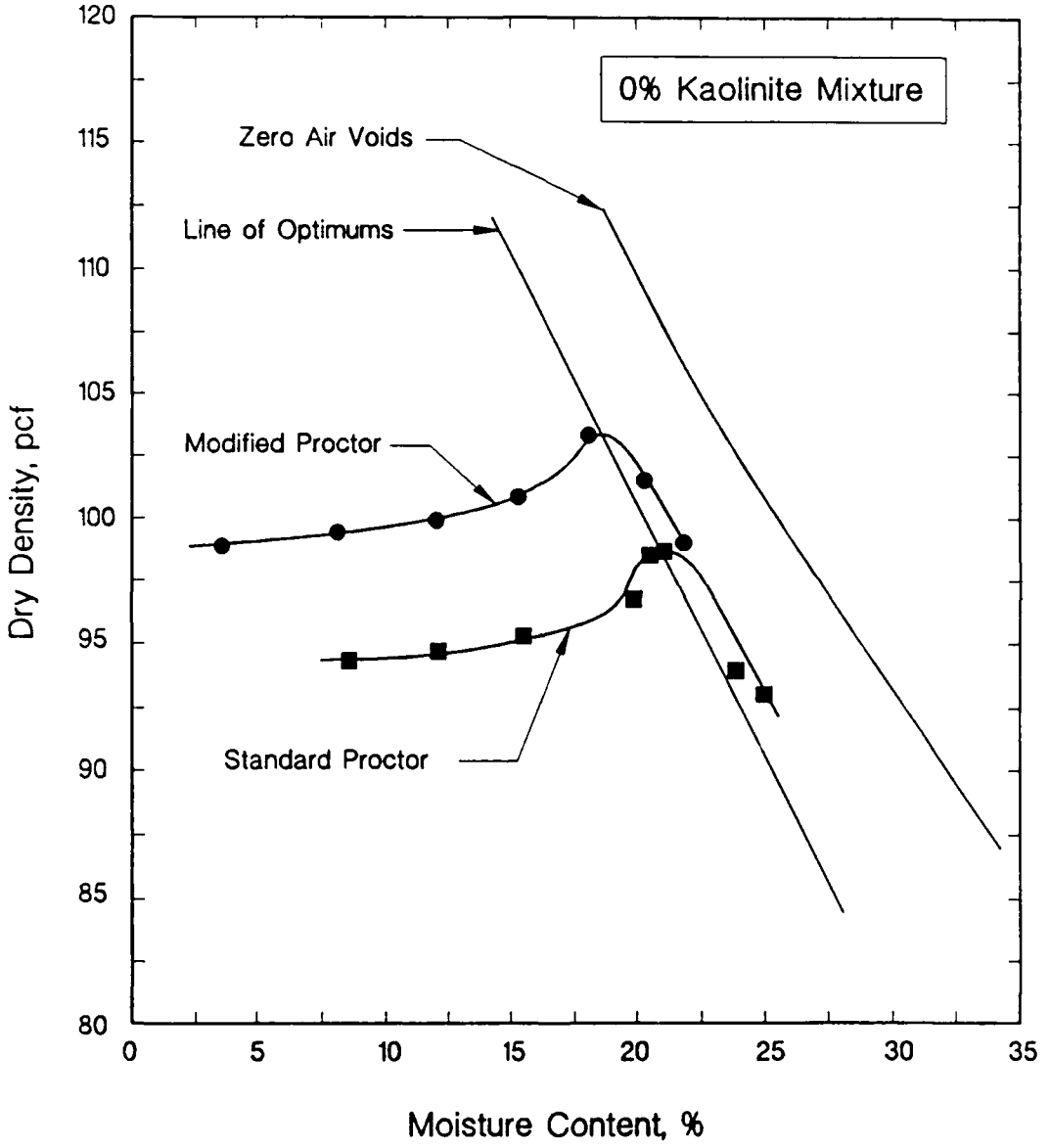


Figure 8. Compaction Curves and Line of Optimums for 0% Kaolinite-Silt Mixture

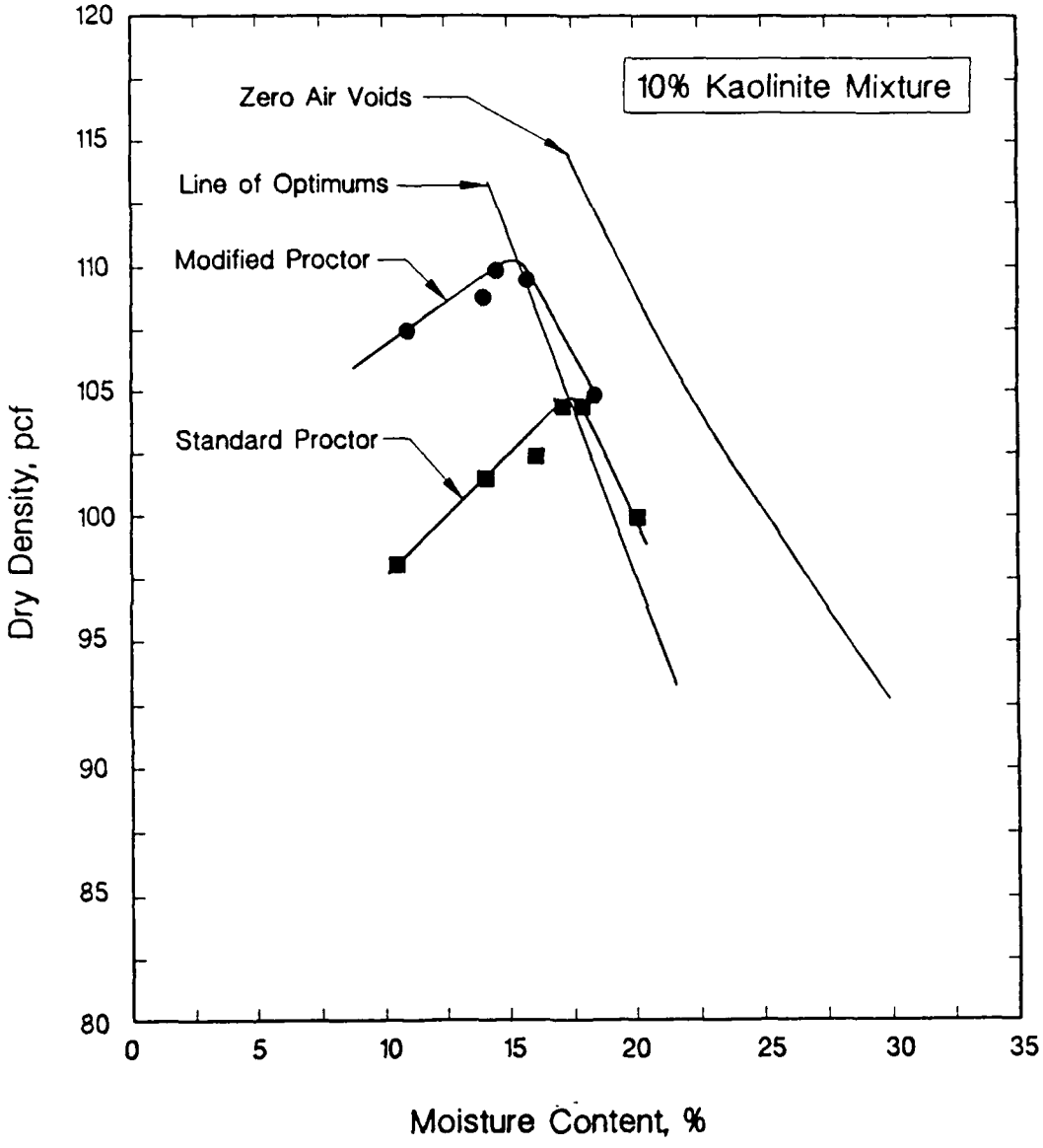


Figure 9. Compaction Curves and Line of Optimums for 10% Kaolinite-Silt Mixture

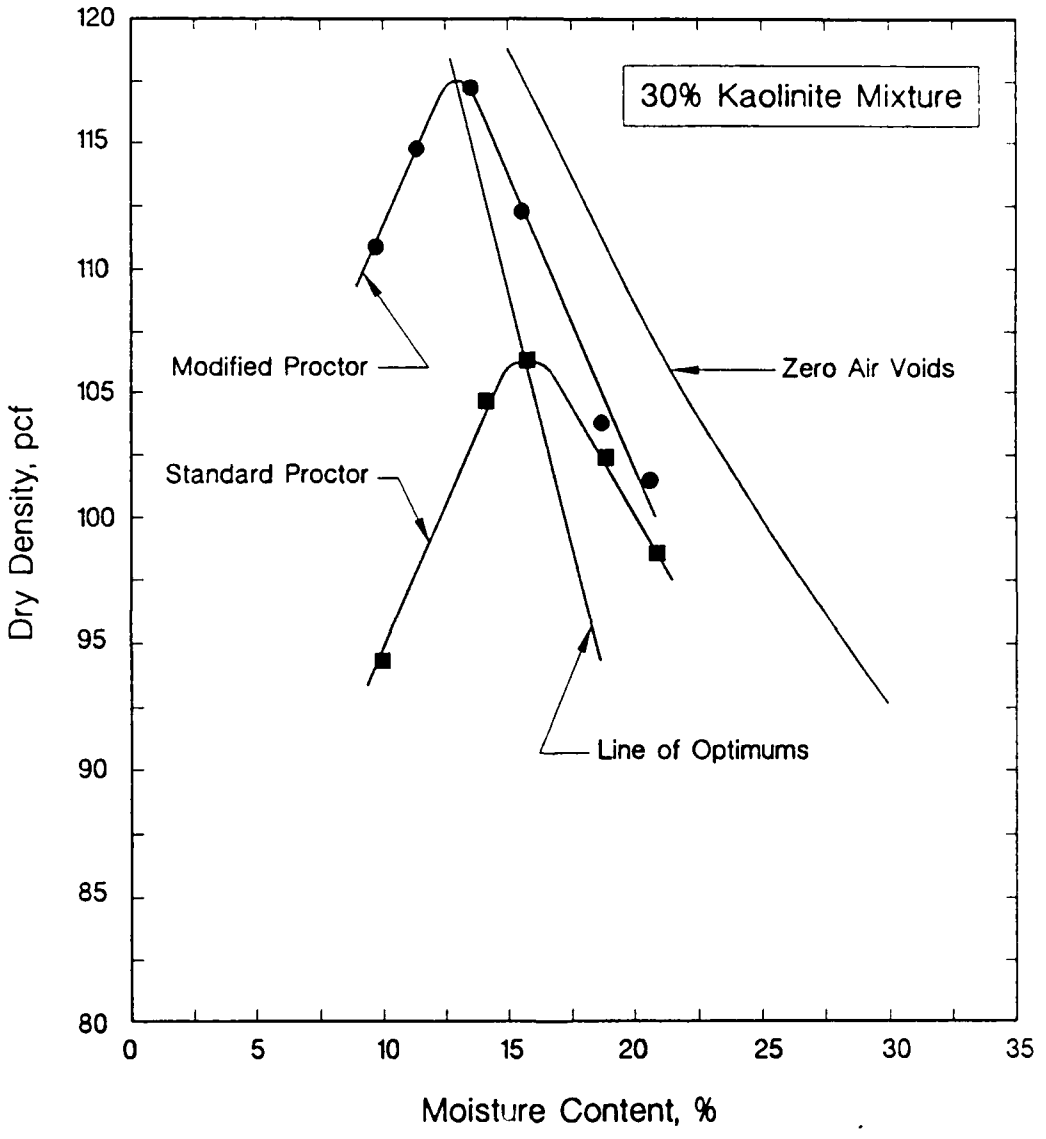


Figure 10. Compaction Curves and Line of Optimums for 30% Kaolinite-Silt Mixture

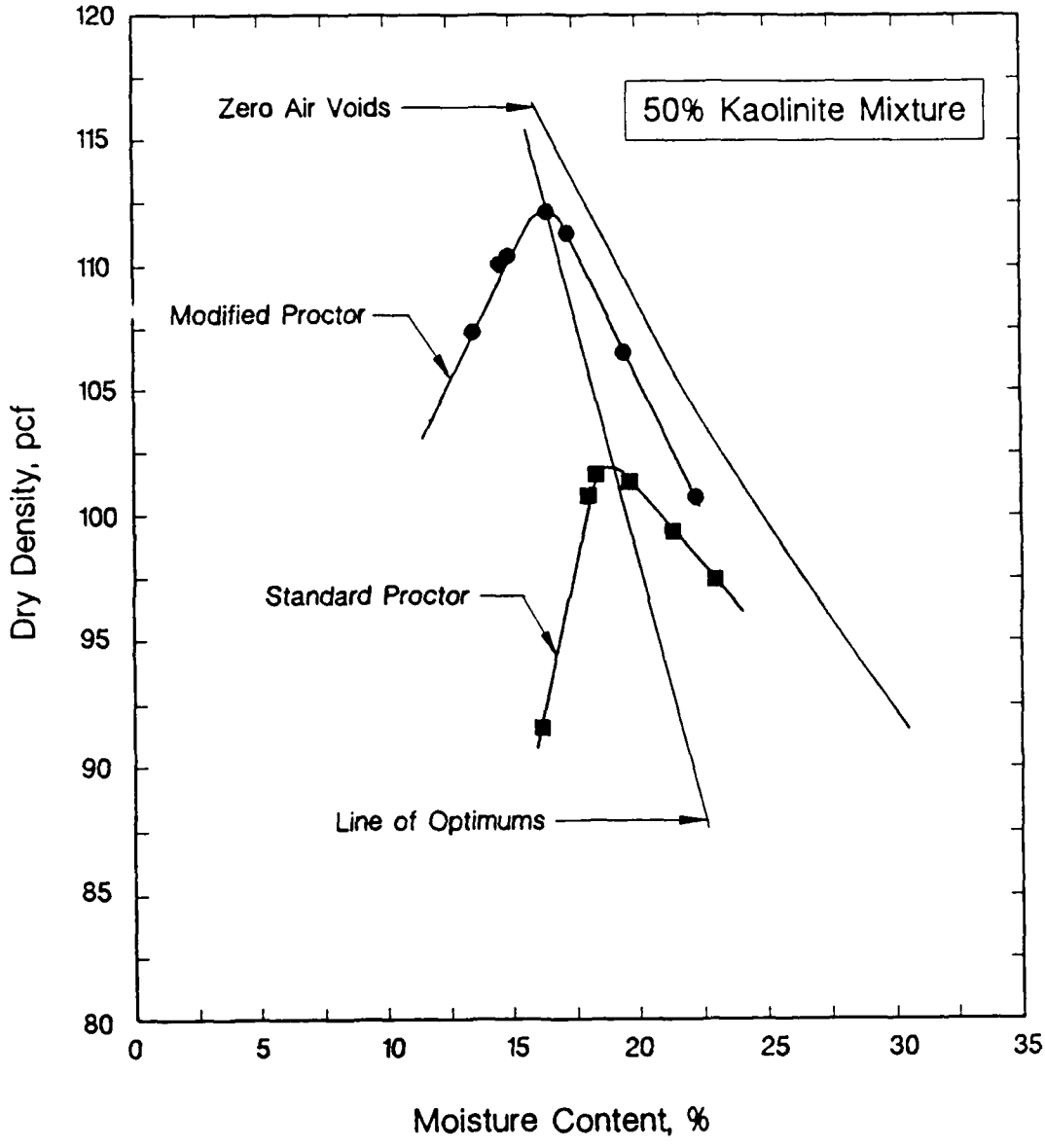


Figure 11. Compaction Curves and Line of Optimums for 50% Kaolinite-Silt Mixture

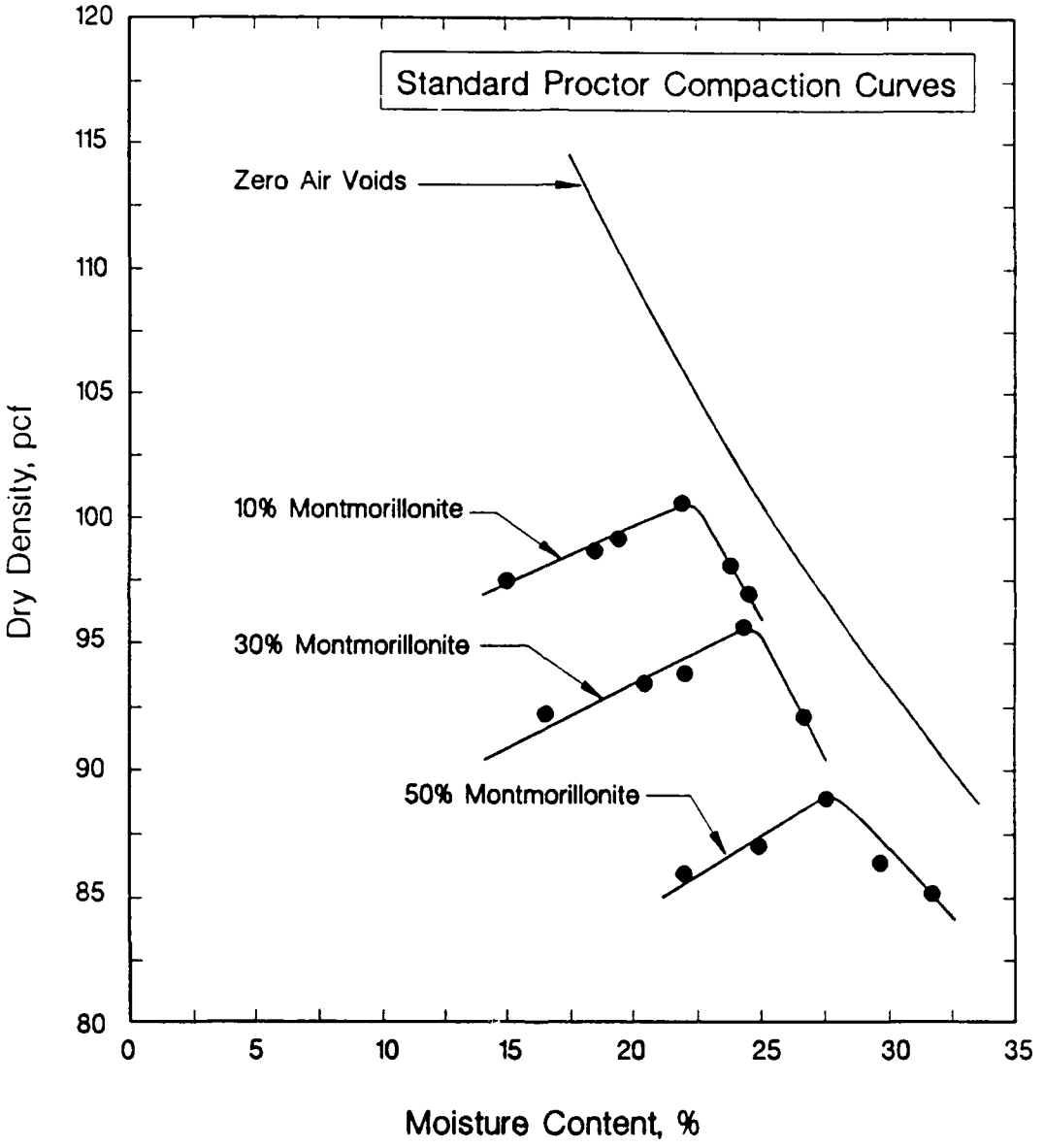


Figure 12. Standard Proctor Compaction Curves for Montmorillonite-Silt Mixtures

## Oedometer Tests

33. The main objective of this study was to characterize the shear behavior of normally consolidated silts and clayey-silts. Therefore, the triaxial tests had to be performed at effective confining pressures which insured normally consolidated behavior. It was also anticipated that removing the overconsolidation due to compaction would greatly facilitate the interpretation and comparison of the test results. Investigation of the effects of overconsolidation due to compaction was beyond the scope of this research.

34. To estimate the effective confining pressure required to insure normally consolidated behavior, an oedometer test was conducted to measure the preconsolidation pressure for each Standard Proctor relative compaction and clay percentage. The effective confining pressures used in the drained and undrained triaxial tests were usually 1.2 to 3.0 times larger than the measured preconsolidation pressures to insure that the overconsolidation due to compaction was overcome.

35. The oedometer test specimens were compacted directly into the fixed oedometer ring at the appropriate dry density and water content. A modified Harvard compaction apparatus was used to compact the test specimens. This apparatus controls the height of each lift and thus the amount of soil compacted into each lift. Therefore, the appropriate amount of soil is weighed and compacted in four lifts to obtain the desired dry density or relative compaction. Four lifts are used to create the 0.4 inch thick test specimens. The top of each lift was scarified before the next lift was placed to insure an adequate bond between lifts. The one-dimensional oedometer tests were performed in accordance with ASTM (1990) Standard D2435-80.

36. Figures 13 through 16 show the effective stress relationships from the oedometer tests on the 0, 10, 30 and 50% kaolinite-silt mixtures, respectively. It can be seen that the stiffness of the silt mixtures increased as the amount of kaolinite decreased. It can be seen from Figure 13 that the 0% kaolinite mixture exhibited a very flat stress-strain curve. As a result, the maximum preconsolidation pressure for the 0% kaolinite mixture ranged from 11 to 18 tsf. Effective confining pressures of 11 to 20 tsf were used for this mixture because pressures greater than 20 tsf could not be obtained. These large confining stresses required the use of stainless steel triaxial containers instead of the standard Plexiglass containers.

37. As the percentage of kaolinite increased, the slope of the stress-strain curve

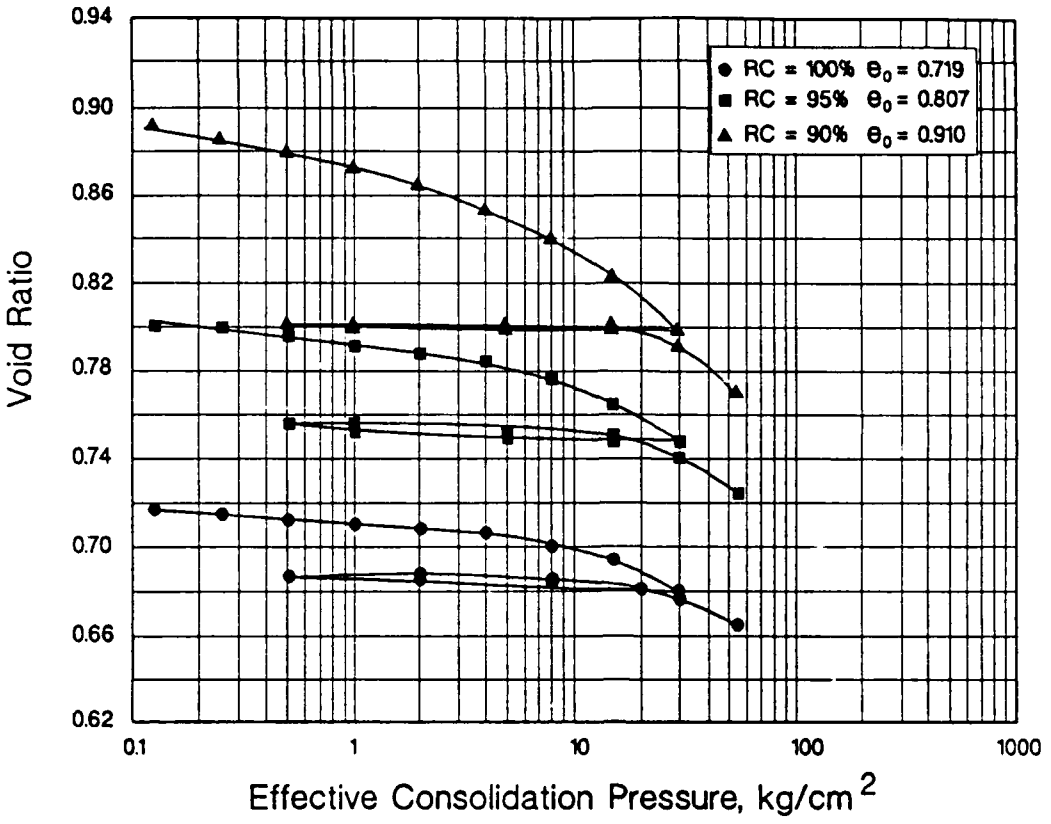


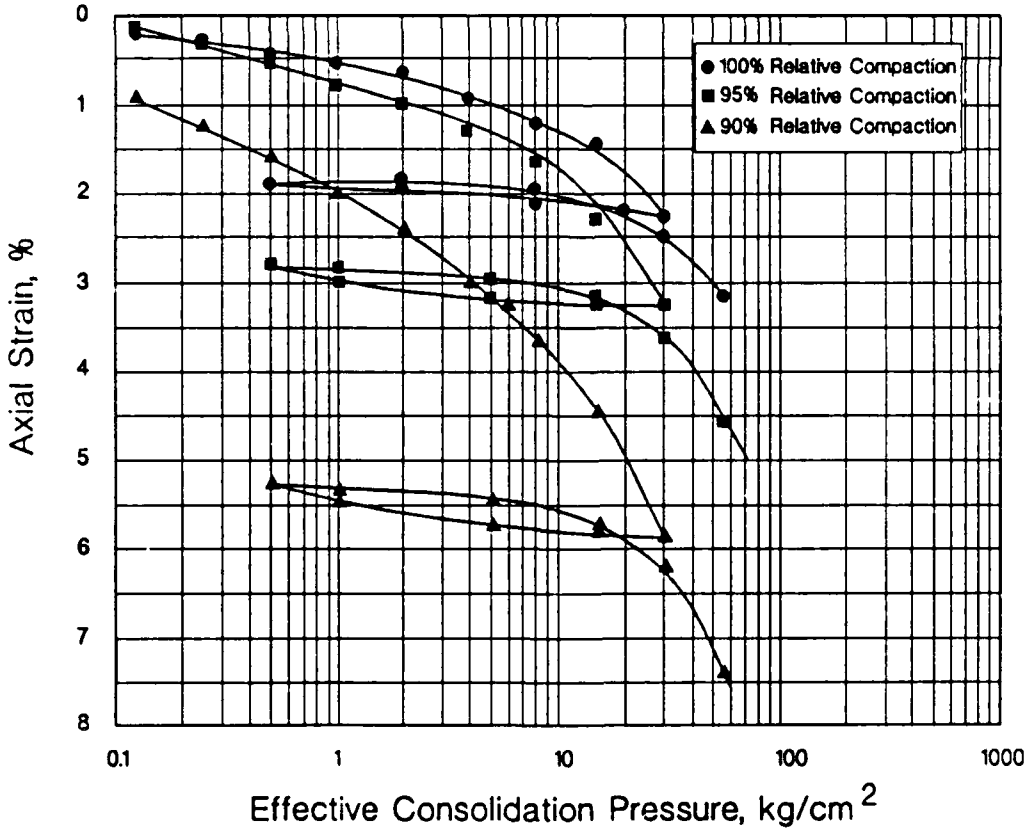


Figure 13. Oedometer Test Results for 0% Kaolinite-Silt Mixture

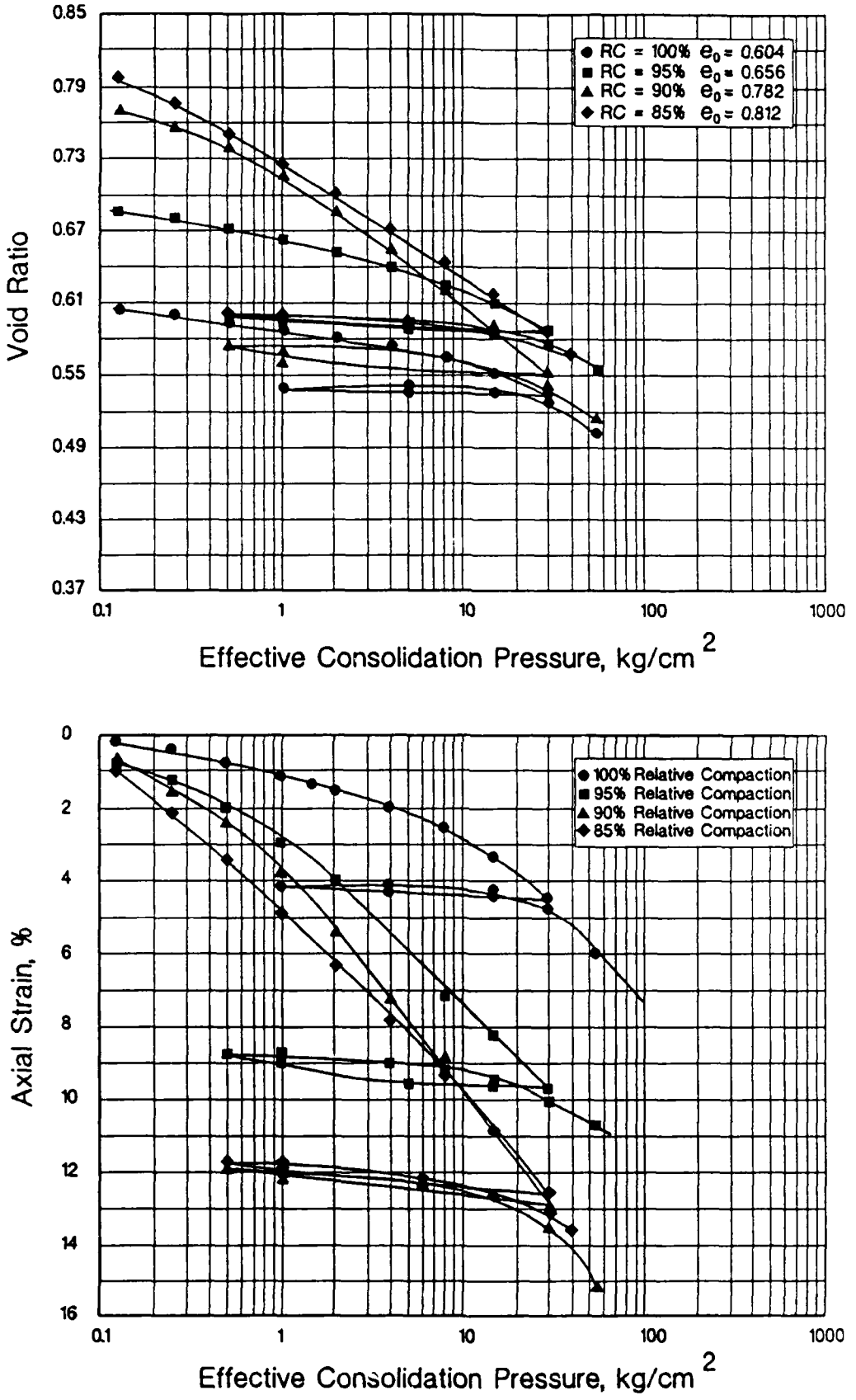


Figure 14. Oedometer Test Results for 10% Kaolinite-Silt Mixture

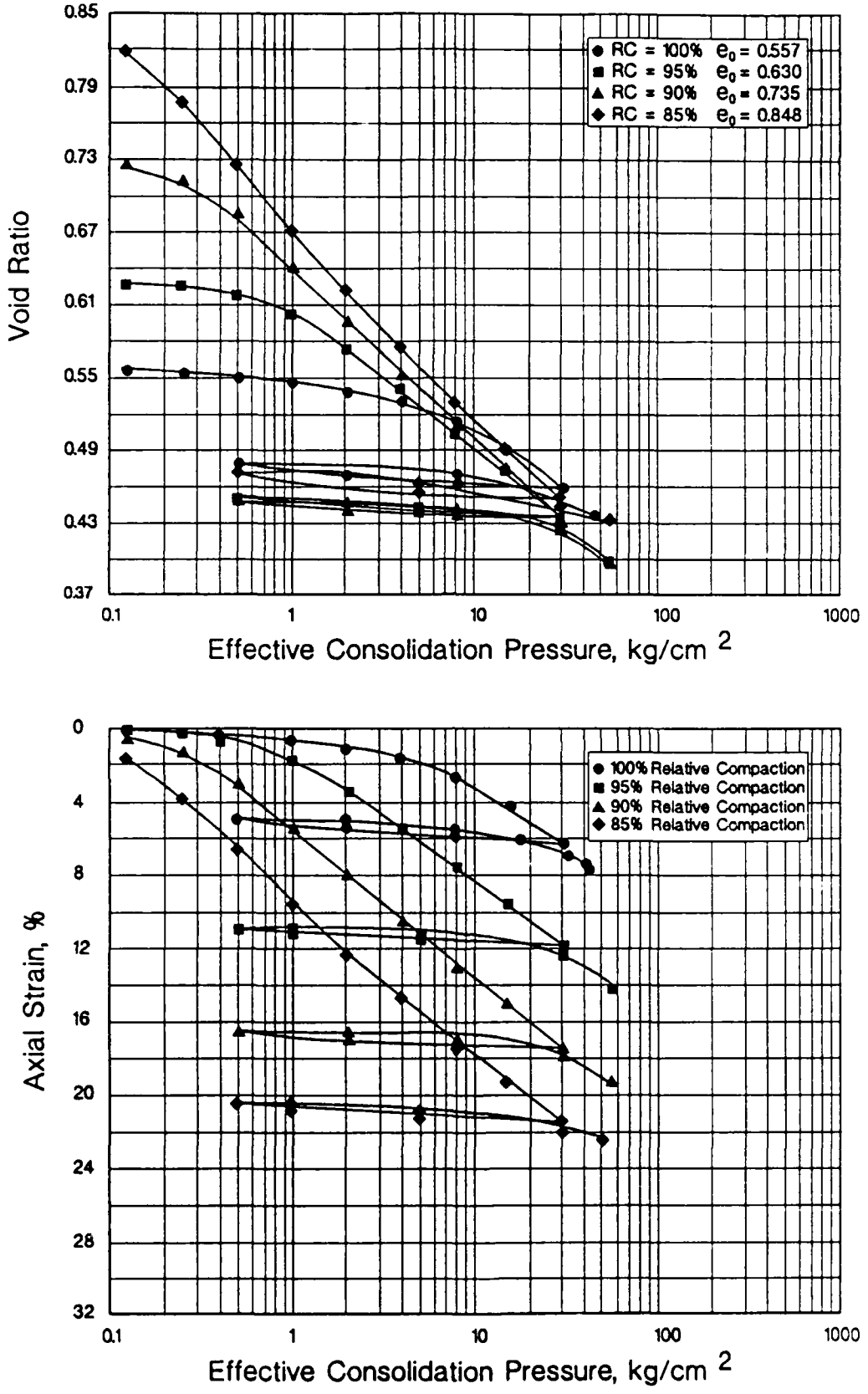


Figure 15. Oedometer Test Results for 30% Kaolinite-Silt Mixture

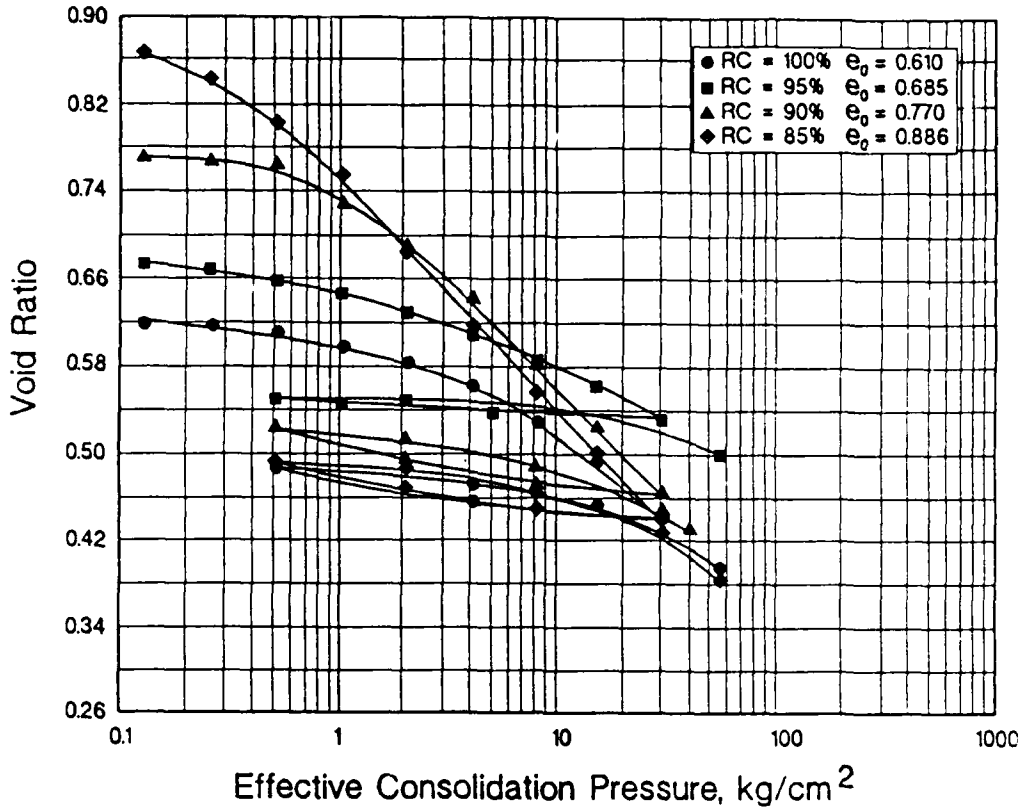


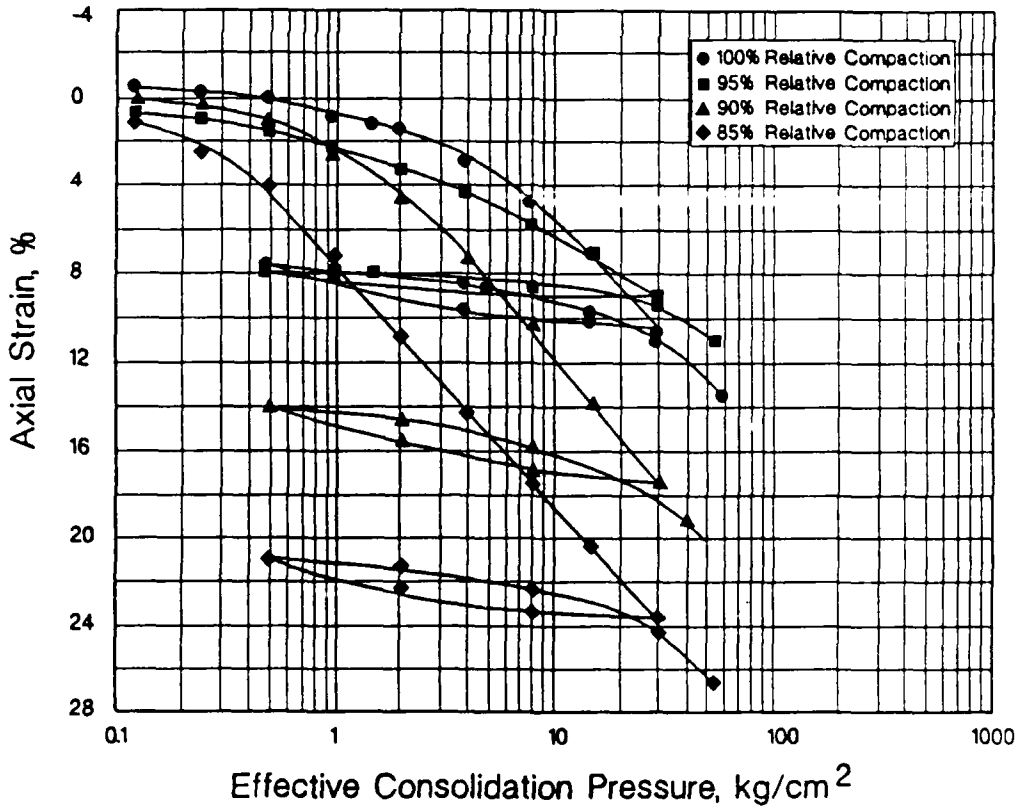


Figure 16. Oedometer Test Results for 50% Kaolinite-Silt Mixture

increased and the maximum preconsolidation pressure decreased. The maximum preconsolidation pressure also decreased as the relative compaction decreased from 100 to 85% of the Standard Proctor maximum. It can be seen from Table 5 that the 50% kaolinite mixture had a preconsolidation pressure of only 1.4 to 2.0 tsf. Therefore, the effective confining pressure for this mixture ranged from 3 to 9 tsf and the Plexiglass containers could be used.

38. Figure 17 shows the effective stress relationships from the oedometer tests on the 10, 30 and 50% montmorillonite-silt mixtures. It can be seen that the maximum preconsolidation pressure decreased as the amount of montmorillonite increased. The range of effective confining pressures used for the montmorillonite-silt mixtures ranged from 3 to 20 tsf as shown in Table 5.

Table 5. Compressibility Parameters of the Silt-Clay Mixtures

| % Clay | Standard Proctor Relative Compaction | Maximum Preconsolidation Pressure (tsf) | $C_c$ | $C_r$ | $C_{\varepsilon c}$ | $C_{\varepsilon r}$ | Effective Triaxial Confining Pressures (tsf) |
|---|---|---|---|---|---|---|---|
| 0% Kao | 100 | 18 | 0.061 | 0.0041 | 0.0355 | 0.0024 | 2.1-17.1 |
| 0% Kao | 95 | 13 | 0.081 | 0.0045 | 0.0410 | 0.0025 | 7.9-16.4 |
| 0% Kao | 90 | 11 | 0.1051 | 0.0067 | 0.0550 | 0.0035 | 8.0-12.9 |
| 0% Kao | 85 | N/A | N/A | N/A | N/A | N/A | N/A |
| 10% Kao | 100 | 14.7 | 0.0702 | 0.0069 | 0.0430 | 0.0043 | 9.8-17.0 |
| 10% Kao | 95 | 1.6 | 0.0813 | 0.0093 | 0.0480 | 0.0055 | 11.7-17.4 |
| 10% Kao | 90 | 1 | 0.1139 | 0.0099 | 0.0639 | 0.0056 | 3.0-15.4 |
| 10% Kao | 85 | 0.5 | 0.1202 | 0.0101 | 0.0670 | 0.0056 | 3.1-14.5 |
| 30% Kao | 100 | 9.6 | 0.1220 | 0.0117 | 0.0782 | 0.0075 | 10.2-17.6 |
| 30% Kao | 95 | 1 | 0.1236 | 0.0118 | 0.0790 | 0.0078 | 8.3-15.5 |
| 30% Kao | 90 | 0.35 | 0.1388 | 0.0120 | 0.0812 | 0.0080 | 4.1-15.5 |
| 30% Kao | 85 | 0.25 | 0.1483 | 0.0131 | 0.0813 | 0.0081 | 3.1-17.3 |
| 50% Kao | 100 | 6 | 0.1674 | 0.0154 | 0.1040 | 0.0096 | 9.2-17.4 |
| 50% Kao | 95 | 2.0 | 0.1297 | 0.0114 | 0.0770 | 0.0067 | 8.2-15.4 |
| 50% Kao | 90 | 1.4 | 0.2071 | 0.0174 | 0.1170 | 0.0098 | 4.0-10.0 |
| 50% Kao | 85 | 0.5 | 0.2137 | 0.0196 | 0.1220 | 0.0112 | 3.5-9.3 |
| 10% Mont | 100 | 16 | 0.0793 | 0.0082 | 0.047 | 0.0055 | 11.3-16.9 |
| 30% Mont | 100 | 6.5 | 0.2032 | 0.0206 | 0.116 | 0.0118 | 10.3-16.9 |
| 50% Mont | 100 | 6.4 | 0.322 | 0.143 | 0.178 | 0.0720 | 8.7-15.5 |

Notes:
1.) Kao = Kaolinite
2.) Mont = Montmorillonite
3.) N/A = Not Available
4.) $C_c$ and $C_r$ obtained from void ratio-effective stress curves
5.) $C_{\varepsilon c}$ and $C_{\varepsilon r}$ obtained from axial strain-effective stress curves

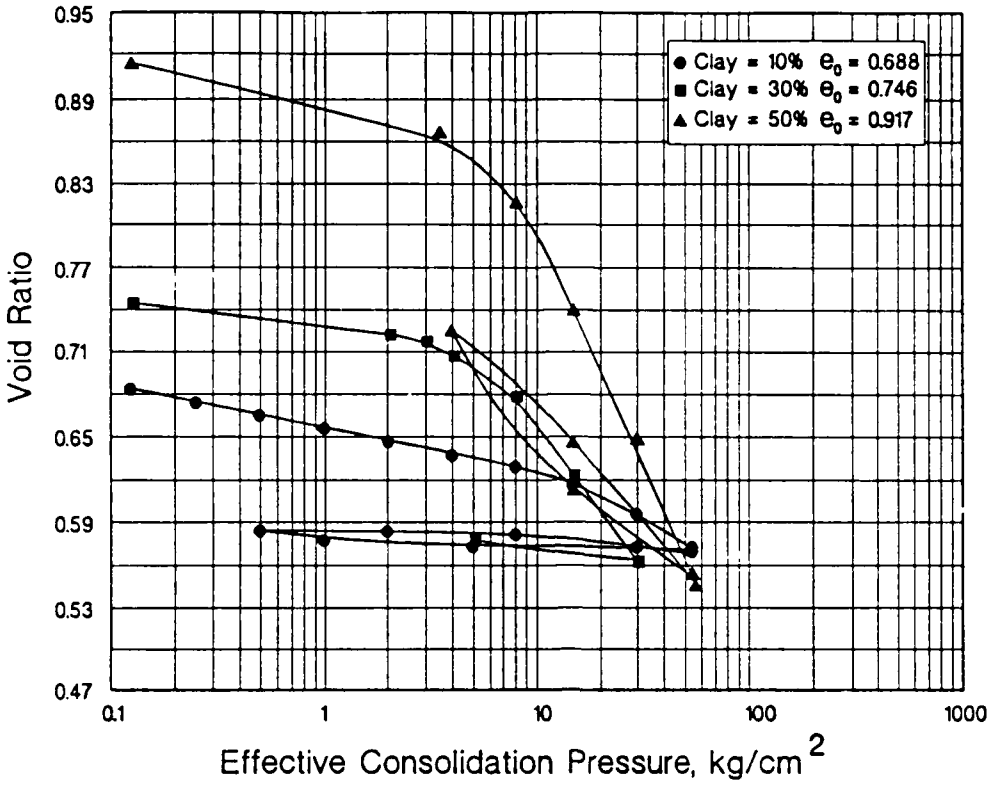


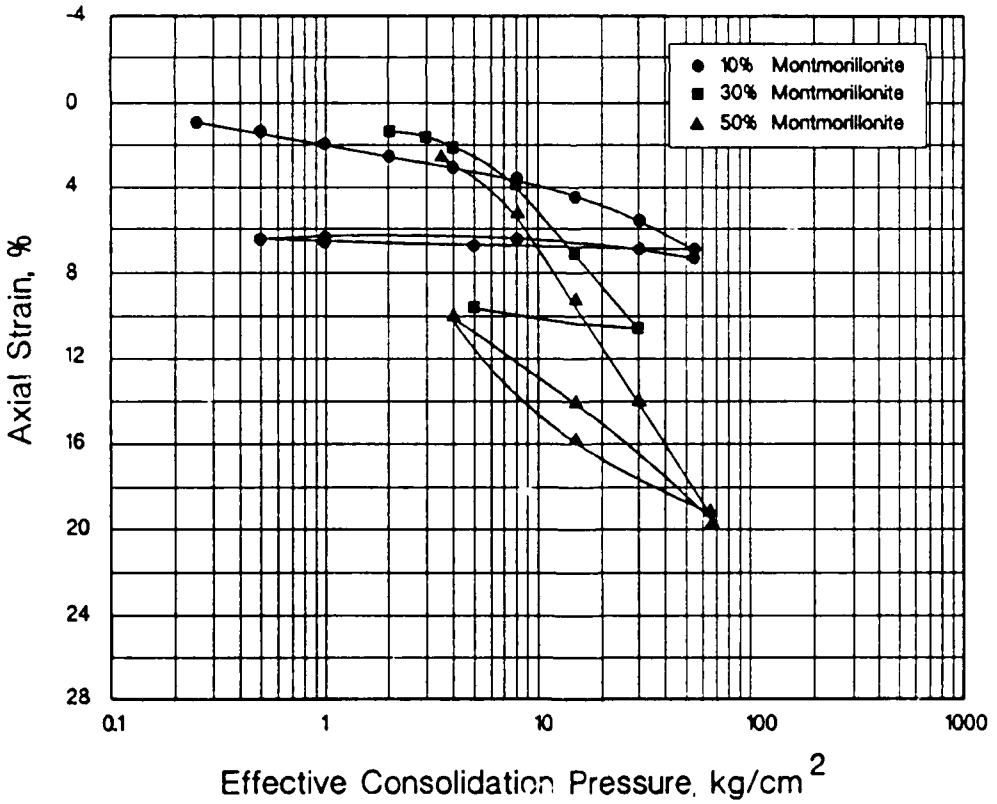


Figure 17. Oedometer Test Results for 10, 30, and 50% Montmorillonite-Silt Mixtures

# PART V: TRIAXIAL TEST PROCEDURES

## Preparation of Triaxial Test Specimens

39. The bulk samples of each kaolinite and montmorillonite-silt mixture were obtained using the dry mixing process described in paragraphs 25 and 26. The triaxial test specimens were trimmed from the compacted samples of the various silt mixtures. Each mixture was compacted into a six inch diameter Proctor compaction mold. To obtain the dry density corresponding to Standard Proctor relative compactions of 85, 90, 95 and 100%, the silt mixtures were compacted in five one-inch lifts. A special compaction apparatus, described by Houston and Chan (1983), was used to compact the appropriate weight of soil into each lift. The height of each lift was fixed by adjusting the depth to which the tamper could penetrate. The depth was set using a series of one-inch spacer blocks. Each lift was then tamped approximately 50 times or until all the soil was compacted into the predetermined lift height. The hand-held tamper was moved around the compaction mold until all the soil was compacted into the one-inch lift. The diameter of the tamper is approximately 1.4 inches. The amount of soil compacted in each lift was calculated based on the desired relative compaction and water content.

40. To facilitate the saturation of the test specimens, carbon dioxide gas was injected into the compaction mold as the soil was being rained in. The carbon dioxide, which is heavier than air, displaced the air trapped in the soil during the raining process. Carbon dioxide dissolves during the back pressure saturation process which greatly reduces the time required to obtain full saturation, Chan (1990).

41. The top of each lift was scarified before the next lift was placed to insure an adequate bond between lifts. Five one-inch lifts were compacted in the six-inch diameter mold to create a compacted silt plug with a volume of a 0.082 cu ft. Each plug was carefully extruded from the mold using a hydraulic jack. The plug was then cut into four sections using a seven-inch long surgical razor blade or a fine wire saw. A triaxial test specimen was trimmed from each section so that four test specimens were obtained from each plug. This resulted in four triaxial test specimens which had a similar compaction history and thus comparable shear strength and stress-strain characteristics.

42. The 1.4 inch diameter and 3.5 inch long triaxial test specimens were trimmed

using a GEONOR trimming lathe. A very fine wire saw was used to trim the 0 and 10% kaolinite mixtures and a surgical razor blade was used for the 30 and 50% kaolinite mixtures. A 3.5 inch long miter box was used to obtain the final triaxial test specimen after the trimming was completed. The water content and dry density of each test specimen was determined before inserting the specimen into the triaxial apparatus.

43. A set of five GEONOR triaxial cells with Plexiglass and stainless steel containers were used for the testing. The cells were connected to volume change/pore pressure measurements devices which could be read electronically. The porous stones at the top and bottom of the test specimens were either cleaned in a sonic cleaner or boiled for ten minutes before each test. Two membranes, i.e. prophylactics, were carefully rolled over each test specimen. To reduce the amount of air trapped in the system, the membranes were carefully rolled over the test specimen and any wrinkles in either membrane were removed. Each membrane was secured with two O-rings at the top and bottom of the specimen. If the effective confining pressure was to exceed 10 tsf, a heavier membrane was used as the second membrane and installed using a membrane expander. The heavier membrane is approximately 0.007 inches thick and reduced the potential for puncture at these high pressures. In both cases a thin coating of silicone lubricant was applied to the first membrane to reduce any friction which might develop between the membranes.

44. To promote drainage in the consolidated-drained (S) triaxial tests, the specimens were wrapped in filter paper. Portions of the filter paper were cut out to reduce the strength of the filter paper as described by Bishop and Henkel (1962). These slotted pieces of filter paper are sometimes referred to as Bishop's pajamas. The appropriate strain rate for the consolidated-drained (S) and undrained (R) triaxial tests was determined using the procedure described by Gibson and Henkel (1954) and the coefficient of consolidation measured during consolidation of each test specimen. The values of coefficient of consolidation were verified using the oedometer test results described in paragraphs 33 through 38. The axial strain rate used for the consolidated-drained (S) tests was a function of the clay content and clay mineral. The triaxial tests on the 0 and 10% kaolinite-silt mixtures were performed using a strain rate of 0.05% (0.0018 in/min). Strain rates of 0.013% (0.00048 in/min) and 0.01% (0.00036 in/min) were used for the 30 and 50% kaolinite-silt mixtures, respectively. The drained triaxial tests on the montmorillonite-silt mixtures were performed using a strain rate of 0.002% (0.000072 in/min). The

consolidated-undrained (R) tests on the kaolinite-silt mixtures were conducted at a strain rate of 0.086% (0.003 in/min).

Specimen Saturation

45. After the entire triaxial cell was assembled and a small cell pressure was applied to the test specimen, a vacuum of less than 1 tsf was then applied to the specimen. The vacuum was applied through an air/water interface and removed most of the air and carbon dioxide from the specimen. The vacuum was usually maintained for approximately 20 minutes. After 20 minutes, the vacuum pump was turned off and deionized water was allowed to slowly percolate into the specimen for 10 to 15 minutes. In most of the tests, this resulted in the solution of most, if not all, of the carbon dioxide and a nearly saturated test specimen. The triaxial cell was then connected to the volume change/pore pressure measuring device and a small back pressure was applied. The back pressure and cell pressure were then incrementally raised until the back pressure reached approximately 1 tsf. The test specimen was allowed to stabilize overnight under this pressure condition. In all of the tests, the cell pressure and back pressure were applied using a GEONOR constant pressure system which utilized dead weights to generate pressure. This prevented any significant variations in the cell and back pressures due to variations in the compressor or air pressure system.

46. Saturation of the test specimen was confirmed using Skempton's (1954) pore pressure coefficient 'B'. The B-value, the change in pore pressure divided by the change in cell pressure, was measured after the specimen came into equilibrium under a back pressure of approximately 1 tsf. In accordance with Black and Lee (1973) and Bishop and Henkel (1962), the desired B-value for the consolidated-drained (S) tests was 95% or greater and 99.7% or greater for the consolidated-undrained (R) tests. If the B-value did not meet these criterion, the cell and back pressure were incrementally increased, using the technique described by Houston and Chan (1983), until they were achieved. The rate and size of the increment were carefully controlled to insure that no part of the specimen was overconsolidated.

47. It was found that the 0 and 10% kaolinite test specimens required a back pressure of only 1 tsf and approximately one day of back pressure to achieve the saturation criteria. The 30 and 50% kaolinite specimens required back pressures as high as 5 to 6 tsf and durations of up to seven days to achieve the saturation criteria. After saturation was

obtained, the consolidated-drained (S) and consolidated-undrained (R) triaxial tests were performed in accordance with the Corps of Engineers Laboratory Soils Testing Manual (Office 1970).

# PART VI: KAOLINITE-SILT TRIAXIAL TEST RESULTS

## Isotropically Consolidated-Drained Triaxial Tests

48. It can be seen from Table 2 that 56 isotropically consolidated-drained (S) triaxial tests were performed on the kaolinite-silt mixtures. The following paragraphs will describe the effect of 1.) dry density or relative compaction, 2.) kaolinite content, and 3.) effective confining pressure on the drained stress-strain behavior of normally consolidated silts and clayey-silts. Figure 18 provides a comparison of the stress-strain curves for Standard Proctor relative compactions of 90 and 100% and a kaolinite content of 0%. It can be seen that the magnitude of relative compaction has a large effect on the measured stiffness and the maximum deviator stress. The relative compaction of 100% results in a maximum deviator stress that is 10 to 12 tsf higher and an initial tangent modulus that is approximately 10 to 20% larger than the 90% relative compaction specimen at the same effective confining pressure. In addition, the shear behavior of the two specimens is noticeably different. The low (0 and 10%) kaolinite mixtures usually exhibited a small amount of strain softening and a large degree of dilation. The high (30 and 50%) kaolinite mixtures usually exhibited a ductile deviator stress curve and a contractive behavior. The maximum deviator stress, i.e. failure, usually occurred at 8 to 10% axial strain in the low kaolinite mixtures while an axial strain of 17 to 20% was required to reach failure in the high kaolinite mixtures.

49. Figure 19 provides a comparison of the stress-strain curves for Standard Proctor relative compactions of 85 and 100% at a kaolinite content of 50%. It can be seen that there is only a small effect of relative compaction on the measured stiffness and maximum deviator stress with a kaolinite content of 50% The maximum deviator stresses differ by less than 1 tsf and the initial tangent moduli are approximately equal. Therefore, it was concluded that the effect of relative compaction on the maximum deviator stress and stiffness is very small when the kaolinite or clay content is greater than 30%. However, it can be seen that relative compaction has a large influence on the volumetric strain at axial strains greater than 6%. In contrast, relative compaction had a large affect on both the maximum deviator stress and the volumetric strain at kaolinite or clay contents less than 10%.

50. This result could have a large impact on the field compaction of silts and clayey-silts. If the clay content is greater than 30% there appears to be little increase (approximately 1 tsf) in the maximum deviator stress from specifying a field relative

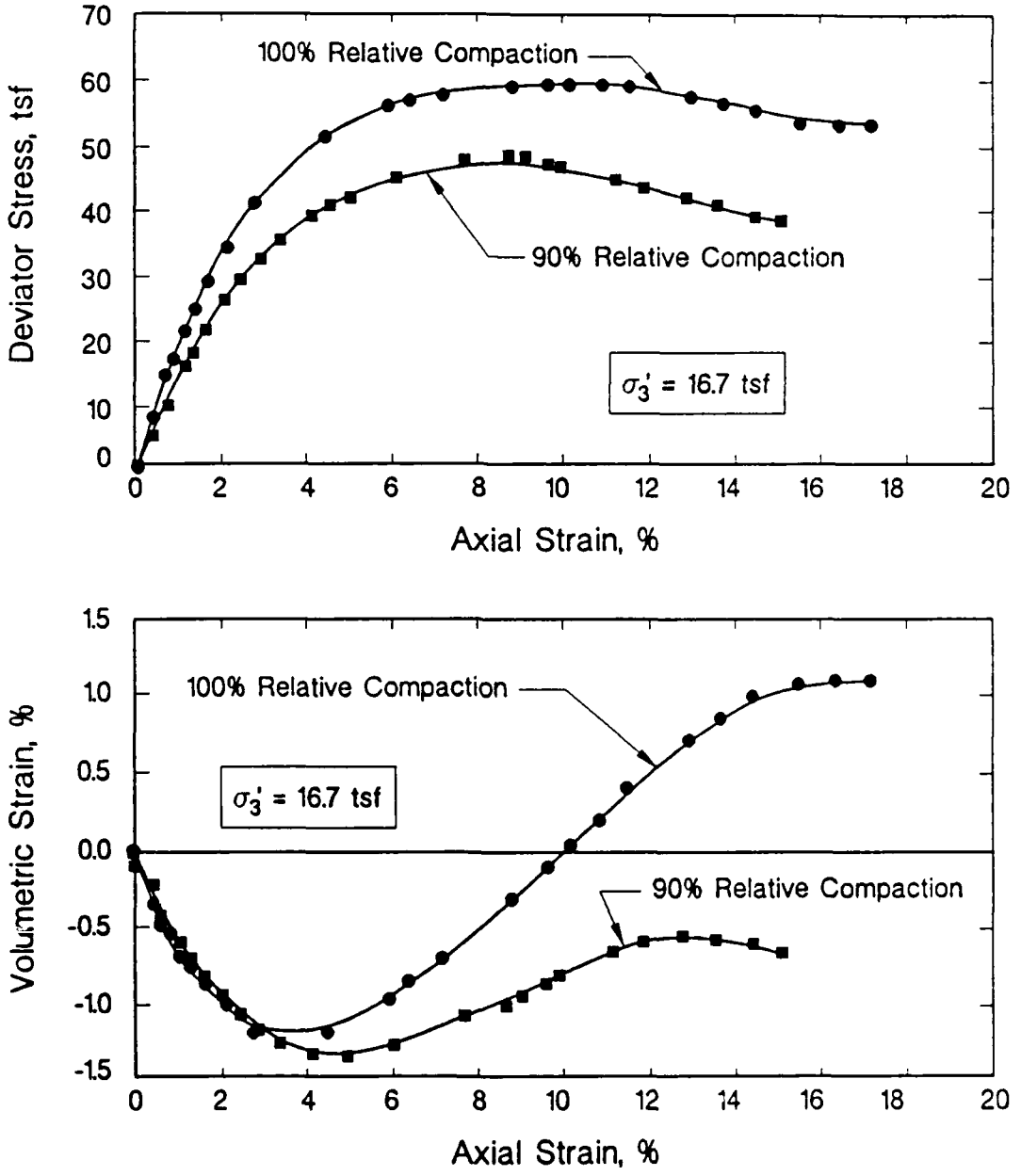


Figure 18. Effect of Relative Compaction on Stress-Strain Behavior in Consolidated-Drained (S) Triaxial Tests on 0% Kaolinite Mixtures

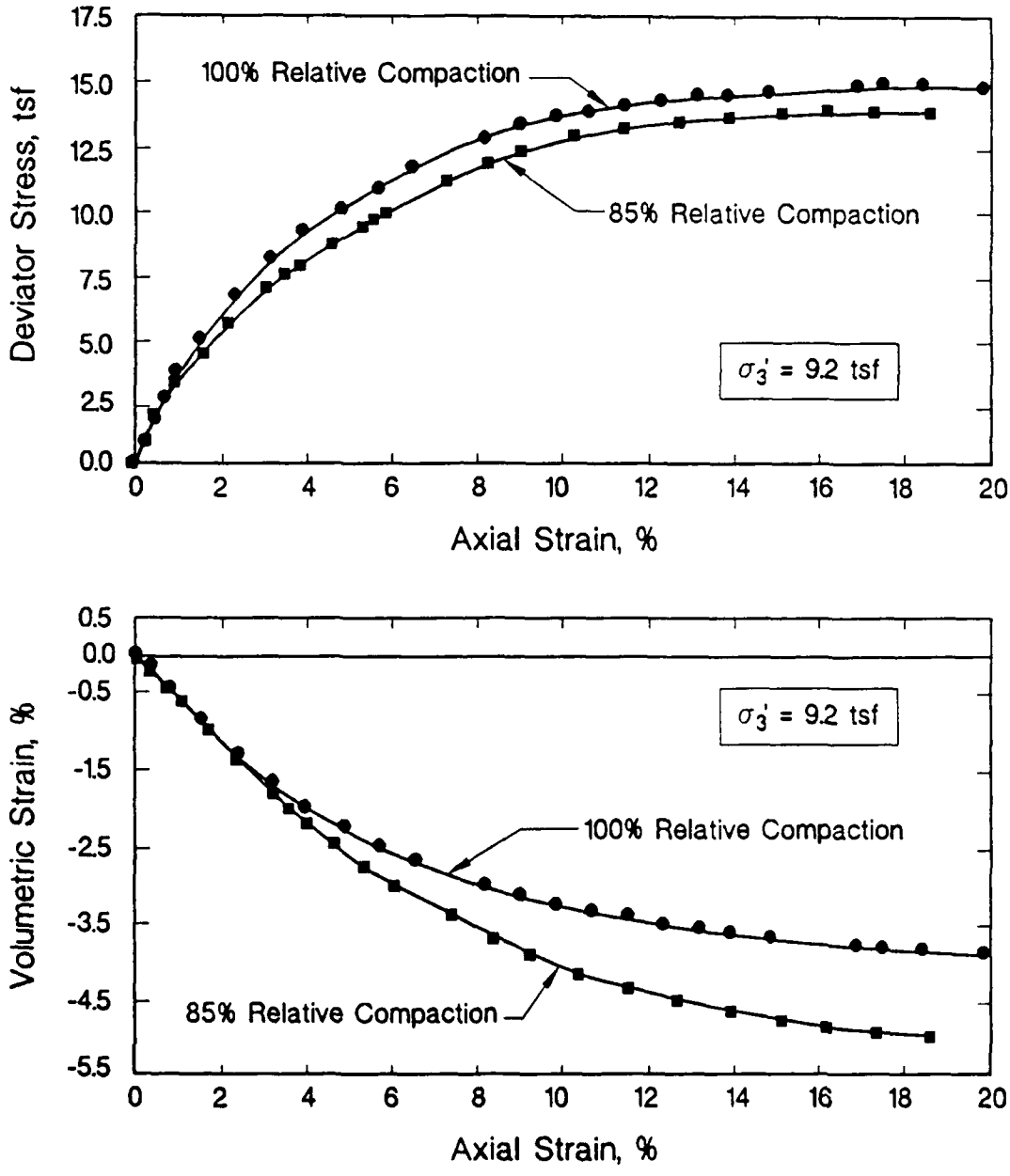


Figure 19. Effect of Relative Compaction on Stress-Strain Behavior in Consolidated-Drained (S) Triaxial Tests on 50% Kaolinite Mixtures

relative compaction greater than 90%. This increase in strength and stiffness due to the increased relative compaction is probably minimal compared to the cost of obtaining a relative compaction greater than 90%. However, increasing the relative compaction may result in a substantial decrease in the volumetric strain or field displacement. On the other hand, if the clay content is less than 10% there appears to be a substantial increase in strength and stiffness as the relative compaction increases from 90 to 100%.

51. Figure 20 provides a comparison of the stress-strain curves for kaolinite contents of 0 and 30%. The 0% curves are typical of the behavior at low (0 and 10%) kaolinite mixtures while the 30% curves are representative of the high (30 and 50%) mixtures. It can be seen that the 0% kaolinite specimen typically exhibits a much larger initial tangent modulus and maximum deviator stress than the 30% kaolinite specimen. The initial tangent modulus for the 0 and 30% kaolinite specimens are $4.0 \times 10^6$ psf (190,000 kPa) and $1.7 \times 10^6$ psf (80,000 kPa), respectively. The effective stress friction angle for the 0 and 30% kaolinite specimens are 38.6 and 25.5, respectively.

52. In summary, the amount of clay or kaolinite controls the stress-strain and shear strength parameters of the specimen. If the clay content is less than 10%, the specimen appears to exhibit strength characteristics similar to a sand. Therefore, the silt controls the engineering properties of the test specimen when the clay content is less than 10%. If the kaolinite content is 30% or greater, the specimen exhibits strength characteristics similar to a clay. Based on these results, the transition point between sand and clay behavior appears to occur at a kaolinite content between 10 and 30%. Additional testing is needed to clarify the kaolinite content which precisely corresponds to the transition point.

53. Figures 21 and 22 illustrate the effect of effective confining pressure on the stress-strain behavior of 0 and 30% kaolinite, respectively. These curves are typical of the low and high kaolinite mixtures, respectively. It can be seen from Figure 21 that at very large effective confining pressures, e.g. 15.6 to 20 tsf, the 0% kaolinite mixture still exhibited dilation. As expected, the amount of dilation increases as the effective confining pressure decreased. Initially it was thought that the test specimens were exhibiting overconsolidated behavior and thus the effective confining pressures were not high enough to create a normally consolidated condition. Since special provisions had already been made to obtain a confining pressure of 20 tsf, an extensive literature search was conducted to determine if this was overconsolidated or normally consolidated behavior.

54. Fleming and Duncan (1990) presented triaxial test results on a low plasticity silt,

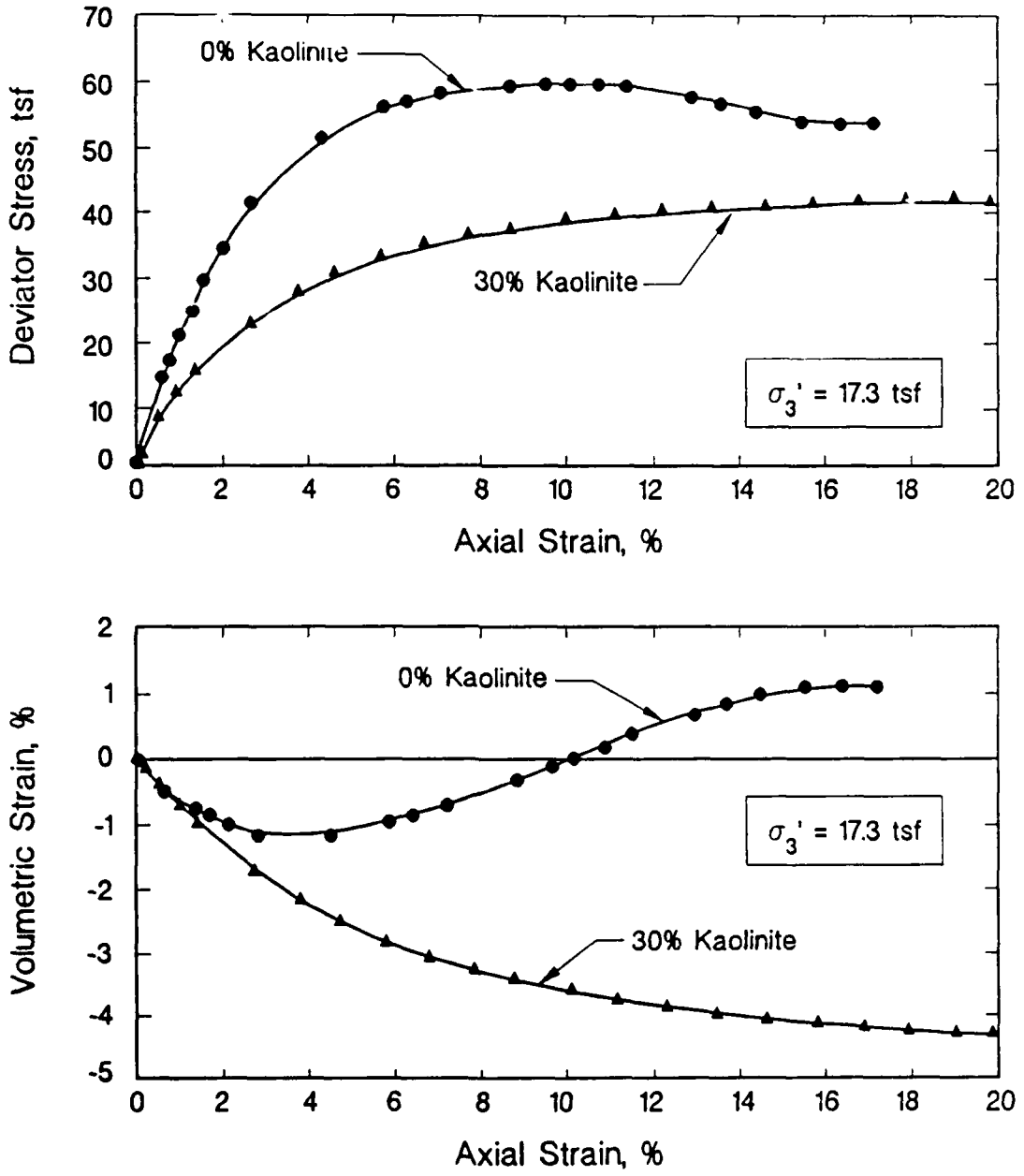


Figure 20. Effect of Kaolinite Content on Stress-Strain Behavior in Consolidated-Drained (S) Triaxial Tests

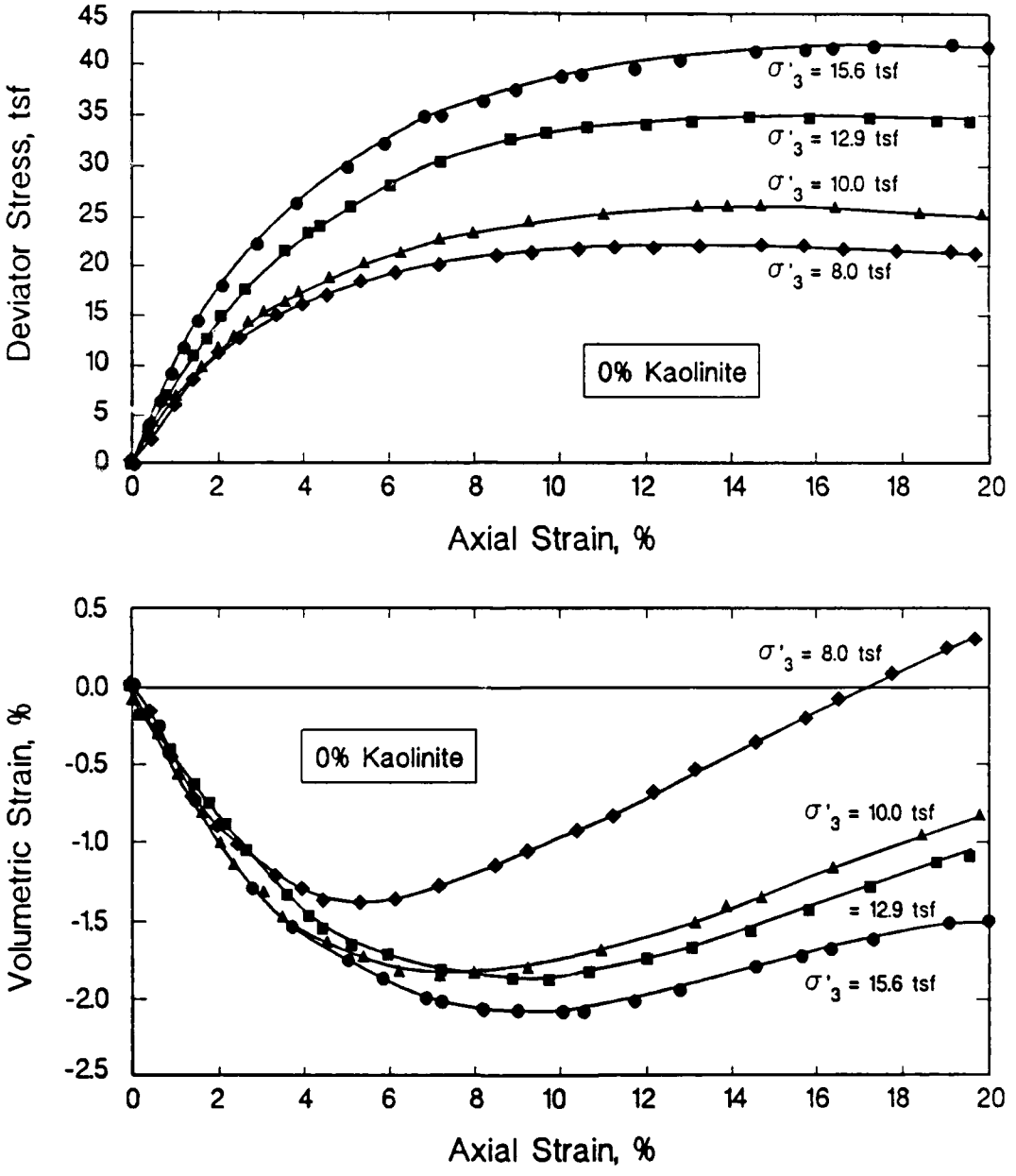


Figure 21. Effect of Effective Confining Pressure on the Drained Stress-Strain Behavior of 0% Kaolinite Mixtures

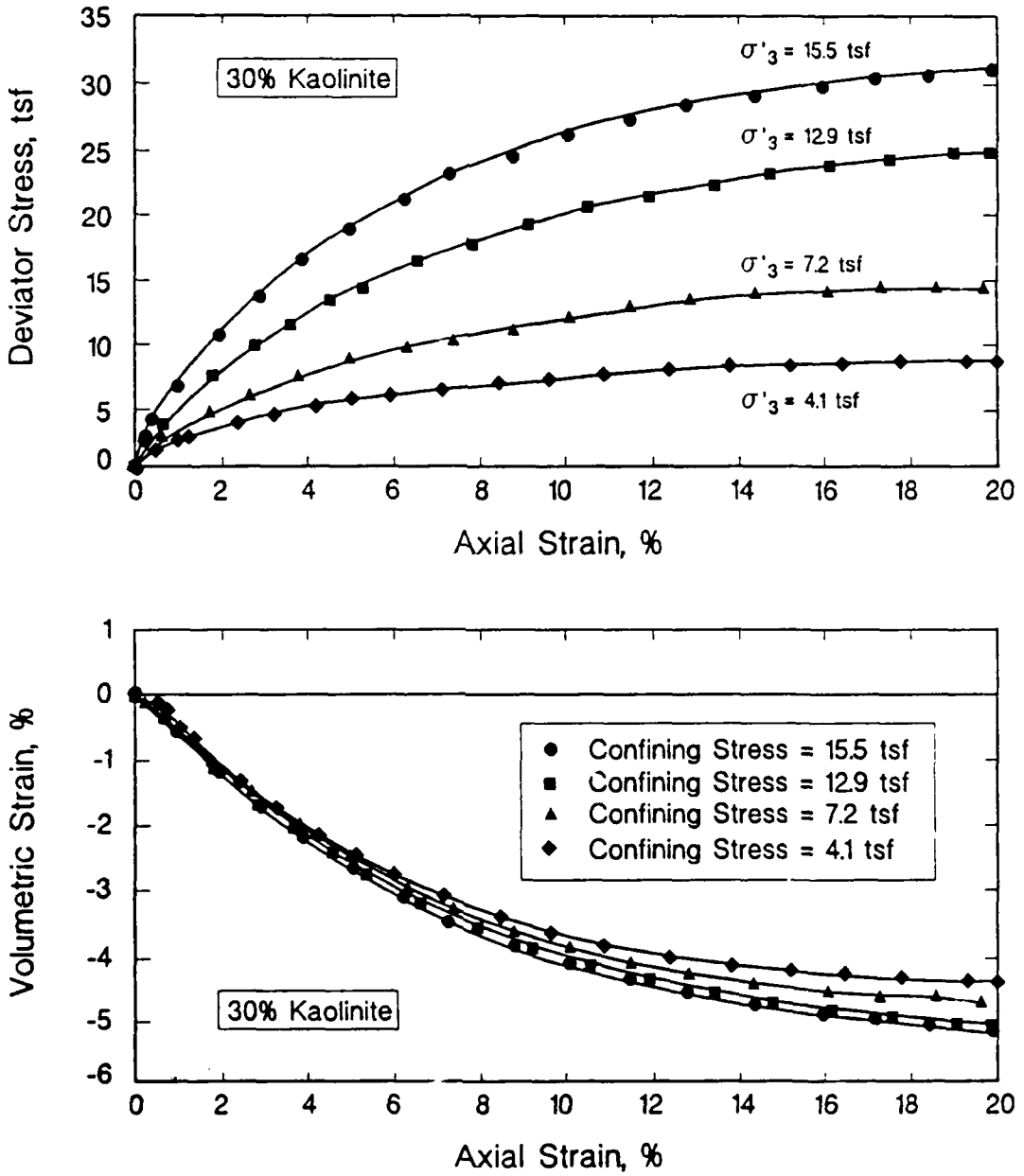


Figure 22. Effect of Effective Confining Pressure on the Drained Stress-Strain Behavior of 30% Kaolinite Mixtures

with a clay fraction of 20 to 22%, from the Beaufort Sea in Alaska. The triaxial test specimens were obtained by consolidating a slurry of the silt in a one-dimensional consolidometer. The triaxial test specimens were then trimmed from the consolidated slurry. Therefore, the Alaskan silt was truly is a normally consolidated condition. Even though the test specimens were normally consolidated, the stress-strain curves from isotropically consolidated-drained and undrained triaxial tests still exhibited dilation. Based on this data it was determined that the dilation exhibited in the 0% kaolinite mixtures was representative of normally consolidated behavior and the effective confining pressures were adequate. It should be noted that the triaxial test specimens consolidated to confining pressures less than 8 tsf exhibited a sharp increase in the initial tangent modulus and effective stress friction angle. Therefore, it was anticipated that a confining pressure of 8 to 10 tsf was the transition point between overconsolidated and normally consolidated behavior. It may thus be concluded that normally consolidated silts dilate and the amount of dilation is a function of the effective confining pressure.

55. Figure 22 illustrates the effect of effective confining pressure on the stress-strain behavior of silt with a 30% kaolinite content. It can be seen that effective confining pressures ranging from 4.1 to 15.5 tsf resulted in a contractive behavior. It can also be seen that there is a larger effect of confining pressure on the deviator stress than the volumetric strain. Therefore, the transition point from sand to clay behavior again appears to occur between a kaolinite content of 10 and 30%.

56. Table 6 presents the effective stress Mohr-Coulomb strength parameters obtained from the isotropically consolidated-drained (S) triaxial tests. The failure criteria used to obtain these parameters is the maximum deviator stress or an axial strain of 20%. It should be noted that a specimen at 0% kaolinite and a relative compaction of 85% could not be obtained because the sample liquefied during compaction due to the high water content. It can be seen that all of the kaolinite-silt mixtures exhibited an effective stress cohesion of zero. This also indicates that the test specimens were in a normally consolidated condition at the time of shearing. At a relative compaction of 100%, the effective stress friction angle ranged from 38.6 degrees for the 0% kaolinite mixture to 26.7 degrees for the 50% kaolinite mixture. Therefore, an increase in kaolinite content from 0 to 50% results in a 12 degree decrease in the effective stress friction angle.

57. It can also be seen from Table 6 that the effect of relative compaction on the effective stress friction angle decreases significantly as the clay content approaches 50%.

Table 6 - Effective Stress Mohr-Coulomb Strength Parameters for Kaolinite-Silt Mixtures from Consolidated-Drained Triaxial Tests

| % Clay | Standard Proctor Relative Compaction | Average and (Range) of Initial Dry Density (pcf) | Average and (Range) of Initial Water Content (%) | Range of Effective Confining Pressure (tsf) | Effective Stress Cohesion (psf) | Effective Stress Friction Angle (degrees) |
|---|---|---|---|---|---|---|
| 0% Kao | 100 | 98 (94.7-98.8) | 27 (26.1-28.9) | 2.1-17.1 | 0 | 38.6 |
| 0% Kao | 95 | 97 (96.9-97.9) | 27 (26.7-27.4) | 7.9-16.4 | 0 | 34.8 |
| 0% Kao | 90 | 96 (95.5-97.6) | 28 (26.9-28.6) | 8.0-12.9 | 0 | 29.5 |
| 0% Kao | 85 | NA | NA | NA | NA | NA |
| 10% Kao | 100 | 104 (102.8-105.2) | 23 (22.3-23.5) | 9.8-17.0 | 0 | 36.5 |
| 10% Kao | 95 | 101 (99.9-102.4) | 25 (23.9-25.2) | 11.7-17.4 | 0 | 34.6 |
| 10% Kao | 90 | 101 (100.5-101.1) | 25 (24.5-24.9) | 3.0-15.4 | 0 | 33.7 |
| 10% Kao | 85 | 101 (99.5-101.3) | 25 (24.4-25.5) | 3.1-14.5 | 0 | 33 |
| 30% Kao | 100 | 110 (108.3-111.7) | 19 (18.3-20.2) | 10.2-17.6 | 0 | 32.5 |
| 30% Kao | 95 | 109 (107.0-110.2) | 20 (19.2-20.8) | 8.3-15.5 | 0 | 31.5 |
| 30% Kao | 90 | 108 (105.3-110.2) | 20 (19.2-21.8) | 4.1-15.5 | 0 | 30 |
| 30% Kao | 85 | 109 (105.5-111.0) | 20 (18.8-21.7) | 3.1-17.3 | 0 | 29.9 |
| 50% Kao | 100 | 106 (104.4-107.9) | 21 (19.7-21.6) | 9.2-17.4 | 0 | 26.7 |
| 50% Kao | 95 | 102 (99.2-103.4) | 23 (22.2-24.7) | 8.2-15.4 | 0 | 26.1 |
| 50% Kao | 90 | 104 (101.7-105.6) | 22 (20.9-23.2) | 4.0-10.0 | 0 | 25.9 |
| 50% Kao | 85 | 104 (102.5-105.5) | 21 (20.2-22.7) | 3.5-9.3 | 0 | 25.5 |

NOTES:
1.) Kao = Kaolinite
2.) NA = Not Available

For example, at 0% kaolinite the friction ranged from 29.5 to 38.6 degrees. Therefore, the friction angle increased approximately 7.1 degrees when the relative compaction increased from 90 to 100%. The range of friction angle for the 50% kaolinite mixture was approximately 1 degree, 25.5 to 26.7, for relative compactions of 85 to 100%, respectively. This result could also have a large impact on the field compaction of silts and clayey-silts.

58. Mitchell (1976) reported that the peak effective stress friction angle of pure kaolinite ranges from 26 to 30 degrees. Therefore, from Table 6 it may be concluded that the kaolinite controls the shear strength of the 30 and 50% kaolinite-silt mixtures. The friction angle for the 10% kaolinite is 33 to 36.5 degrees and appears to be controlled by the strength of the silt instead of the kaolinite. This also implies that the transition point between sand and clay behavior in drained conditions occurs at a kaolinite content between 10 and 30%.

59. Table 7 presents the hyperbolic stress-strain parameters obtained from the isotropically consolidated-drained (S) triaxial tests. These parameters were obtained using the procedure recommended by Duncan et al. (1980) in which the deviator stresses at 70 and 95% of the maximum deviator stress are used to estimate the initial tangent modulus. Figure 23 presents a typical comparison of the actual and hyperbolic stress-strain curves for the 30 and 50% kaolinite-silt mixtures. It can be seen that the hyperbolic model provides an excellent representation of the deviator stress and volumetric strain curves. This is mainly due to these kaolinite-silt mixtures exhibiting a contractive shear behavior.

60. Figure 24 presents a typical comparison of the actual and hyperbolic stress-strain curves for the 0 and 10% kaolinite silt mixtures. It can be seen that the hyperbolic parameters provide an excellent representation of the deviator stress curve for axial strains less than 12%. However, at axial strains greater than approximately 6%, the volumetric strain curve exhibits a dilative behavior. Since the hyperbolic stress-strain model does not account for dilation, the model provides a poor representation of the volumetric strain behavior. Therefore, the hyperbolic parameters presented in Table 7 will provide an accurate estimate of the volume change behavior at axial strains less than 6%. At axial strains greater than 6%, the reported hyperbolic parameters will over estimate the volumetric strain.

61. It can be seen from Table 7 that the influence of relative compaction on the modulus number increases as the kaolinite content decreases. The modulus number

Table 7 - Effective Stress Hyperbolic Stress-Strain Parameters for Kaolinite-Silt Mixtures from Consolidated-Drained Triaxial Tests

| % Clay | Standard Proctor Relative Compaction | Average and (Range) of Initial Dry Density (pcf) | Average and (Range) of Initial Water Content (%) | ange of Effective Confining Pressure (tsf) | Effective Stress Cohesion (psf) | Effective Stress Friction Angle (degrees) | Modulus Number K | Modulus Exponent n | Bulk Modulus Number Kb | Bulk Modulus Exponent m | Failure Ratio Rf |
|---|---|---|---|---|---|---|---|---|---|---|---|
| 0% Kao | 100 | 98 (94.7-98.8) | 27 (26.1-28.9) | 2.1-17.1 | 0 | 38.6 | 174 | 1.01 | 101 | 0.96 | 0.73 |
| 0% Kao | 95 | 97 (96.9-97.9) | 27 (26.7-27.4) | 7.9-16.4 | 0 | 34.8 | 118 | 1.06 | 63 | 0.97 | 0.76 |
| 0% Kao | 90 | 96 (95.5-97.6) | 28 (26.9-28.6) | 8.0-12.9 | 0 | 29.5 | 81 | 1.03 | 42 | 0.95 | 0.76 |
| 0% Kao | 85 | NA | NA | NA | NA | NA | NA | NA | NA | NA | NA |
| 10% Kao | 100 | 104 (102.8-105.2) | 23 (22.1-23.5) | 9.8-17.0 | 0 | 36.5 | 163 | 1.00 | 84 | 0.93 | 0.78 |
| 10% Kao | 95 | 103 (101.8-104.9) | 23 (23.2-23.7) | 11.7-17.4 | 0 | 34.6 | 101 | 1.00 | 54 | 0.93 | 0.76 |
| 10% Kao | 90 | 103 (101.8-104.9) | 23 (22.3-24.1) | 3.0-15.4 | 0 | 33.7 | 83 | 1.00 | 36 | 0.93 | 0.69 |
| 10% Kao | 85 | 102 (101.4-104.3) | 24 (22.7-24.4) | 3.1-14.5 | 0 | 33 | 68 | 1.00 | 29 | 0.93 | 0.7 |
| 30% Kao | 100 | 115 (113.4-116.3) | 17 (16.2-17.6) | 10.2-17.6 | 0 | 32.5 | 95 | 1.00 | 28 | 0.9 | 0.82 |
| 30% Kao | 95 | 115 (112.7-116.4) | 17 (16.2-17.9) | 8.3-15.5 | 0 | 31.5 | 50 | 1.00 | 20 | 0.9 | 0.76 |
| 30% Kao | 90 | 114 (110.2-116.7) | 18 (16.0-19.2) | 4.1-15.5 | 0 | 30 | 38 | 1.00 | 18 | 0.9 | 0.73 |
| 30% Kao | 85 | 114 (110.3-117.3) | 17 (15.8-19.2) | 3.1-17.3 | 0 | 29.9 | 27 | 1.00 | 16 | 0.9 | 0.65 |
| 50% Kao | 100 | 111 (108.5-113.4) | 18 (16.9-19.3) | 9.2-17.4 | 0 | 26.7 | 44 | 1.02 | 30 | 0.78 | 0.74 |
| 50% Kao | 95 | 107 (104.3-109.5) | 20 (18.8-21.7) | 8.2-15.4 | 0 | 26.1 | 34 | 1.02 | 25 | 0.78 | 0.72 |
| 50% Kao | 90 | 109 (106.4-111.1) | 19 (18.0-20.5) | 4.0-10.0 | 0 | 25.9 | 32 | 1.02 | 21 | 0.78 | 0.67 |
| 50% Kao | 85 | 108 (105.7-110.0) | 20 (18.6-20.9) | 3.5-9.3 | 0 | 25.5 | 28 | 1.02 | 19 | 0.78 | 0.61 |

NOTES:
1.) Kao = Kaolinite
2.) NA = Not Available

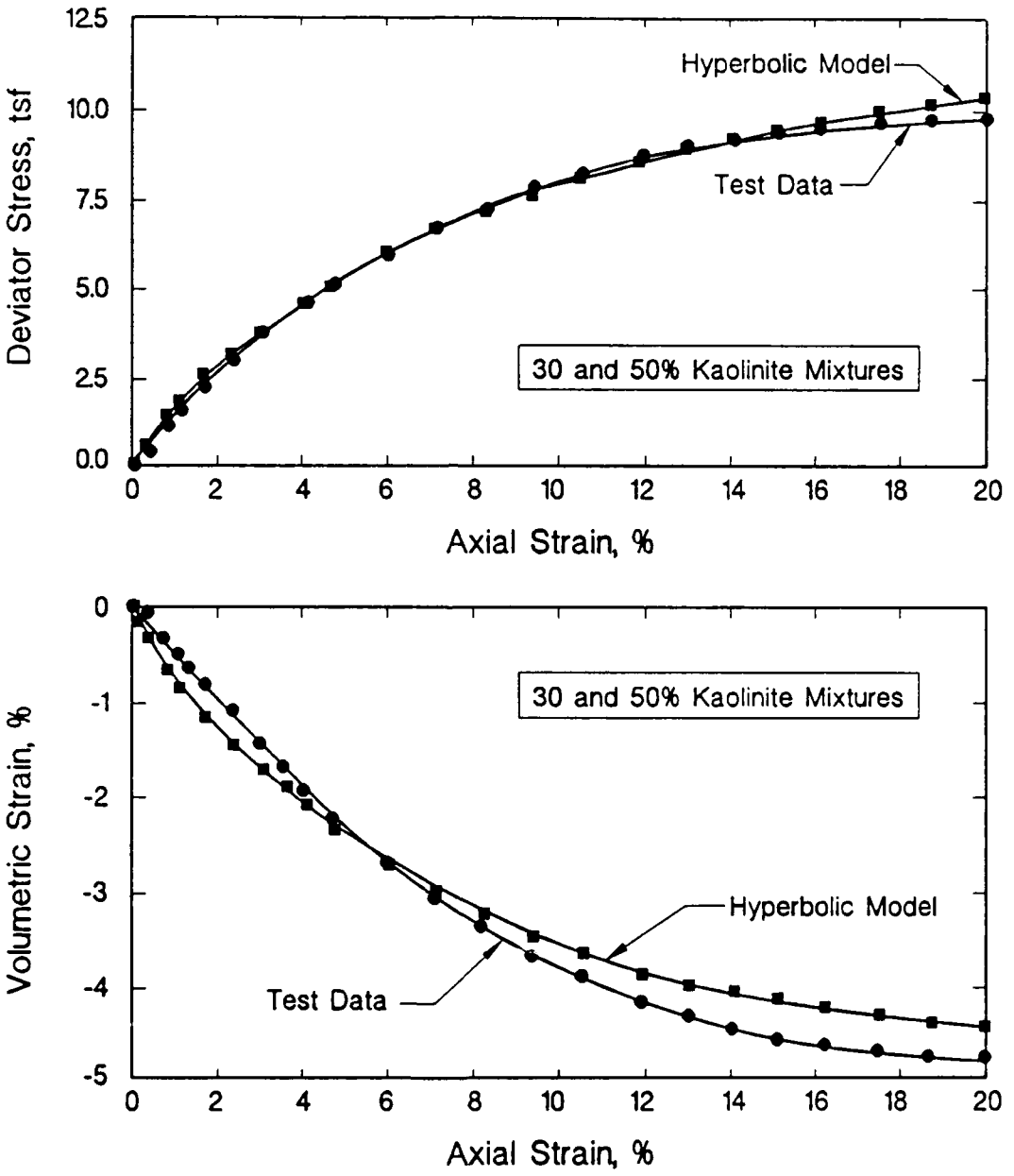


Figure 23. Comparison of Measured and Drained Hyperbolic Stress-Strain Curves for the 30 and 50% Kaolinite Mixtures

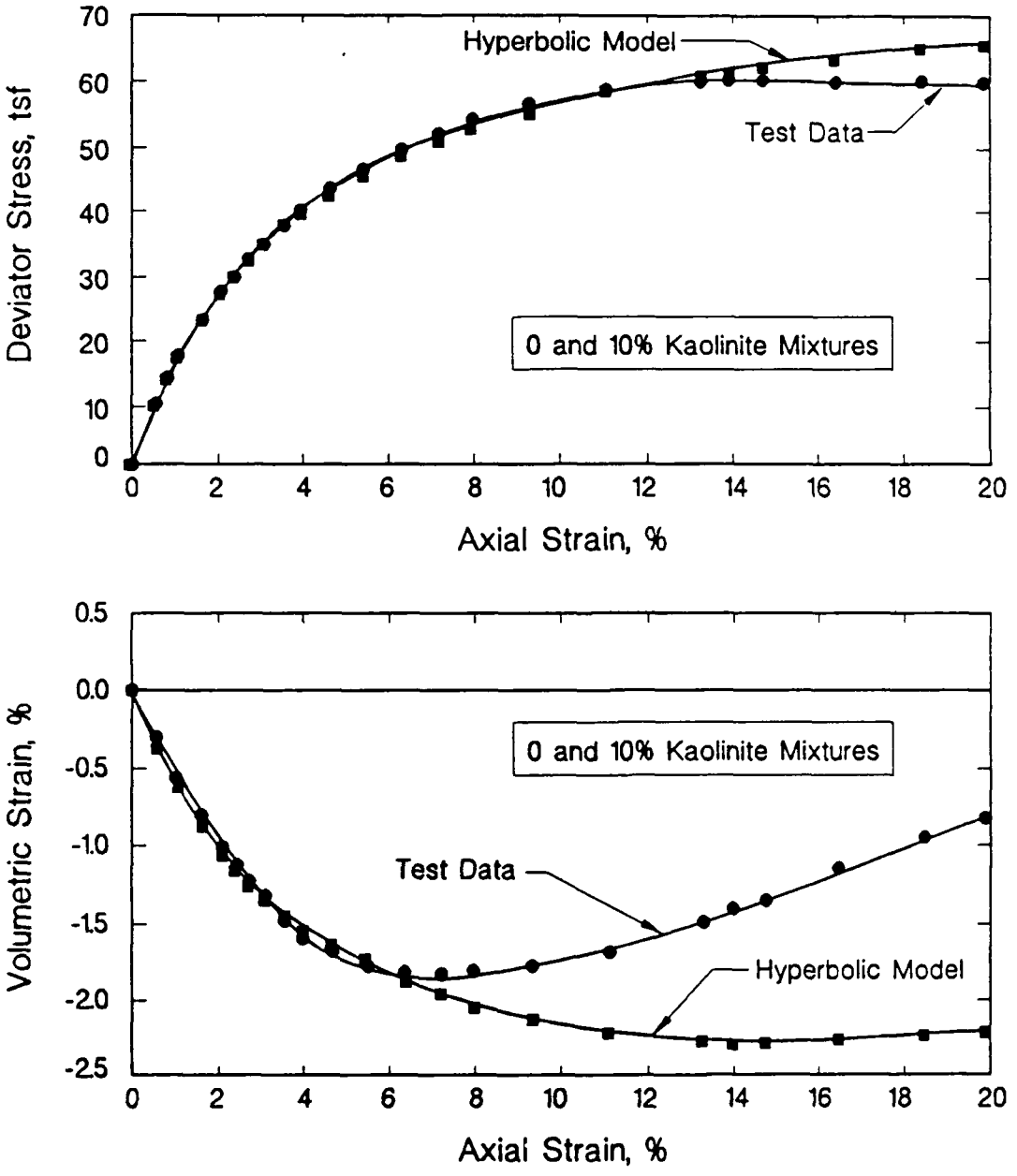


Figure 24. Comparison of Measured and Drained Hyperbolic Stress-Strain Curves for the 0 and 10% Kaolinite Mixtures

ranged from 81 to 174 for 0% kaolinite and only 28 to 44 for the 50% kaolinite mixture. In addition, the higher the kaolinite content, the softer or lower the modulus number. From Table 7 it can be seen that modulus exponent was approximately equal to unity for all of the mixtures. This is in good agreement with the fact that the test specimens were normally consolidated. In fact, it can be shown using critical state soil mechanics that the modulus exponent should be equal to 1.0 if the specimen is normally consolidated.

62. It can be seen from Table 7 that the relative compaction and kaolinite content had a similar effect on the bulk modulus number as it did on the modulus number. The bulk modulus number was obtained using the volumetric strain at 70 and 95% of the maximum deviator stress as recommended by Duncan et al. (1980). The bulk modulus exponent was also equal to unity due to the normally consolidated nature of the test specimens. The failure ratio for all of the mixtures varied from 0.61 to 0.82 and did not have a discernible pattern. However, the small variations in the failure ratio did not significantly effect the shape of the stress-strain curve predicted by the hyperbolic stress-strain model.

63. In summary, Tables 6 and 7 provide an excellent database of effective stress strength and hyperbolic stress-strain parameters for normally consolidated silts and clayey-silts. The hyperbolic and shear strength parameters for natural silt deposits can be estimated from these tables using the insitu dry density and water content. Tables 6 an 7 also illustrate the effects of clay content, effective confining pressure, and soil density on the Mohr-Coulomb strength and hyperbolic stress-strain parameters. These results provide an excellent insight into the drained stress-strain response of silts and clayey-silts to field loadings. It should be noted that the hyperbolic stress-strain model does not account for dilation. Therefore, the dilative behavior observed in the volumetric strain curves for kaolinite contents less than or equal to 10%, will not be accurately modeled. The hyperbolic parameters in Table 7 only provide an accurate representation of the volume change characteristics at axial strains less than approximately 6% for kaolinite contents of 10% or less due to this dilative behavior. However, the deviator stress curves were accurately modeled to an axial strain of 12%. In the 30 and 50% kaolinite-silt mixtures, the hyperbolic model provided an excellent representation of the measured soil behavior for axial strains less than or equal to 20%.

## Isotropically Consolidated-Undrained Triaxial Tests

64. It can be seen from Table 2 that 50 isotropically consolidated-undrained (R)

triaxial tests were performed on the kaolinite-silt mixtures. The following paragraphs will describe 1.) the differences between the drained and undrained stress-strain behavior, 2.) the effect of dry density or relative compaction, 3.) the effect of kaolinite or clay content, and 4.) the effect of effective confining pressure on the undrained behavior of normally consolidated silts and clayey-silts. Figures 25 and 26 provide a comparison of the stress-strain curves from consolidated-drained and consolidated-undrained triaxial tests, respectively. The Standard Proctor relative compaction for the tests shown in these Figures is 100%. The differences in drained behavior exhibited by the low (0 and 10%) and high (30 and 50%) kaolinite content can be seen in Figure 25. In general, the deviator stress curve for the low kaolinite mixtures exhibits a ductile behavior and the volumetric strain curve indicates a large amount of dilation. At large axial strains, it can be seen that the amount of dilation usually decreased resulting in a small amount of strain softening. The high kaolinite mixtures exhibit a strain hardening deviator stress curve while showing a contractive volume change behavior.

65. It can be seen from Figure 26 that the low kaolinite mixtures exhibit a strain hardening deviator stress curve and a dilative pore pressure response. Before strain hardening occurred, the undrained deviator stress curves usually exhibited a large change in slope at an axial strain of 1 to 2%. This coincides with the initiation of dilation and thus a decrease in the pore pressure. Based on these results the strain hardening behavior was attributed to dilation and the development of negative pore pressures. Due to the limitations of the hyperbolic model, the undrained deviator stress curve for the low kaolinite mixtures could only be accurately modeled to an axial strain of 1 to 2%.

66. The high kaolinite mixtures exhibited a ductile deviator stress curve and a contractive or positive pore pressure response. As a result, the undrained behavior of the high kaolinite mixtures was accurately modeled by the hyperbolic relationships. In summary, the drained and undrained behavior of the high and low kaolinite mixtures differed significantly. The low kaolinite mixtures exhibited a ductile behavior in drained conditions and a strain hardening behavior in undrained conditions. Conversely, the high kaolinite mixtures exhibited a drained strain hardening behavior and a ductile behavior in undrained conditions.

67. Figure 27 provides a comparison of the stress-strain curves for Standard Proctor relative compactions of 90 and 100% at a low (0 and 10%) kaolinite content. It can be seen that both specimens exhibit a strain hardening behavior. However, the amount of

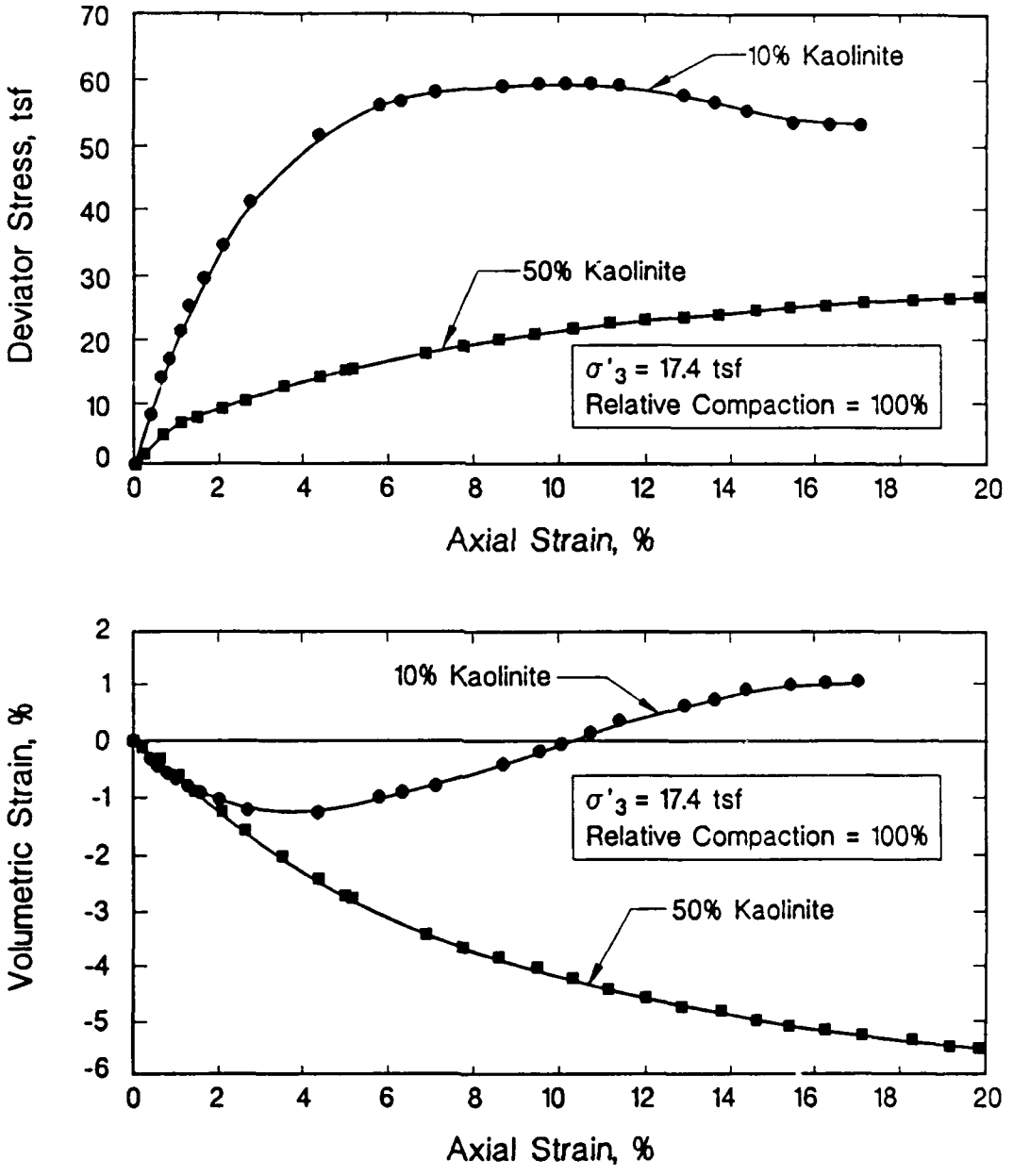


Figure 25. Comparison of Consolidated-Drained Stress-Strain Behavior

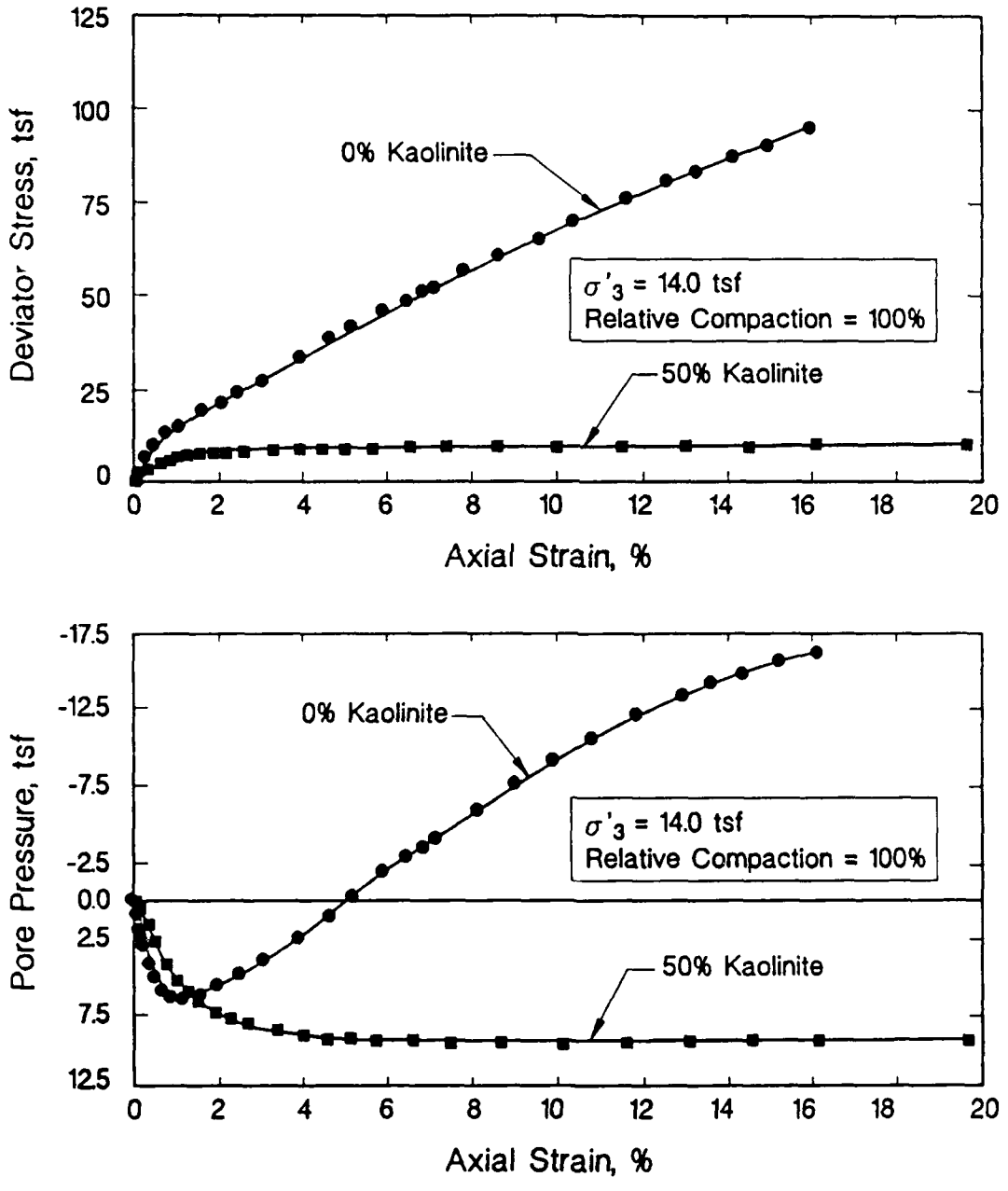


Figure 26. Comparison of Consolidated-Undrained Stress-Strain Behavior

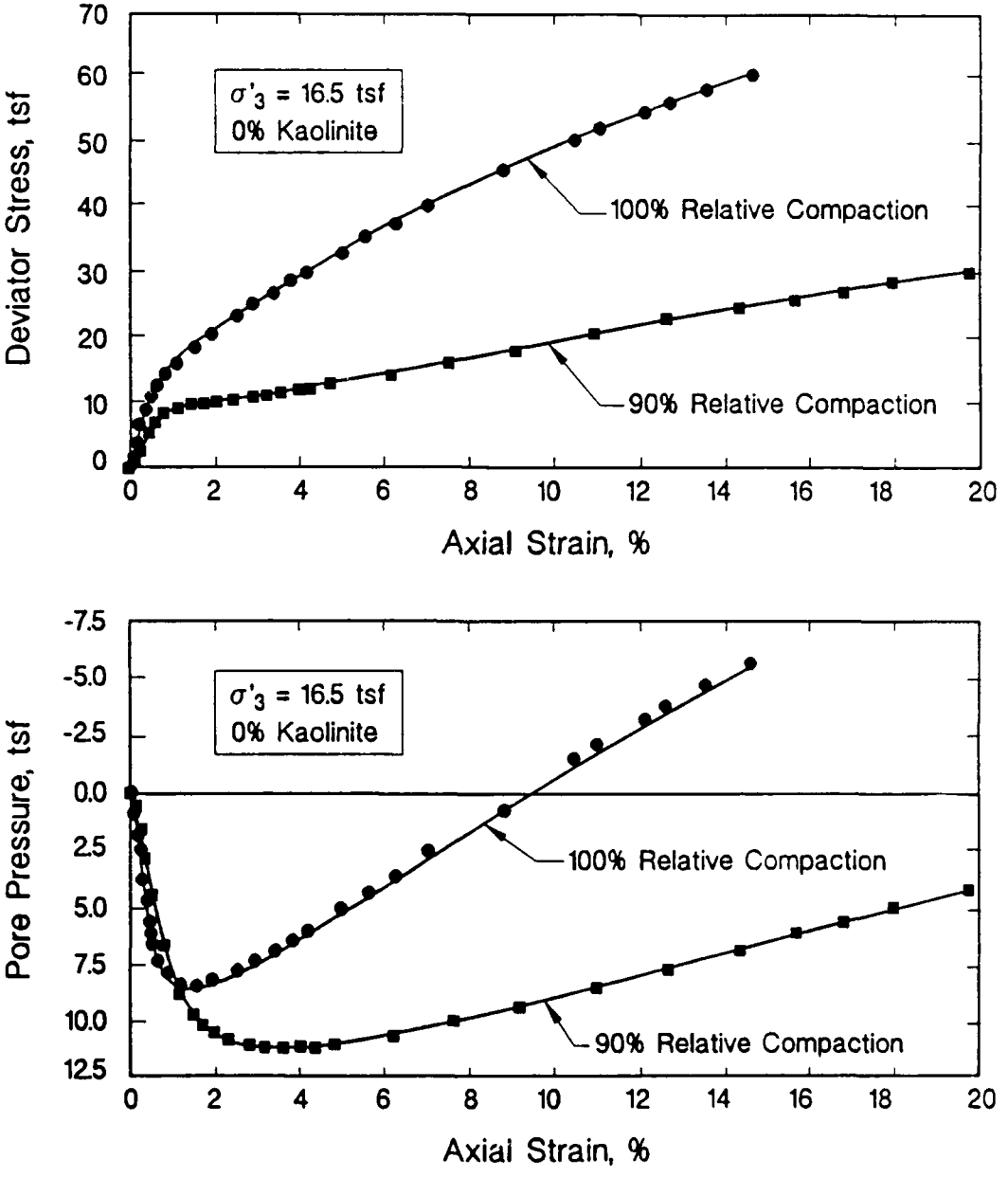


Figure 27. Effect of Relative Compaction on Stress-Strain Behavior in Consolidated-Undrained (R) Triaxial Tests on 0% Kaolinite Mixtures

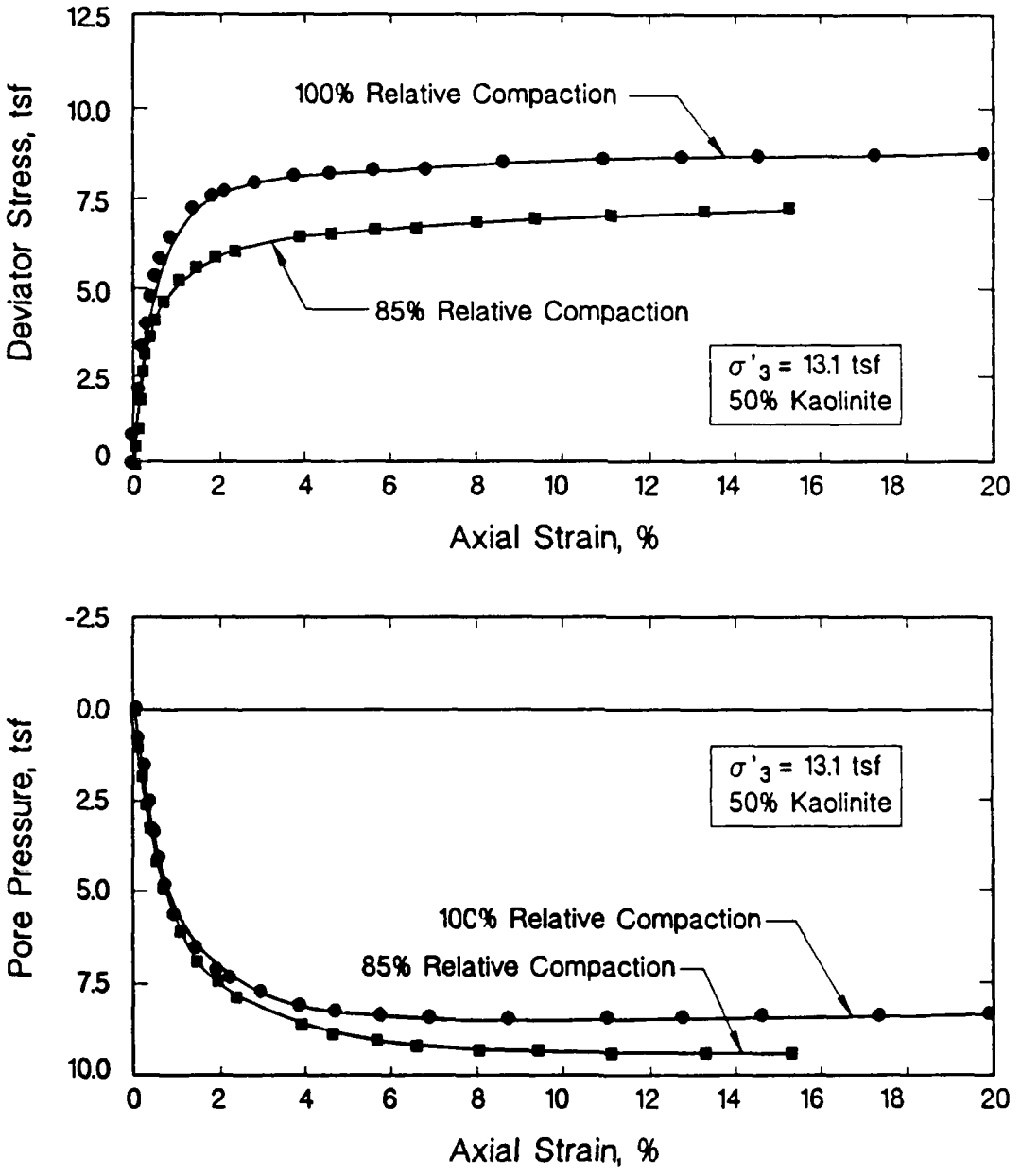


Figure 28. Effect of Relative Compaction on Stress-Strain Behavior in Consolidated-Undrained (R) Triaxial Tests on 50% Kaolinite Mixtures

hardening is substantially larger for the 100% relative compaction. The 100% relative compaction specimen also exhibited a larger amount of dilation. It can also be seen that the 10% difference in the relative compaction also resulted in a large increase in the undrained modulus and maximum deviator stress.

68. Figure 28 provides a comparison of the stress-strain curves for Standard Proctor relative compactions of 85 and 100% at high kaolinite contents. It can be seen that the deviator stress and pore pressure response do not differ significantly for these relative compactions. Therefore, it was concluded that the effect of relative compaction on the undrained response is very small when the kaolinite content is greater than or equal to 30% and very large when the kaolinite is 10% or less. This result was also observed in the consolidated-drained triaxial tests and could have a large impact on compaction specifications for silts and clayey-silts. These results suggest that for silts with clay contents greater than or equal to 30%, the increase in strength for relative compactions greater than 90% may not warrant the costs associated with the increased compactive effort.

69. Figure 26 presents a comparison of the undrained stress-strain curves for low and high kaolinite contents. As described previously, the higher the kaolinite or clay content the weaker and more ductile the stress-strain behavior. Based on these results, the undrained, as well as the drained, transition point between sand and clay behavior appears to occur at a kaolinite content between 10 and 30%. Therefore, the amount of clay present will determine the shear characteristics of the silt and thus the hyperbolic and shear strength parameters.

70. Figure 29 illustrates the effect of effective confining pressure on the stress-strain behavior of the low (0 and 10%) kaolinite mixtures. It can be seen that the effective confining pressures ranged from 6.1 to 16.6 tsf and the pore pressure response was dilative for all of the tests. Even though the specimens exhibited dilation, it was anticipated that effective confining pressures of 8 to 10 tsf were adequate to insure a normally-consolidated condition. This is described in more detail in paragraphs 53 and 54. Figure 30 presents the effect of effective confining pressure on the stress-strain behavior of the high (30 and 50%) kaolinite mixtures. It can be seen that effective confining pressures ranging from 3.7 to 13.3 tsf all of the tests showed a positive pore pressure response.

71. Table 8 presents the total and effective stress Mohr-Coulomb strength parameters from the consolidated-undrained (R) triaxial tests. The failure criteria used to

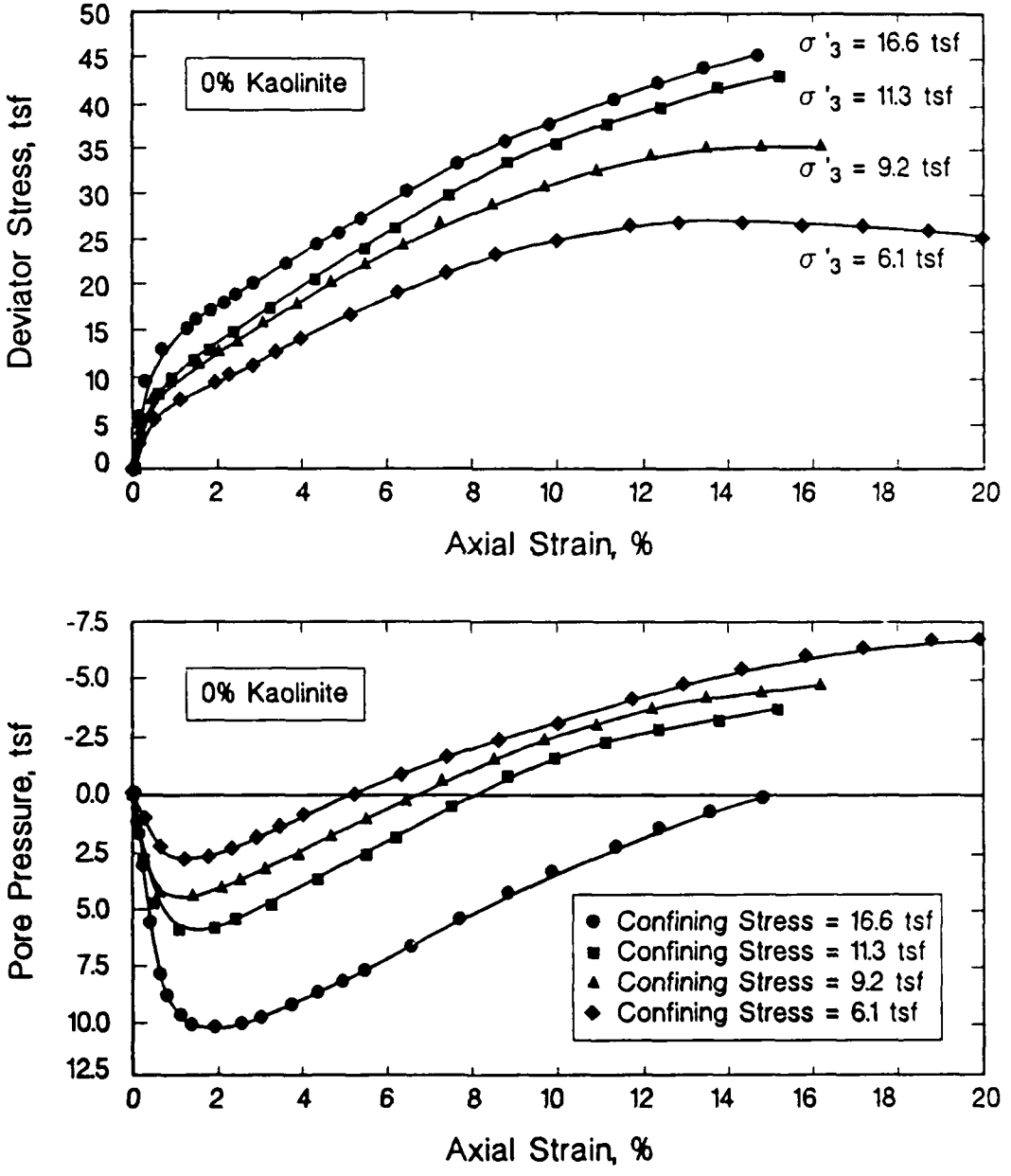


Figure 29. Effect of Effective Confining Pressure on the Undrained Stress-Strain Behavior of 0% Kaolinite Mixtures

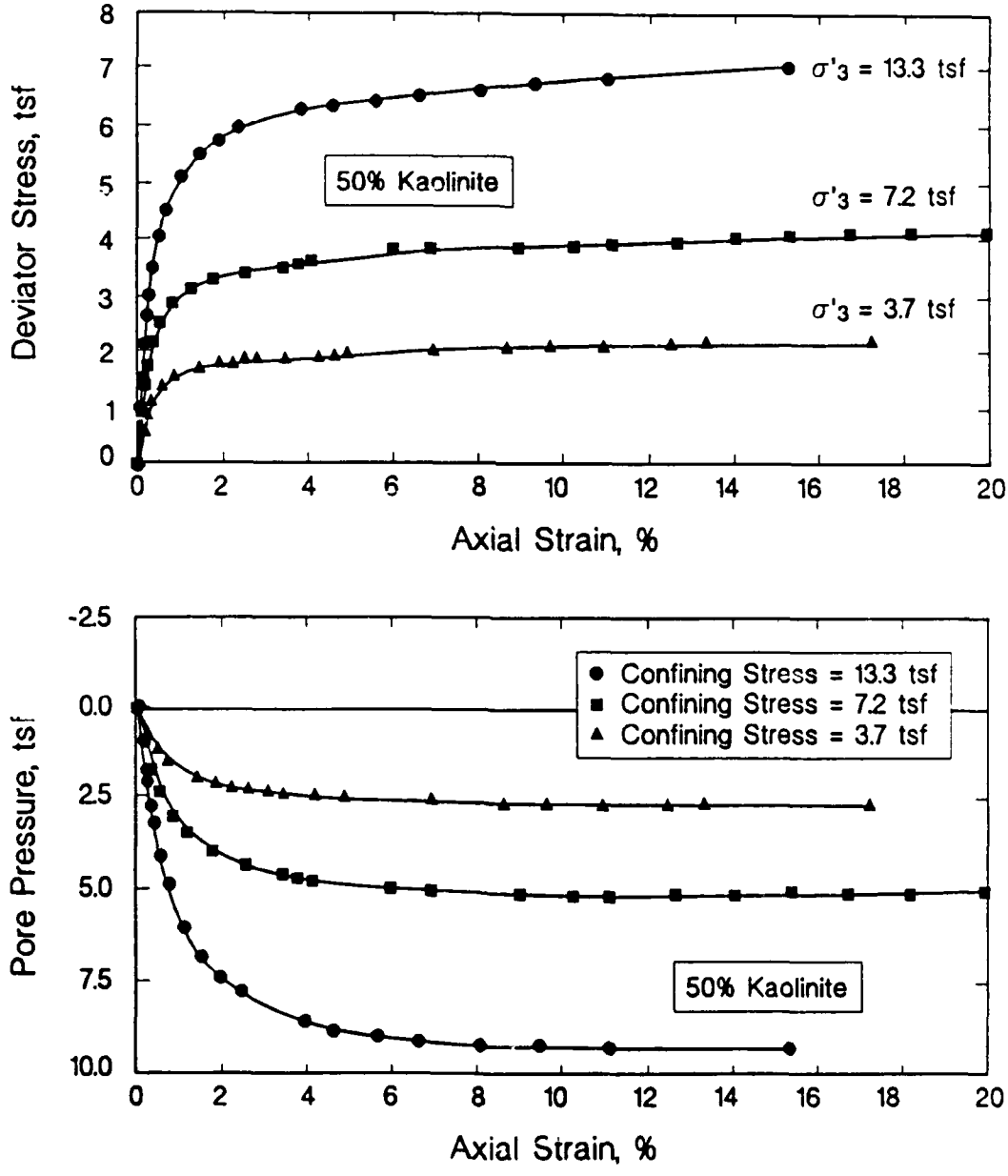


Figure 30. Effect of Effective Confining Pressure on the Undrained Stress-Strain Behavior of 50% Kaolinite Mixtures

Table 8 - Total and Effective Stress Mohr-Coulomb Strength Parameters for Kaolinite-Silt Mixtures from Consolidated-Undrained Triaxial Tests

| % Clay | Standard Proctor Relative Compaction | Initial Average and (Range) of Dry Density (pcf) | Initial Average and (Range) of Water Content (%) | Range of Effective Confining Pressure (tsf) | Total Stress Cohesion (psf) | Total Stress Friction Angle (degrees) | Effective Stress Cohesion (psf) | Effective Stress Friction Angle (degrees) |
|---|---|---|---|---|---|---|---|---|
| 0% Kao | 100 | 97 (95.0-99.3) | 27 (25.8-28.6) | 11.3-16.4 | 0 | 18.0 | 0 | 37.5 |
| 0% Kao | 95 | 95 (89.8-96.7) | 29 (27.5-32.5) | 6.1-16.6 | 0 | 17.8 | 0 | 35.8 |
| 0% Kao | 90 | 94 (94.1-94.8) | 29 (28.8-29.3) | 8.7-16.5 | 0 | 15.7 | 0 | 33.0 |
| 0% Kao | 85 | NA | NA | NA | NA | NA | NA | NA |
| 10% Kao | 100 | 106 (105.4-105.9) | 22 (21.7-22.1) | 13.8-16.9 | 0 | 17.9 | 0 | 36.4 |
| 10% Kao | 95 | 103 (102.6-102.9) | 24 (23.5-23.7) | 10.3-16.3 | 0 | 16.8 | 0 | 34.8 |
| 10% Kao | 90 | 100 (98.7-101.0) | 25 (24.6-26.0) | 5.2-16.9 | 0 | 15.6 | 0 | 34.4 |
| 10% Kao | 85 | 104 (103.2-105.9) | 23 (21.8-23.3) | 4.2-17.3 | 0 | 14.5 | 0 | 34.1 |
| 30% Kao | 100 | 113 (112.3-113.0) | 18 (17.8-18.1) | 9.2-15.4 | 0 | 15.5 | 0 | 31.5 |
| 30% Kao | 95 | 107 (106.1-108.5) | 21 (20.1-21.4) | 3.1-12.8 | 0 | 14.6 | 0 | 30.9 |
| 30% Kao | 90 | 110 (106.9-112.4) | 19 (18.1-20.9) | 4.1-15.9 | 0 | 12.6 | 0 | 29.2 |
| 30% Kao | 85 | 109 (105.5-111.0) | 20 (18.9-21.7) | 3.1-13.3 | 0 | 12.3 | 0 | 28.8 |
| 50% Kao | 100 | 103 (100.0-105.1) | 22 (21.2-24.3) | 6.7-14.3 | 0 | 14.9 | 0 | 27.8 |
| 50% Kao | 95 | 103 (101.6-105.3) | 22 (21.1-23.5) | 7.2-15.4 | 0 | 14.3 | 0 | 26.5 |
| 50% Kao | 90 | 103 (101.5-103.7) | 23 (22.0-23.3) | 7.6-13.3 | 0 | 12.5 | 0 | 25.9 |
| 50% Kao | 85 | 102 (99.7-105.0) | 23 (21.3-24.4) | 3.7-13.3 | 0 | 12.1 | 0 | 25.5 |

NOTES:
1.) Kao = Kaolinite
2.) NA = Not Available

obtain the total stress friction angle was the deviator stress at the minimum value of p' on a p'-q' diagram. It should be noted that p' is the sum of the effective principal stresses, i.e. $\sigma'_1$ and $\sigma'_3$, divided by two and q' is the deviator stress divided by two. The effective stress friction angle was obtained from the best fit failure envelope on the p'-q' diagram. Test specimens with 0% kaolinite and a relative compaction of 85% could not be obtained because the sample liquefied during compaction due to the high water content.

72. From Table 8 it can be seen that the effective stress cohesion for all the mixtures was zero. This also indicates that the test specimens were normally consolidated. The effective stress friction angle ranged from 37.5 degrees for the 0% kaolinite mixture to 25.5 degrees for the 50% kaolinite mixture. As expected these friction angles are in excellent agreement with the effective stress friction angles obtained from the consolidated-drained triaxial tests, see Table 6.

73. The total stress friction angle ranged from 18.0 degrees for the 0% kaolinite mixture to 12.1 degrees for the 50% kaolinite mixture. The range of the effective stress friction angle was 12 degrees, 37.5 to 25.5 degrees, which is approximately two times larger than the 5.9 degree range observed in the total stress friction angle. However, the total stress friction angle decreased with increasing kaolinite content in a similar pattern as the effective stress friction angle. It can also be seen from Table 8 that the effect of relative compaction on the total and effective stress friction angles decreased significantly as the kaolinite content increased. As observed in the consolidated-drained triaxial test results, the effective stress friction angles for the low (0 and 10%) kaolinite mixtures are representative of a sand while the high (30 and 50%) kaolinite mixtures are more representative of cohesive soils. Therefore, the drained and undrained test results both indicate that the transition point between sand and clay behavior occurs at a kaolinite content between 10 and 30%.

74. Table 9 presents the hyperbolic stress-strain parameters obtained from the undrained triaxial tests. These parameters were obtained using the total stress friction angle and the best geometric agreement between the measured and hyperbolic stress-strain curves. Figure 31 presents a typical comparison of the actual and hyperbolic stress-strain curves for the high kaolinite mixtures. Due to the ductile stress-strain behavior of the high kaolinite mixtures, the hyperbolic model provides an excellent representation of the actual stress-strain curve. Since the test specimens were undrained during shear, there was no volume change during shear. Therefore, the bulk modulus number and exponent were not

Table 9 - Total Stress Hyperbolic Stress-Strain Parameters for Kaolinite-Silt Mixtures from Consolidated-Undrained Triaxial Tests

| % Clay | Standard Proctor Relative Compaction | Average and (Range) of Initial Dry Density (pcf) | Average and (Range) of Initial Water Content (%) | Range of Effective Confining Pressure (tsf) | Total Stress Cohesion (psf) | Total Stress Friction Angle (degrees) | Effective Stress Cohesion (psf) | Effective Stress Friction Angle (degrees) | Modulus Number K | Modulus Exponent n | Failure Ratio Rf |
|---|---|---|---|---|---|---|---|---|---|---|---|
| 0% Kao | 100 | 97 (95.0-99.3) | 27 (25.8-28.6) | 11.3-16.4 | 0 | 18.0 | 0 | 37.5 | 215 | 1.00 | 0.65 |
| 0% Kao | 95 | 95 (89.8-96.7) | 29 (27.5-32.5) | 6.1-16.6 | 0 | 17.8 | 0 | 35.8 | 210 | 1.00 | 0.65 |
| 0% Kao | 90 | 94 (94.1-94.8) | 29 (28.8-29.3) | 8.7-16.5 | 0 | 15.7 | 0 | 33.0 | 205 | 1.00 | 0.65 |
| 0% Kao | 85 | NA | NA | NA | NA | NA | NA | NA | NA | NA | NA |
| 10% Kao | 100 | 106 (105.4-105.9) | 22 (21.7-22.1) | 13.8-16.9 | 0 | 17.9 | 0 | 36.4 | 210 | 1.00 | 0.84 |
| 10% Kao | 95 | 103 (102.6-102.9) | 24 (23.5-23.7) | 10.3-16.3 | 0 | 16.8 | 0 | 34.8 | 205 | 1.00 | 0.84 |
| 10% Kao | 90 | 100 (98.7-101.0) | 25 (24.6-26.0) | 5.2-16.9 | 0 | 15.6 | 0 | 34.4 | 200 | 1.00 | 0.84 |
| 10% Kao | 85 | 104 (103.2-105.9) | 23 (21.8-23.3) | 4.2-17.3 | 0 | 14.5 | 0 | 34.1 | 180 | 1.00 | 0.84 |
| 30% Kao | 100 | 113 (112.3-113.0) | 18 (17.8-18.1) | 9.2-15.4 | 0 | 15.5 | 0 | 31.5 | 180 | 1.00 | 0.95 |
| 30% Kao | 95 | 107 (106.1-108.5) | 21 (20.1-21.4) | 3.1-12.8 | 0 | 14.6 | 0 | 30.9 | 175 | 1.00 | 0.95 |
| 30% Kao | 90 | 110 (106.9-112.4) | 19 (18.1-20.9) | 4.1-15.9 | 0 | 12.6 | 0 | 29.2 | 170 | 1.00 | 0.95 |
| 30% Kao | 85 | 109 (105.5-111.0) | 20 (18.9-21.7) | 3.1-13.3 | 0 | 12.3 | 0 | 28.8 | 165 | 1.00 | 0.95 |
| 50% Kao | 100 | 103 (100.0-105.1) | 22 (21.2-24.3) | 6.7-14.3 | 0 | 14.9 | 0 | 27.8 | 150 | 1.00 | 1.00 |
| 50% Kao | 95 | 103 (101.6-105.3) | 22 (21.1-23.5) | 7.2-15.4 | 0 | 14.3 | 0 | 26.5 | 147 | 1.00 | 1.00 |
| 50% Kao | 90 | 103 (101.5-103.7) | 23 (22.0-23.3) | 7.6-13.3 | 0 | 12.5 | 0 | 25.9 | 145 | 1.00 | 1.00 |
| 50% Kao | 85 | 102 (99.7-105.0) | 23 (21.3-24.4) | 3.7-13.3 | 0 | 12.1 | 0 | 25.5 | 142 | 1.00 | 1.00 |

NOTES:
1.) Kao = Kaolinite
2.) NA = Not Available

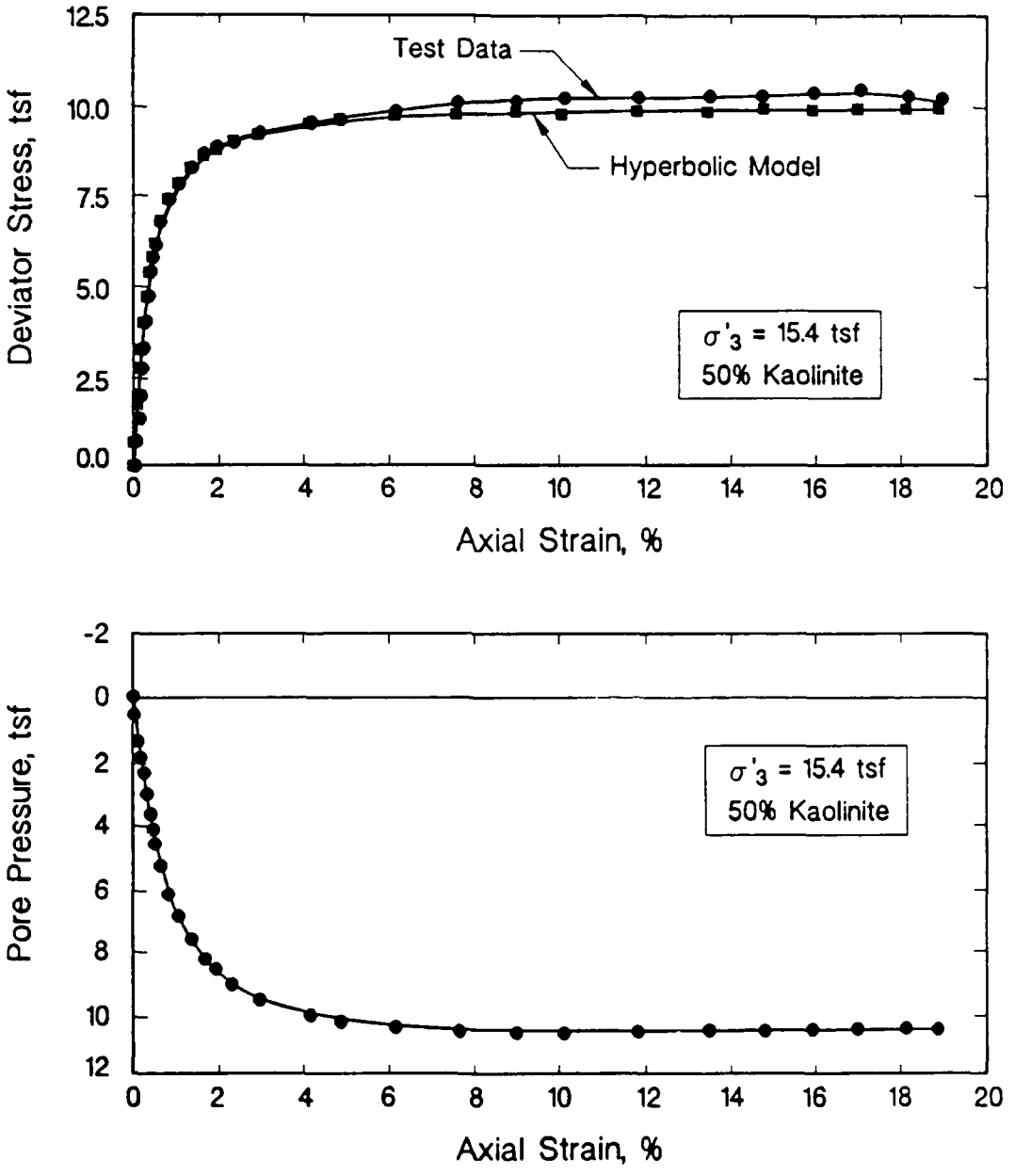


Figure 31. Comparison of Measured and Actual Undrained Hyperbolic Stress-Strain Curves for the 30 and 50% Kaolinite Mixtures

calculated for the undrained tests. All of the test specimens were saturated, i.e. B-value greater than 99.7%, thus poisson's ratio can be assumed to be approximately 0.5 for these tests.

75. It can be seen from Figure 32 that the geometric matching criterion had a large influence on the hyperbolic parameters for the low kaolinite mixtures. It can be seen that the hyperbolic model is in excellent agreement with the measured data for axial strains less than 2%. Since the hyperbolic model does not account for strain hardening, the agreement at axial strains greater than 2% is poor. However, it was decided that modeling the initial portion of the deviator stress curve is more important than the behavior at large strains. Therefore, the hyperbolic parameters presented in Table 9 for the low (0 and 10%) kaolinite mixtures should only be used for small strain (less than 5%) problems.

76. In summary, Table 8 provides an excellent database of the total and effective stress strength parameters for normally consolidated silts and clayey-silts. Table 9 provides a database of total stress hyperbolic parameters for the various kaolinite-silt mixtures. The hyperbolic stress-strain and shear strength parameters for natural silt deposits can be estimated from Table 8 and 9 using the insitu density and water content. It should be noted that the hyperbolic parameters for the low kaolinite mixtures only model the actual deviator stress curve at axial strains less than 5%. Table 8 and 9 also provide an insight to the effects of clay content, effective confining pressure, and soil density on the undrained response of normally consolidated silts and clayey-silts.

# PART VII: MONTMORILLONITE-SILT TRIAXIAL TEST RESULTS

## Isotropically Consolidated-Drained Tests

77. It can be seen from Table 2 that 10 isotropically consolidated-drained (S) triaxial tests were performed on mixtures of montmorillonite and silt. These tests were performed to investigate the effect of clay mineralogy on the transition between sand and clay behavior, and the drained strength and stress-strain parameters. Only a Standard Proctor relative compaction of 100% and the four clay percentages, 0, 10, 30, and 50%, were used. Figure 33 presents a comparison of the stress-strain curves for the low (0 and 10%) montmorillonite and kaolinite mixtures. It can be seen that the kaolinite mixtures exhibit a higher modulus and shear strength than the montmorillonite mixtures. The montmorillonite mixtures exhibited a contractive volume change behavior while the kaolinite mixtures were dilative.

78. Figure 34 presents a comparison of the stress-strain curves for the high (30 and 50%) montmorillonite and kaolinite mixtures. It can be seen that the modulus and strength of the kaolinite-silt mixtures are substantially higher than the montmorillonite-silt mixtures. From Figures 33 and 34 it may be concluded that the montmorillonite has a larger influence on the stress-strain response of the silt than kaolinite. This is probably due to the intrinsic activity and mechanincal properties of montmorillonite.

79. Table 10 presents the effective stress Mohr-Coulomb strength parameters obtained from the consolidated-drained triaxial tests on the montmorillonite-silt mixtures. The failure criteria used to obtain these parameters is the maximum deviator stress or an axial strain of 20%. It can be seen that the effective stress cohesion measured for all of the montmorillonite-silt mixtures was zero. This indicates that the test specimens were in a normally consolidated condition at the time of shearing.

80. From Table 8 it can be seen that the effective stress friction angle ranged from 38.6 degrees for the 0% montmorillonite to 14.3 degrees for 50% montmorillonite mixture. By comparing Tables 6 and 10 it may be seen that the effective stress friction angle for the 30 and 50% montmorillonite mixtures are substantially lower than the corresponding angles for the kaolinite-silt mixtures. Mitchell (1976) reported that the peak effective stress friction angle of pure montmorillonite ranges from 6 to 10 degrees. Therefore, the difference in the friction angle between the montmorillonite and kaolinite mixtures appears to be due to the montmorillonite. In addition, the effective stress friction angle for

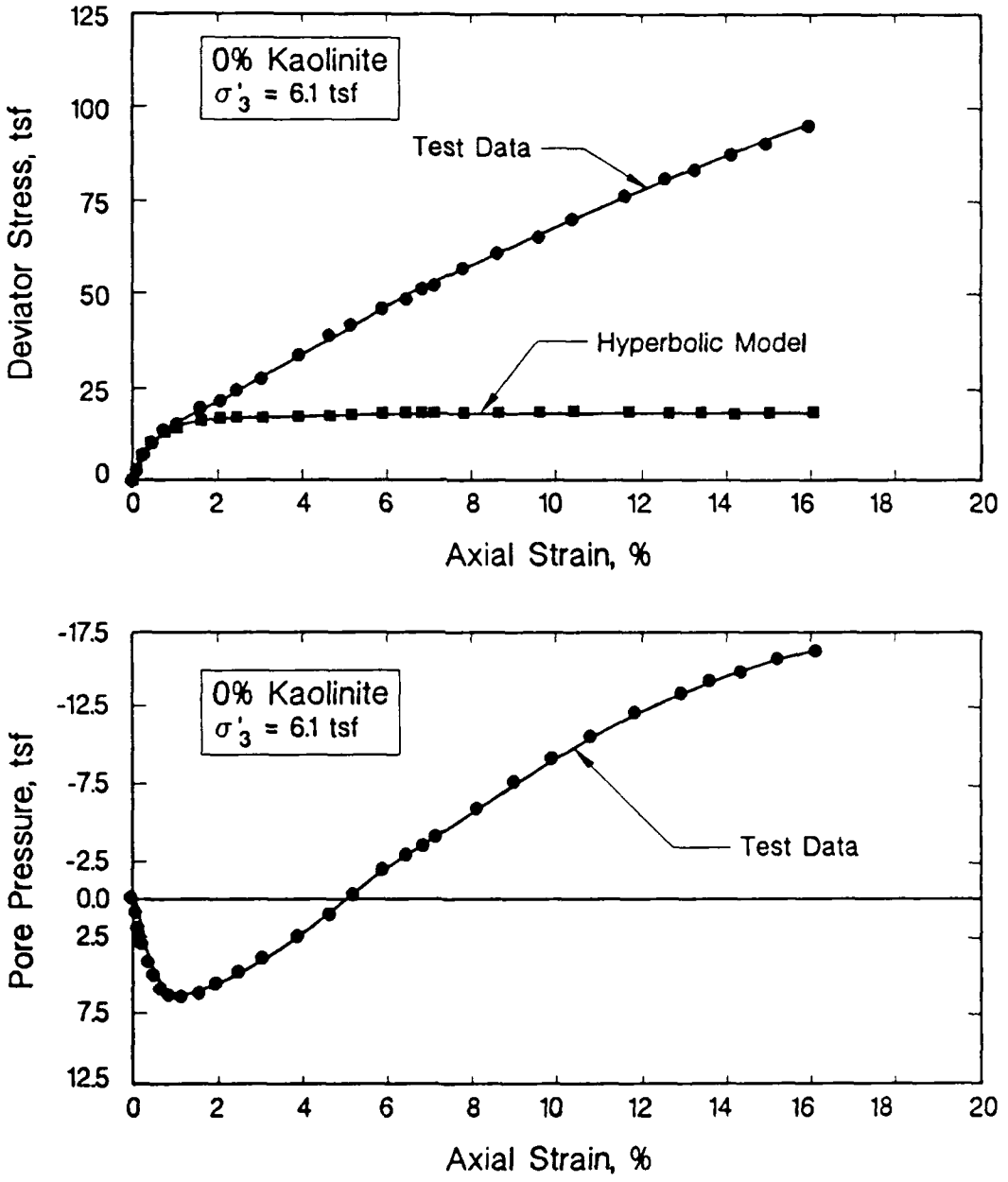


Figure 32. Comparison of Measured and Actual Undrained Hyperbolic Stress-Strain Curves for the 0 and 10% Kaolinite Mixtures

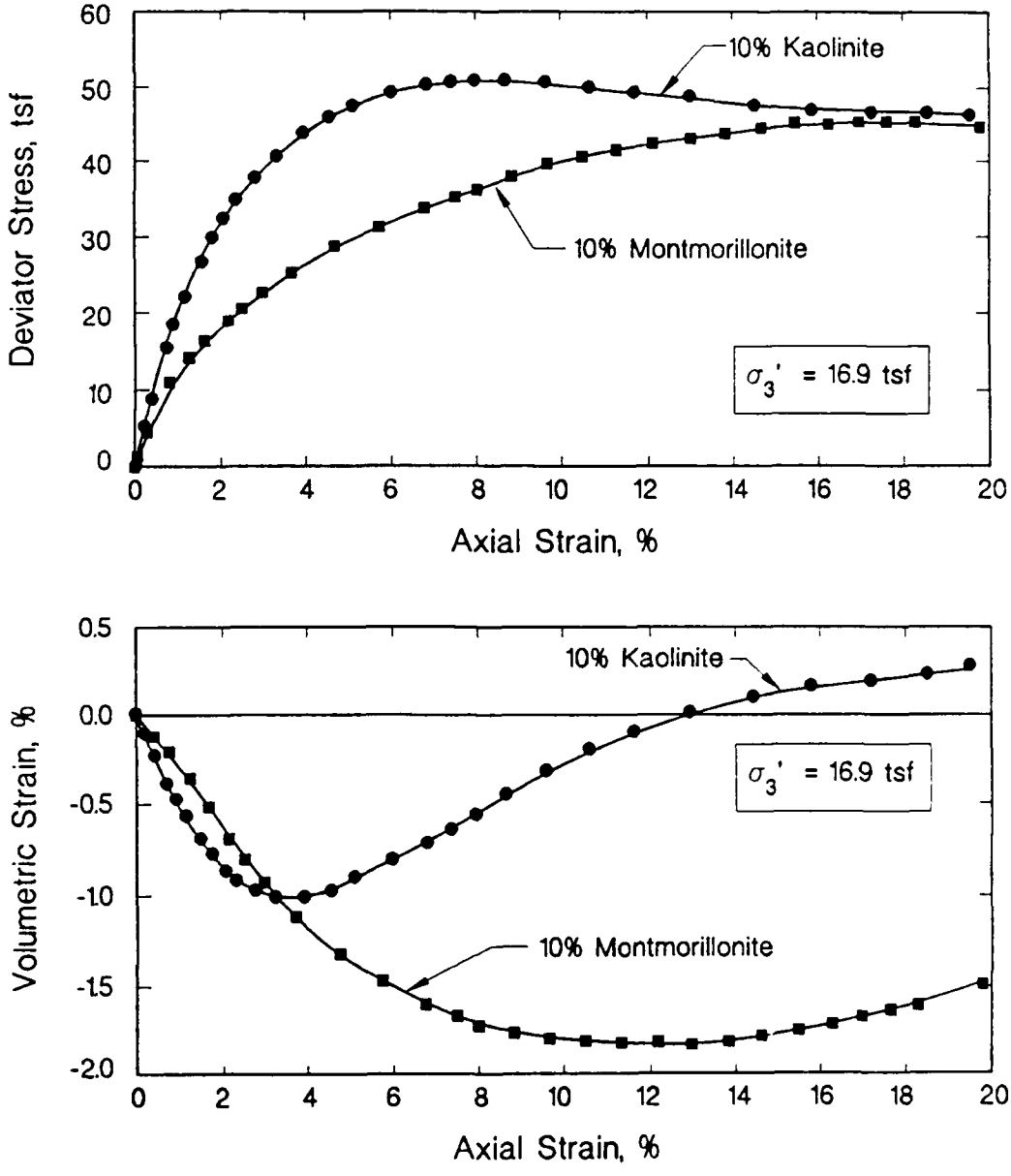


Figure 33. Comparison of Drained Stress-Strain Behavior for 10% Kaolinite and 10% Montmorillonite Mixtures

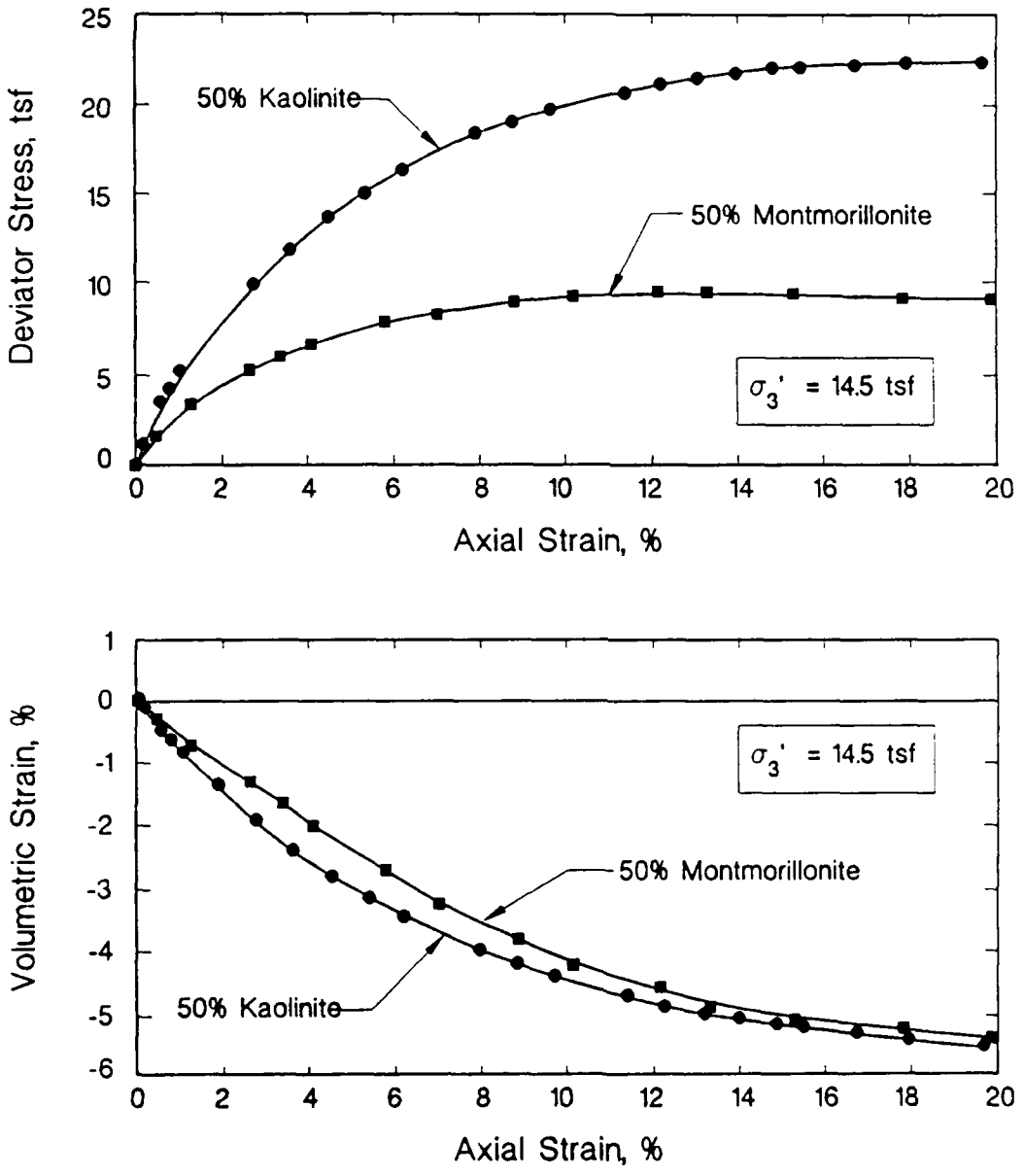


Figure 34. Comparison of Drained Stress-Strain Behavior for 50% Kaolinite and 50% Montmorillonite Mixtures

Table 10 - Effective Stress Mohr-Coulomb Strength Parameters for Montmorillonite-Silt Mixtures from Consolidated-Drained Triaxial Tests

| % Clay | Standard Proctor Relative Compaction | Average and (Range) of Initial Dry Density (pcf) | Average and (Range) of Initial Water Content (%) | Range of Effective Confining Pressure (tsf) | Effective Stress Cohesion (psf) | Effective Stress Friction Angle (degrees) |
|---|---|---|---|---|---|---|
| 0% Mont | 100 | 98 (94.7-98.8) | 27 (26.1-28.9) | 2.1-17.1 | 0 | 38.6 |
| 10% Mont | 100 | 103 (101.5-104.5) | 24 (22.8-24.6) | 11.3-16.9 | 0 | 35.0 |
| 30% Mont | 100 | 103 (102.3-104.9) | 24 (22.6-24.1) | 10.3-16.9 | 0 | 20.0 |
| 50% Mont | 100 | 94 (92.0-96.2) | 30 (28.0-31.0) | 8.7-15.5 | 0 | 14.3 |

NOTES:
1.) Mont = Montmorillonite

the 10% montmorillonite mixture is 1.5 degrees lower than the 10% kaolinite mixture even though the dry density and water content of these mixtures are similar. This indicates that the montmorillonite is starting to control the behavior of the mixture. Therefore, the transition from clay to sand behavior in the montmorillonite mixtures appears to be at or near 10% while the kaolinite transition point is in between 10 and 30%. In summary, the engineering behavior of silts is controlled by the percentage of clay and the clay mineralogy present in the silt.

81. Table 11 summarizes the hyperbolic stress-strain parameters for the montmorillonite-silt mixtures. By comparing Tables 7 and 11, it can be seen that the modulus and bulk modulus numbers for the montmorillonite mixtures are substantially lower than the corresponding kaolinite mixtures. In addition, the hyperbolic parameters also indicate that the transition point between clay and sand behavior is at or near a montmorillonite content of 10%. Tables 10 and 11 can be used to estimate the hyperbolic and shear strength parameters for natural silt deposits which contain montmorillonite, using the insitu water content and density.

Table 11 - Effective Stress Hyperbolic Stress-Strain Parameters for Montmorillonite-Silt Mixtures from Consolidated-Drained Triaxial Tests

| % Clay | Standard Proctor Relative Compaction | Average and (Range) of Initial Dry Density (pcf) | Average and (Range) of Initial Water Content (%) | Range of Effective Confining Pressure (tsf) | Effective Stress Cohesion (psf) | Effective Stress Friction Angle (degrees) | Modulus Number K | Modulus Exponent n | Bulk Modulus Number Kb | Bulk Modulus Exponent m | Failure Ratio Rf |
|---|---|---|---|---|---|---|---|---|---|---|---|
| 0% Mont | 100 | 98 (94.7-98.8) | 27 (26.1-28.9) | 2.1-17.1 | 0 | 38.6 | 174 | 1.01 | 101 | 0.96 | 0.73 |
| 10% Mont | 100 | 103 (101.5-104.5) | 24 (22.8-24.6) | 11.3-16.9 | 0 | 35.0 | 80 | 1.00 | 70 | 0.83 | 0.72 |
| 30% Mont | 100 | 103 (102.3-104.9) | 24 (22.6-24.1) | 10.3-16.9 | 0 | 20.0 | 29 | 1.00 | 15 | 0.83 | 0.78 |
| 50% Mont | 100 | 94 (92.0-96.2) | 30 (28.0-31.0) | 8.7-15.5 | 0 | 14.3 | 24 | 1.00 | 12 | 0.83 | 0.70 |

NOTES:
1.) Mont = Montmorillonite

# PART VIII: INTERPRETATION OF TRIAXIAL TEST RESULTS

## Isotropically Consolidated-Drained Tests

82. Clough and Duncan (1969) present drained hyperbolic stress-strain parameters for the low plasticity silt, Unified Soil Classification symbol of ML, in the foundation soils at Port Allen Lock. It should be noted that these parameters were obtained from consolidation and direct shear test data and not consolidated-drained (S) triaxial test results. However, these hyperbolic stress-strain parameters provide a basis for comparing the drained parameters obtained during this study. Clough and Duncan reported a modulus number of 330, a modulus exponent of 0.6, a failure ratio of 0.85, and a poisson's ratio of 0.2 to 0.3 for the Port Allen Silt. The good agreement between the measured and calculated stresses and deformations at Port Allen Lock suggest that these parameters are representative of the silt deposit.

83. The silt mixture with 0% kaolinite also classified as a low plasticity silt, i.e. ML, and was used for the comparison. It can be seen from Table 7 that the modulus number and exponent were 174 and 1.0, respectively, for a relative compaction of 100%. Therefore, the modulus number is approximately 1.9 times smaller than the value reported by Clough and Duncan. There are several explanations for this discrepancy.

84. The most plausible explanation is that the Port Allen silt has a higher density and may be overconsolidated due to the natural cementation and/or structure of the silt. This is evident by comparing the modulus exponents. The Port Allen silt exhibited a modulus exponent less than 1.0 which corresponds to an overconsolidated condition. Therefore, it was concluded that the large difference in the modulus numbers for the kaolinite-silt mixtures and the Port Allen silt must be due to the natural overconsolidation or cementation which silts and clayey-silts possess. The bluff at WES from which the silt samples were obtained, stands at a vertical slope as do many of the loess slopes in the area. This fact does not correspond with the hyperbolic stress-strain parameters and effective stress friction angles which were measured during this study. Therefore, the natural cementation and/or soil structure of the loess appears to result in a much higher strength and stiffness. During the processing of the silt, all of the cementation and structure was destroyed. Therefore, the measured strength and hyperbolic stress-strain parameters will probably be lower than those back-calculated from field measurements. Future studies on the behavior of silts should involve the testing of undisturbed silt and clayey-silt specimens to quantify the effect of the natural cementation and/or structure of silts on the hyperbolic

stress-strain and Mohr-Coulomb strength parameters.

85. Therefore, the hyperbolic stress-strain and Mohr-Coulomb strength parameters presented herein can be used to estimate the behavior of normally consolidated silts and clayey-silt deposits. The parameters also provide an insight into the effects of clay content, effective confining pressure, and soil density on the strength and hyperbolic stress-strain parameters. These trends can be used to estimate or verify soil parameters for a wide range of densities, clay contents, and effective stresses.

# PART IX: SUMMARY

86. The main objective of this research was to characterize the drained and undrained stress-strain behavior of normally consolidated silts and clayey-silts. To achieve this objective, extensive drained and undrained triaxial tests were conducted on silt mixtures with varying clay contents. The percentages of clay used in the silt mixtures are 0, 10, 30, and 50%. Manufactured kaolinite and montmorillonite were mixed with the silt to investigate the effect of clay mineralogy. The effect of density on the stress-strain behavior was investigated by compacting the triaxial test specimens at Standard Proctor relative compactions of 85, 90, 95, and 100%. The main conclusions of the behavior of normally consolidated silts and clayey-silts are summarized below:

1.) The shear behavior of silt is controlled by the percentage of clay and the clay mineral in the soil. At low clay contents the silt exhibits shear characteristics similar to a sand and at high clay contents the shear behavior is similar to a clay. The transition point from sand to clay behavior is also a function of the clay mineralogy and was found to be between 10 and 30% for the kaolinite-silt mixtures and at or near 10% for the montmorillonite-silt mixtures.

2.) The effect of density on the strength and stress-strain parameters decreased as the clay content increased. At a low clay content (0 and 10%), increasing the Standard Proctor relative compaction from 85 to 100% resulted in a substantial increase in the shear strength and hyperbolic stress-strain parameters. However, at high clay contents (30 and 50%), there was only a small increase in the shear strength and hyperbolic stress-strain parameters when the relative compaction increased from 85 to 100%. Therefore, there appears to be little benefit, in terms of strength and stiffness, of specifying a field relative compaction greater than 90% if the clay content is greater than or equal to 30%. However, the test results suggest that the volumetric strain may be reduced by 25% if the relative compaction is greater than 90%.

3.) At low (0 and 10%) clay contents, the kaolinite-silt mixtures exhibited dilation even though the test specimens were normally consolidated. At high (30 and 50%) clay contents, the volume change behavior was always contractive. Conversely, the montmorillonite-silt mixtures all exhibited a contractive volume change behavior. Therefore, the volume change behavior during shear was a function of the clay content and the clay mineralogy.

4.) Effective confining pressures greater than 8 to 10 tsf were usually required to obtain a normally consolidated condition.

5.) Total stress and effective stress Mohr-Coulomb strength parameters can be estimated for normally consolidated silts and clayey-silts using the insitu water content and density and the database described herein. It can be seen from Tables 6 and 10 that the effective stress friction angle for the kaolinite-silt mixtures ranged from 38.6 to 25.5 and from 38.6 to 14.3 for the montmorillonite-silt mixtures. The effective stress cohesion was measured to be zero for all of the mixtures. This also indicates that the test specimens were in a normally consolidated condition.

6.) Clay mineralogy, as well as percentage of clay, controls the shear behavior of a silt deposit. The more active the clay mineral, the lower the modulus and shear strength of the silt. In addition, increasing the activity reduces the percentage of clay required to reach the transition point between sand and clay behavior.

7.) Tables 6 through 11 can be used to estimate the shear strength and hyperbolic parameters of normally consolidated silts and clayey-silts using the insitu water content and density.

# REFERENCES


1. ASTM (1990). "Soil and Rock, Building Stones; Geotextiles," *Annual Book of ASTM Standards*, American Society for Testing and Materials, Section 4, Volume 04.08, Philadelphia, 953 pp.

2. Bishop, A.W. and Henkel, D.J. (1962). *The Measurement of Soil Properties in the Triaxial Tests*, London, Edward Arnold Ltd., 190 p.

3. Black, D.K. and Lee, K.L. (1973). "Saturating Laboratory Samples by Back Pressure," *Journal of the Soil Mechanics and Foundations Division*, ASCE, Vol. 99, No. SM1, June, pp. 75-93.

4. Chan, C.K. (1990). personnel communications.

5. Chang, C-Y. (1969). "Finite Element Analyses of Soil Movements Caused by Deep Excavation and Dewatering," Dissertation, University of California, Berkeley.

6. Clough, G.W. and Duncan, J.M. (1969). "Finite Element Analyses of Port Allen and Old River Locks," Report No. TE 69-3, University of California, Berkeley, September, pp. 265.

7. Duncan, J.M. Byrne, P., Wong, K.S., and Mabry, P. (1978). "Strength, Stress-Strain and Bulk Modulus Parameters for Finite Element Analyses of Stresses and Movements in Soil Masses," Report No. UCB/GT/78-02, University of California, Berkeley, April.

8. Duncan, J.M. Byrne, P., Wong, K.S., and Mabry, P. (1980). "Strength, Stress-Strain and Bulk Modulus Parameters for Finite Element Analyses of Stresses and Movements in Soil Masses," Report No. UCB/GT/80-01, University of California, Berkeley, August, 1980, pp. 77.

9. Duncan, J.M. and Chang, C-Y. (1970). "Nonlinear Analysis of Stress and Strain in Soils," *Journal of the Soil Mechanics and Foundations Division*, ASCE, Vol. 96, No. SM5, September, pp.

10. Duncan, J.M., Clough, G.W., and Ebeling, R.M. (1990). "Behavior and Design of Gravity Earth Retaining Structures," *Proceedings, Design and Performance of Earth Retaining Structures*, ASCE Specialty Conference, Cornell University, Ithaca, 18-21 June, ASCE, New York, pp. 251-277.

11. Duncan, J.M., Lucia, P.C., and D'Orazio, T.B. (1982). "Finite Element Analyses of Stresses and Movements in Arcadia Dam," Geotechnical Engineering Report NO. UCB/GT/82-07 to U.S. Army Corps of Engineers, Tulsa District, University of California, Berkeley, Sept., 33 pp.

12. Fleming, L.N. and Duncan, J.M. (1990). "Stress-Deformation Characteristics of Alaskan Silt," *Journal of Geotechnical Engineering*, ASCE, Vol. 116, No. GT3, March, pp. 377-393.

13. Gibson, R.E. and Henkel, D.J. (1954). "Influence of Duration of Tests at Constant Rate of Strain on Measured "Drained" Strength," *Geotechnique*, Vol. 4, No. 1, pp. 6-15.

14. Houston, W.N. and Chan, C.K., (1983). "Laboratory Testing Manual," Geotechnical Engineering Report, University of California, Berkeley.

15. Janbu, N. (1963). "Soil Compressibility as Determined by Oedometer and Triaxial Tests," *Proceedings, European Conference on Soil Mechanics and Foundation Engineering*, Wissbaden, Germany, Vol. 1, pp. 19-25.

16. Lupini, J.F., Skinner, A.E., and Vaughan, P.R., (1981) "The Drained Residual Strength of Cohesive Soil," *Geotechnique*, Vol. 31, No. 2, pp. 181-213.

17. Mana, A.I. and Clough, G.W. (1981). "Prediction of Movements for Braced Cuts in Clays," *Journal of Geotechnical Engineering*, ASCE, Vol. 107, No. GT6, June, pp. 759-777.

18. Mitchell, J.K. (1976). *Fundamental of Soil Behavior*, John Wiley and Sons, New York, NY, 422 pp.

19. Mulilis, J.P., Seed, H.B., and Chan, C.K. (1977). "Effects of Sample Preparation on Sand Liquefaction," *Journal of the Soil Mechanics and Foundations Division*, ASCE, Vol. 103, No. GT2, February, pp. 91-108.

20. Office, (1970). Chief of Engineers, Department of the Army, "Engineer Manual: Laboratory Soils Testing," EM 1110-2-1906, Washington, D.C.

21. Seed, H.B., Woodward, R.J., and Lundgren, R. (1964). "Clay Mineralogical Aspects of the Atterberg Limits," *Journal of Soil Mechanics and Foundations Division*, ASCE, Vol. 90, No. SM4, July, pp. 107-131.

22. Seed, R.B. and Duncan, J.M. (1986). "FE Analyses: Compaction-Induced Stresses and Deformations," *Journal of Geotechnical Engineering*, ASCE, Vol. 112, No. GT1, January, pp. 23-43.

23. Skempton, A.W. (1954). "The Pore-Pressure Coefficients A and B," *Geotechnique*, Vol. 4, No. 3, pp. 143-147.

24. Skempton, A.W. (1985). "Residual Strength of Clays in Landslides, Folded Strata and the Laboratory," *Geotechnique*, Vol. 35, No. 1, pp. 3-18.

# APPENDIX A

## Isotropically Consolidated-Drained Triaxial Test Results on Kaolinite-Silt Mixtures

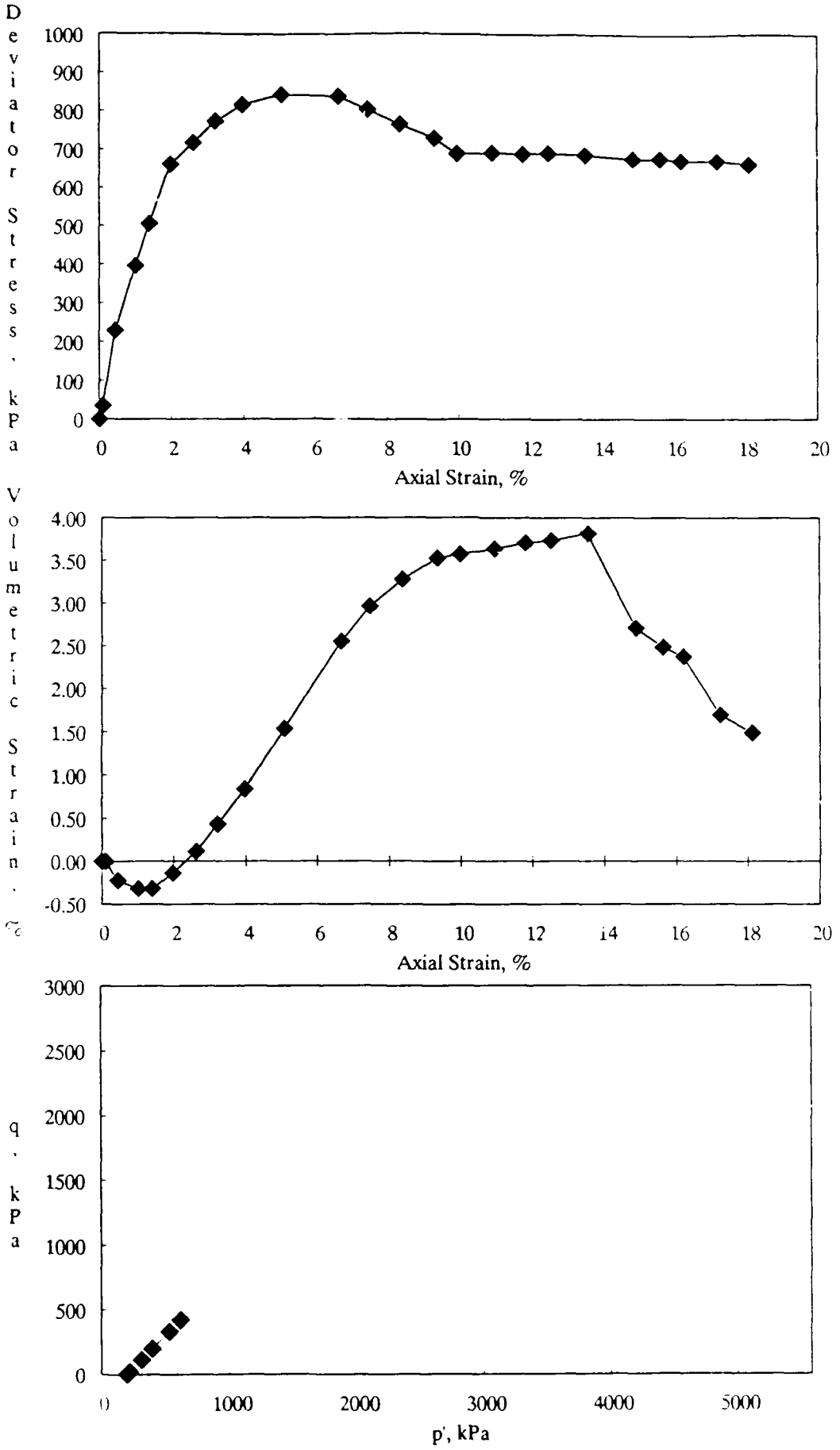


Figure A-1. CD Triaxial Test Results for 0% Kaolinite Mixture at a Standard Proctor Relative Compaction of 100% and an Effective Confining Pressure of 197 kPa.

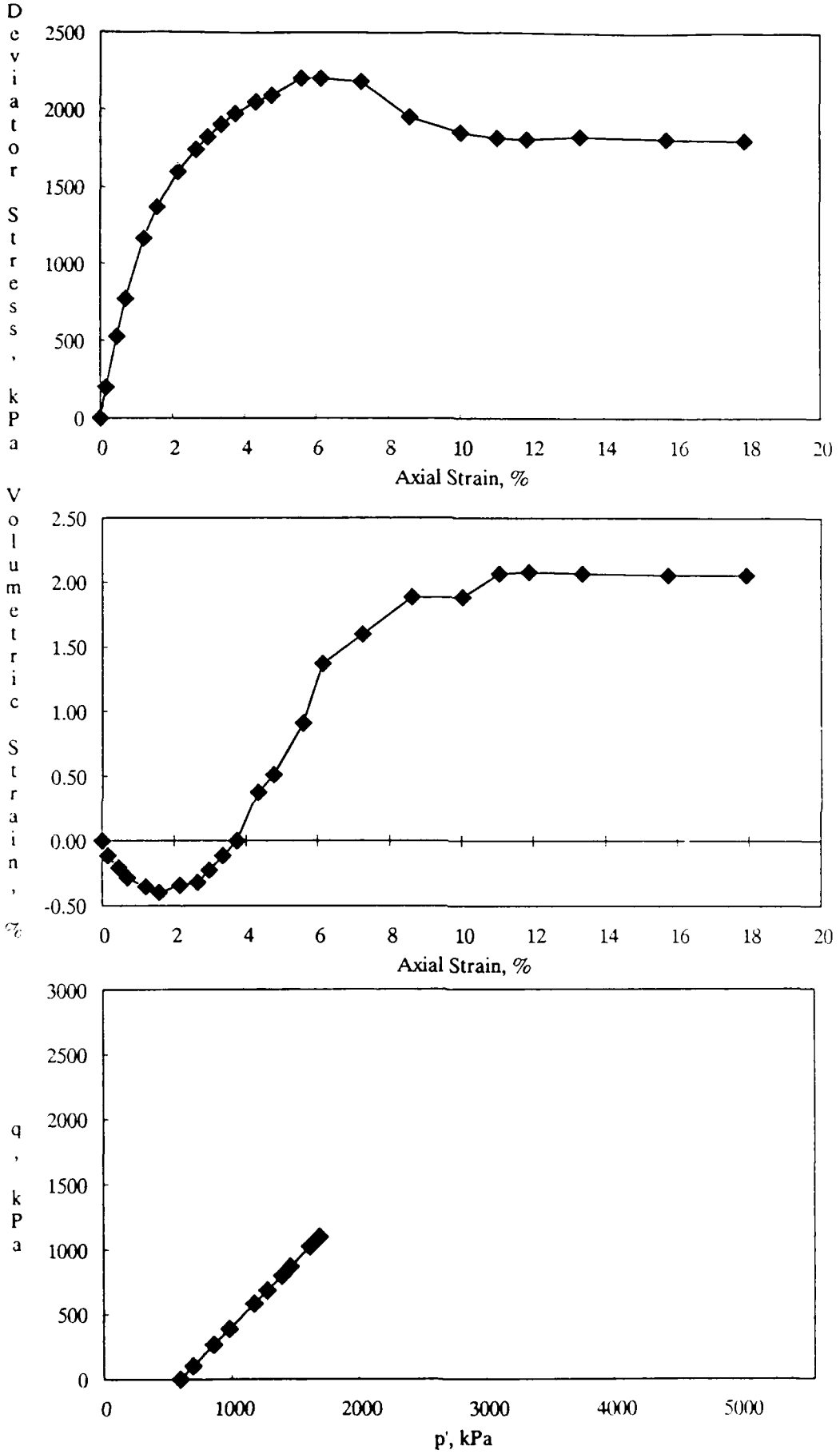


Figure A-2. CD Triaxial Test Results for 0% Kaolinite Mixture at a Standard Proctor Relative Compaction of 100% and an Effective Confining Pressure of 593 kPa.

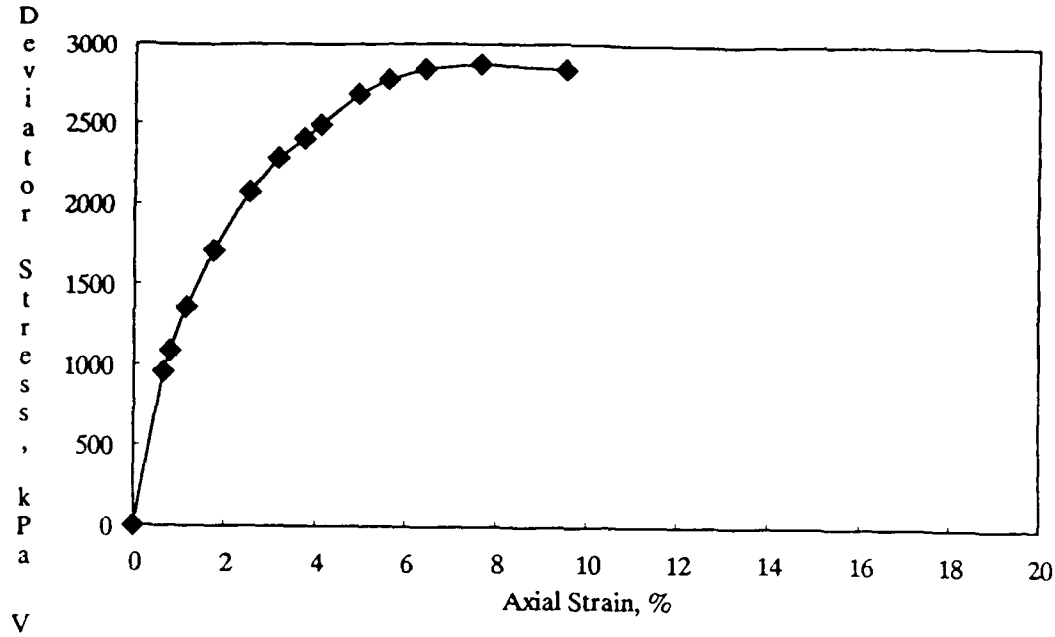


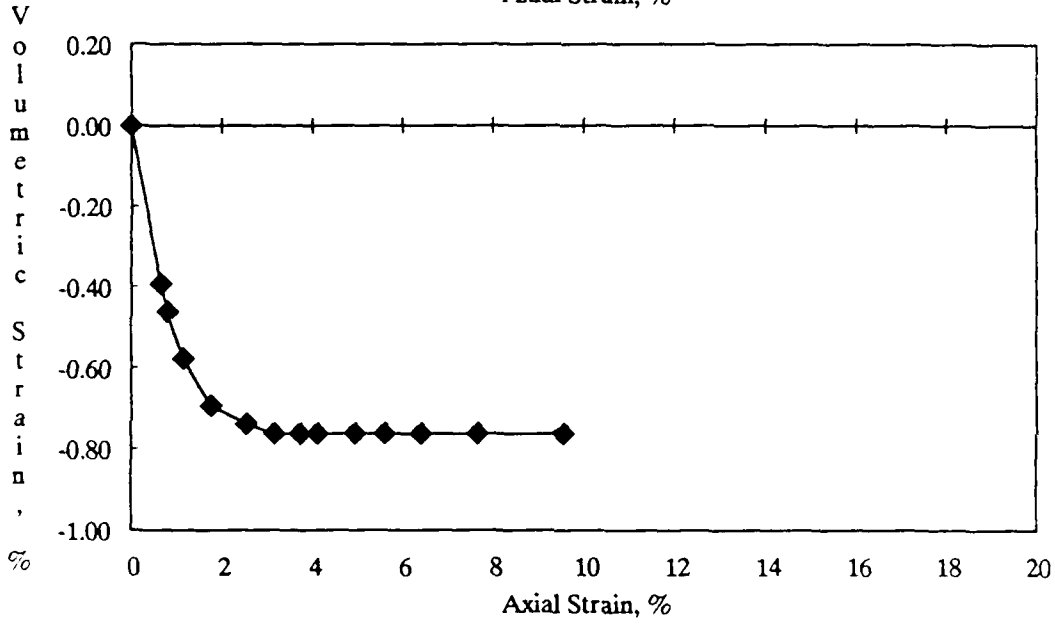


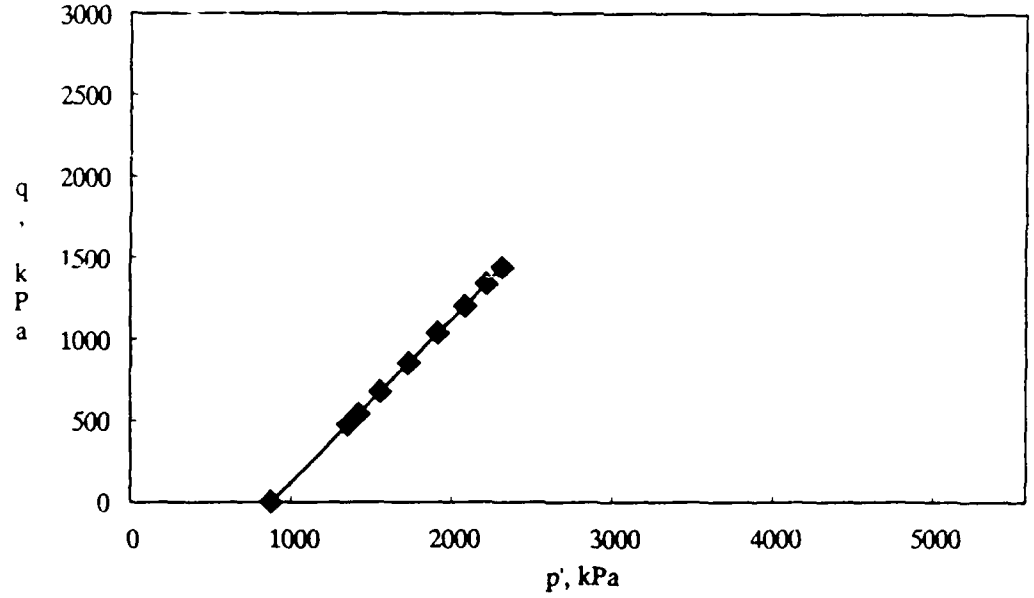


Figure A-3. CD Triaxial Test Results for 0% Kaolinite Mixture at a Standard Proctor Relative Compaction of 100% and an Effective Confining Pressure of 873 kPa.

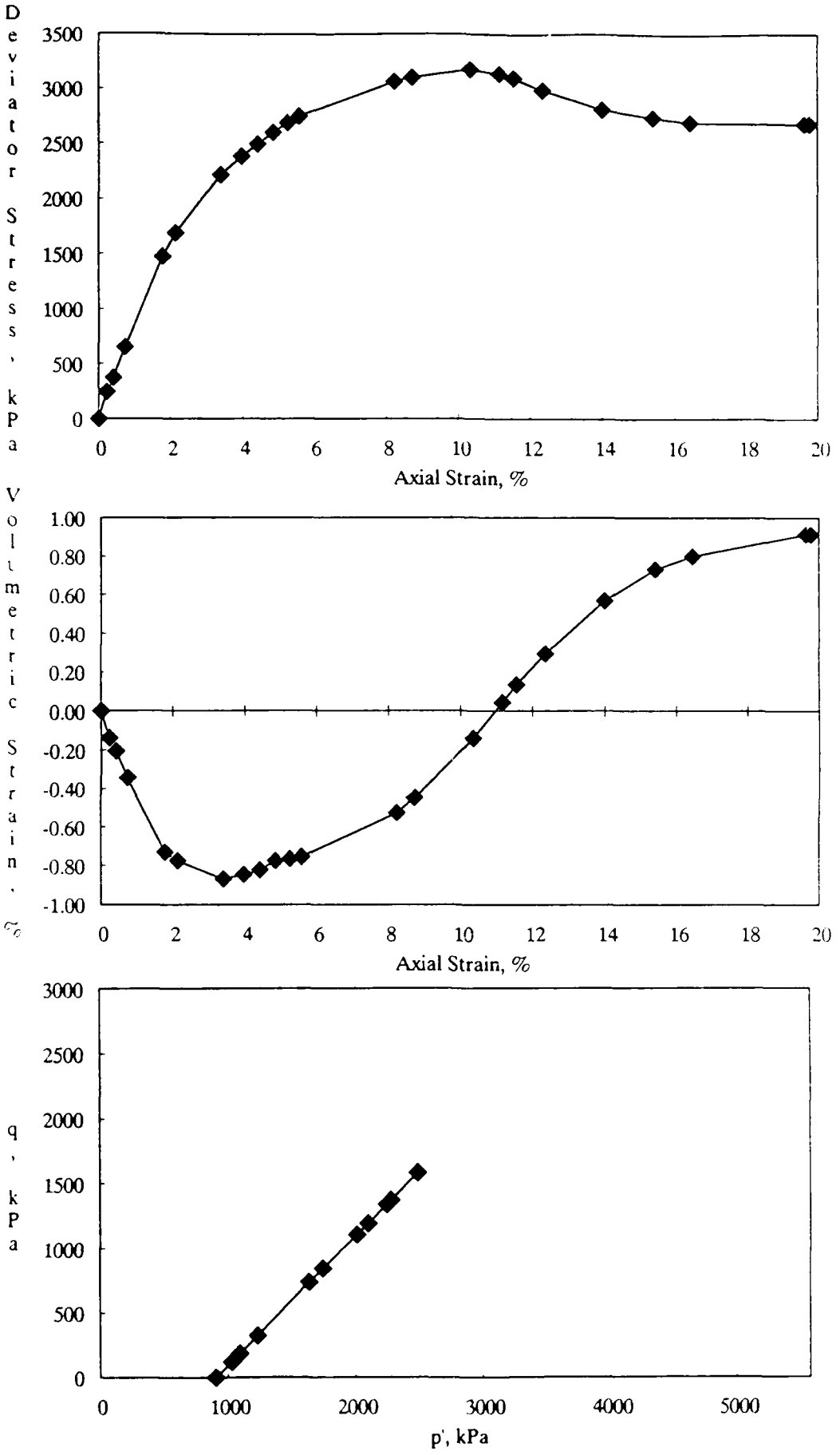


Figure A-4. **CD Triaxial Test Results for 0% Kaolinite Mixture at a Standard Proctor Relative Compaction of 100% and an Effective Confining Pressure of 905 kPa.**

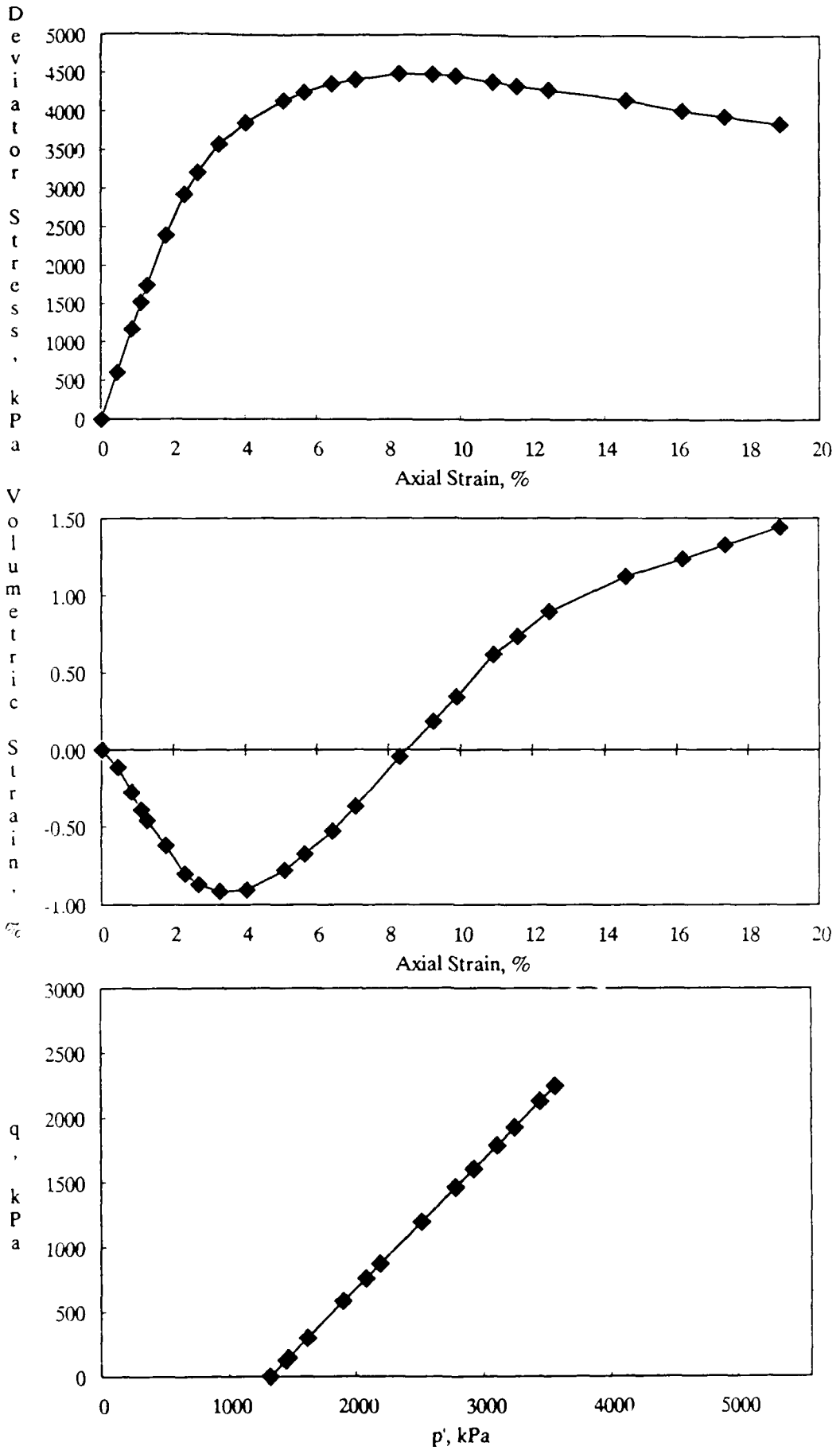


Figure A-5. CD Triaxial Test Results for 0% Kaolinite Mixture at a Standard Proctor Relative Compaction of 100% and an Effective Confining Pressure of 1319 kPa.

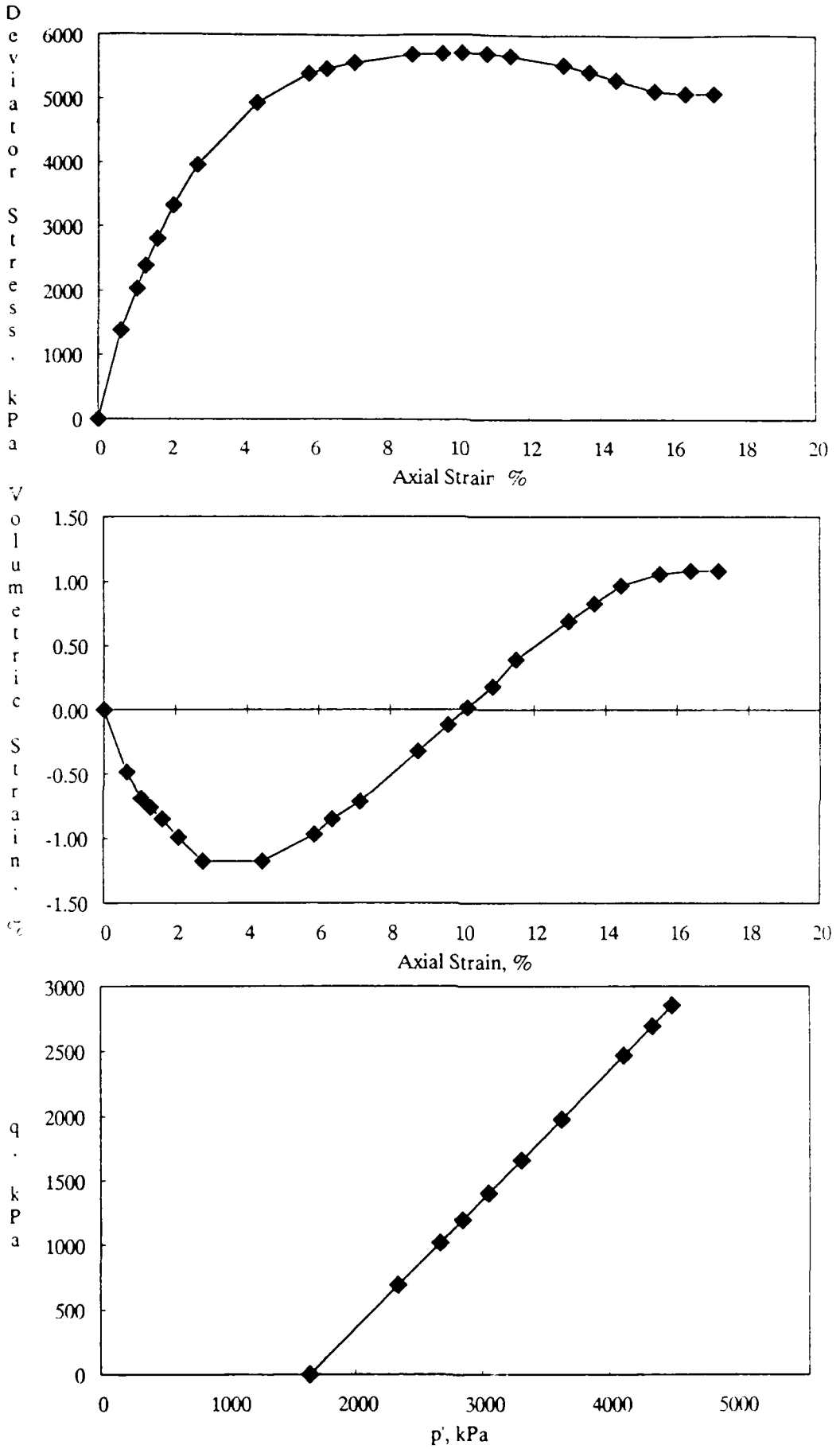


Figure A-6. CD Triaxial Test Results for 0% Kaolinite Mixture at a Standard Proctor Relative Compaction of 100% and an Effective Confining Pressure of 1642 kPa.

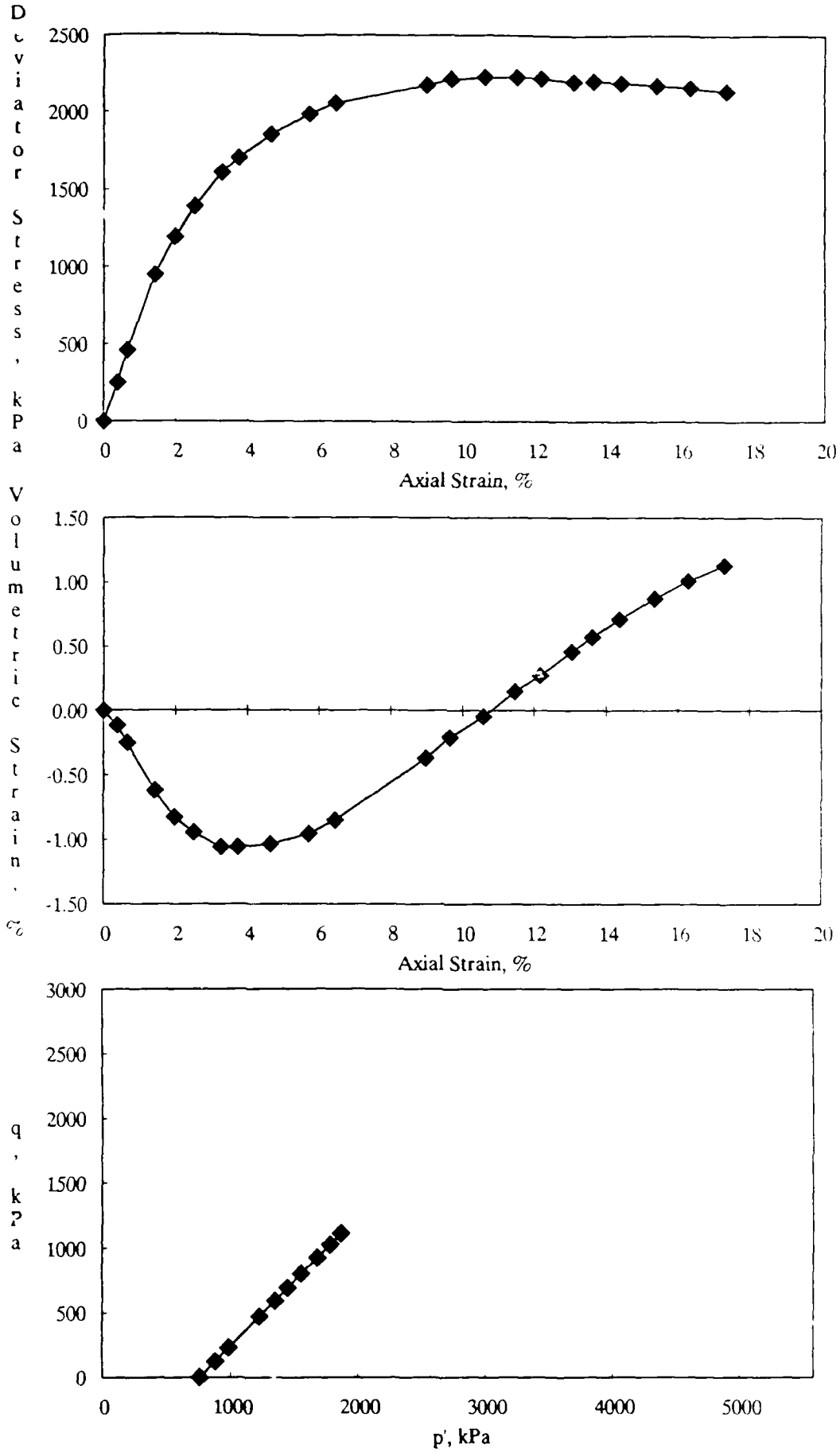


Figure A-7. **CD Triaxial Test Results for 0% Kaolinite Mixture at a Standard Proctor Relative Compaction of 95% and an Effective Confining Pressure of 754 kPa.**

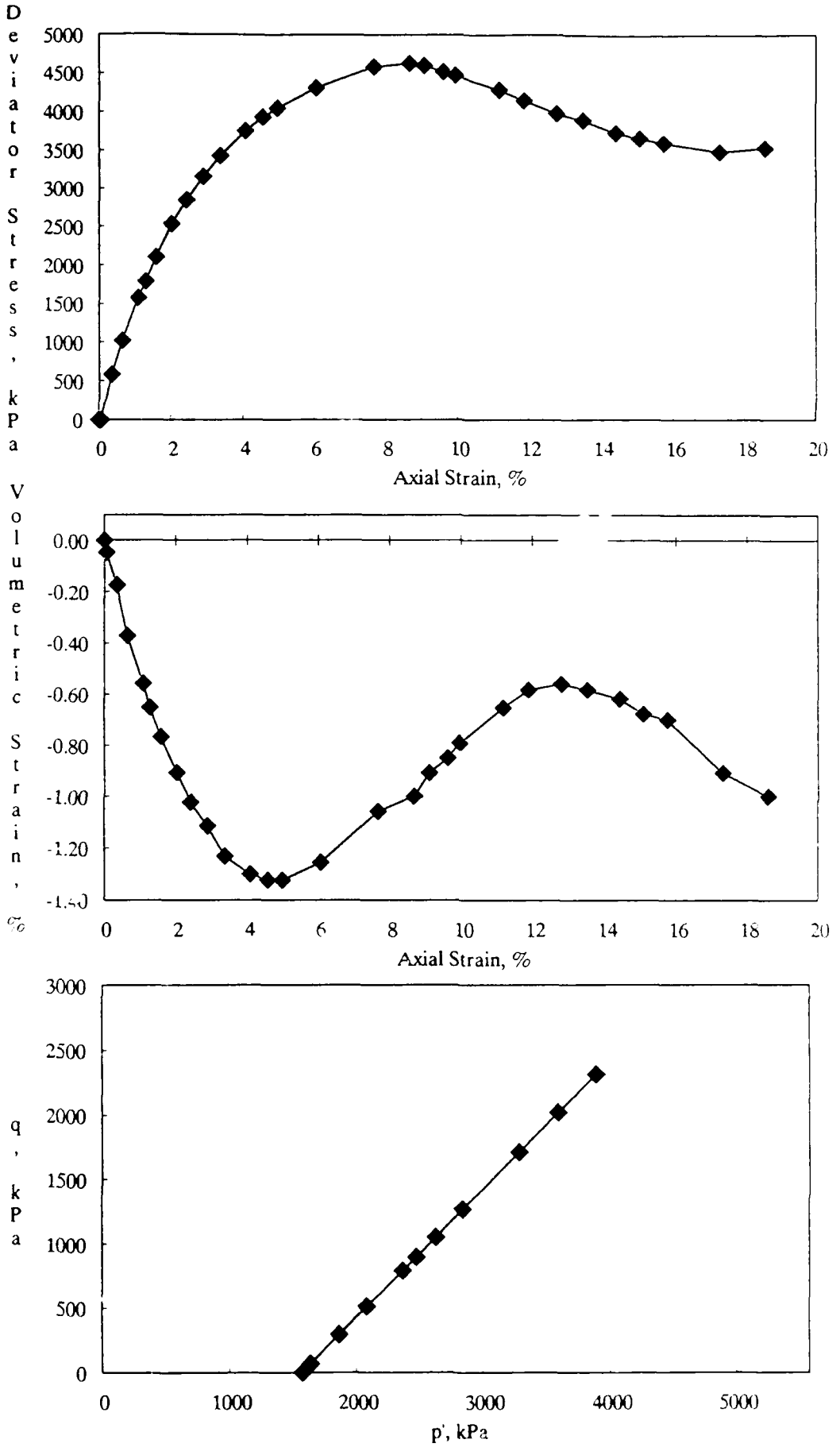


Figure A-8. CD Triaxial Test Results for 0% Kaolinite Mixture at a Standard Proctor Relative Compaction of 95% and an Effective Confining Pressure of 1572 kPa.

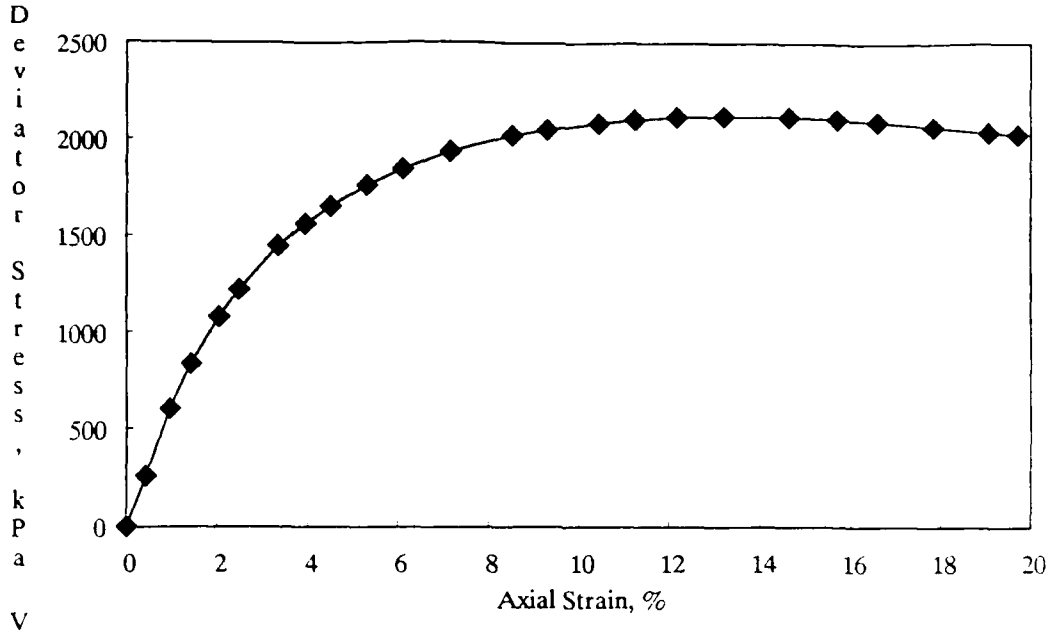


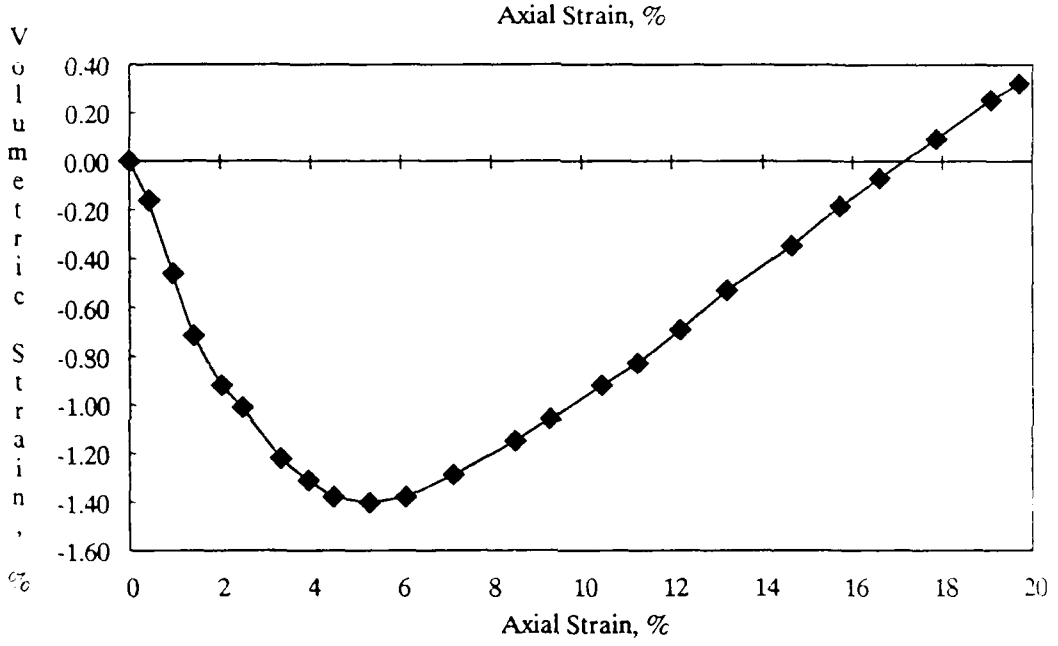


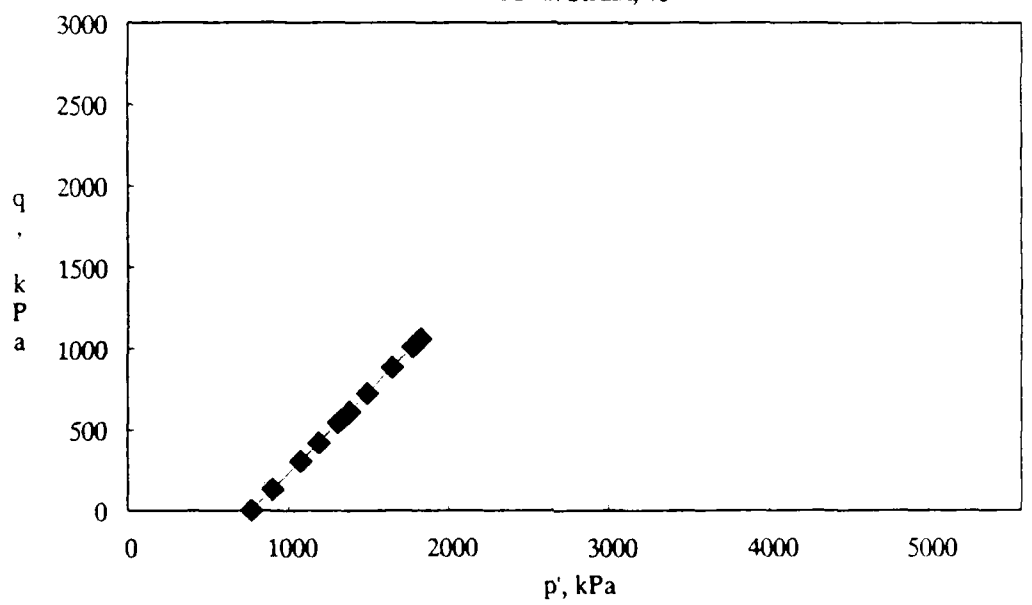


Figure A-9. CD Triaxial Test Results for 0% Kaolinite Mixture at a Standard Proctor Relative Compaction of 90% and an Effective Confining Pressure of 766 kPa.

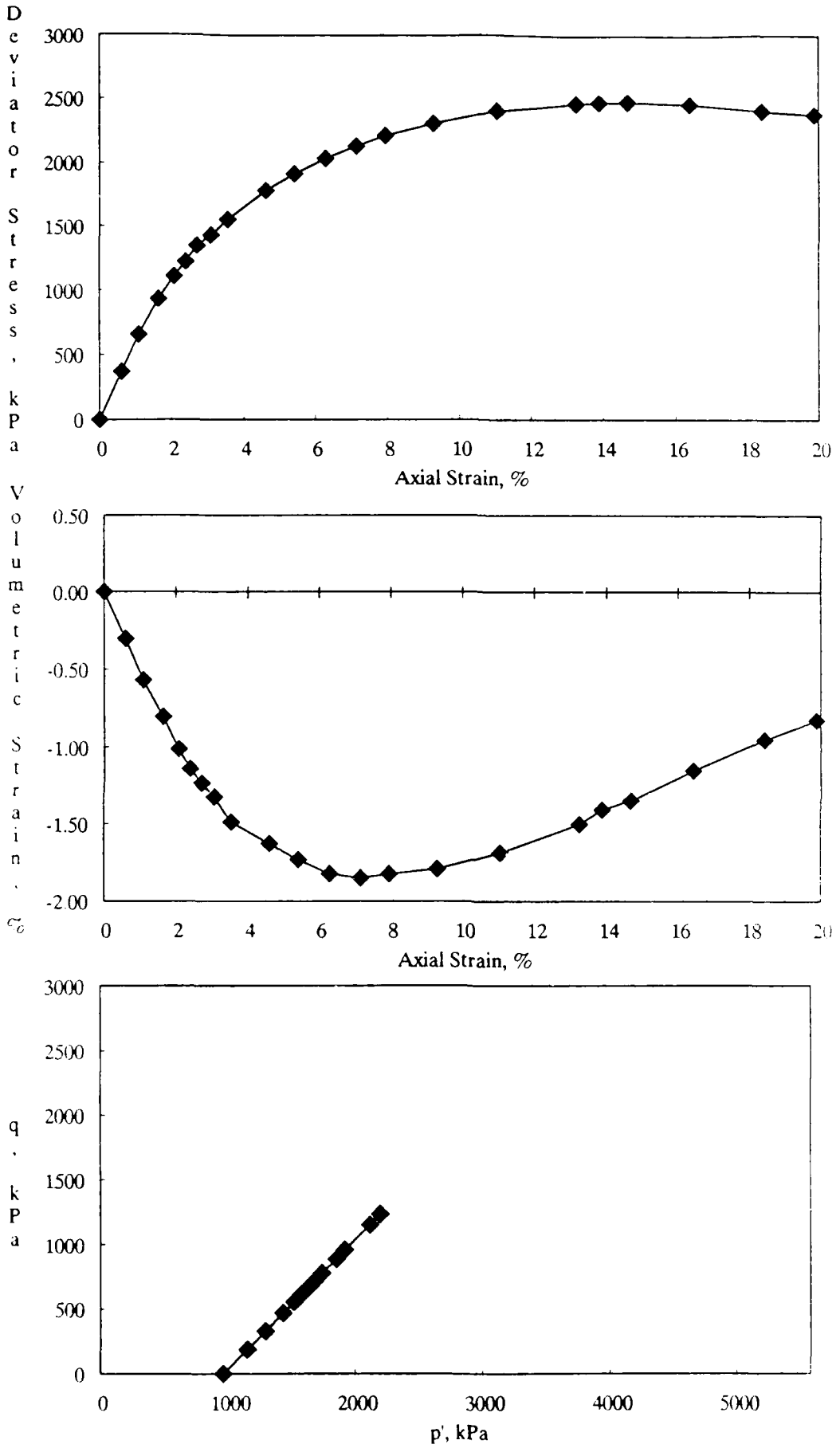


Figure A-10. CD Triaxial Test Results for 0% Kaolinite Mixture at a Standard Proctor Relative Compaction of 90% and an Effective Confining Pressure of 951 kPa.

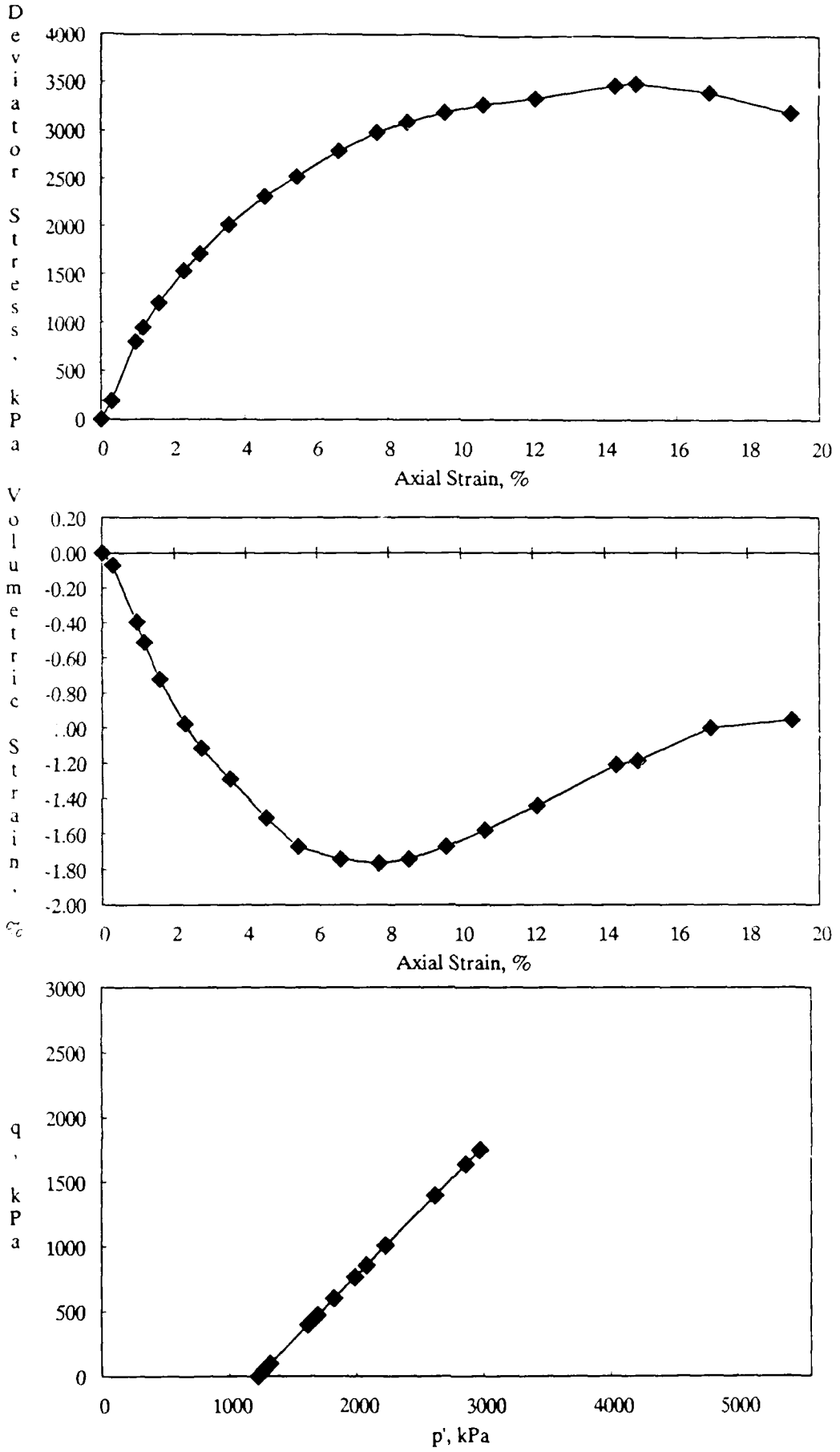


Figure A-11. CD Triaxial Test Results for 0% Kaolinite Mixture at a Standard Proctor Relative Compaction of 90% and an Effective Confining Pressure of 1222 kPa.

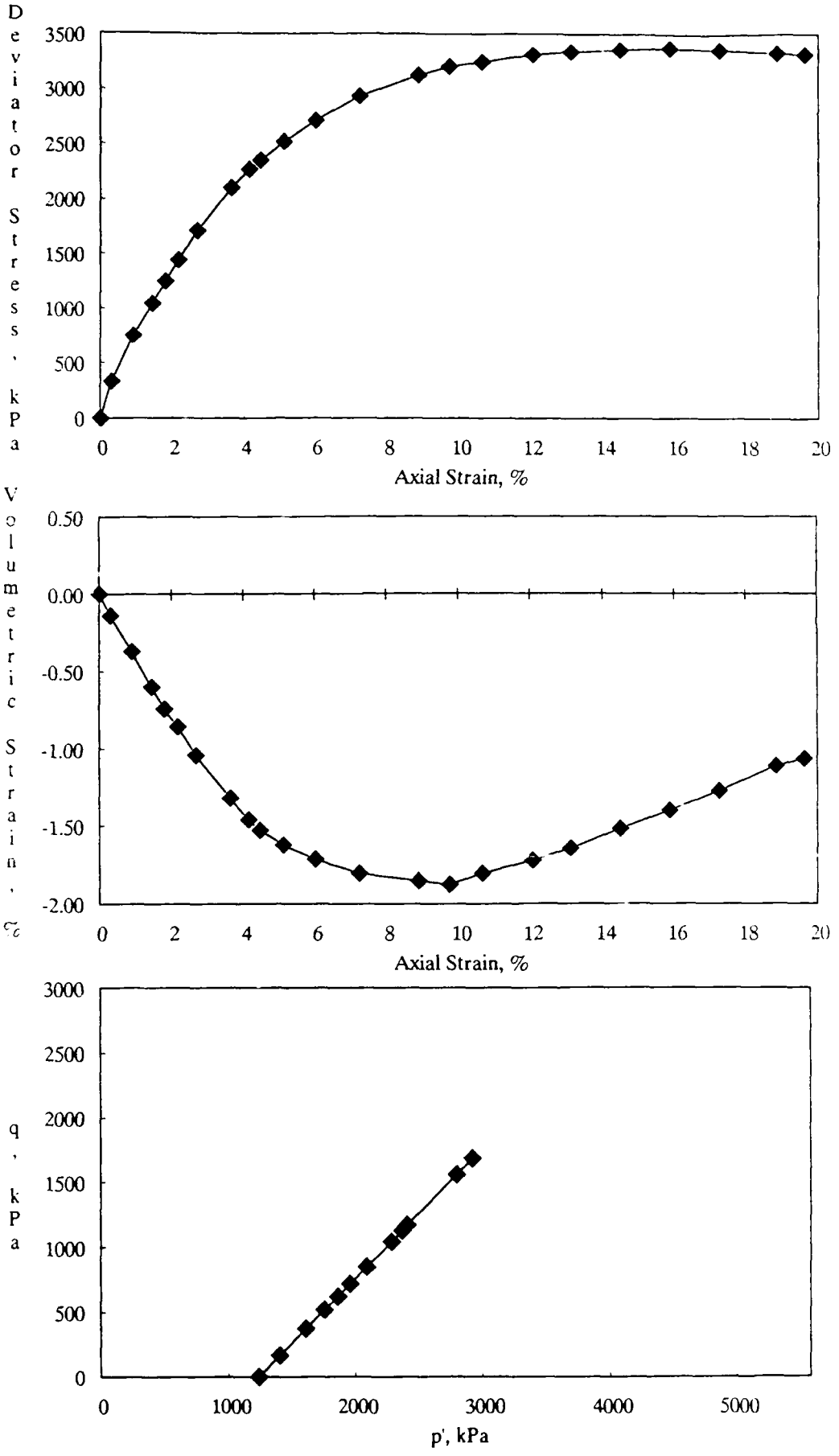


Figure A-12. CD Triaxial Test Results for 0% Kaolinite Mixture at a Standard Proctor Relative Compaction of 90% and an Effective Confining Pressure of 1236 kPa.

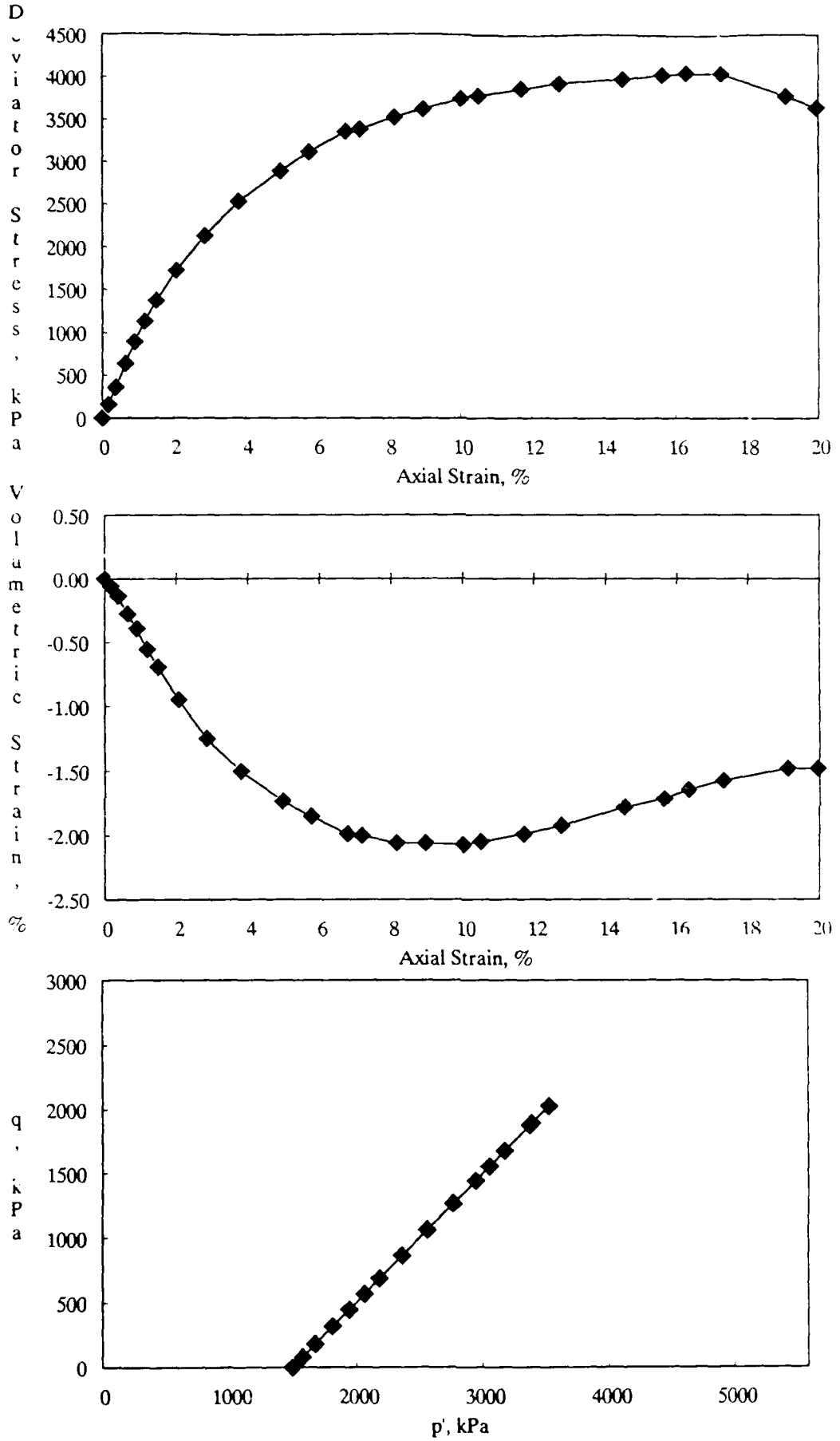


Figure A-13. CD Triaxial Test Results for 0% Kaolinite Mixture at a Standard Proctor Relative Compaction of 90% and an Effective Confining Pressure of 1494 kPa.

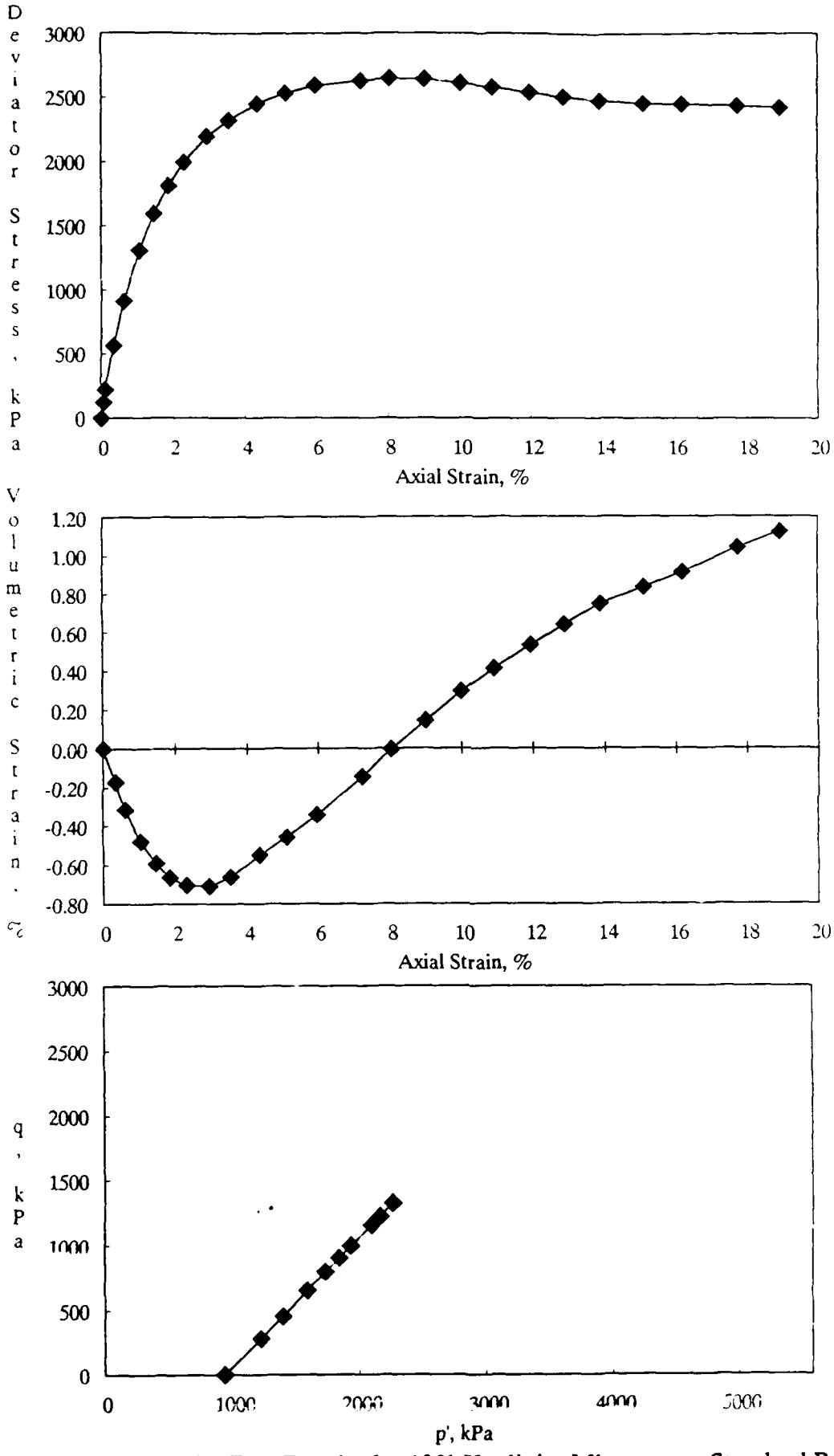


Figure A-14. CD Triaxial Test Results for 10% Kaolinite Mixture at a Standard Proctor Relative Compaction of 100% and an Effective Confining Pressure of 937 kPa.

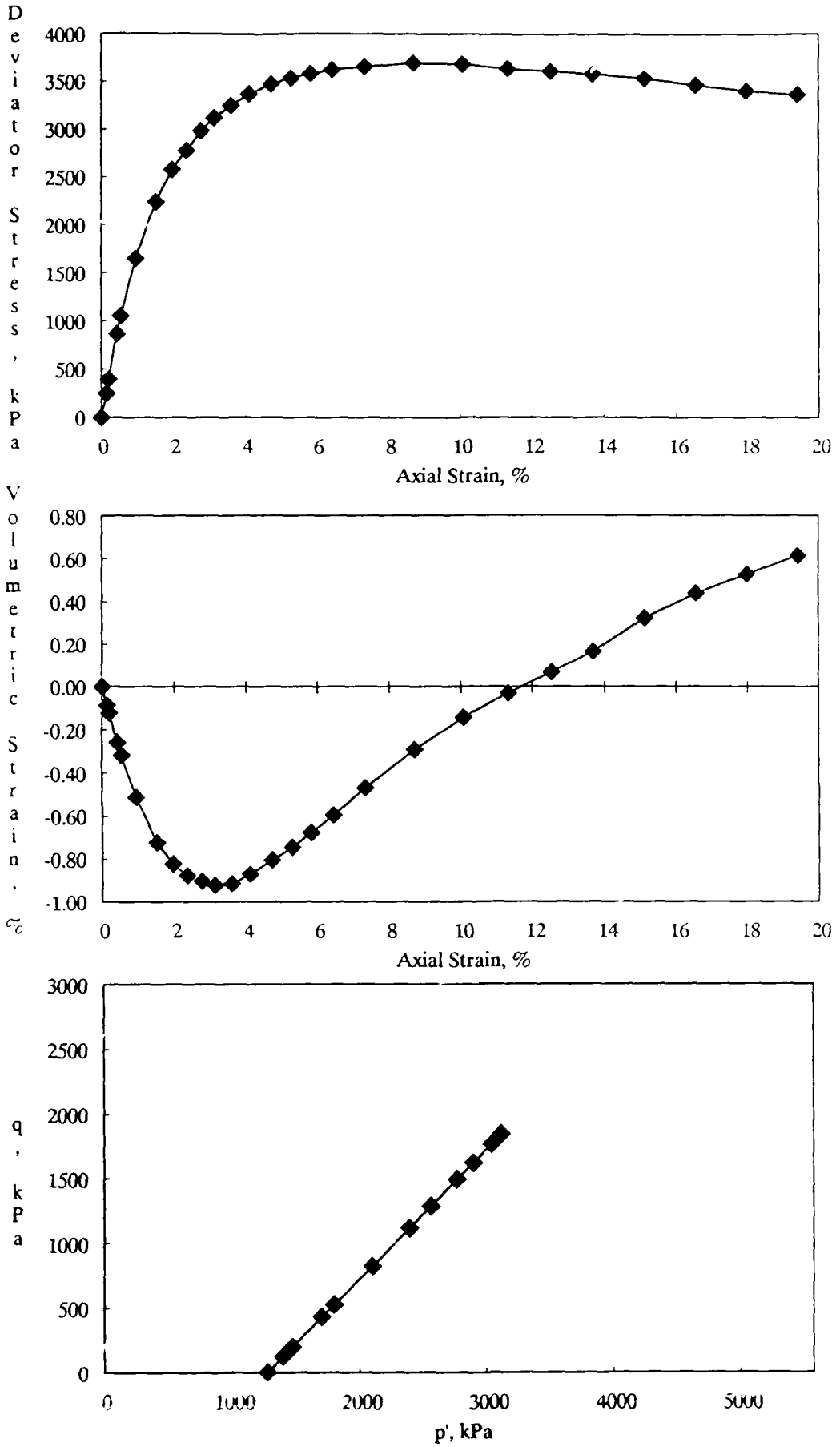


Figure A-15. CD Triaxial Test Results for 10% Kaolinite Mixture at a Standard Proctor Relative Compaction of 100% and an Effective Confining Pressure of 1274 kPa.

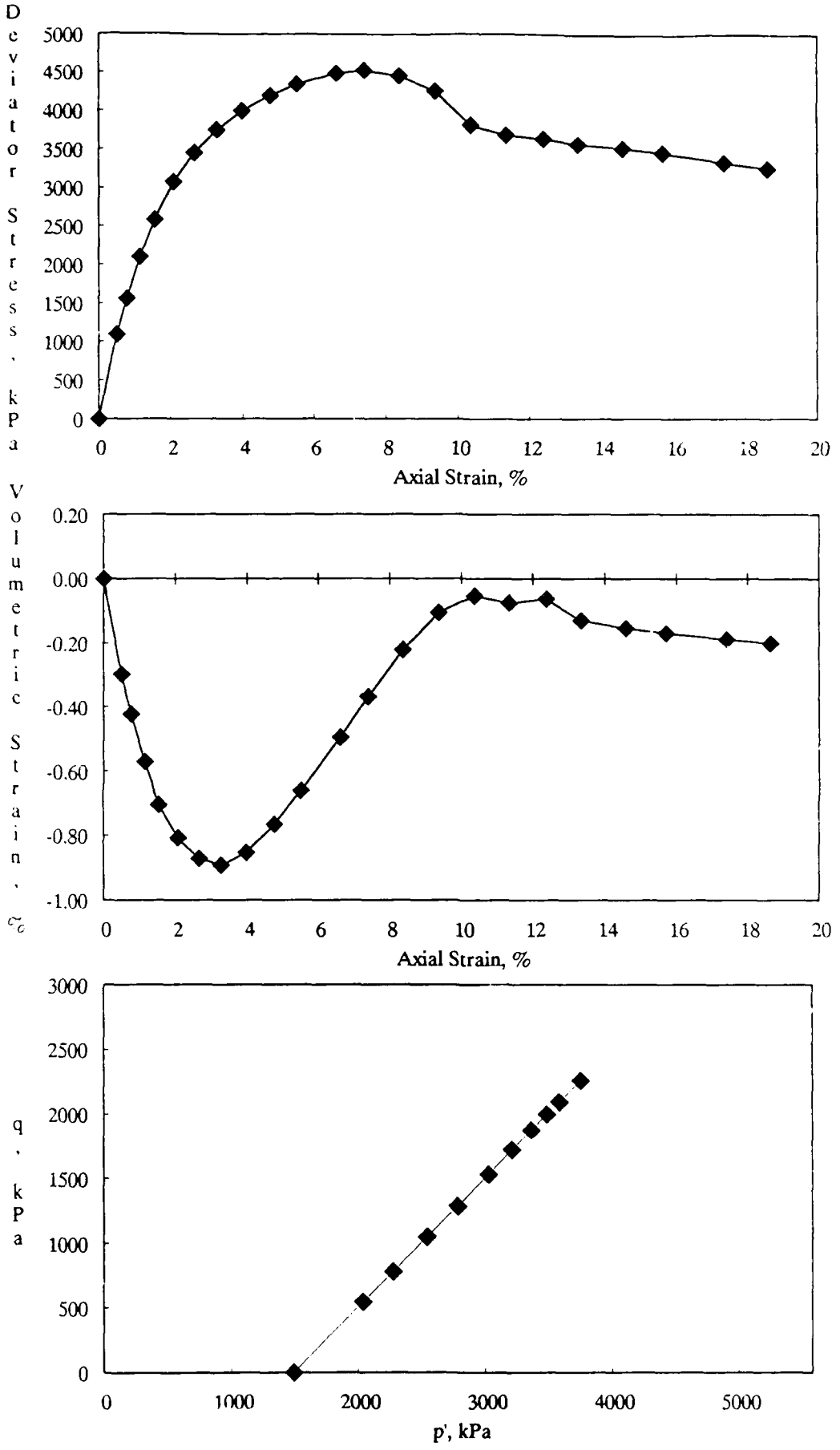


Figure A-16. CD Triaxial Test Results for 10% Kaolinite Mixture at a Standard Proctor Relative Compaction of 100% and an Effective Confining Pressure of 1492 kPa.

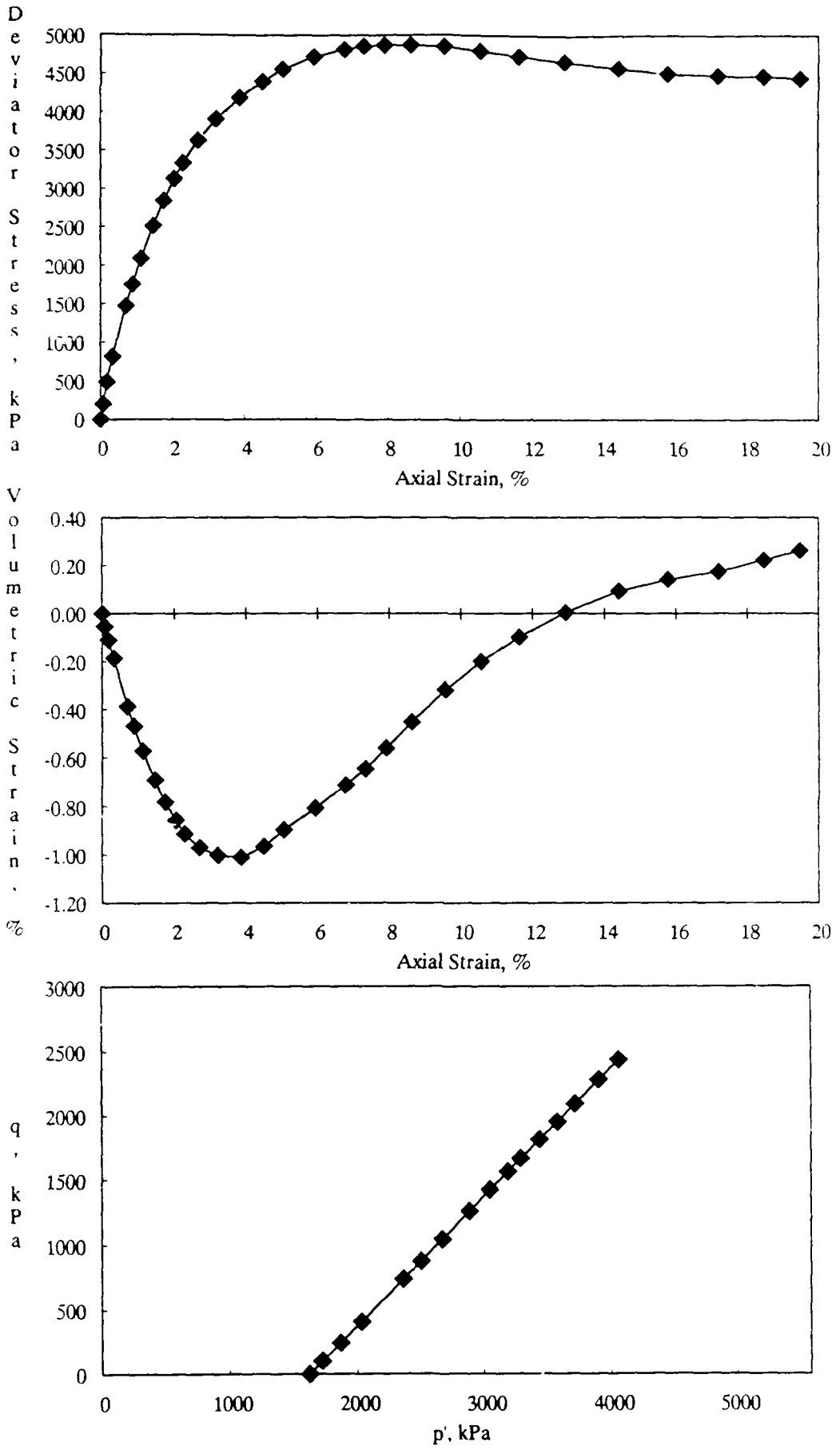


Figure A-17. CD Triaxial Test Results for 10% Kaolinite Mixture at a Standard Proctor Relative Compaction of 100% and an Effective Confining Pressure of 1624 kPa.

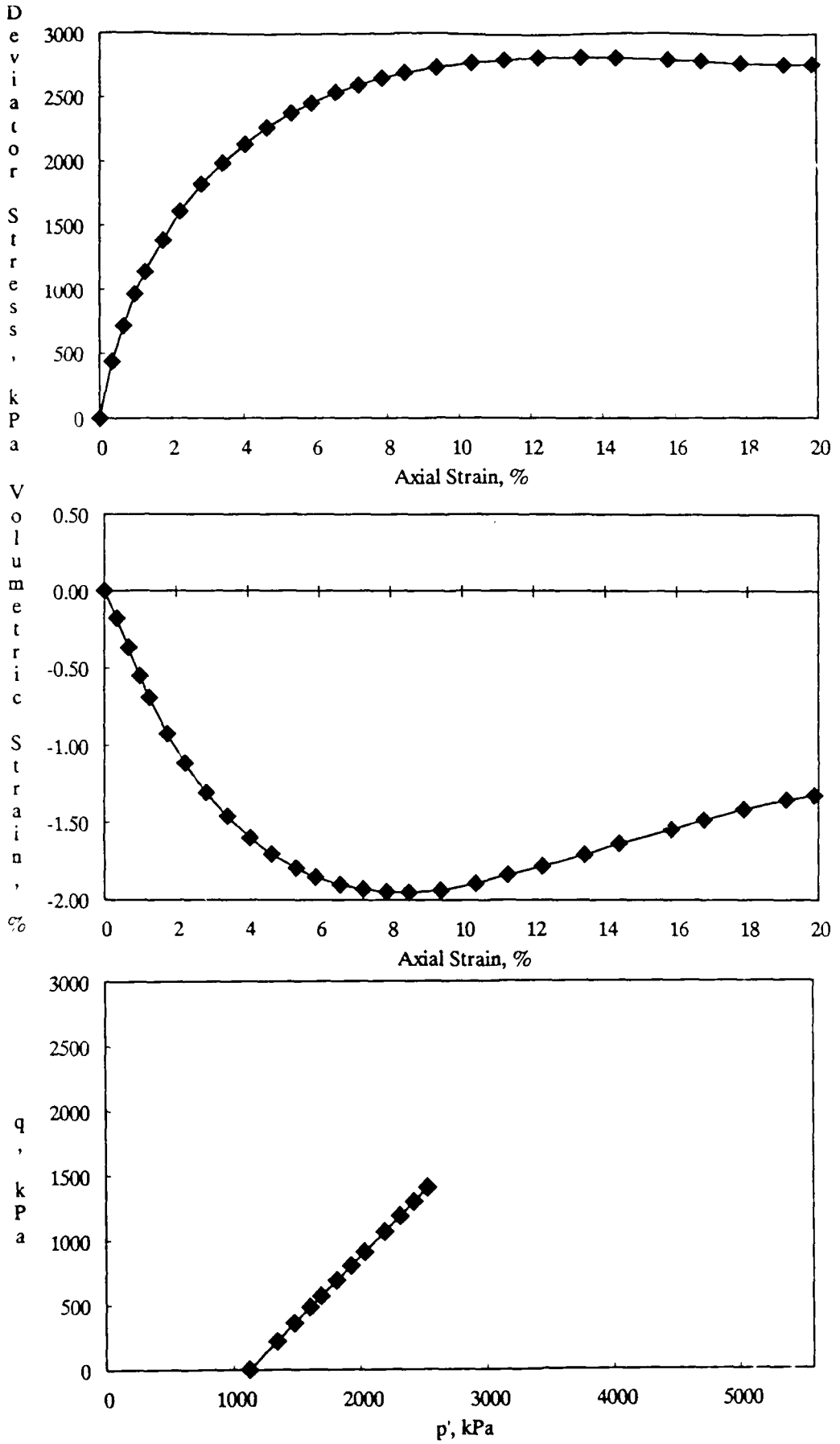


Figure A-18. CD Triaxial Test Results for 10% Kaolinite Mixture at a Standard Proctor Relative Compaction of 95% and an Effective Confining Pressure of 1119 kPa.

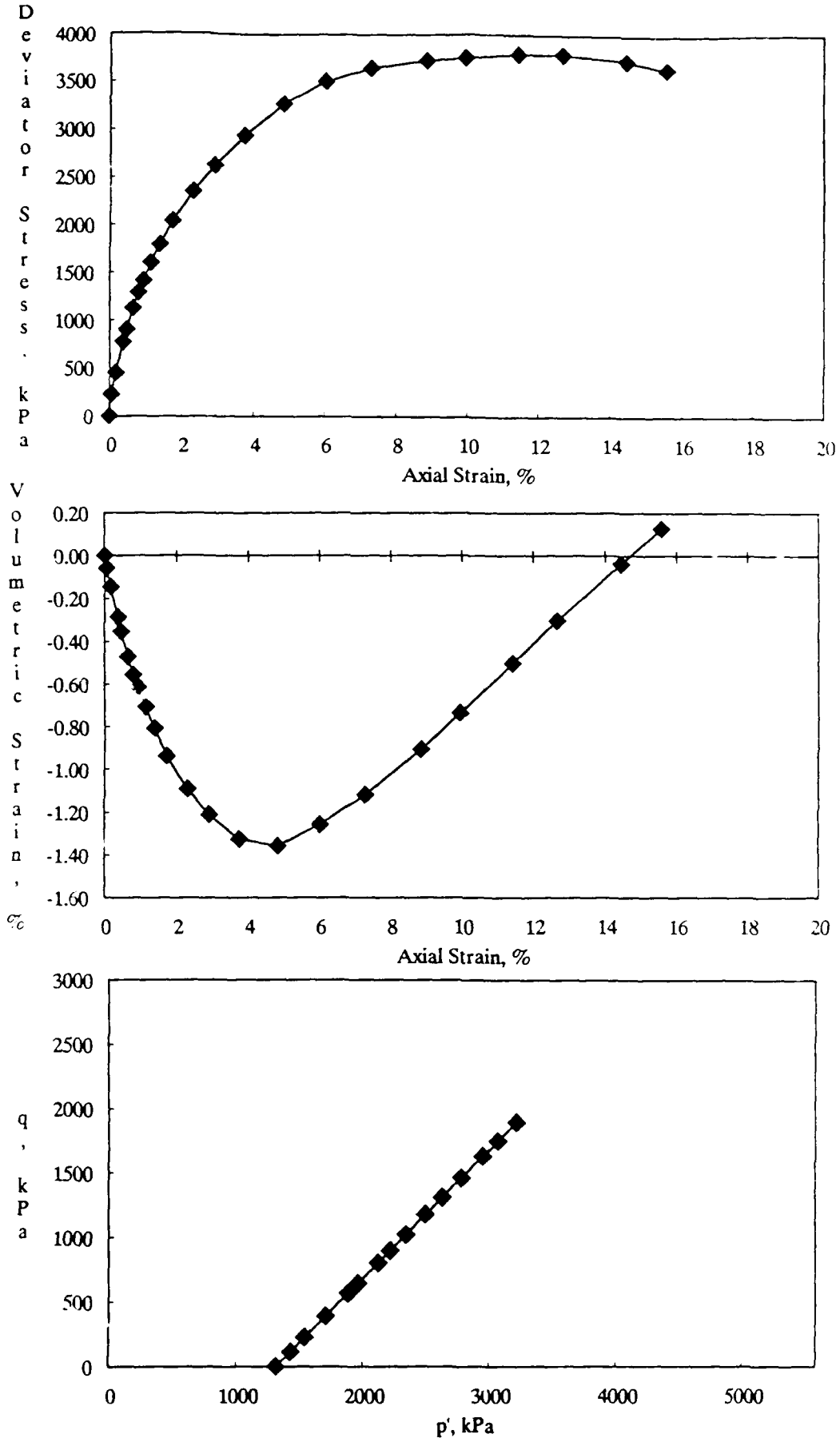


Figure A-19. CD Triaxial Test Results for 10% Kaolinite Mixture at a Standard Proctor Relative Compaction of 95% and an Effective Confining Pressure of 1315 kPa.

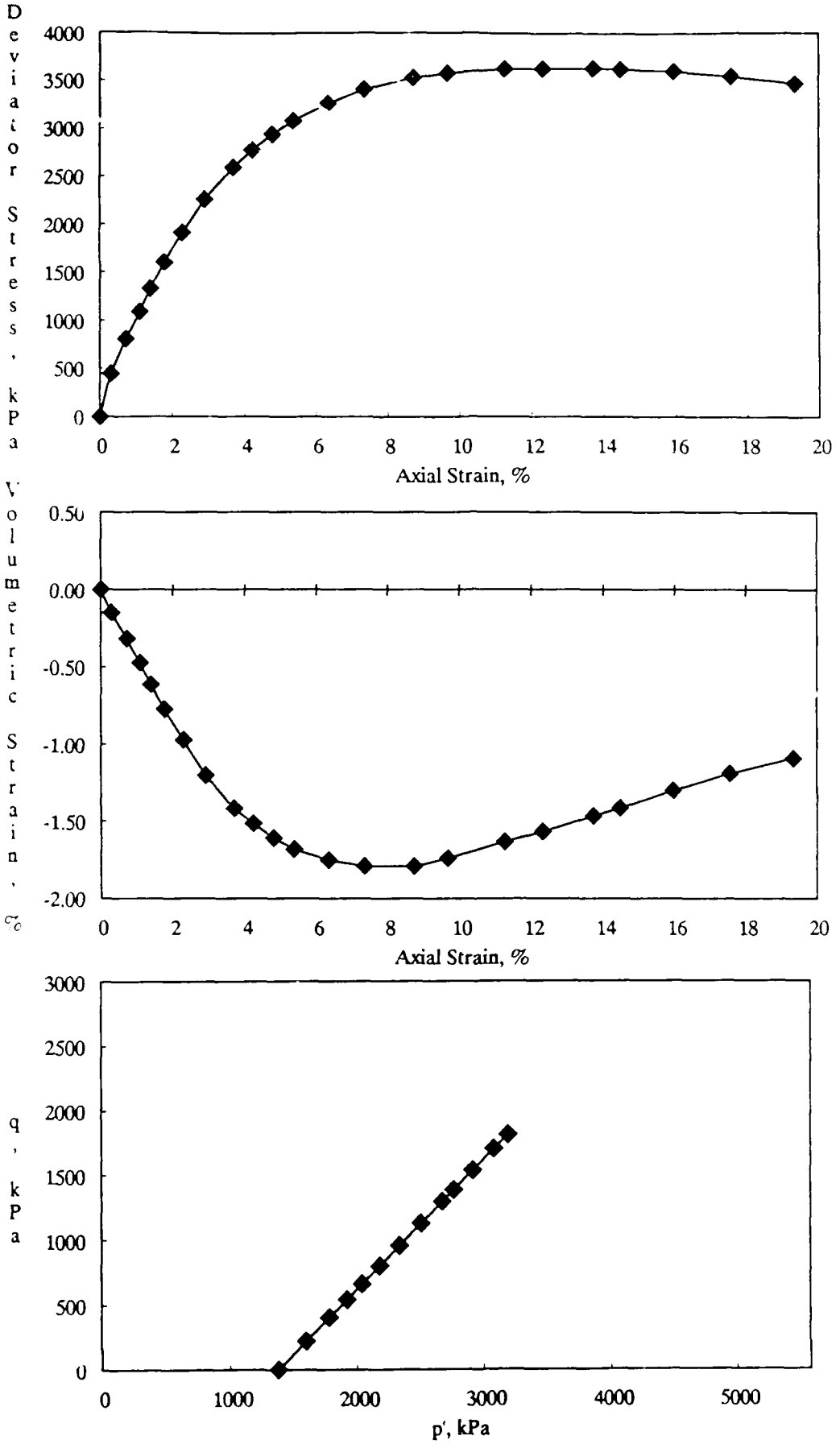


Figure A-20. CD Triaxial Test Results for 10% Kaolinite Mixture at a Standard Proctor Relative Compaction of 95% and an Effective Confining Pressure of 1379 kPa.

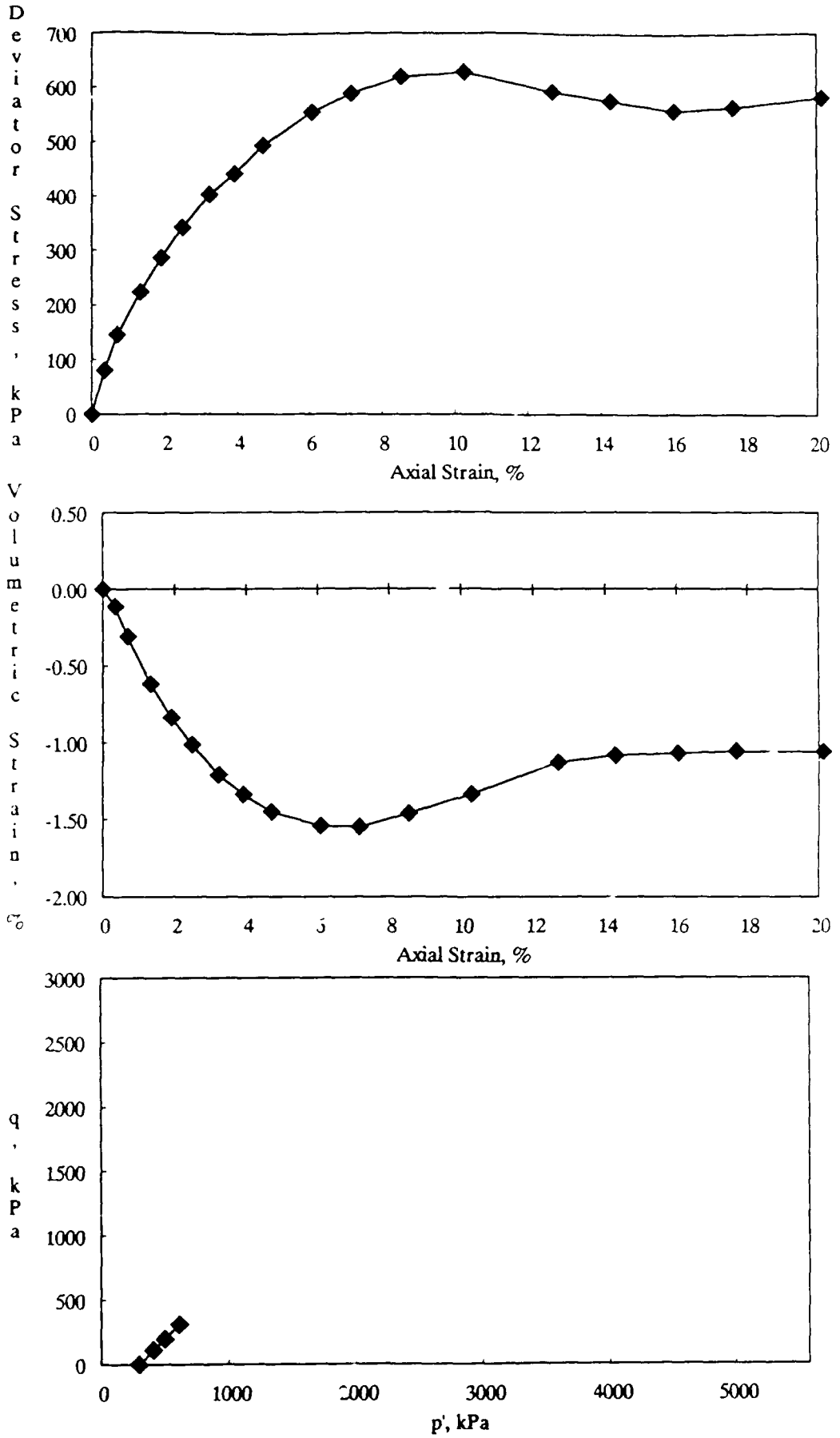


Figure A-21. CD Triaxial Test Results for 10% Kaolinite Mixture at a Standard Proctor Relative Compaction of 90% and an Effective Confining Pressure of 294 kPa.

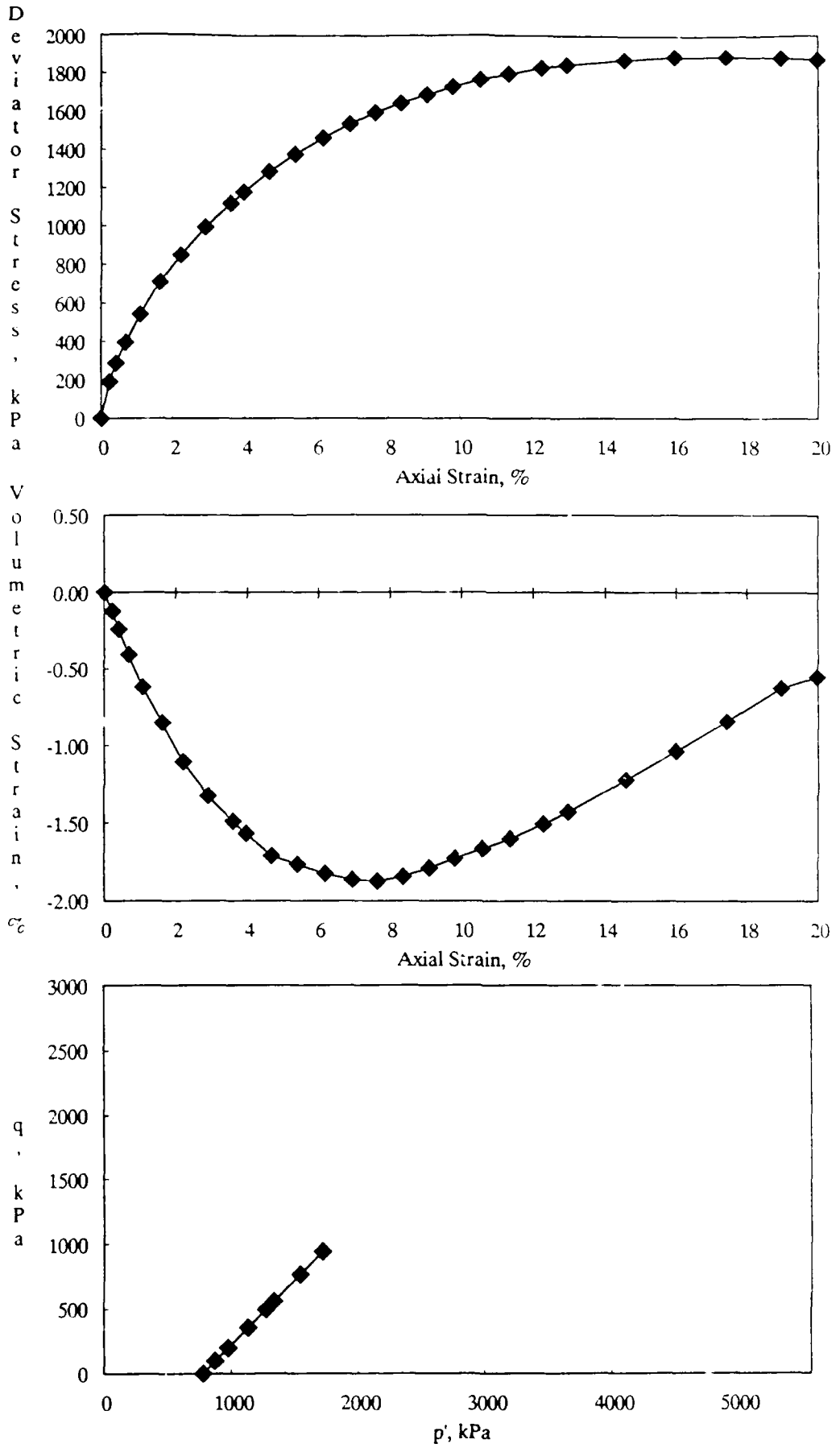


Figure A-22. CD Triaxial Test Results for 10% Kaolinite Mixture at a Standard Proctor Relative Compaction of 90% and an Effective Confining Pressure of 744 kPa.

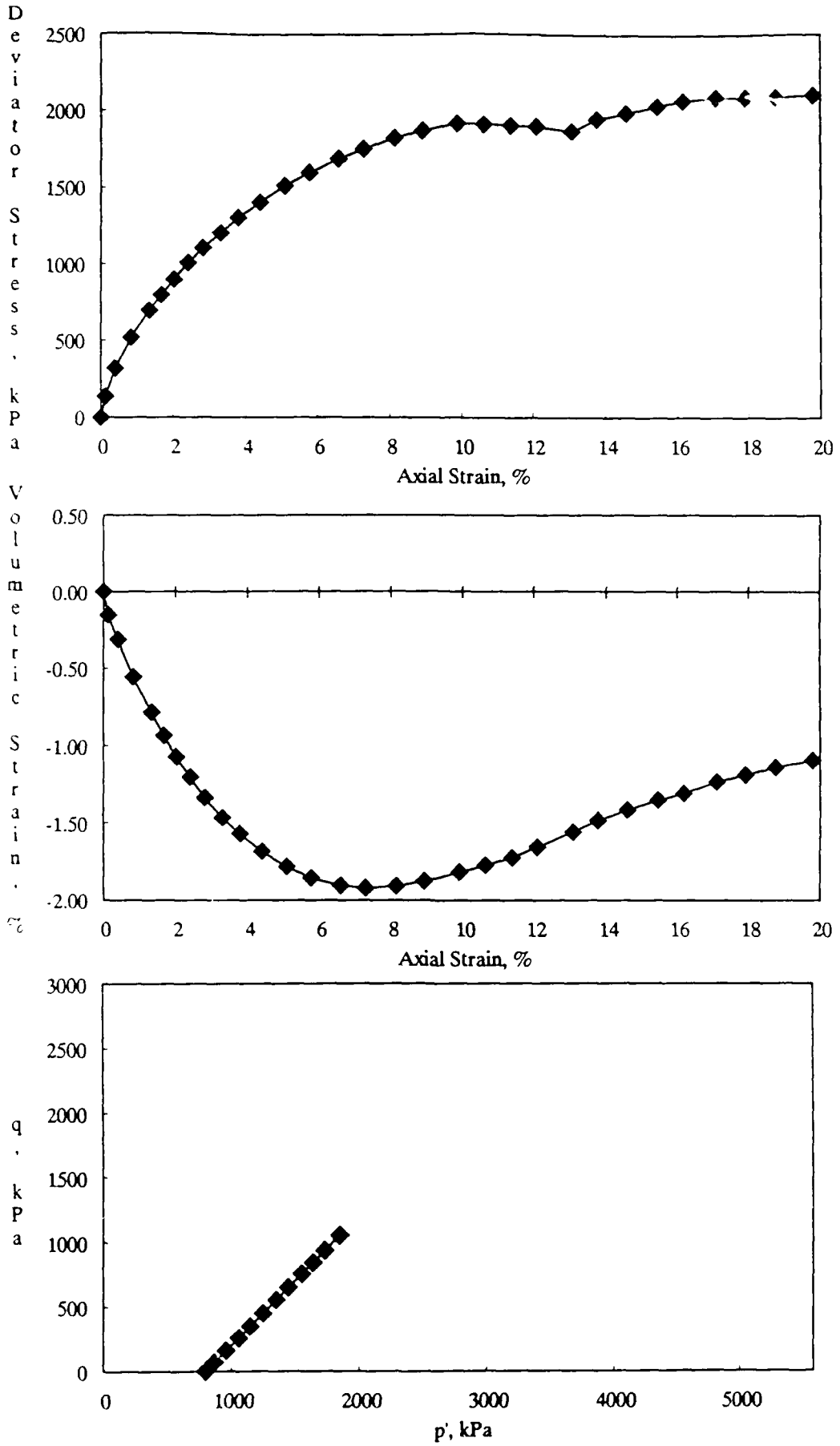


Figure A-23. CD Triaxial Test Results for 10% Kaolinite Mixture at a Standard Proctor Relative Compaction of 90% and an Effective Confining Pressure of 795 kPa.

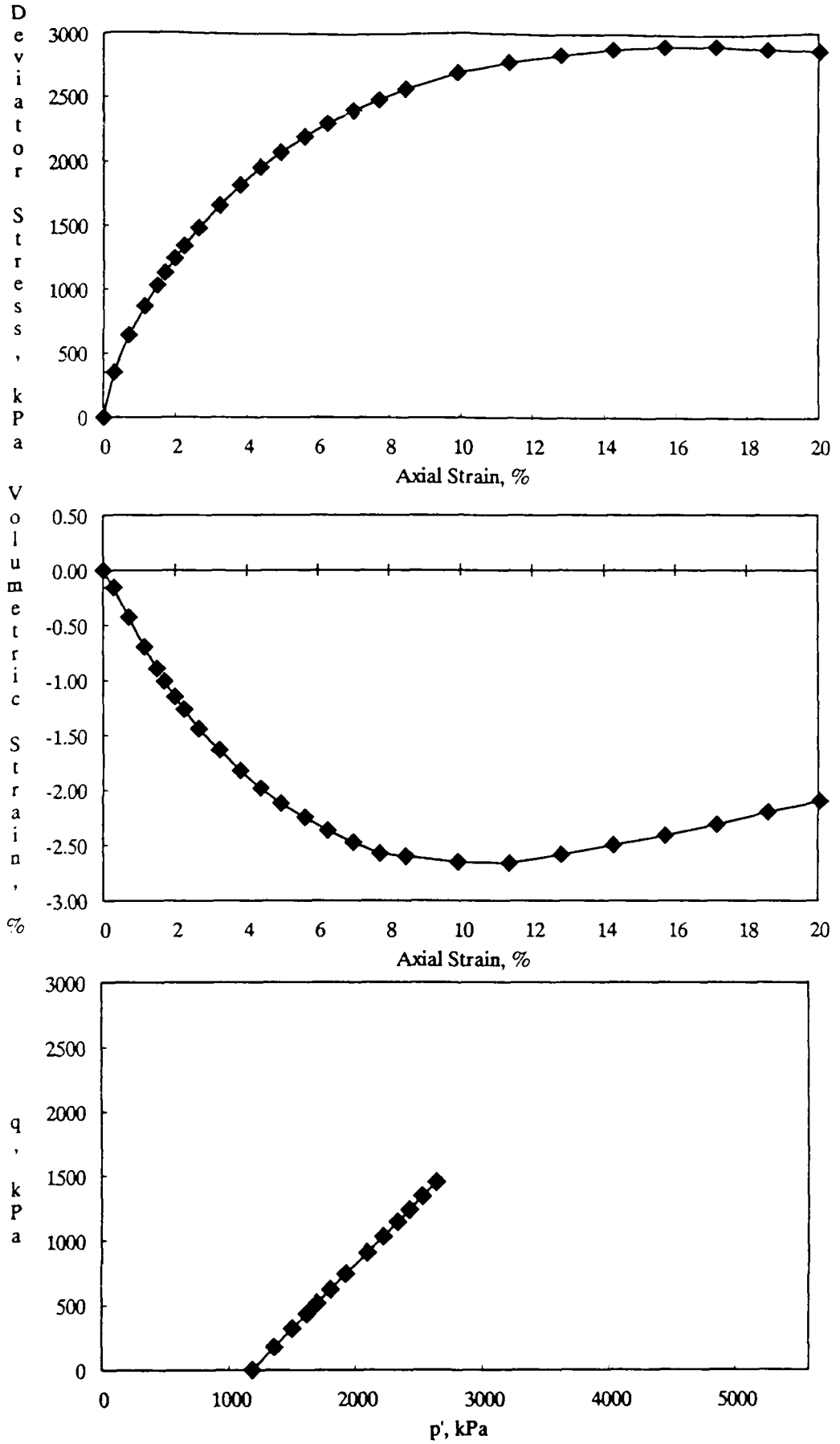


Figure A-24. CD Triaxial Test Results for 10% Kaolinite Mixture at a Standard Proctor Relative Compaction of 90% and an Effective Confining Pressure of 1183 kPa.

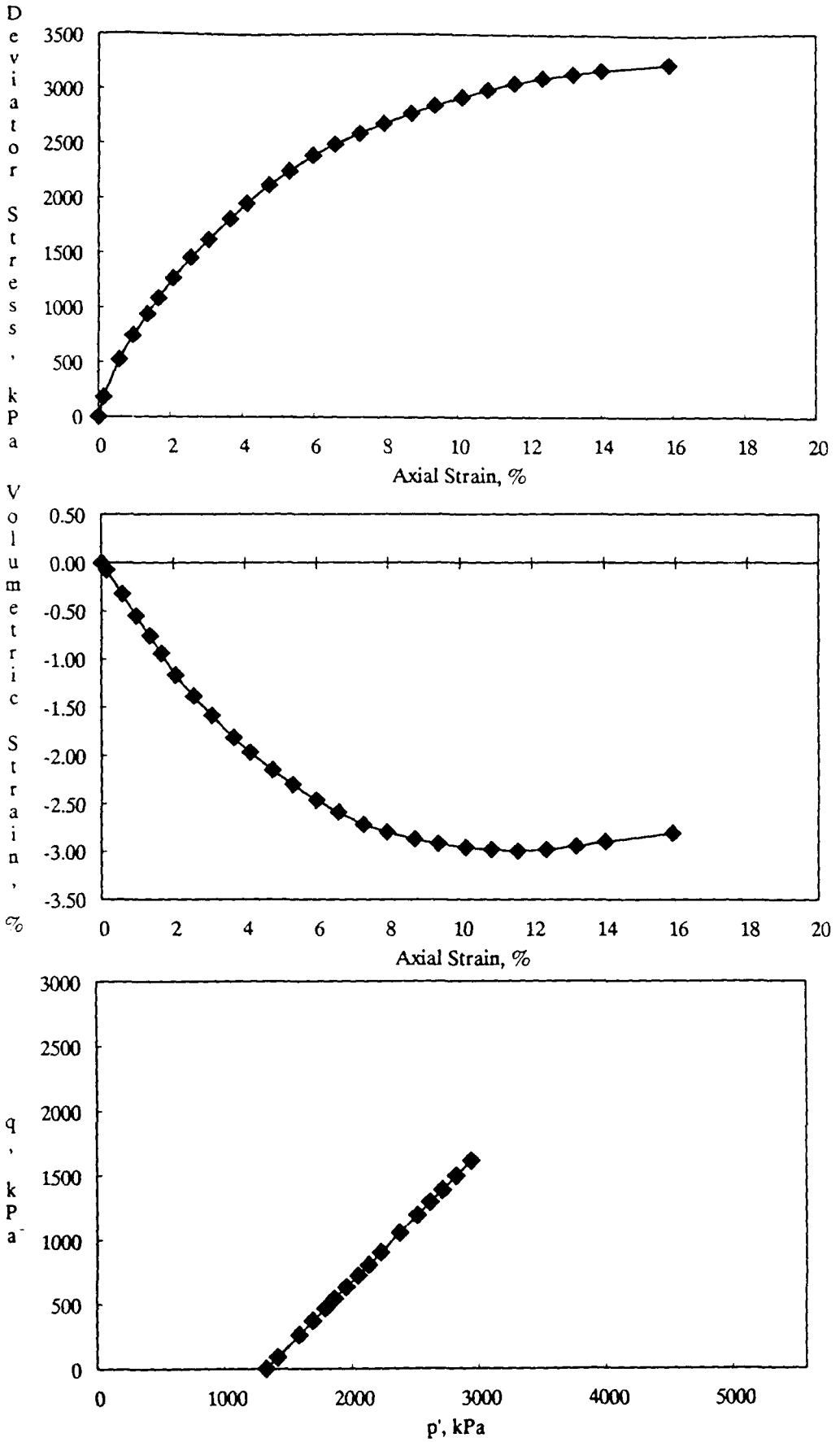


Figure A-25. CD Triaxial Test Results for 10% Kaolinite Mixture at a Standard Proctor Relative Compaction of 90% and an Effective Confining Pressure of 1323 kPa.

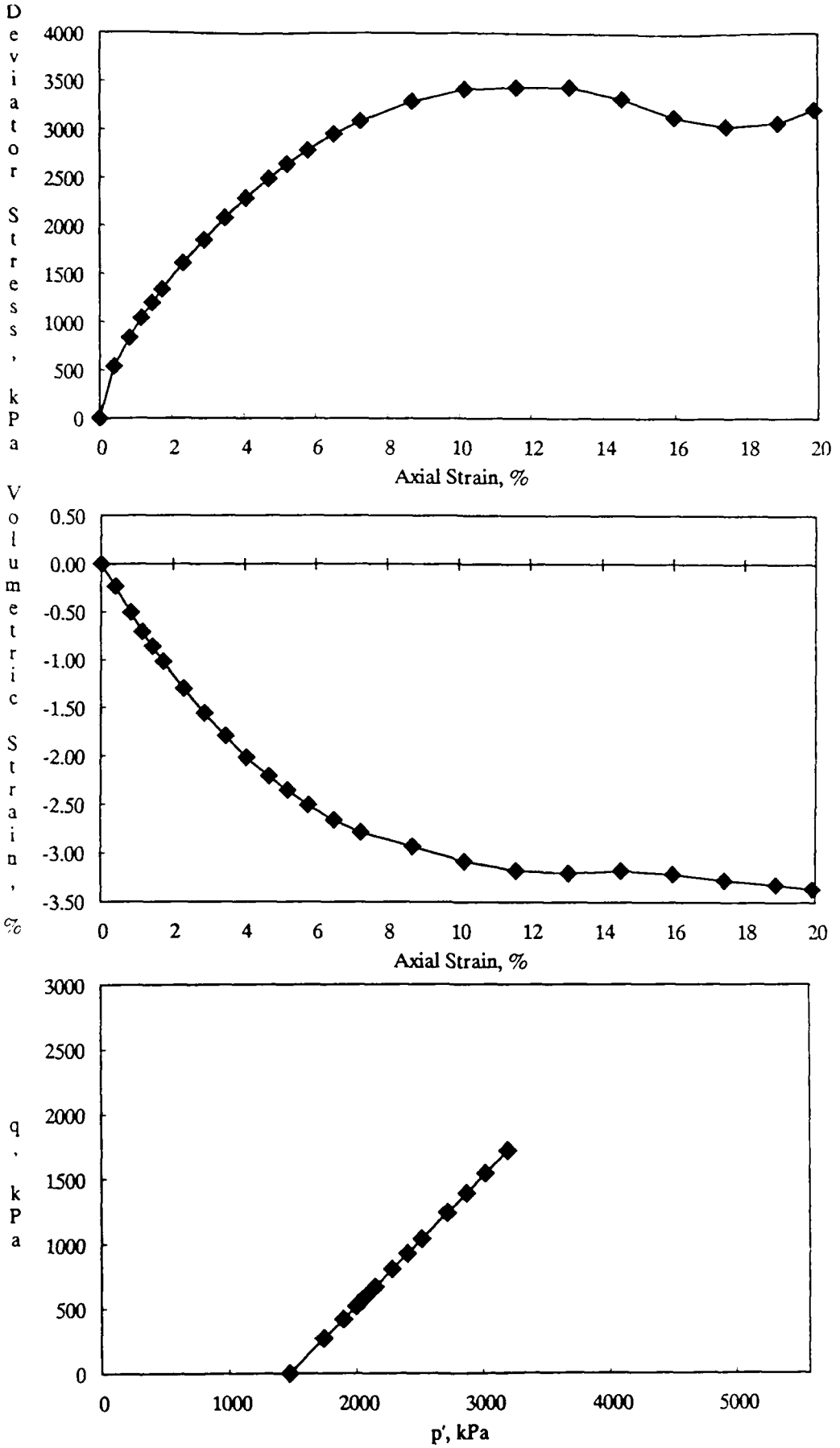


Figure A-26. CD Triaxial Test Results for 10% Kaolinite Mixture at a Standard Proctor Relative Compaction of 90% and an Effective Confining Pressure of 1474 kPa.

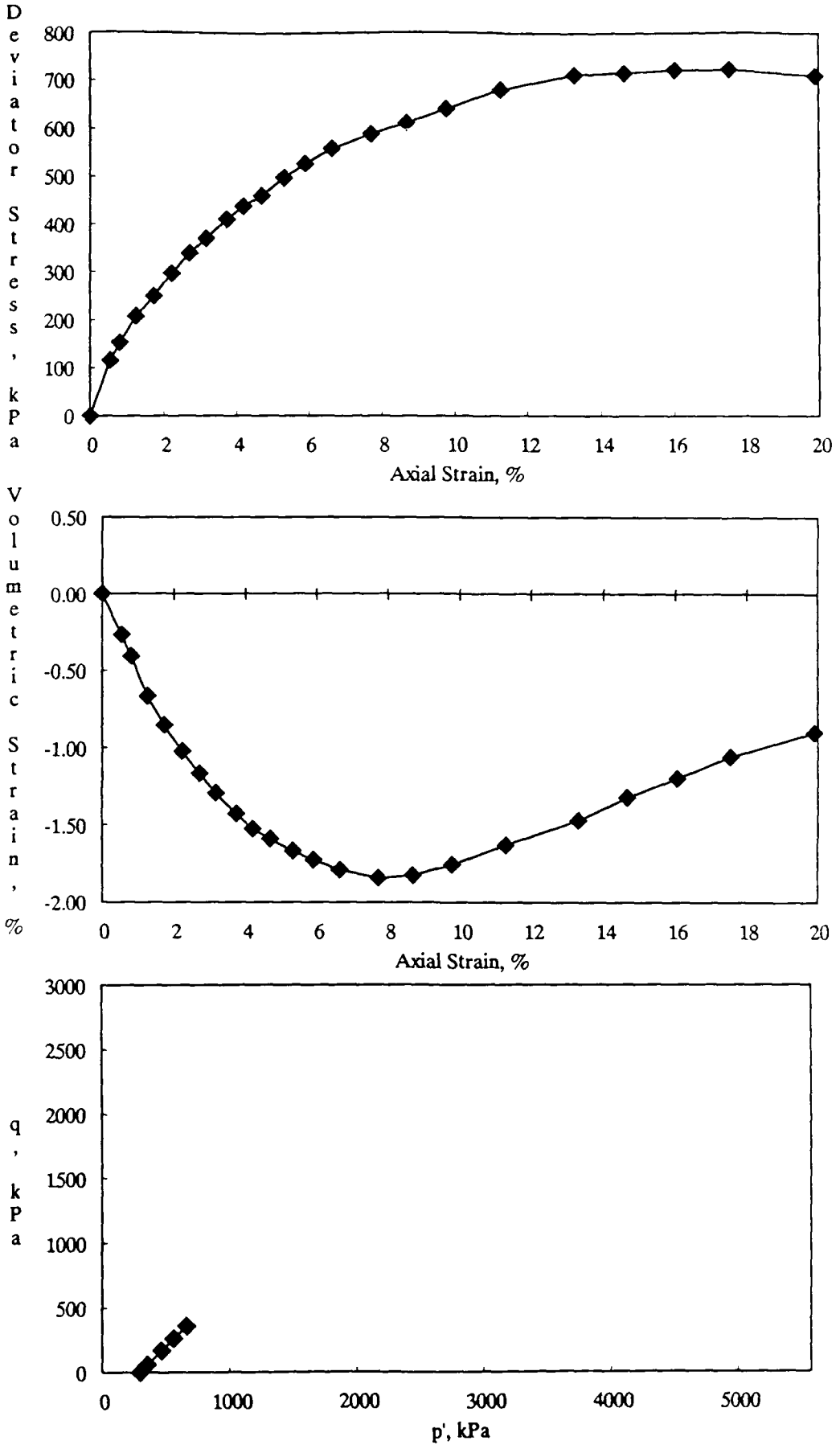


Figure A-27. CD Triaxial Test Results for 10% Kaolinite Mixture at a Standard Proctor Relative Compaction of 85% and an Effective Confining Pressure of 293 kPa.

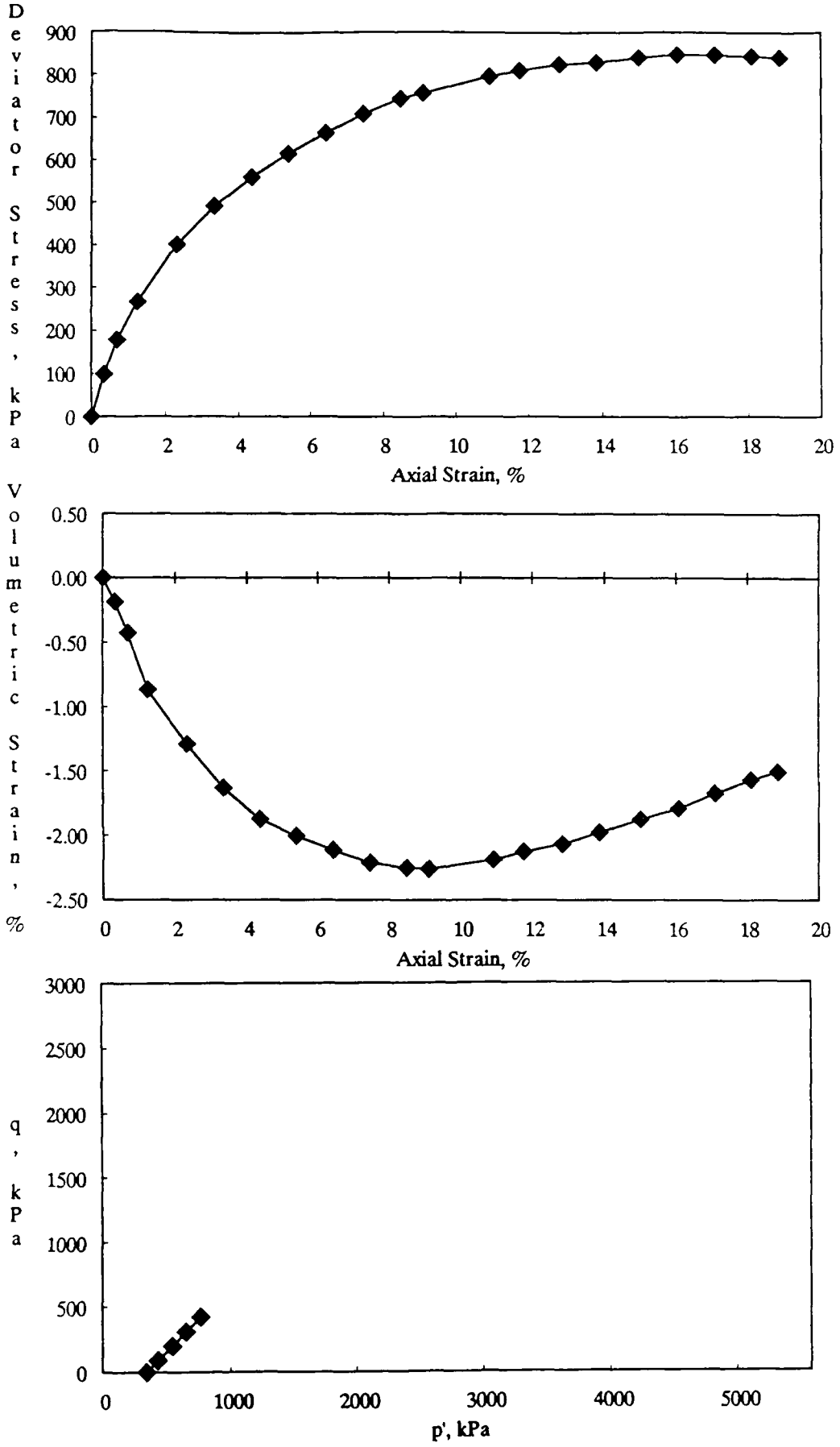


Figure A-28. CD Triaxial Test Results for 10% Kaolinite Mixture at a Standard Proctor Relative Compaction of 85% and an Effective Confining Pressure of 342 kPa.

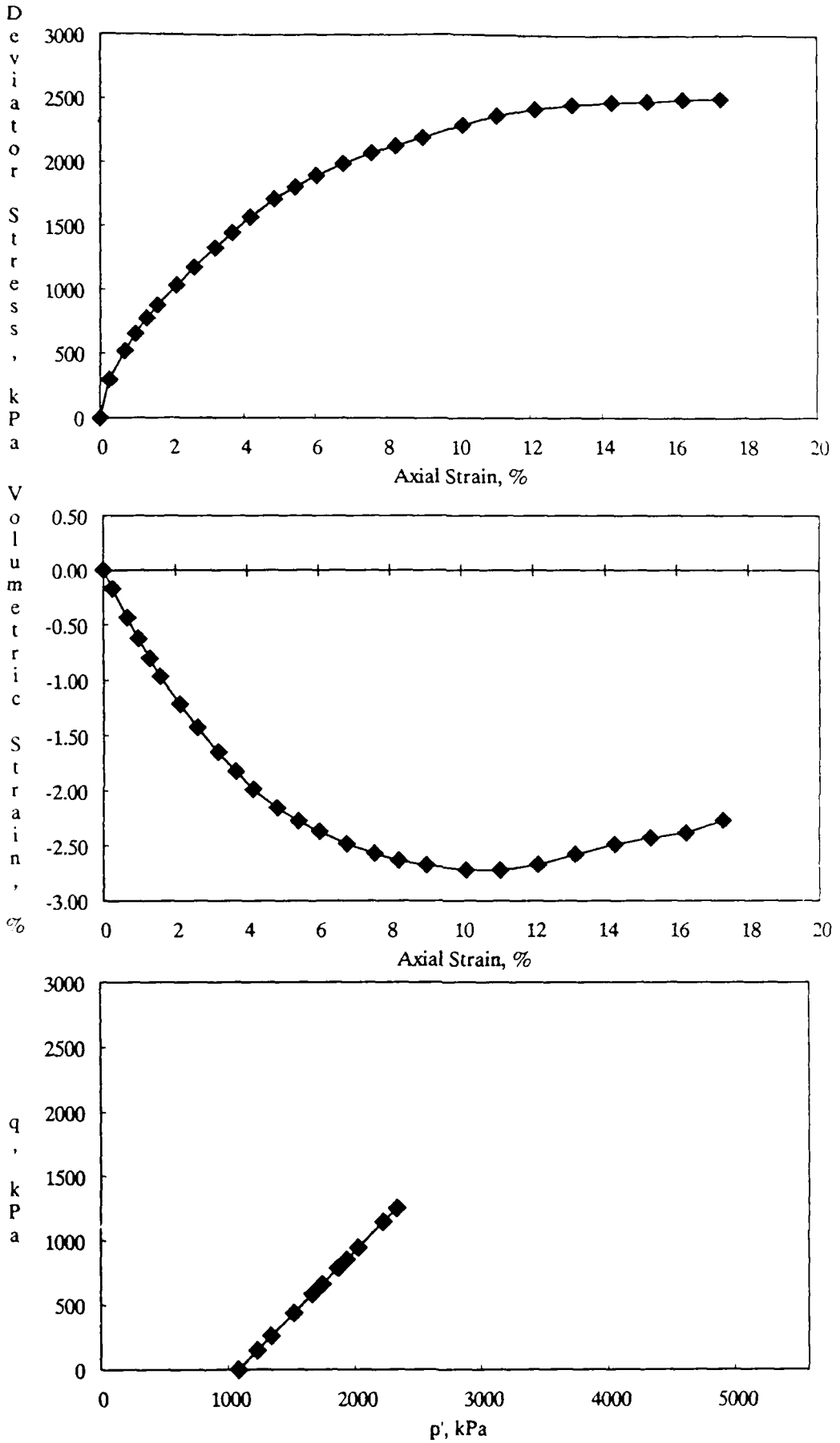


Figure A-29. CD Triaxial Test Results for 10% Kaolinite Mixture at a Standard Proctor Relative Compaction of 85% and an Effective Confining Pressure of 1078 kPa.

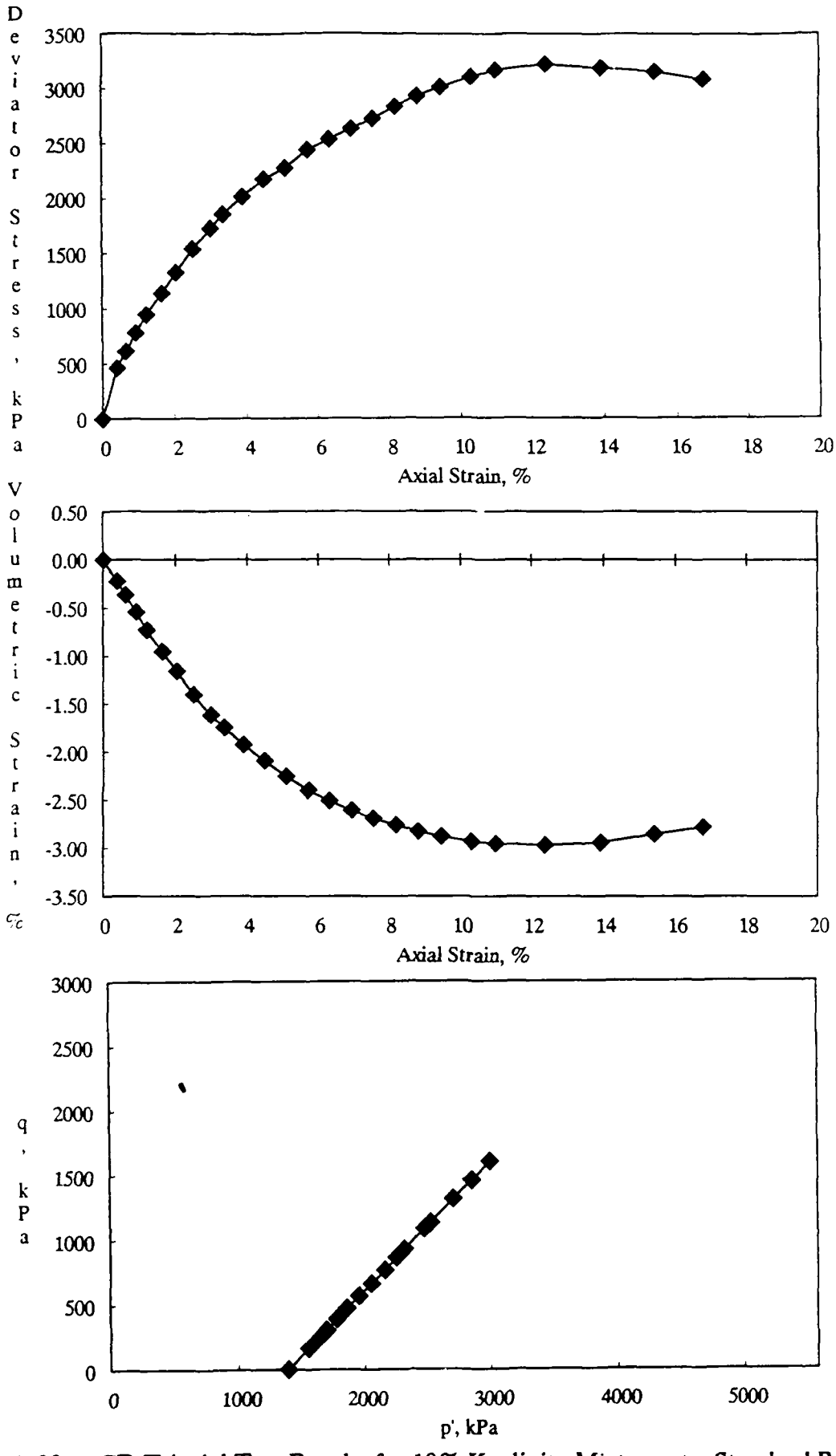


Figure A-30. CD Triaxial Test Results for 10% Kaolinite Mixture at a Standard Proctor Relative Compaction of 85% and an Effective Confining Pressure of 1389 kPa.

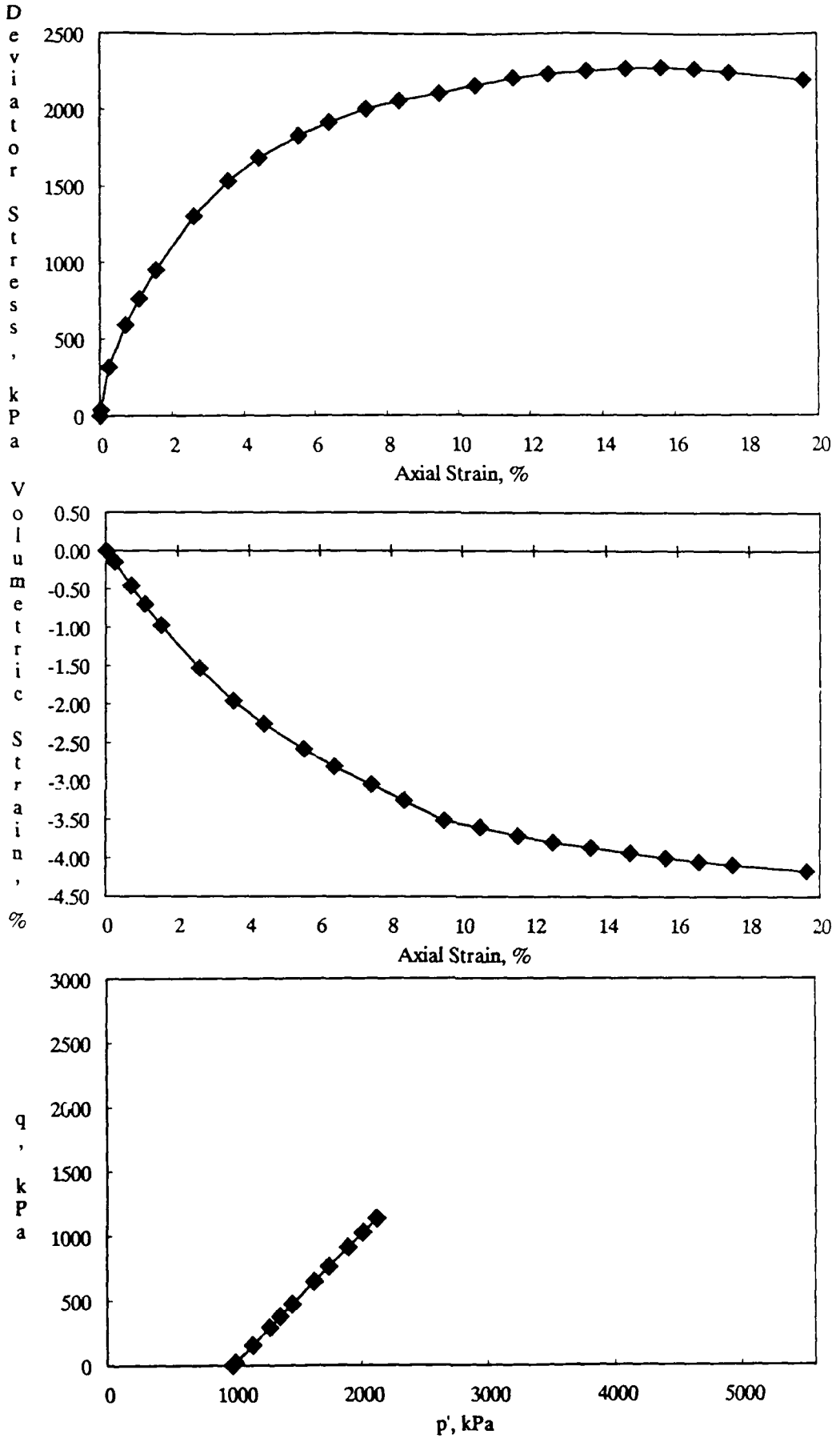


Figure A-31. CD Triaxial Test Results for 30% Kaolinite Mixture at a Standard Proctor Relative Compaction of 100% and an Effective Confining Pressure of 980 kPa.

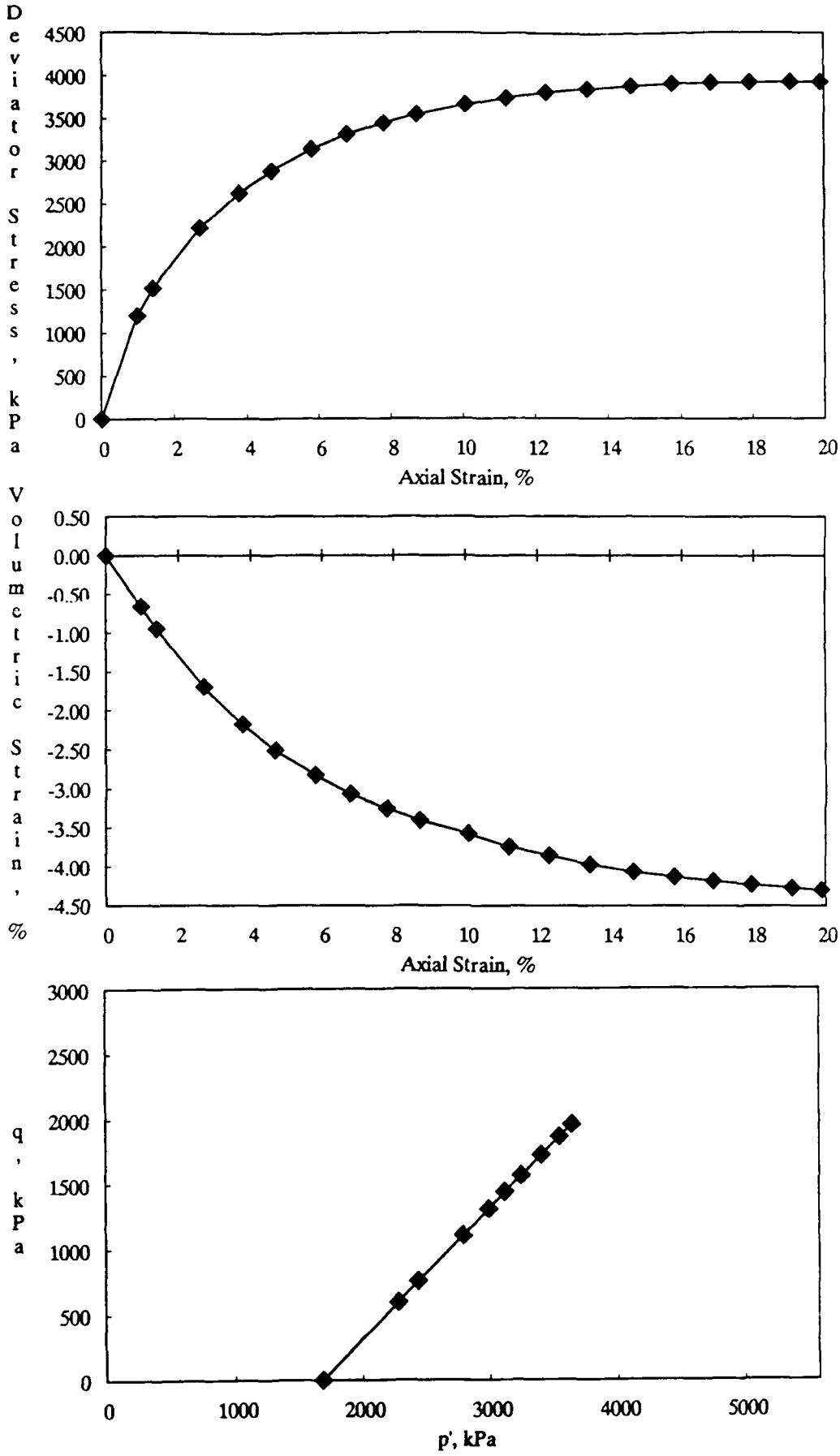


Figure A-32. CD Triaxial Test Results for 30% Kaolinite Mixture at a Standard Proctor Relative Compaction of 100% and an Effective Confining Pressure of 1683 kPa.

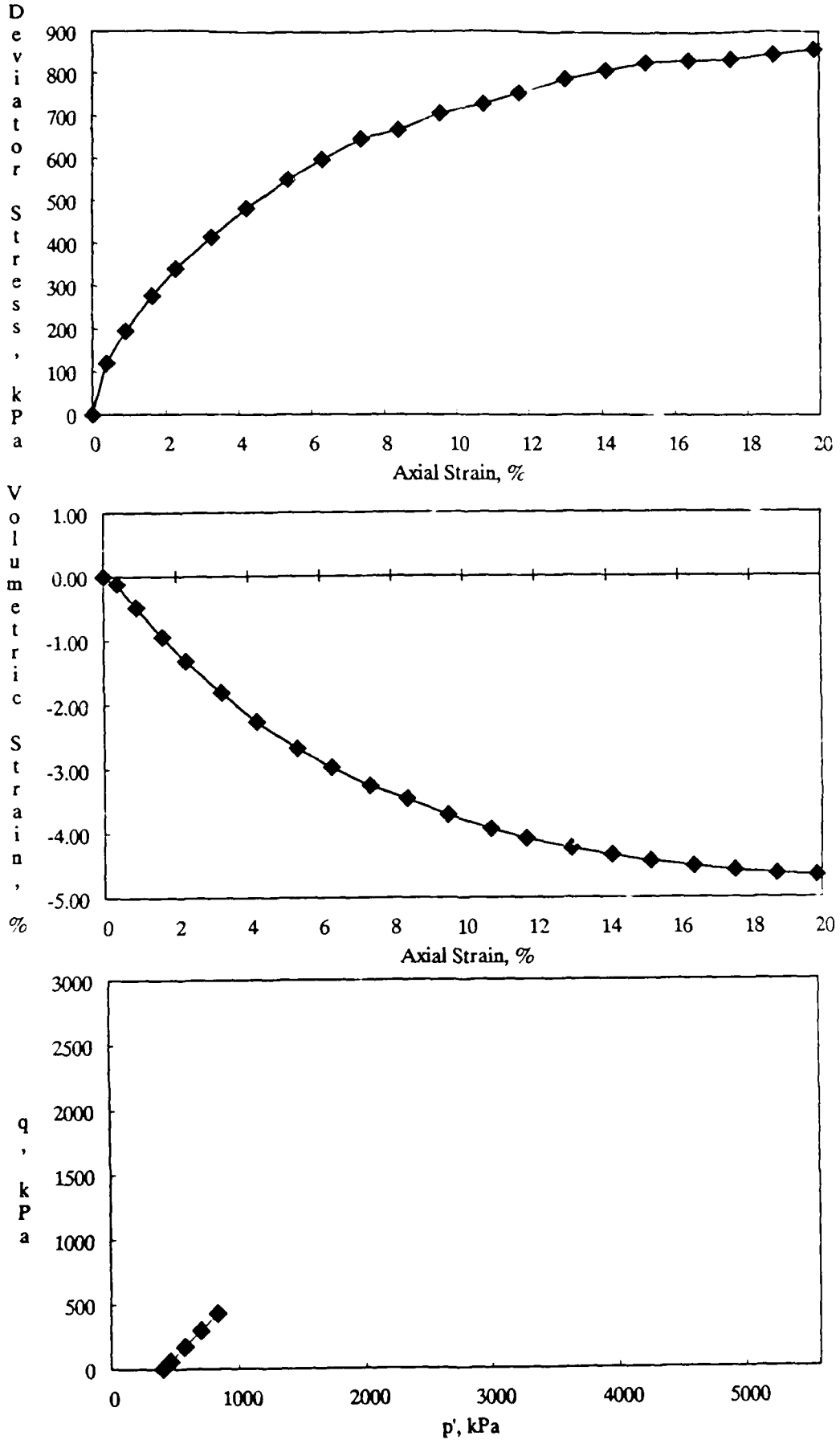


Figure A-33. CD Triaxial Test Results for 30% Kaolinite Mixture at a Standard Proctor Relative Compaction of 95% and an Effective Confining Pressure of 398 kPa.

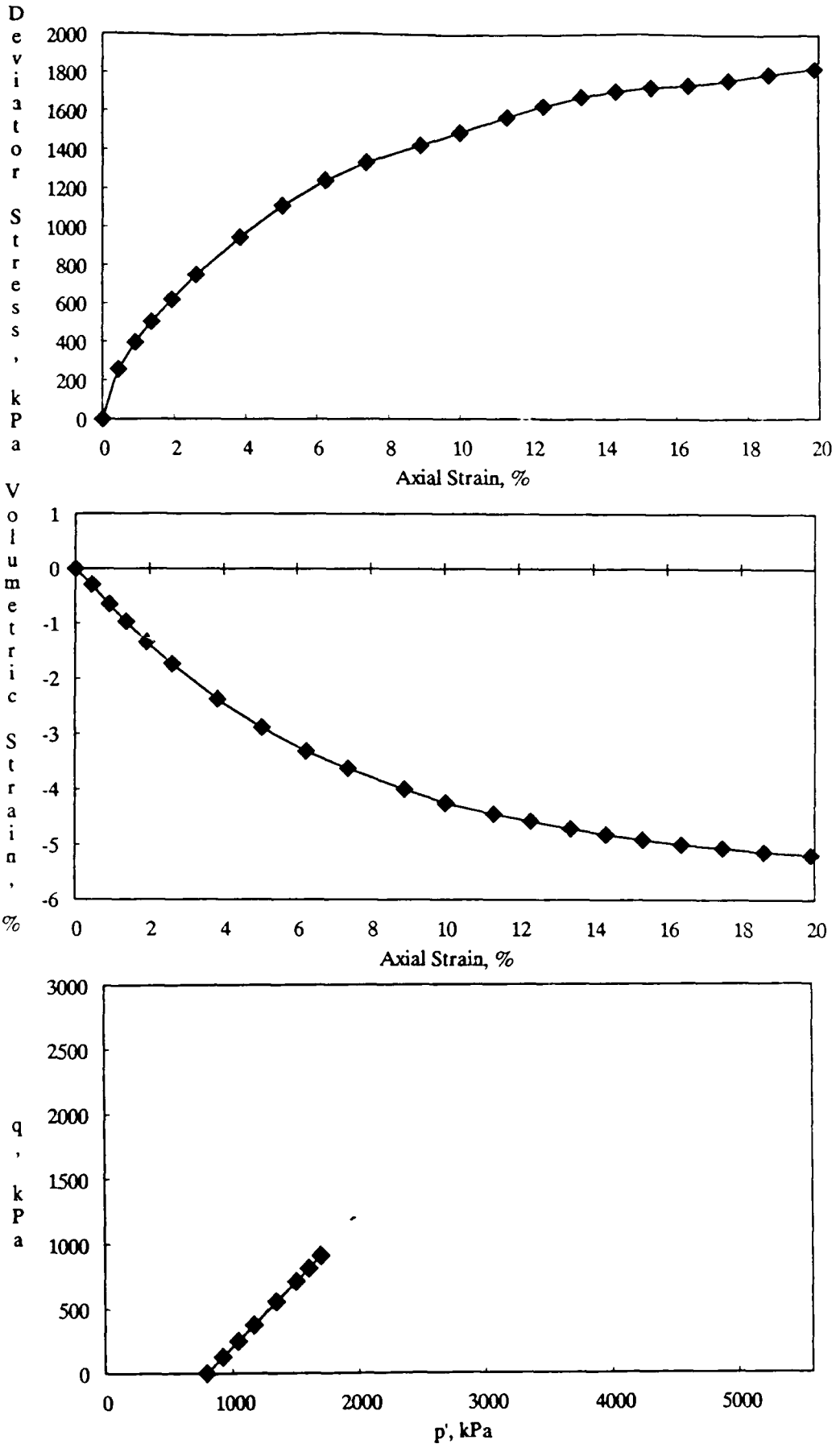


Figure A-34. CD Triaxial Test Results for 30% Kaolinite Mixture at a Standard Proctor Relative Compaction of 95% and an Effective Confining Pressure of 792 kPa.

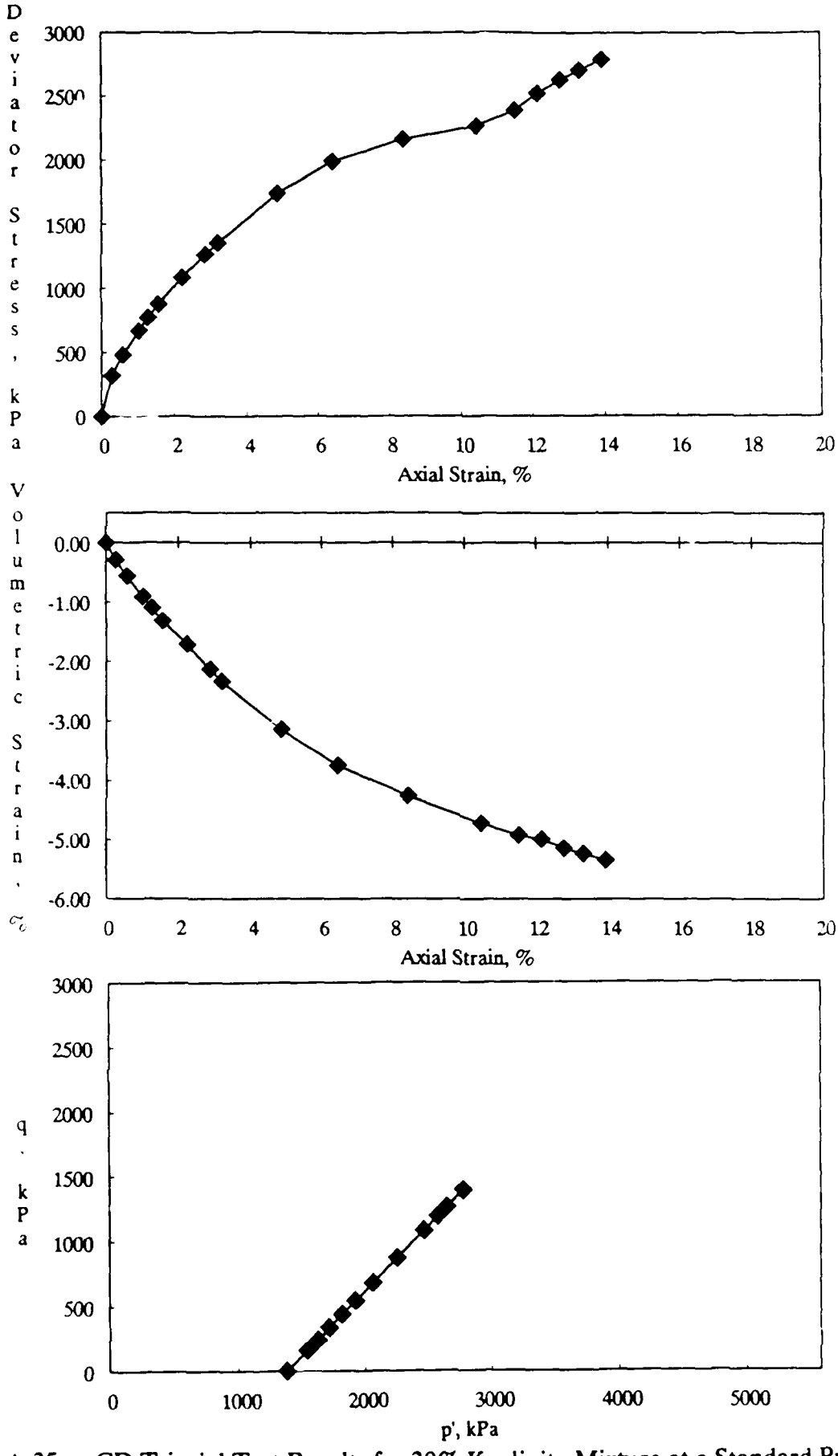


Figure A-35. CD Triaxial Test Results for 30% Kaolinite Mixture at a Standard Proctor Relative Compaction of 95% and an Effective Confining Pressure of 1379 kPa.

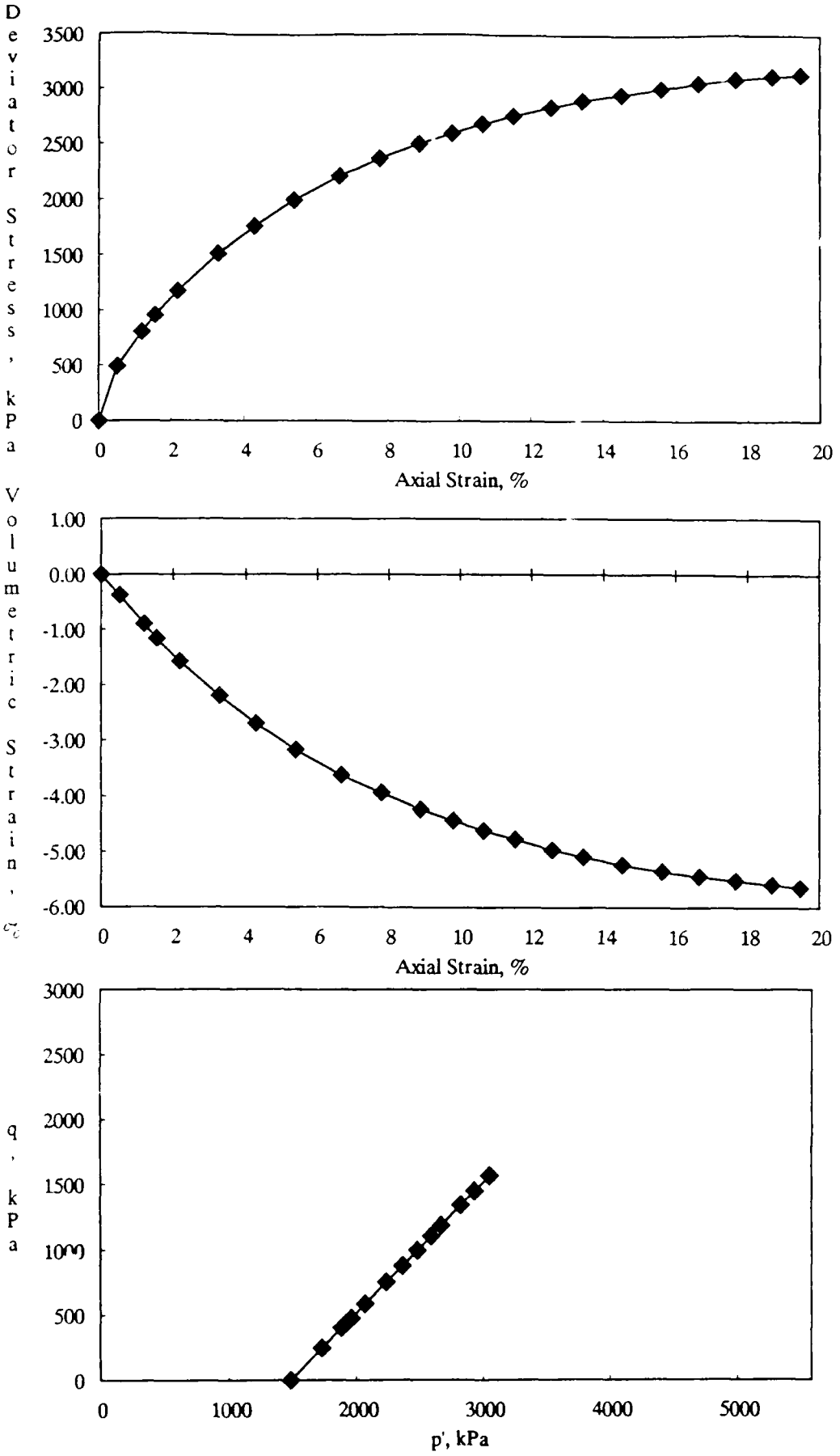


Figure A-36. CD Triaxial Test Results for 30% Kaolinite Mixture at a Standard Proctor Relative Compaction of 95% and an Effective Confining Pressure of 1481 kPa.

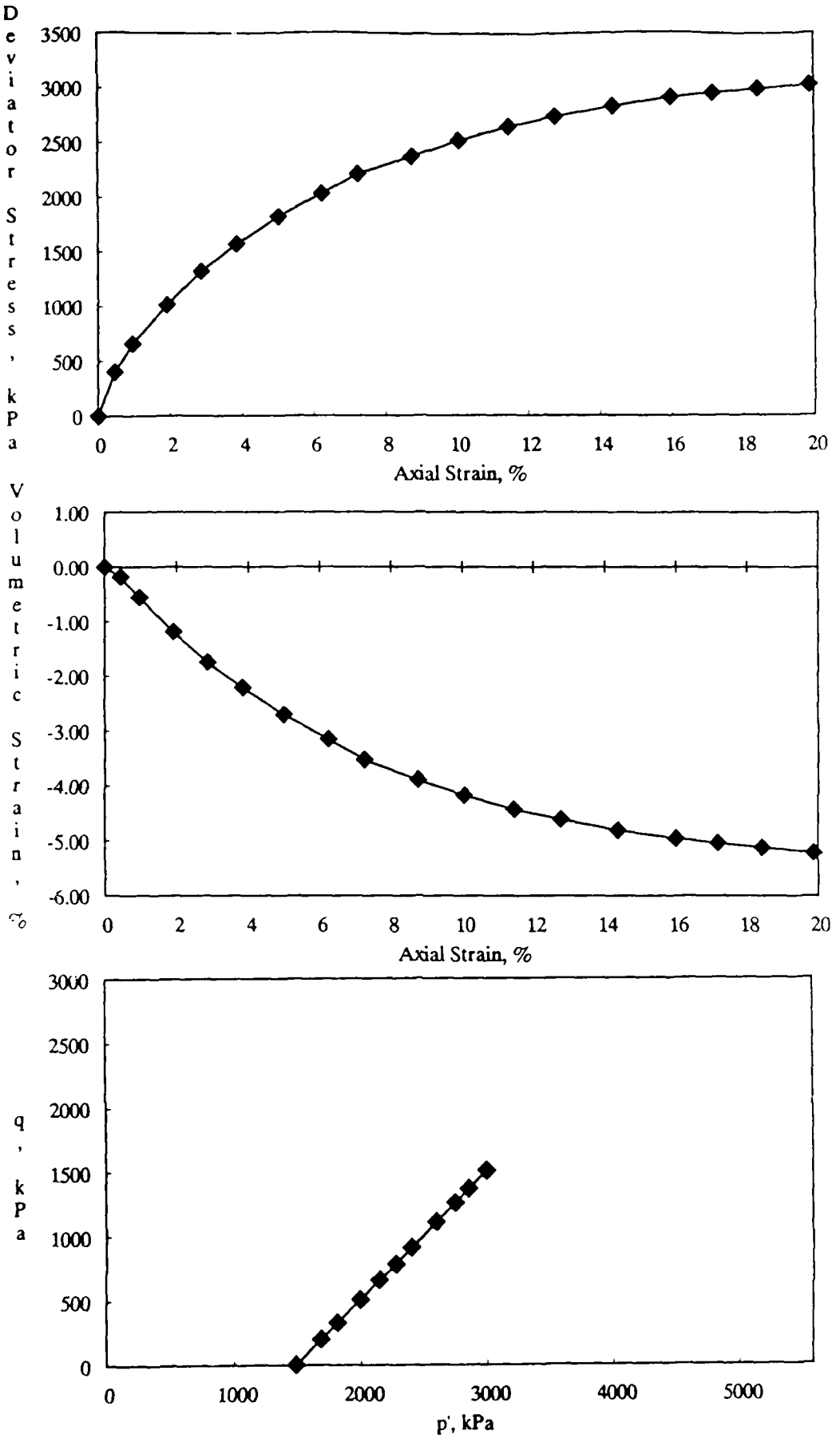


Figure A-37. CD Triaxial Test Results for 30% Kaolinite Mixture at a Standard Proctor Relative Compaction of 95% and an Effective Confining Pressure of 1485 kPa.

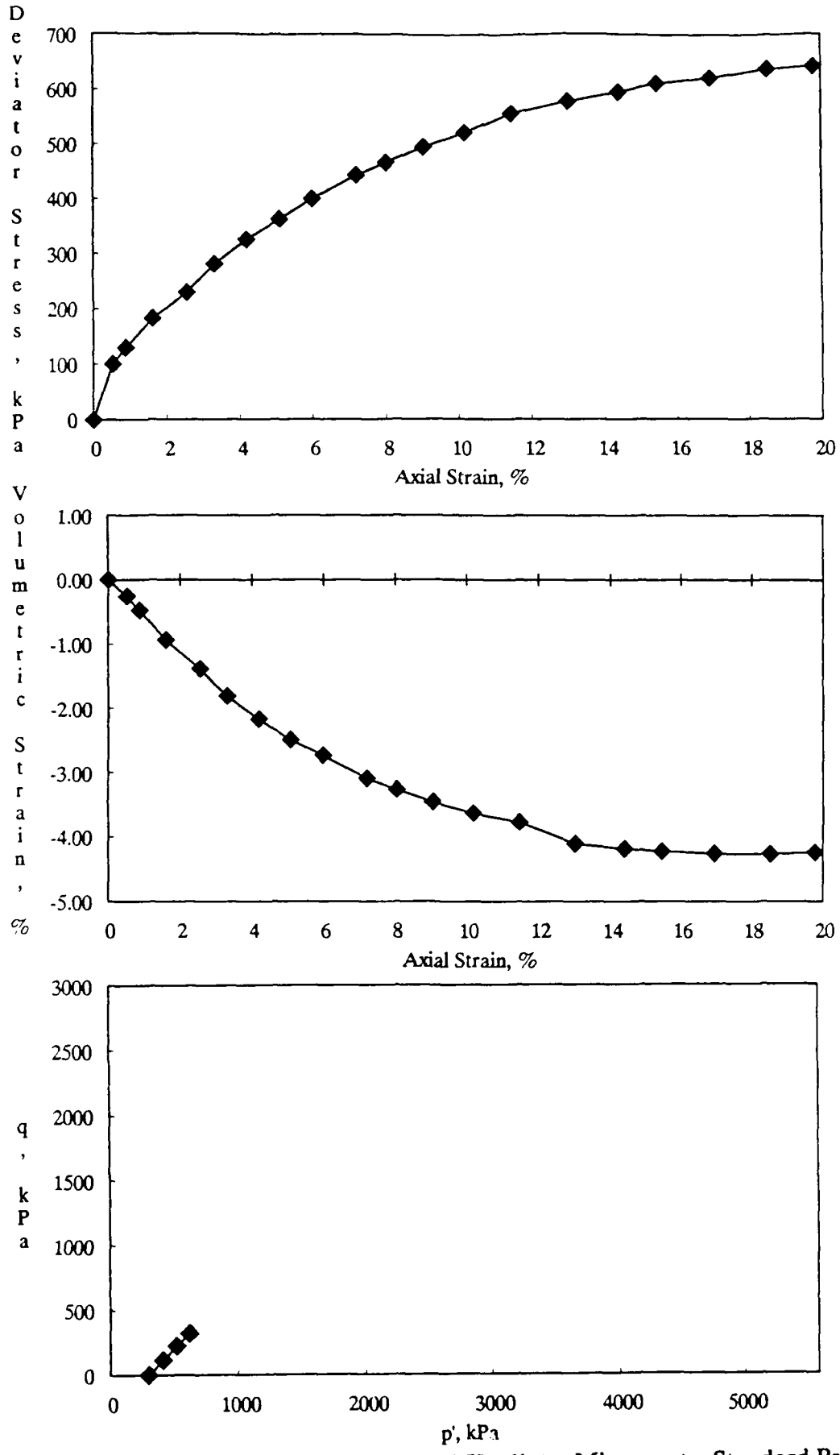


Figure A-38. CD Triaxial Test Results for 30% Kaolinite Mixture at a Standard Proctor Relative Compaction of 90% and an Effective Confining Pressure of 297 kPa.

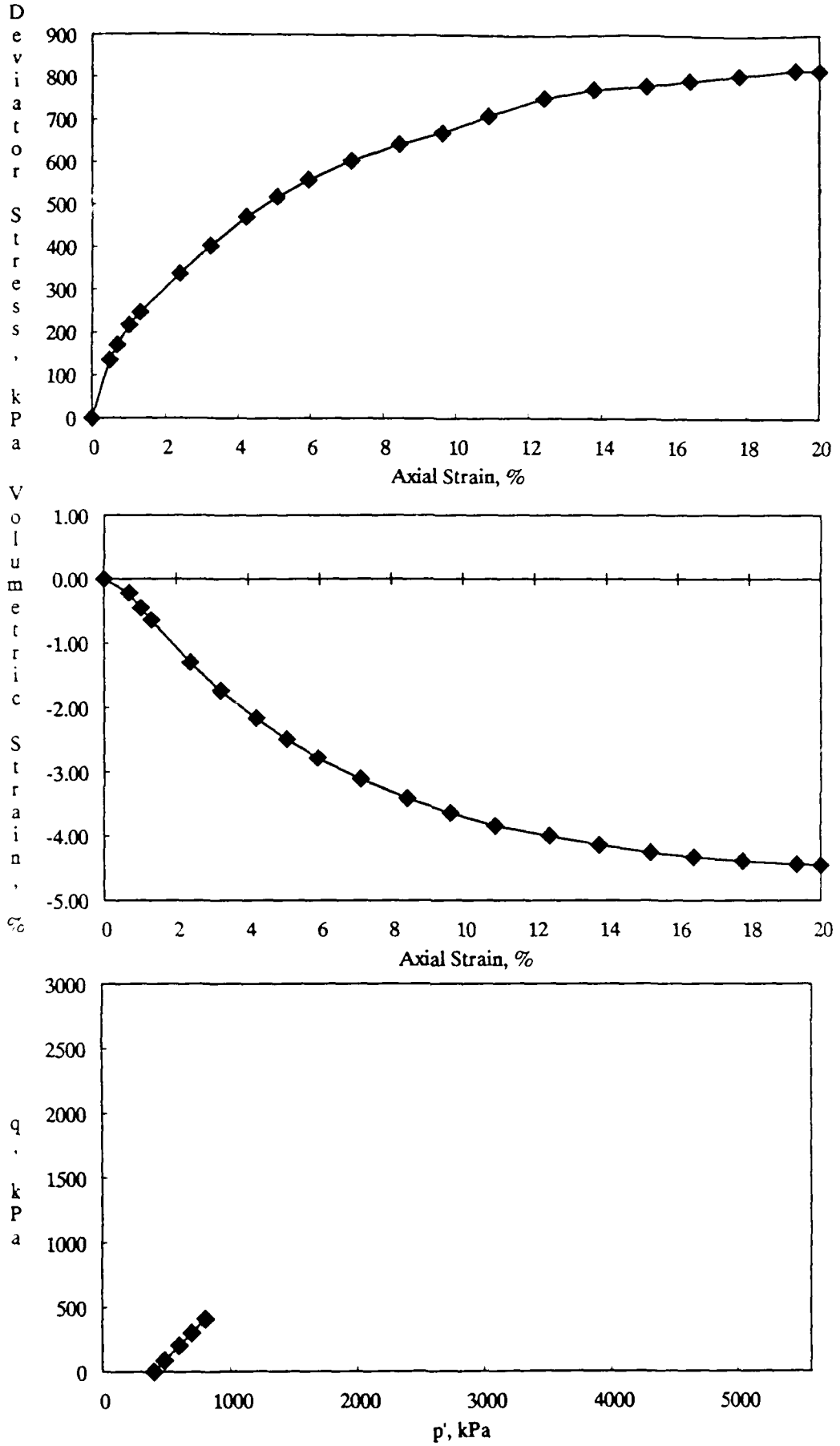


Figure A-39. CD Triaxial Test Results for 30% Kaolinite Mixture at a Standard Proctor Relative Compaction of 90% and an Effective Confining Pressure of 396 kPa.

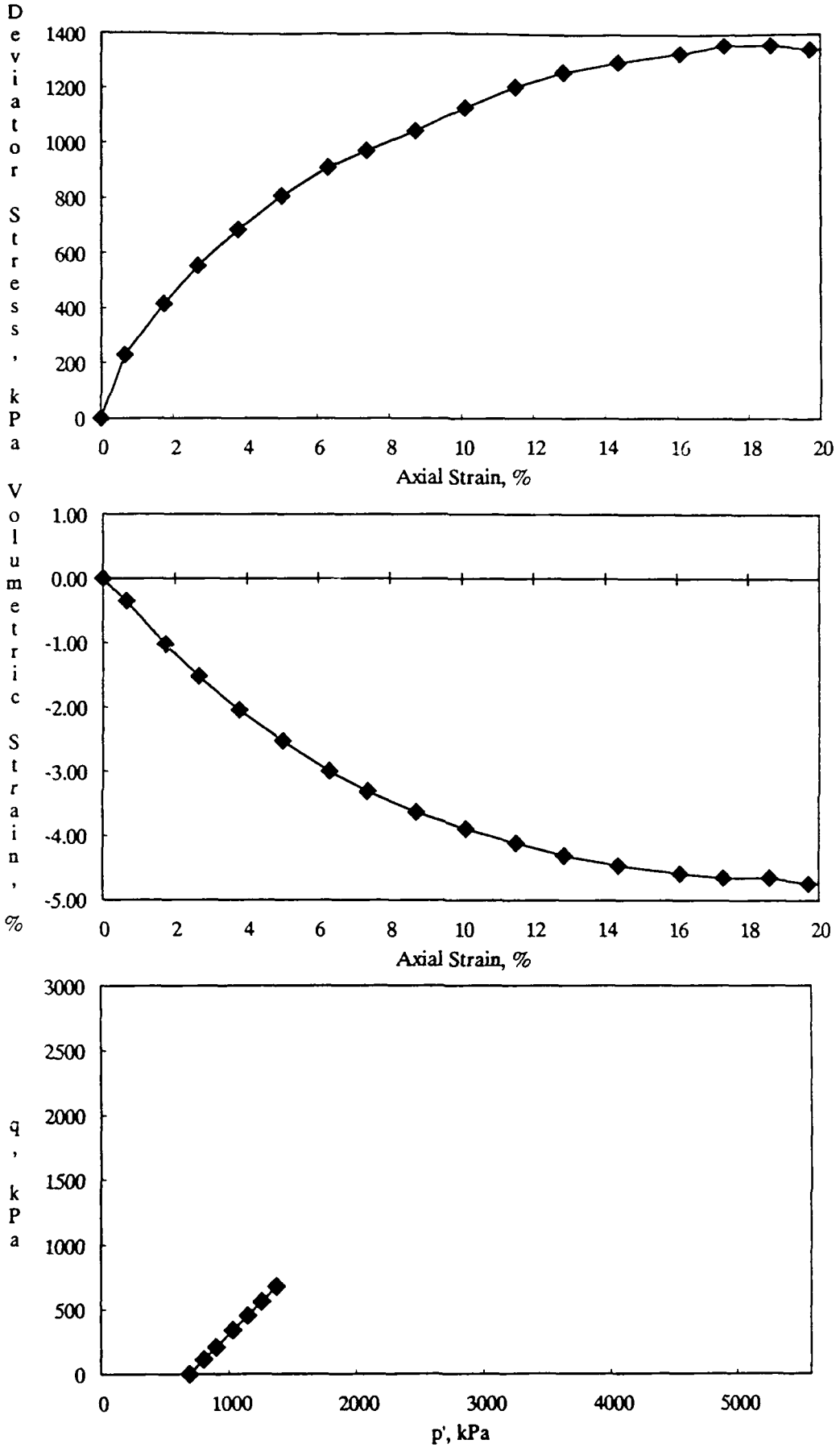


Figure A-40. CD Triaxial Test Results for 30% Kaolinite Mixture at a Standard Proctor Relative Compaction of 90% and an Effective Confining Pressure of 687 kPa.

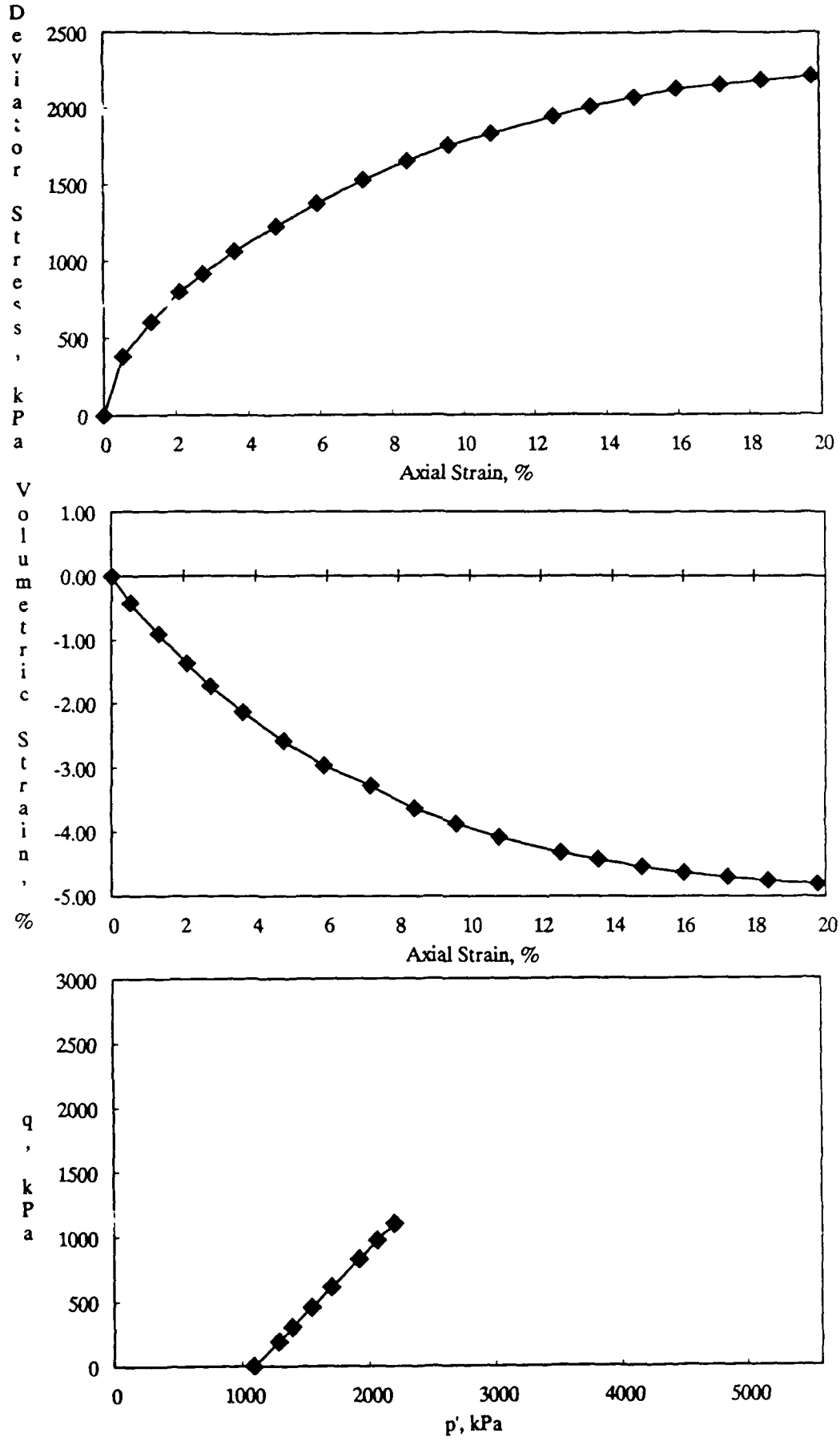


Figure A-41. CD Triaxial Test Results for 30% Kaolinite Mixture at a Standard Proctor Relative Compaction of 90% and an Effective Confining Pressure of 1088 kPa.

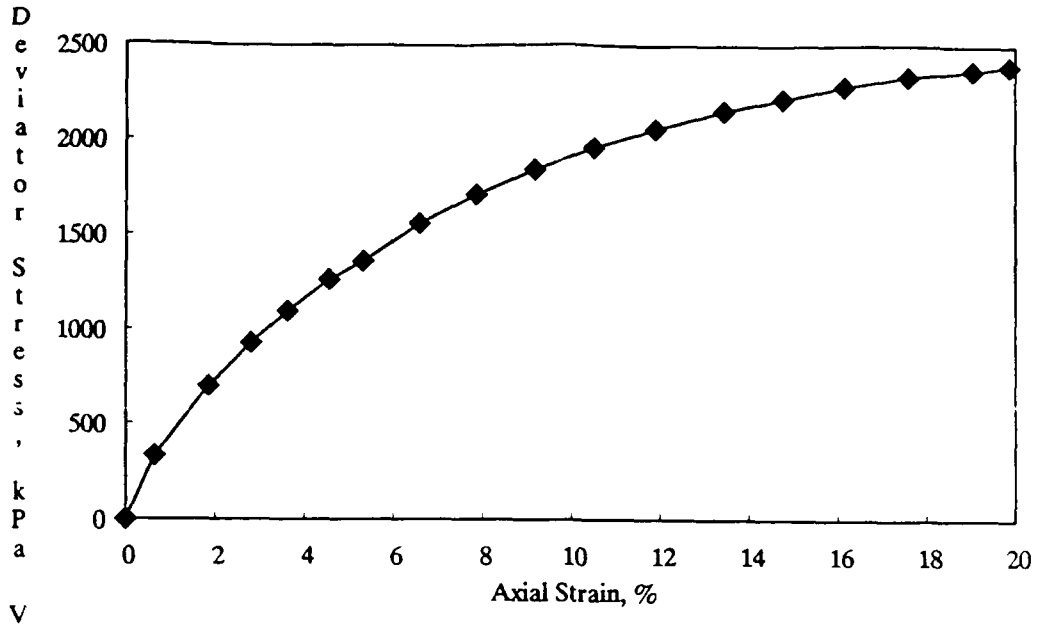


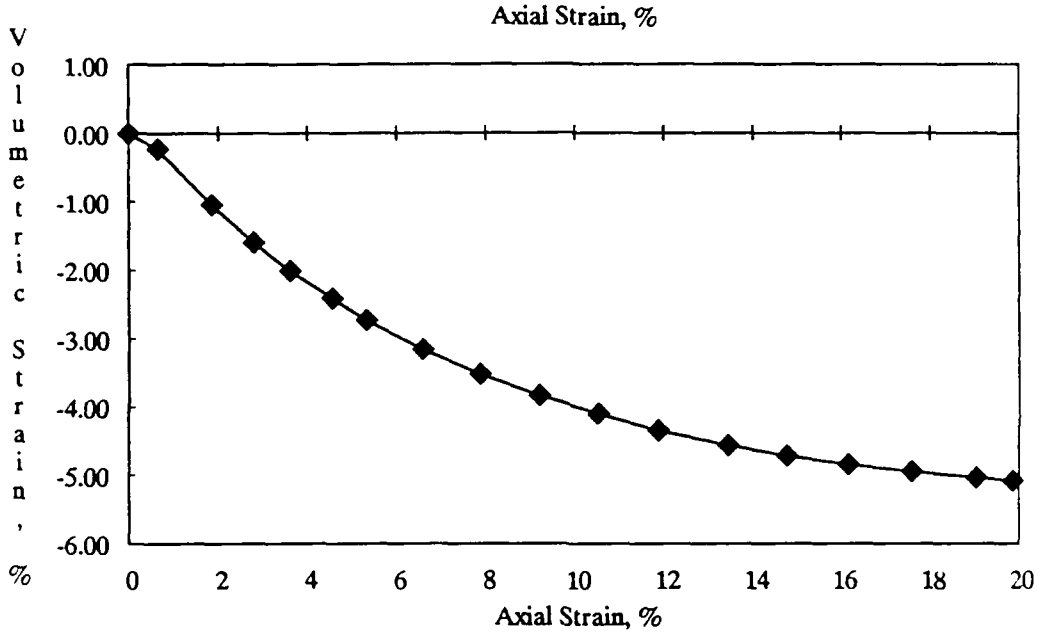


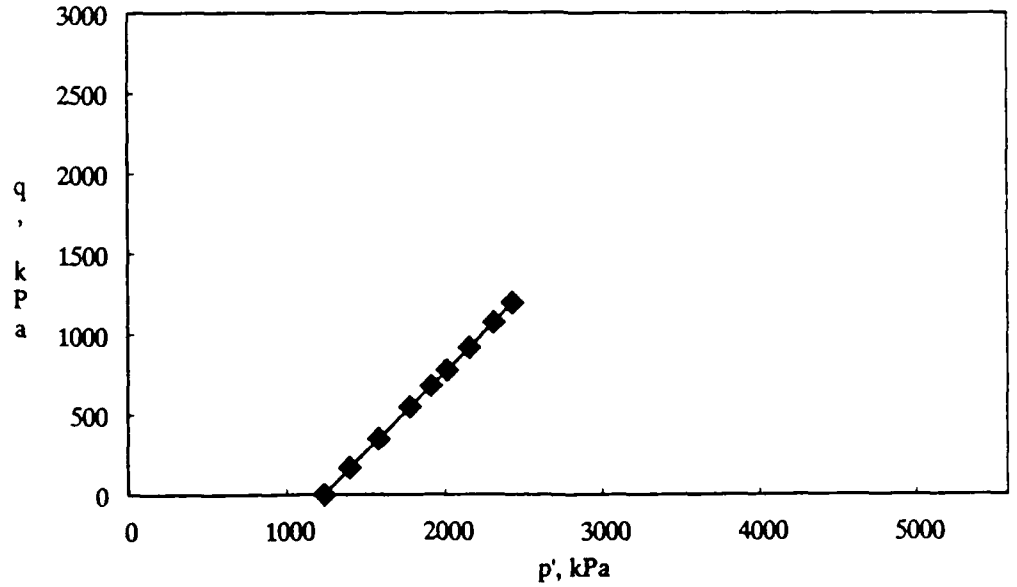


Figure A-42. CD Triaxial Test Results for 30% Kaolinite Mixture at a Standard Proctor Relative Compaction of 90% and an Effective Confining Pressure of 1233 kPa.

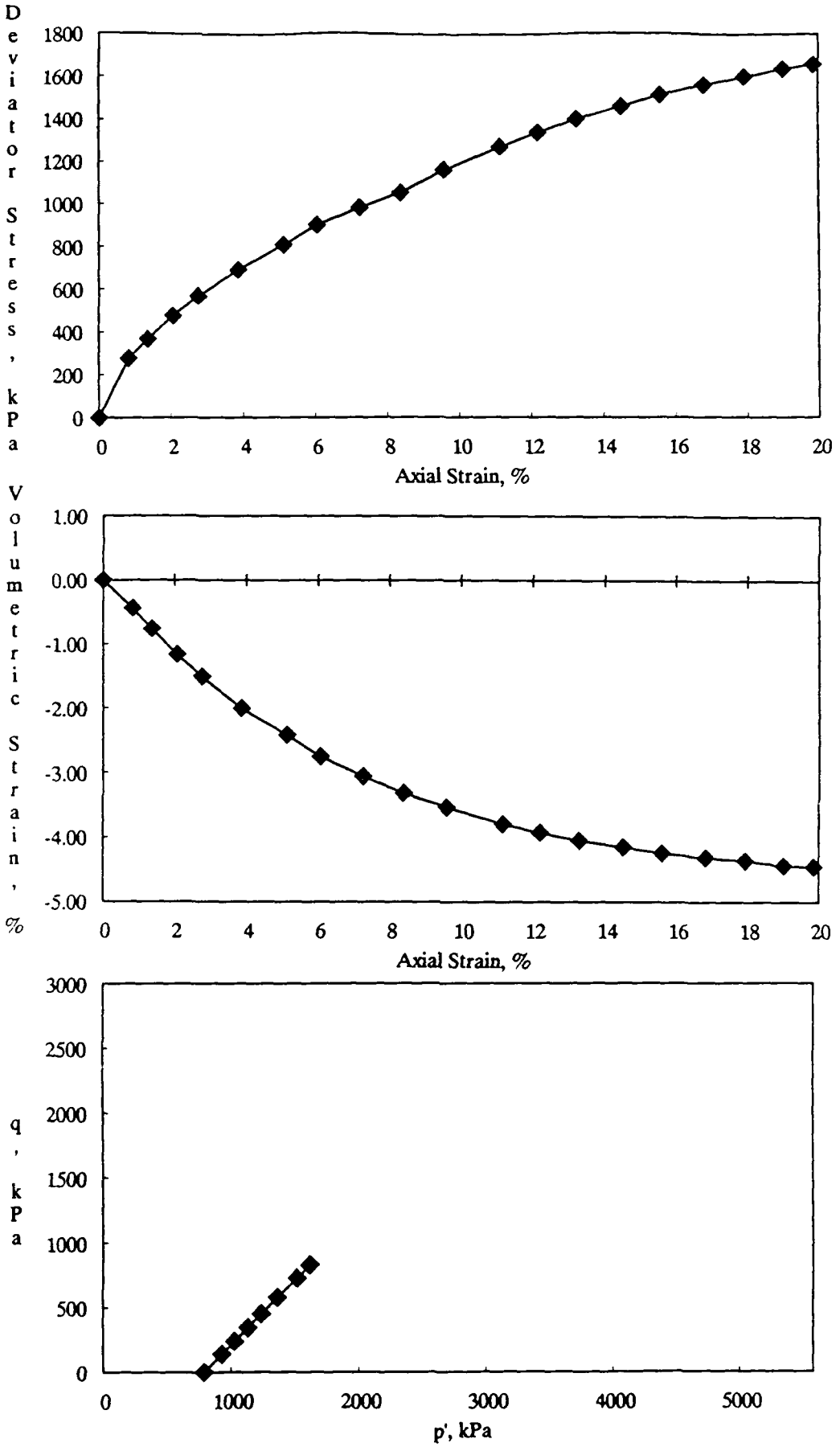


Figure A-43. CD Triaxial Test Results for 30% Kaolinite Mixture at a Standard Proctor Relative Compaction of 85% and an Effective Confining Pressure of 788 kPa.

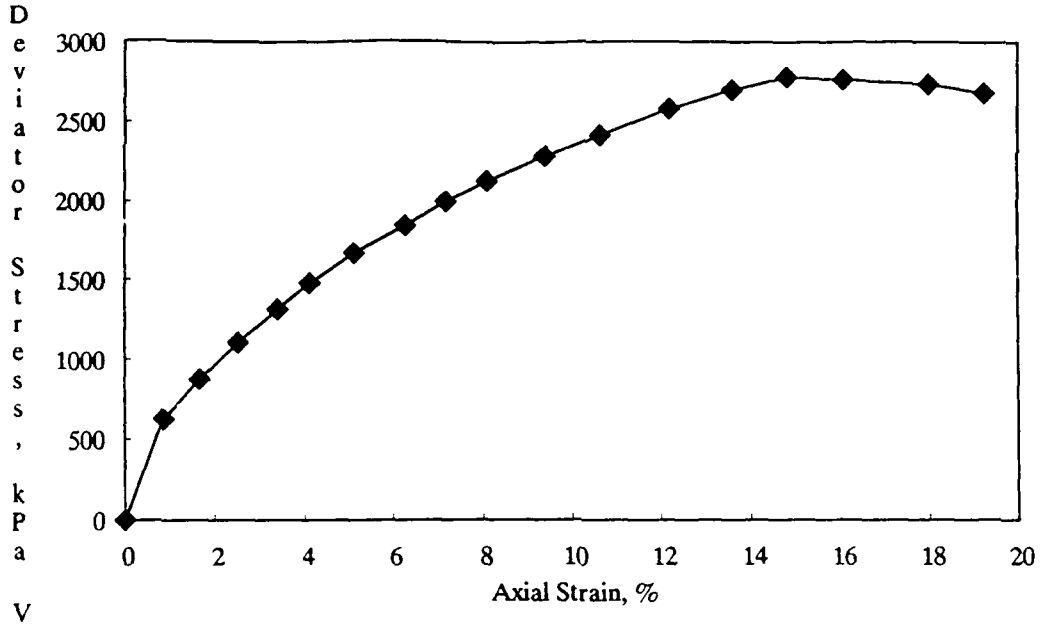


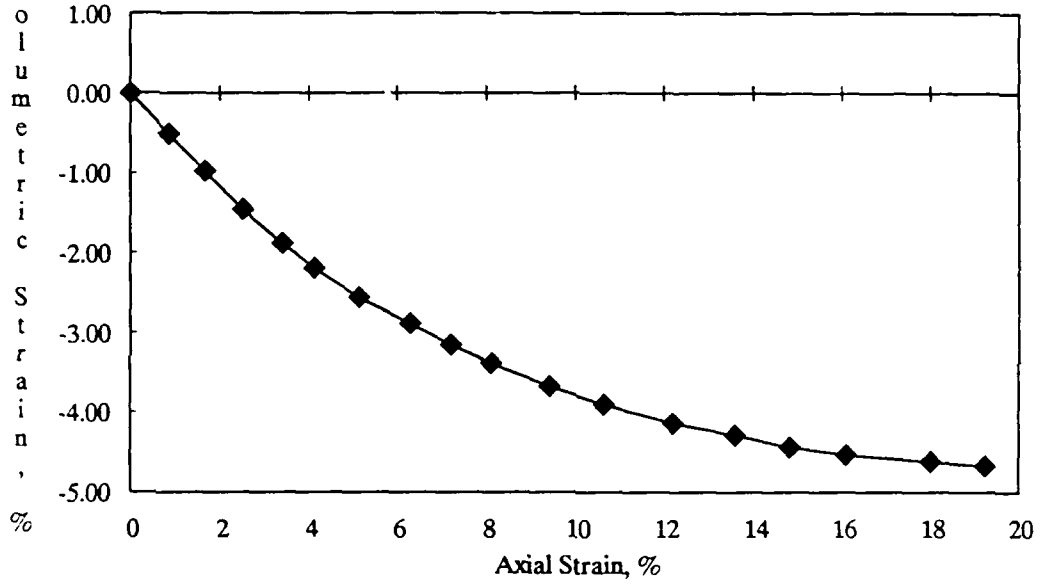


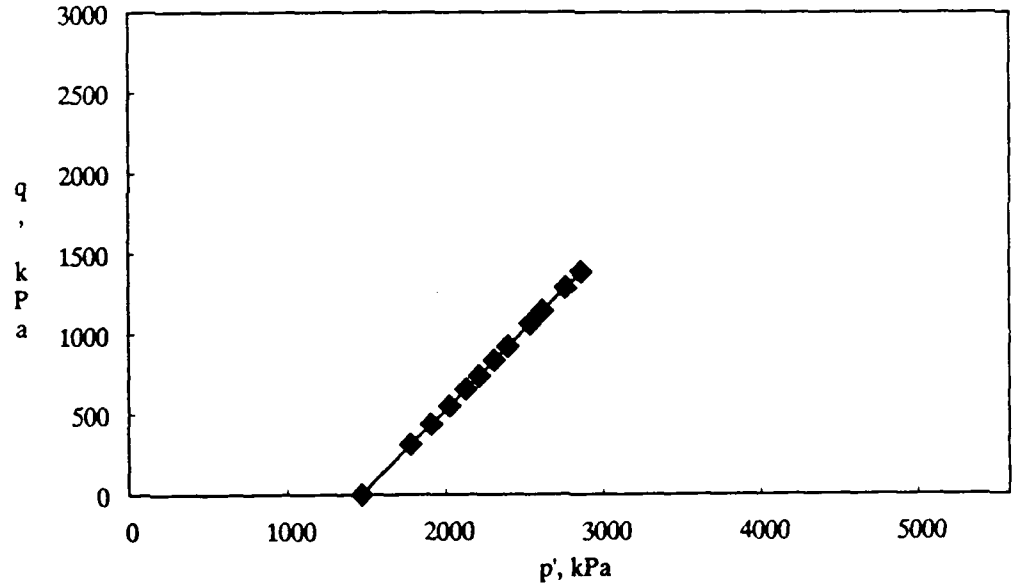


Figure A-44. CD Triaxial Test Results for 30% Kaolinite Mixture at a Standard Proctor Relative Compaction of 85% and an Effective Confining Pressure of 1654 kPa.

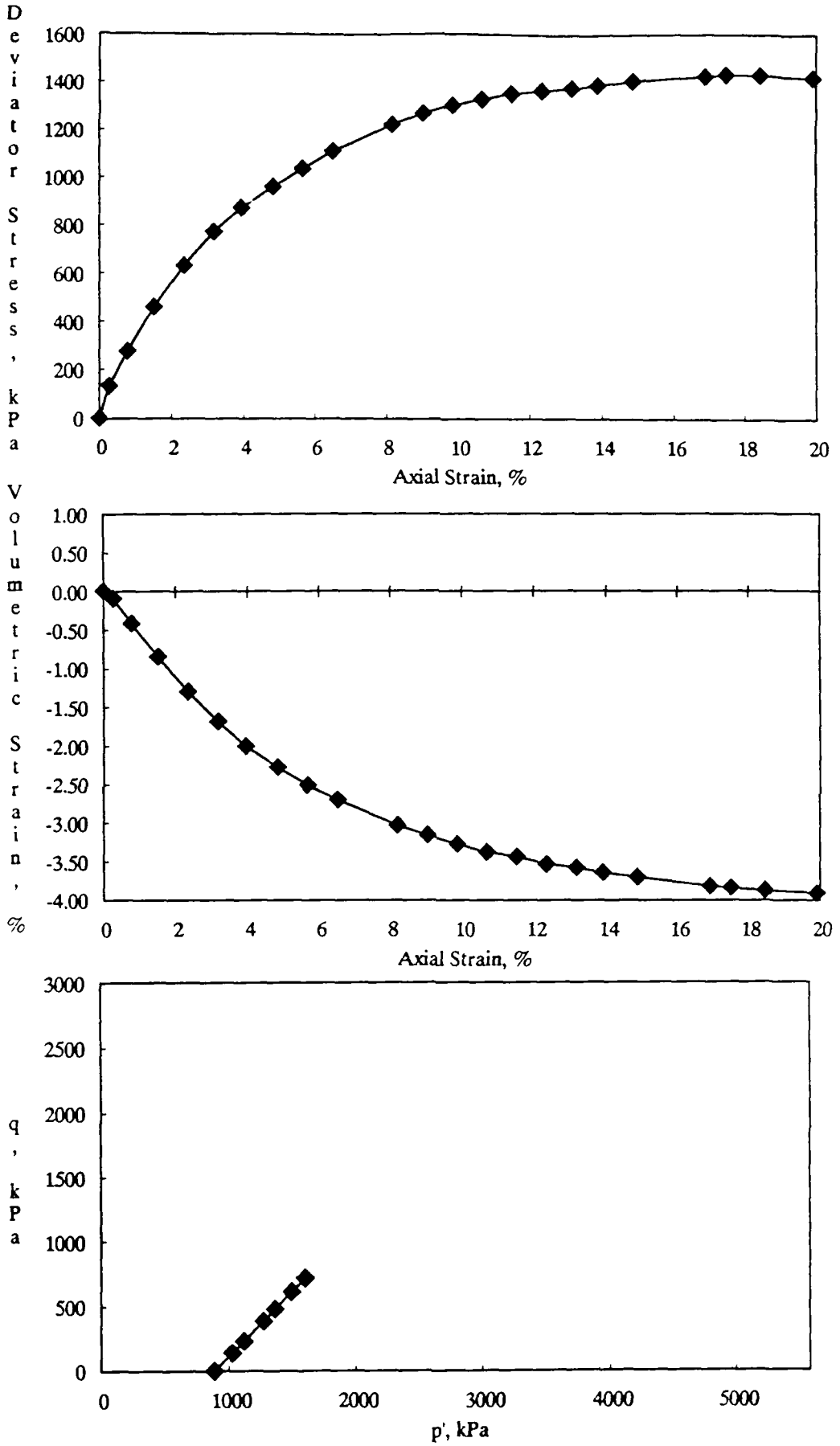


Figure A-45. CD Triaxial Test Results for 50% Kaolinite Mixture at a Standard Proctor Relative Compaction of 100% and an Effective Confining Pressure of 882 kPa.

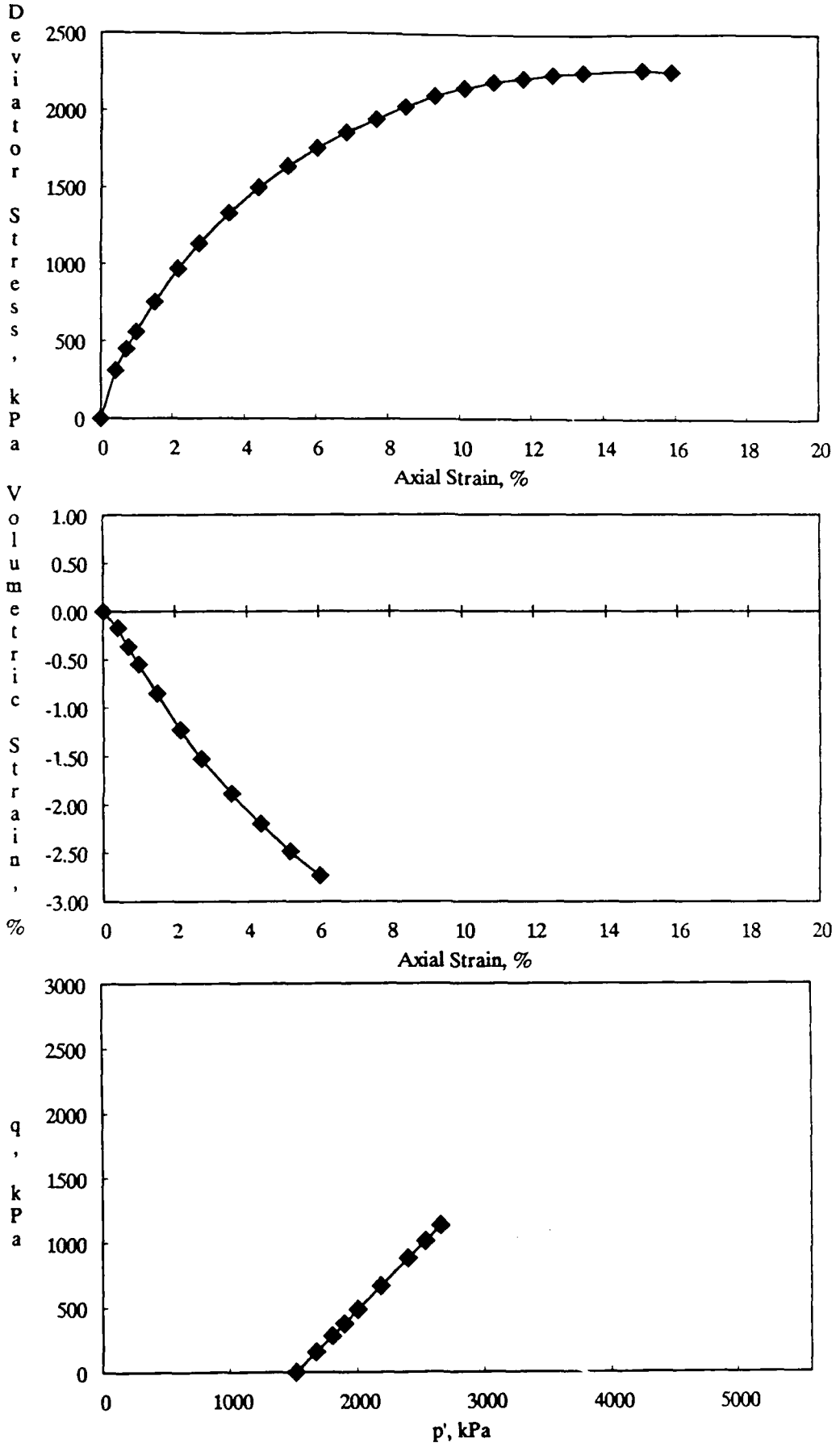


Figure A-46. CD Triaxial Test Results for 50% Kaolinite Mixture at a Standard Proctor Relative Compaction of 100% and an Effective Confining Pressure of 1519 kPa.

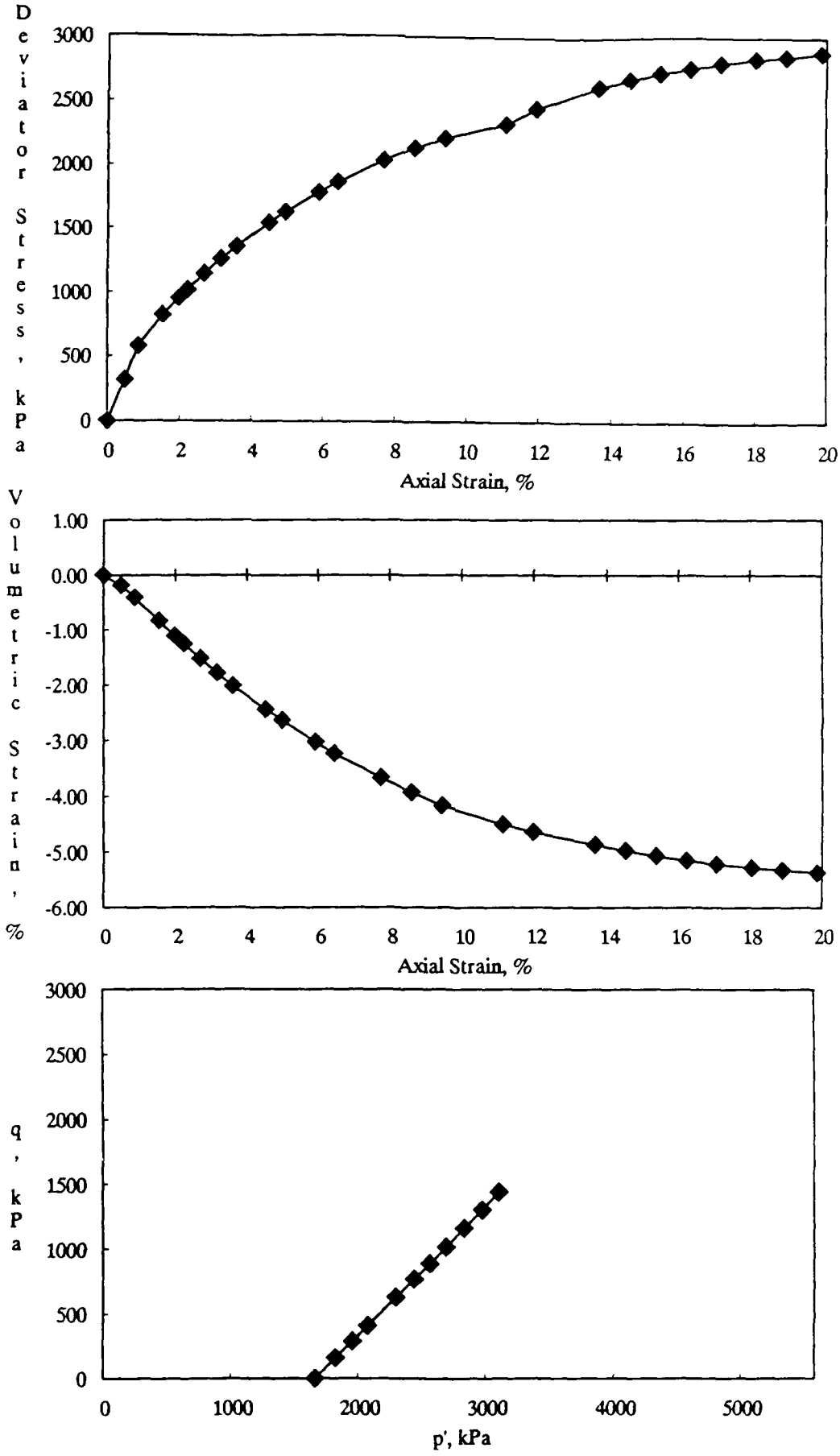


Figure A-47. CD Triaxial Test Results for 50% Kaolinite Mixture at a Standard Proctor Relative Compaction of 100% and an Effective Confining Pressure of 1667 kPa.

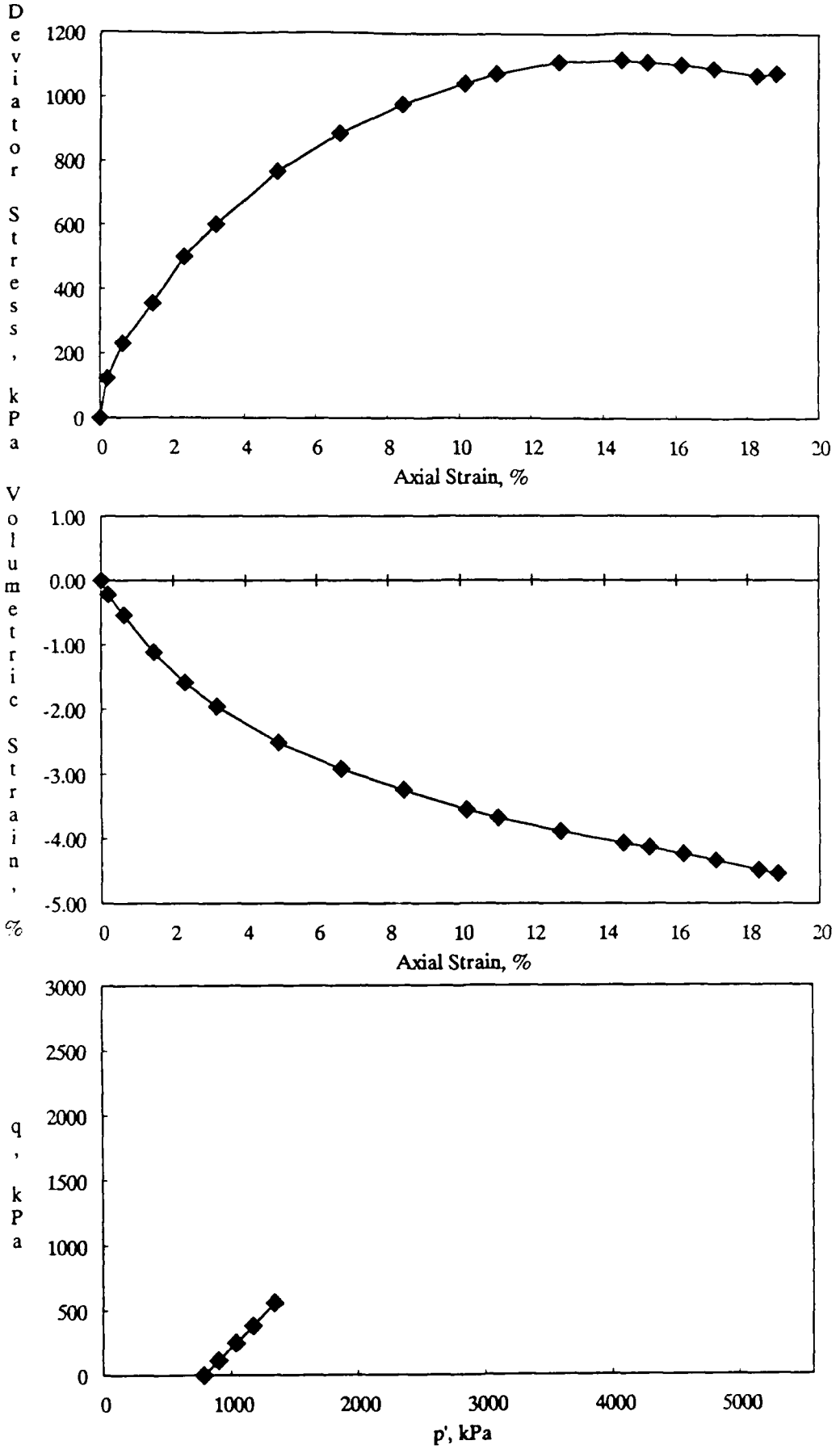


Figure A-48. CD Triaxial Test Results for 50% Kaolinite Mixture at a Standard Proctor Relative Compaction of 95% and an Effective Confining Pressure of 780 kPa.

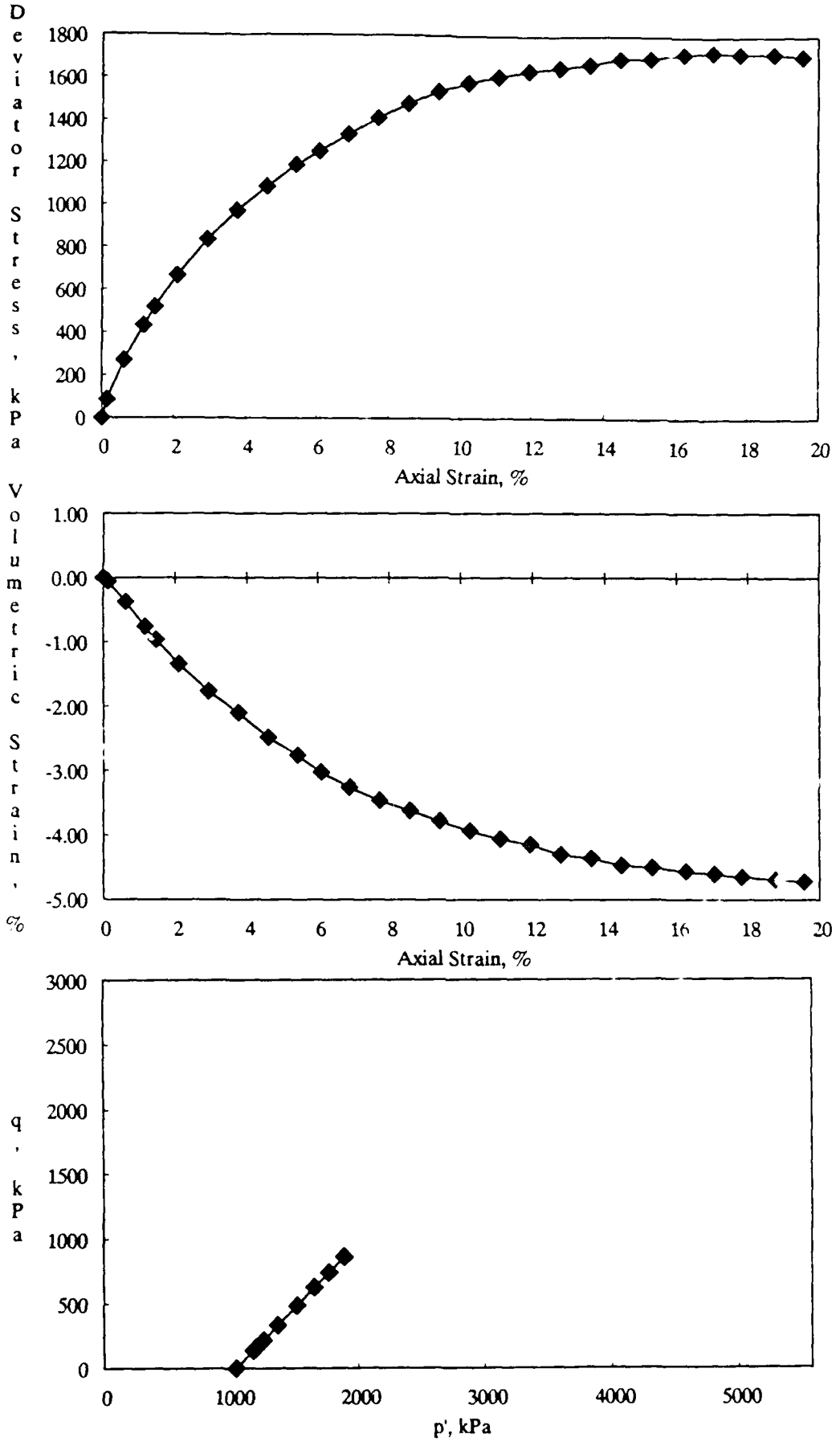


Figure A-49. CD Triaxial Test Results for 50% Kaolinite Mixture at a Standard Proctor Relative Compaction of 95% and an Effective Confining Pressure of 1030 kPa.

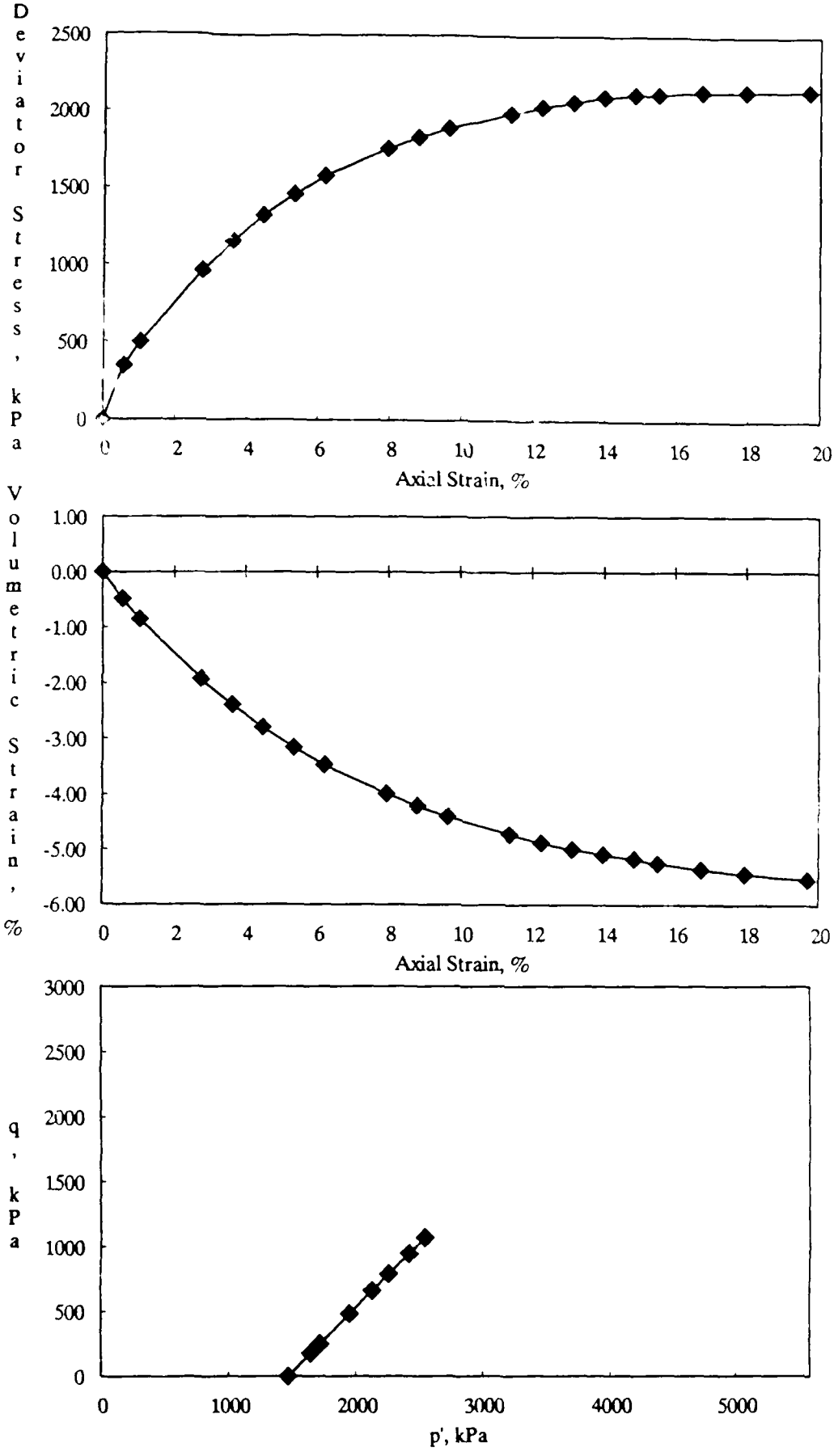


Figure A-50. CD Triaxial Test Results for 50% Kaolinite Mixture at a Standard Proctor Relative Compaction of 95% and an Effective Confining Pressure of 1470 kPa.

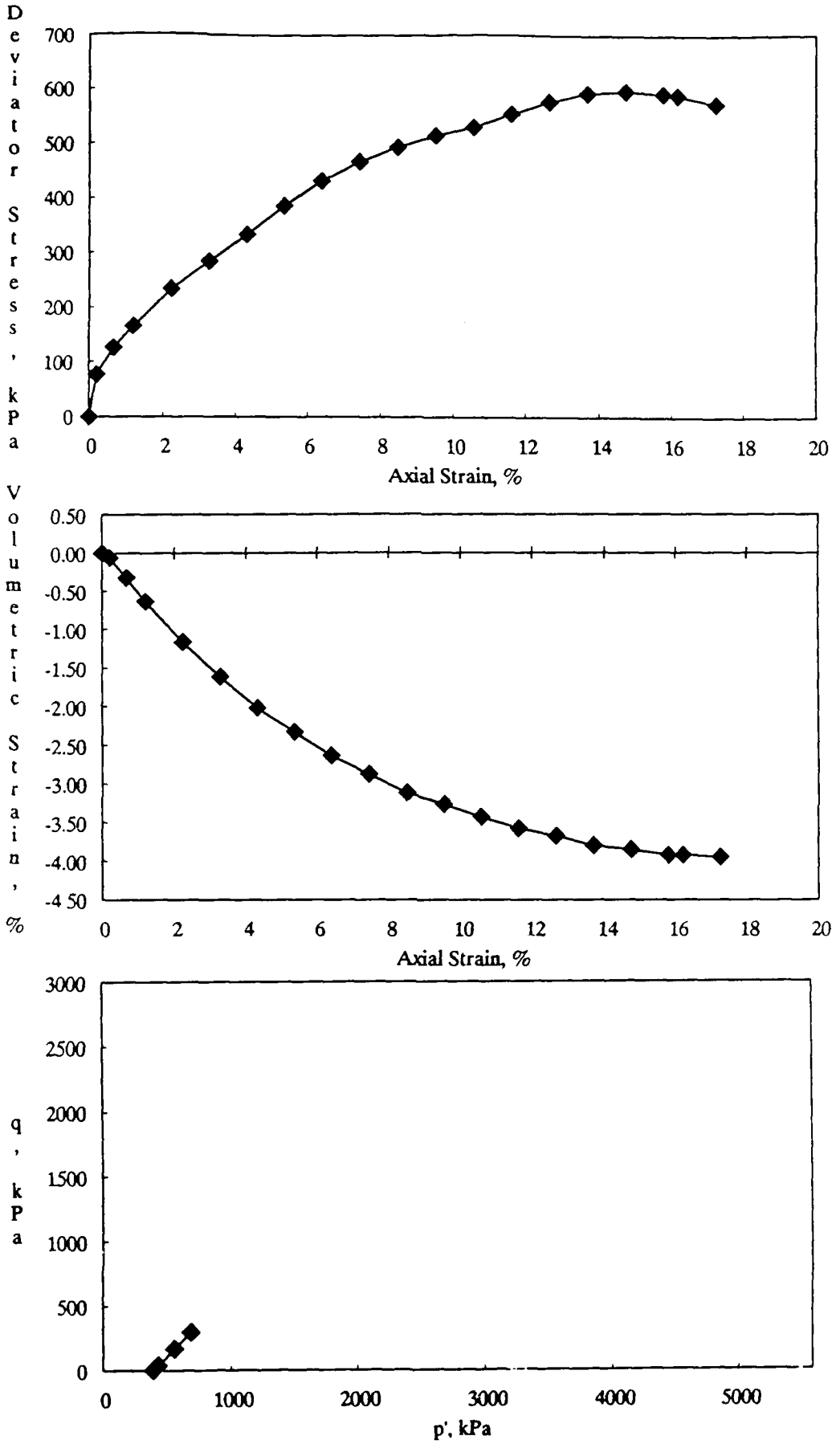


Figure A-51. CD Triaxial Test Results for 50% Kaolinite Mixture at a Standard Proctor Relative Compaction of 90% and an Effective Confining Pressure of 387 kPa.

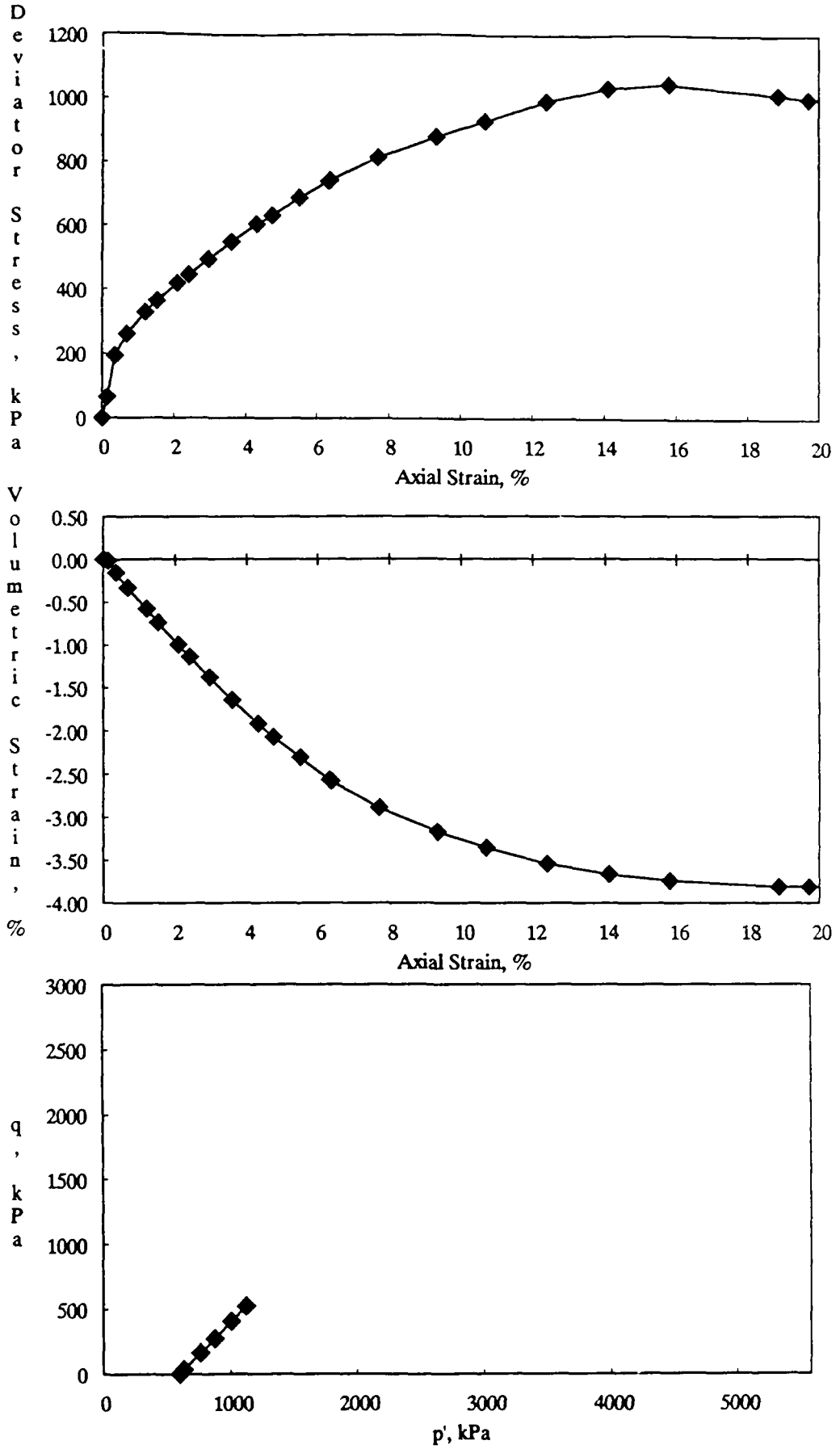


Figure A-52. CD Triaxial Test Results for 50% Kaolinite Mixture at a Standard Proctor Relative Compaction of 90% and an Effective Confining Pressure of 597 kPa.

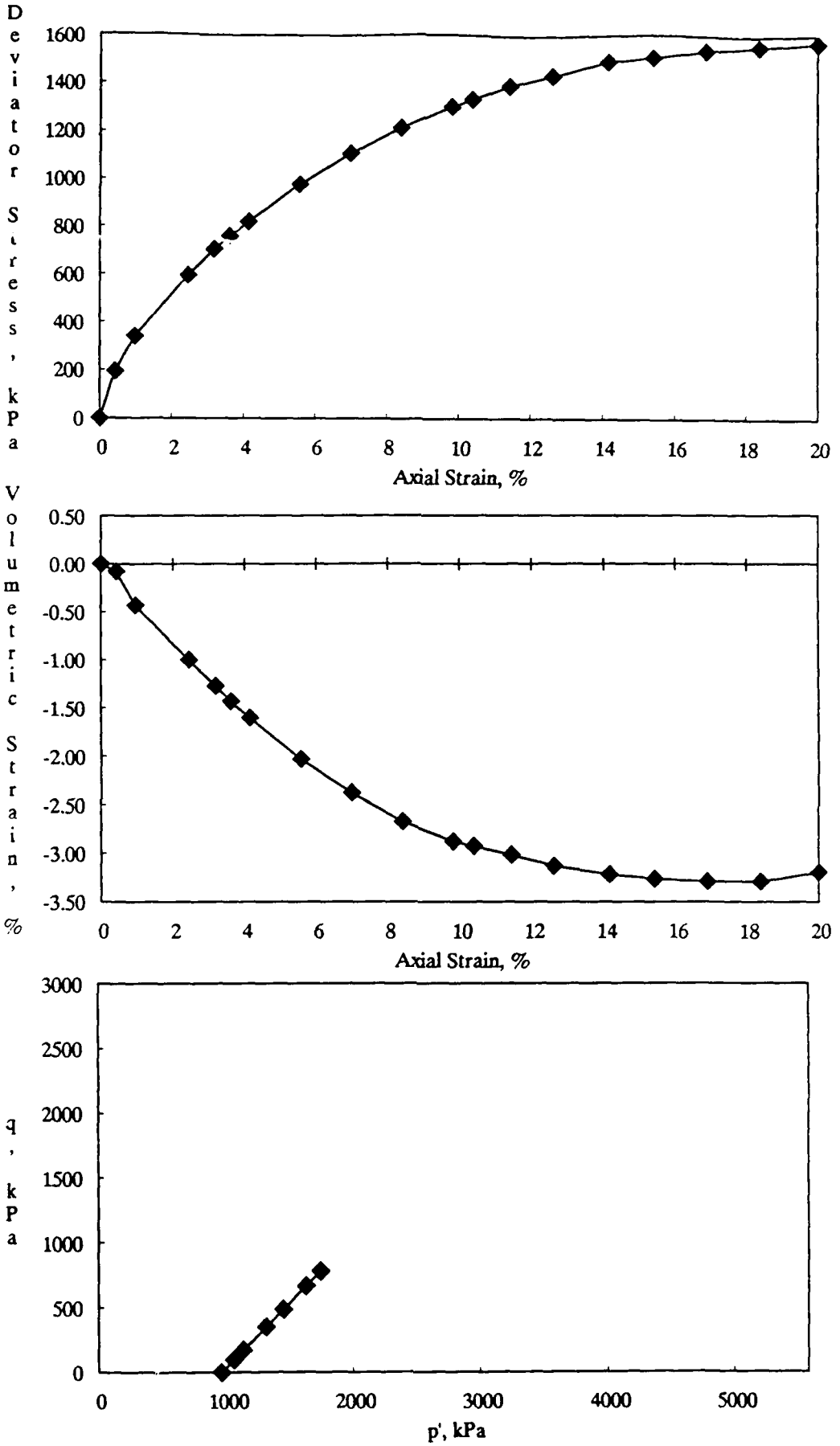


Figure A-53. CD Triaxial Test Results for 50% Kaolinite Mixture at a Standard Proctor Relative Compaction of 90% and an Effective Confining Pressure of 961 kPa.

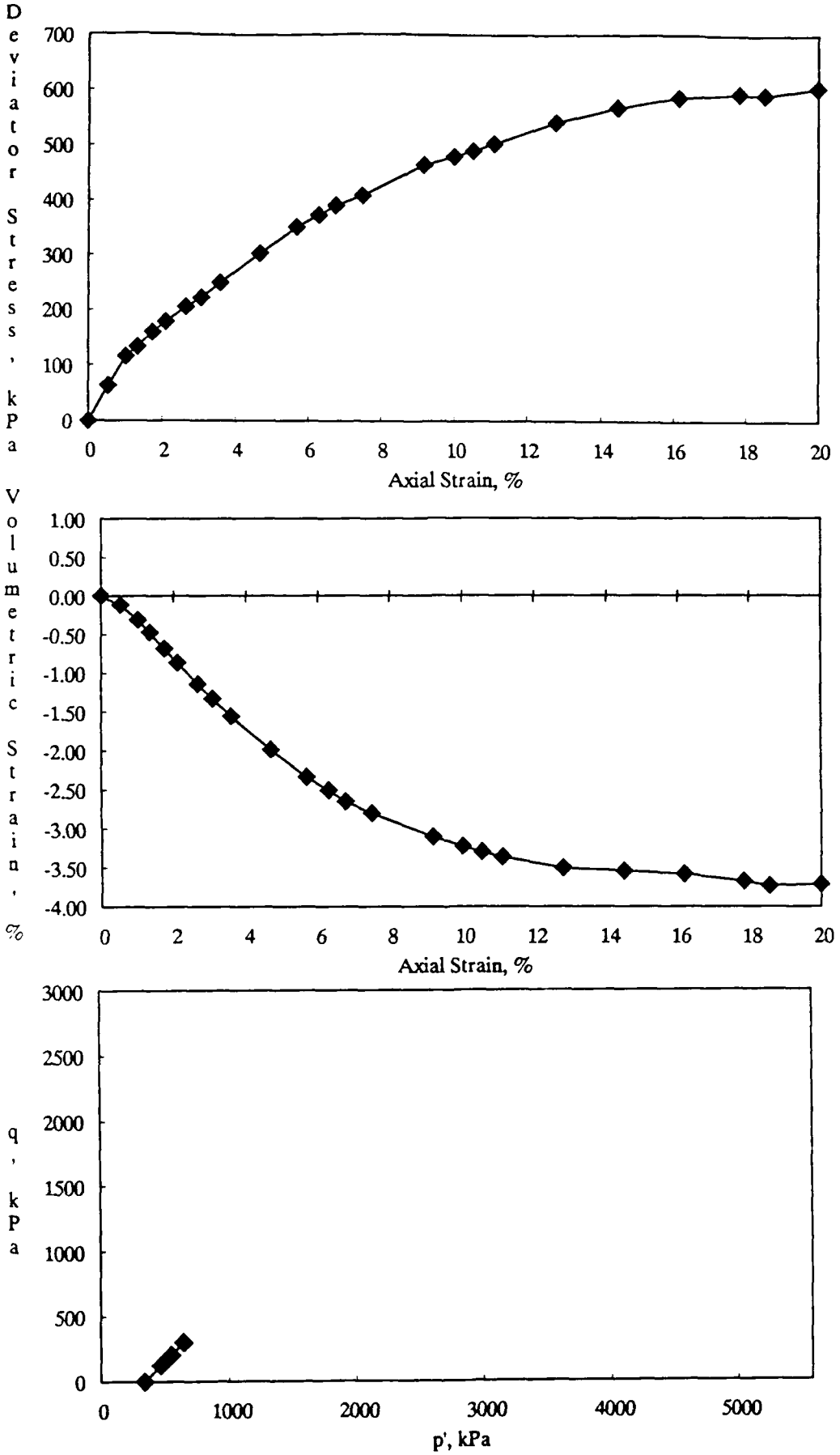


Figure A-54. CD Triaxial Test Results for 50% Kaolinite Mixture at a Standard Proctor Relative Compaction of 85% and an Effective Confining Pressure of 339 kPa.

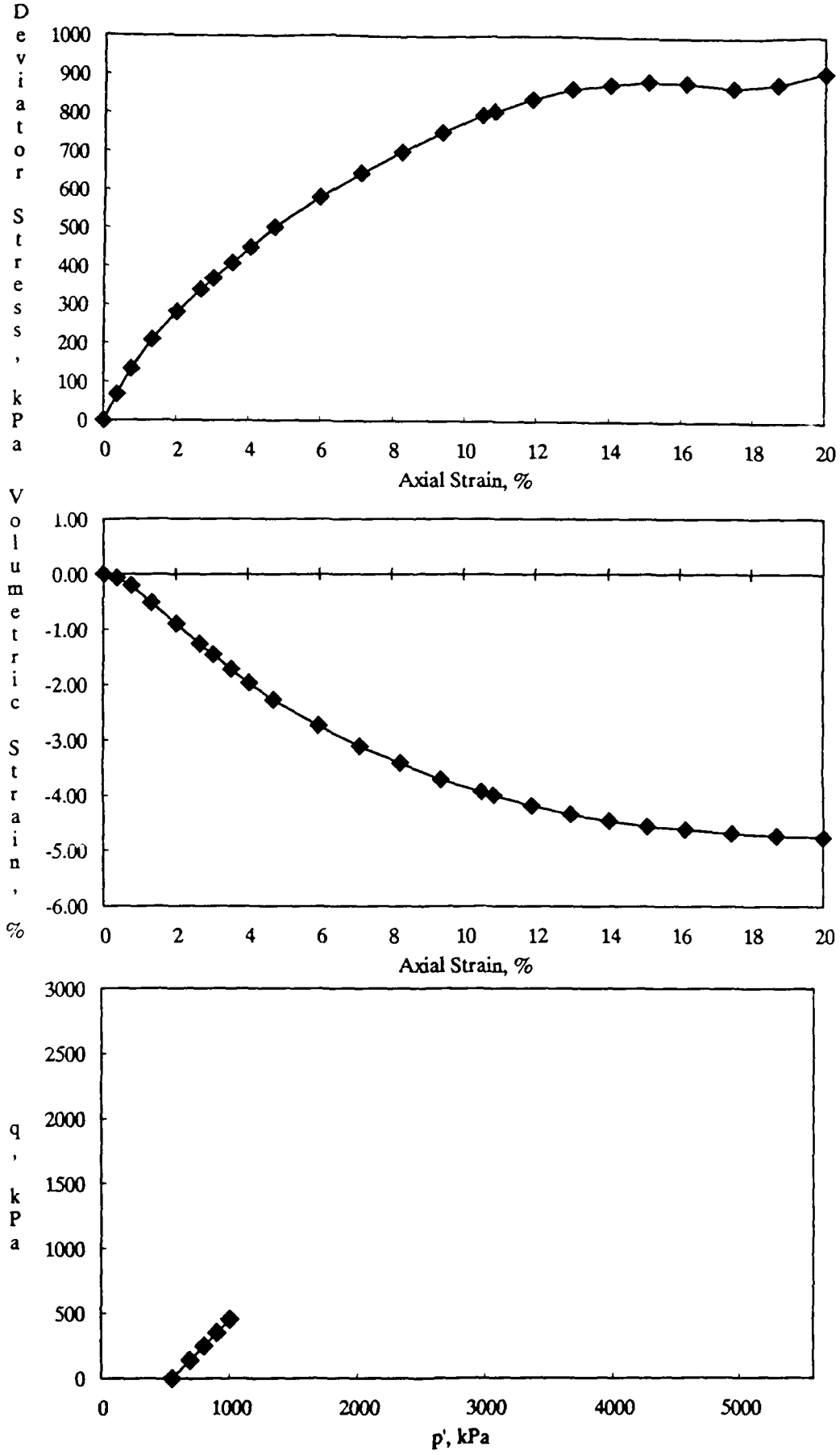


Figure A-55. CD Triaxial Test Results for 50% Kaolinite Mixture at a Standard Proctor Relative Compaction of 85% and an Effective Confining Pressure of 550 kPa.

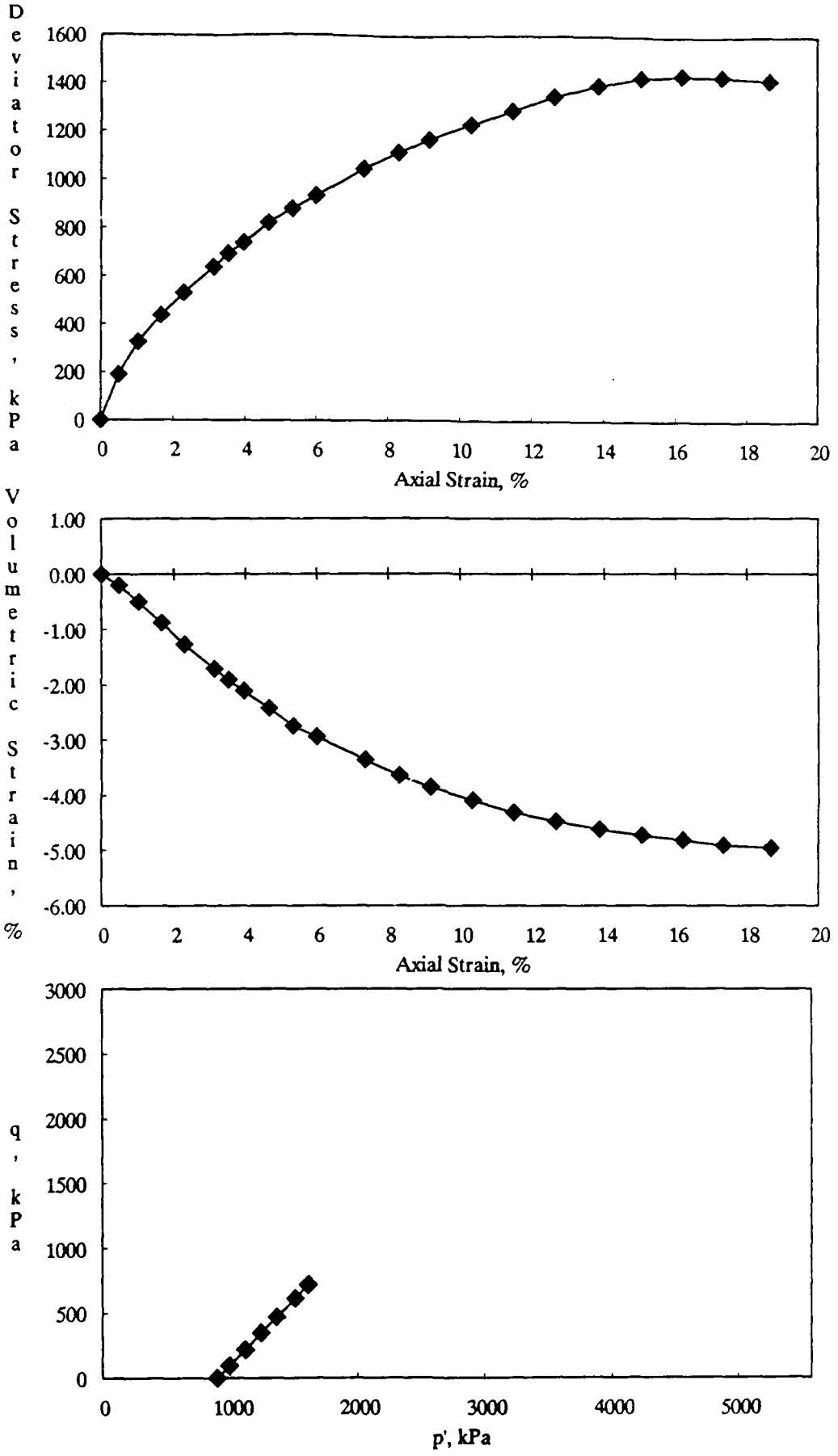


Figure A-56. CD Triaxial Test Results for 50% Kaolinite Mixture at a Standard Proctor Relative Compaction of 85% and an Effective Confining Pressure of 893 kPa.

# APPENDIX B

## Isotropically Consolidated-Undrained Triaxial Test Results on Kaolinite-Silt Mixtures

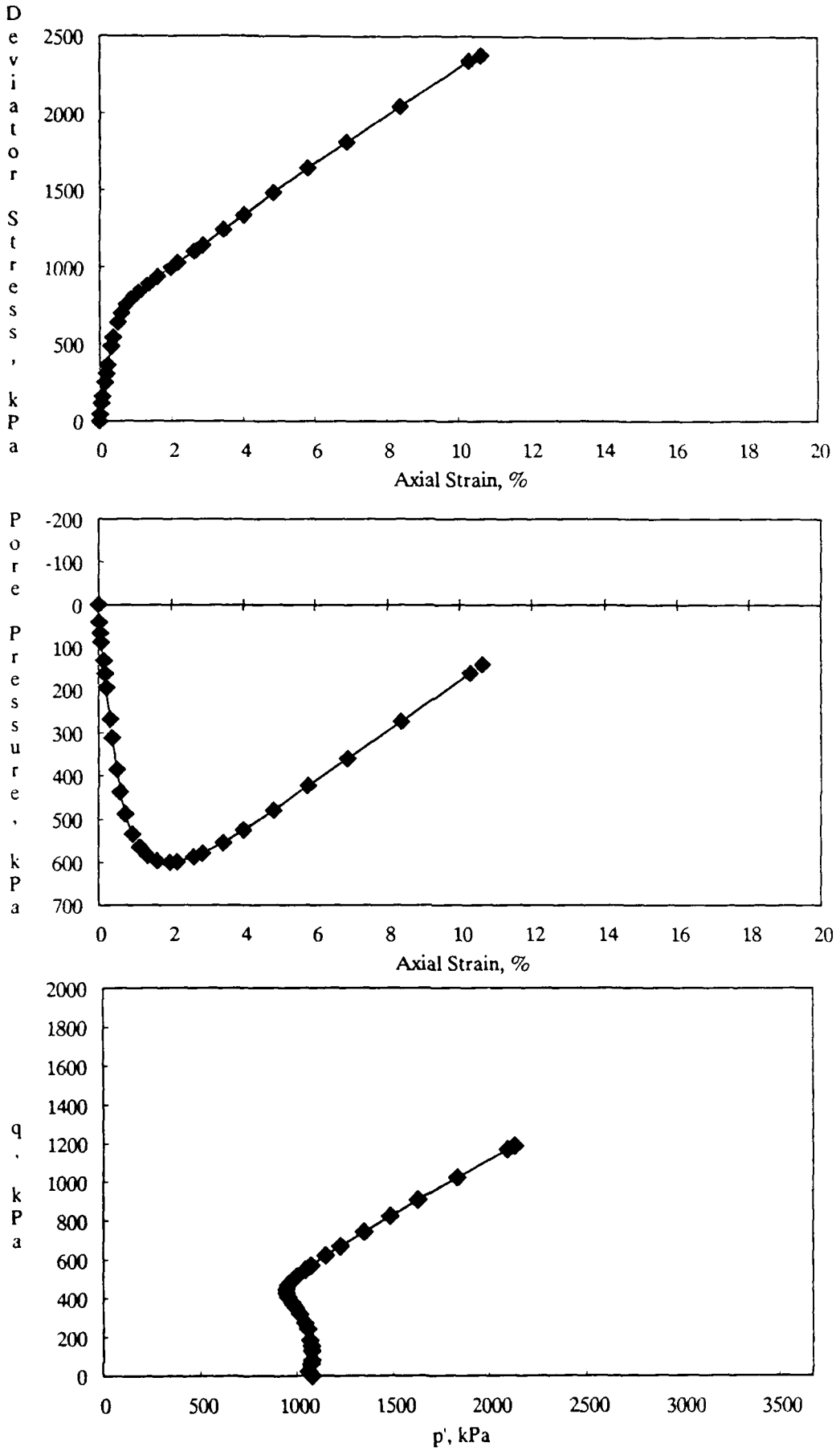


Figure B-1. CU Triaxial Test Results for 0% Kaolinite Mixture at a Standard Proctor Relative Compaction of 100% and an Effective Confining Pressure of 1079 kPa.

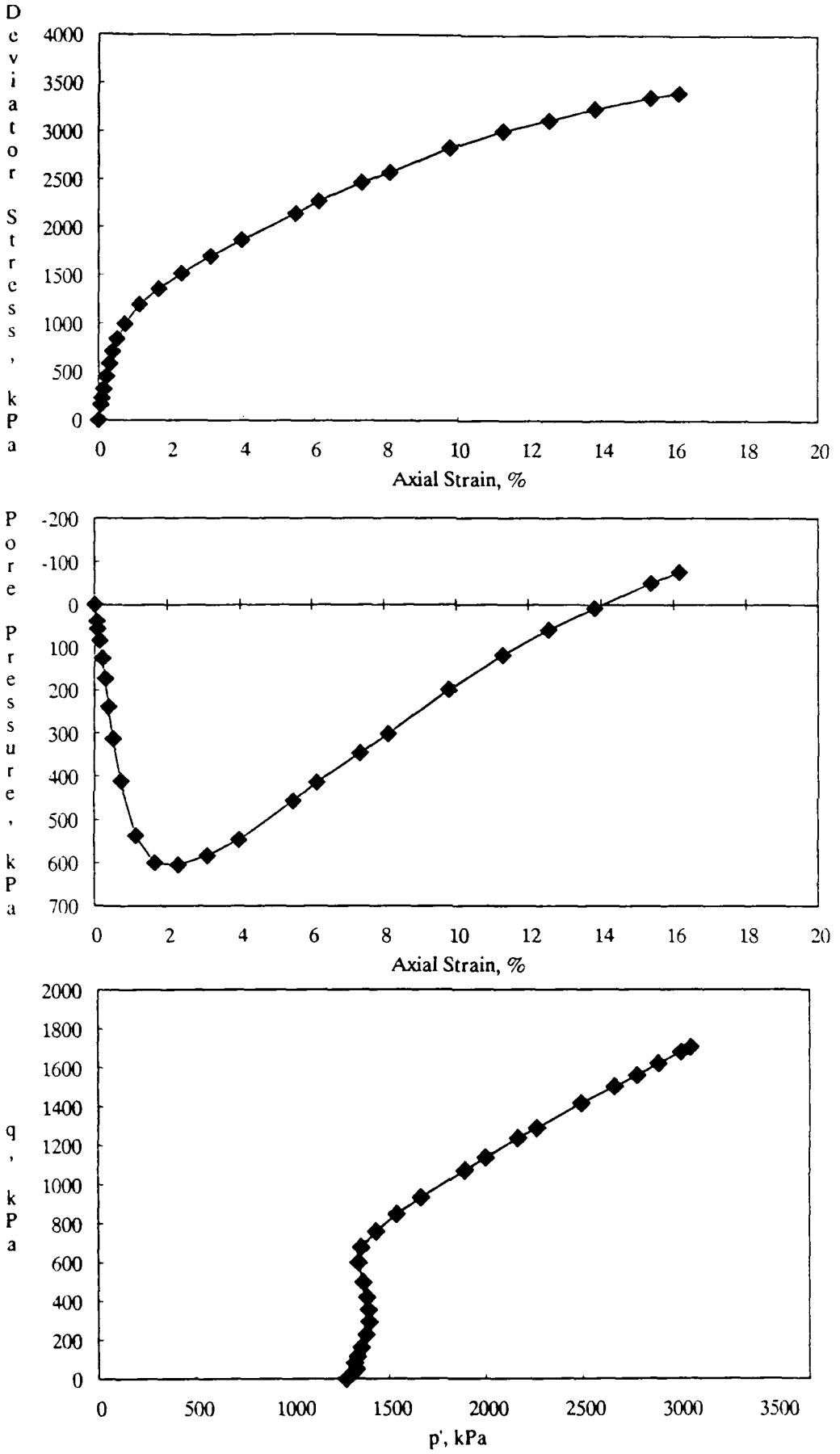


Figure B-2. CU Triaxial Test Results for 0% Kaolinite Mixture at a Standard Proctor Relative Compaction of 100% and an Effective Confining Pressure of 1276 kPa.

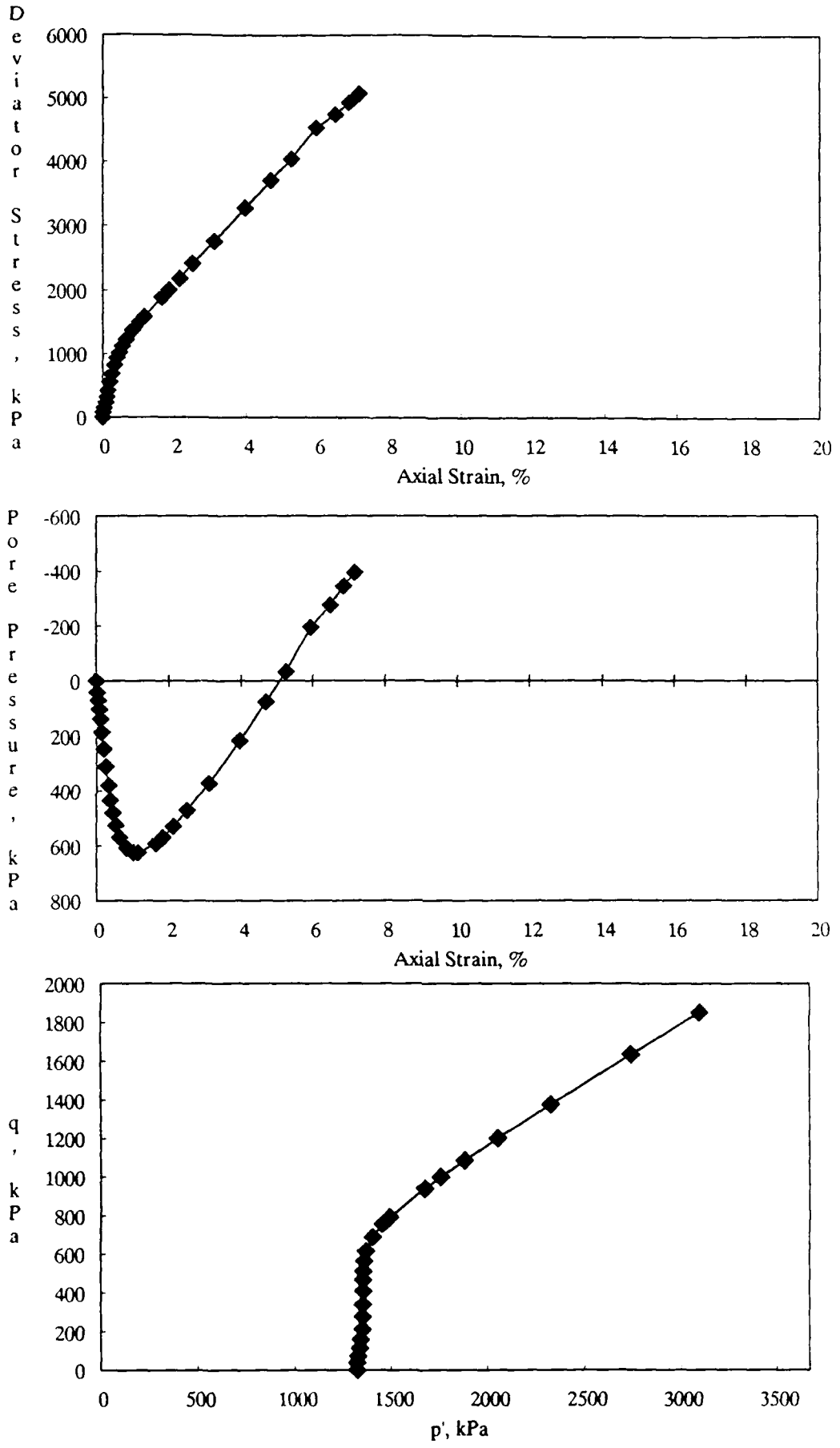


Figure B-3. CU Triaxial Test Results for 0% Kaolinite Mixture at a Standard Proctor Relative Compaction of 100% and an Effective Confining Pressure of 1324 kPa.

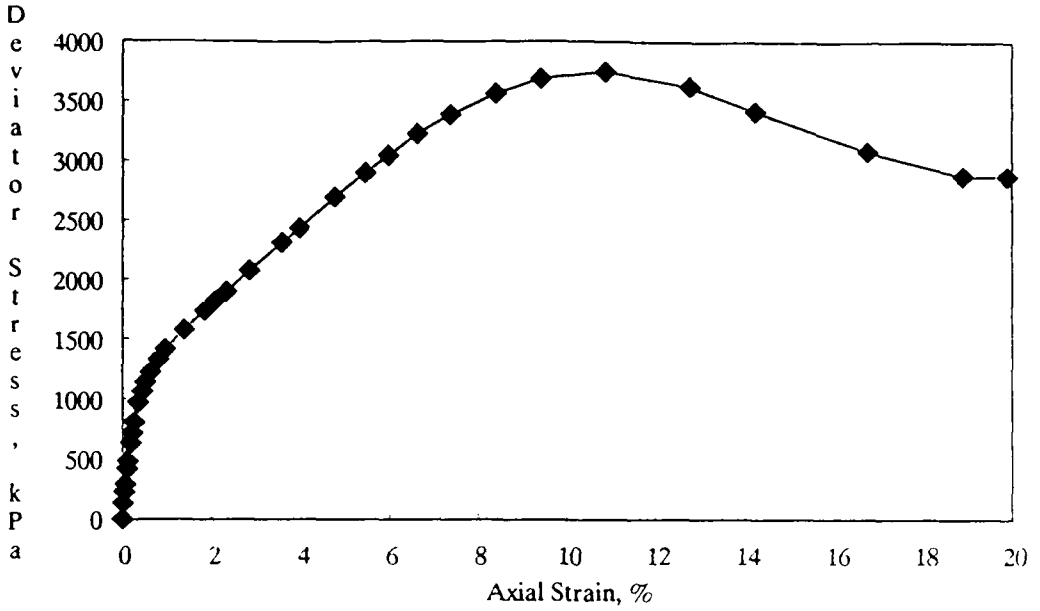


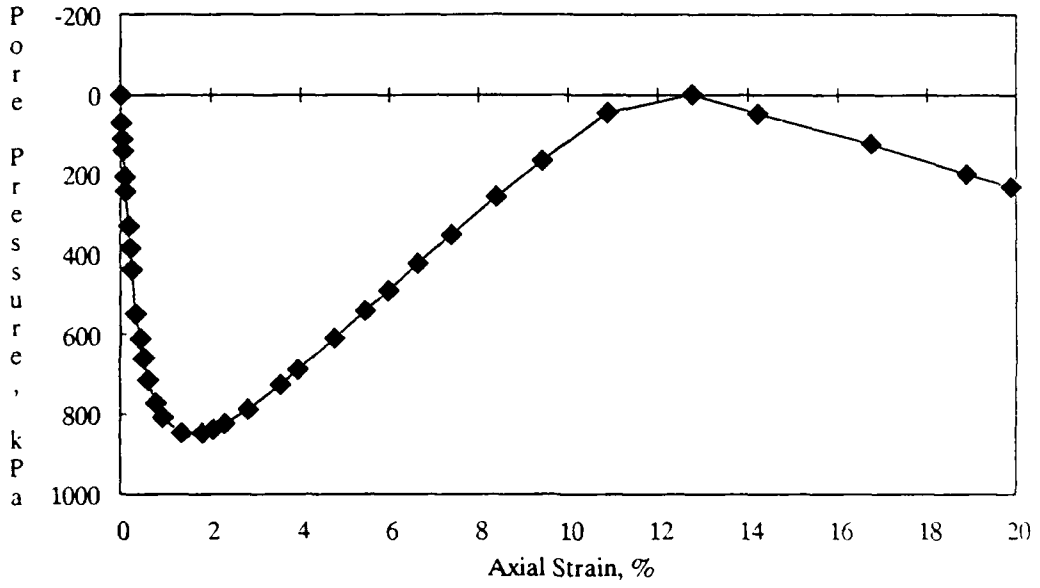


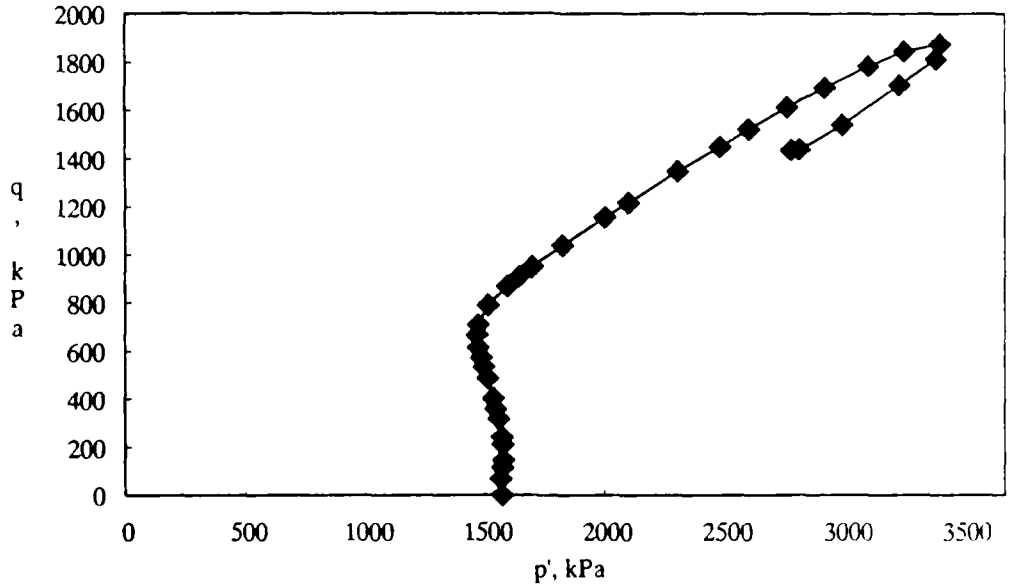


Figure B-4. **CU Triaxial Test Results for 0% Kaolinite Mixture at a Standard Proctor Relative Compaction of 100% and an Effective Confining Pressure of 1569 kPa.**

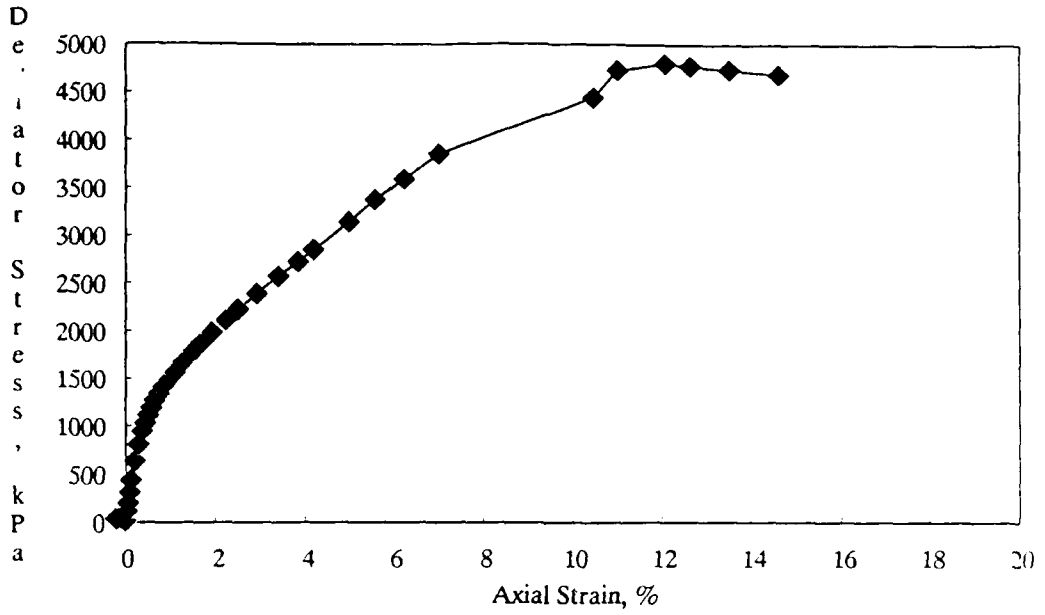


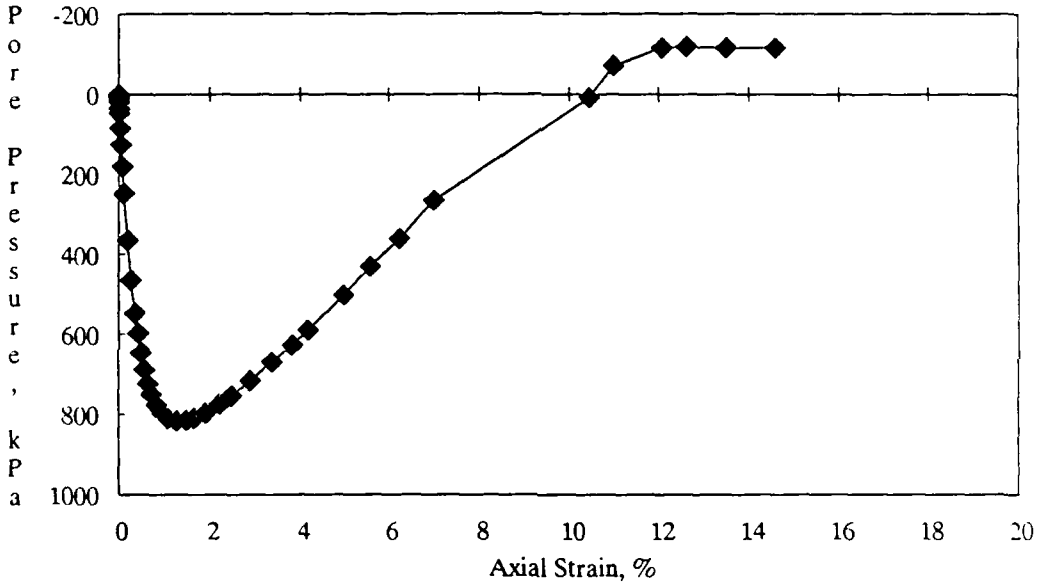


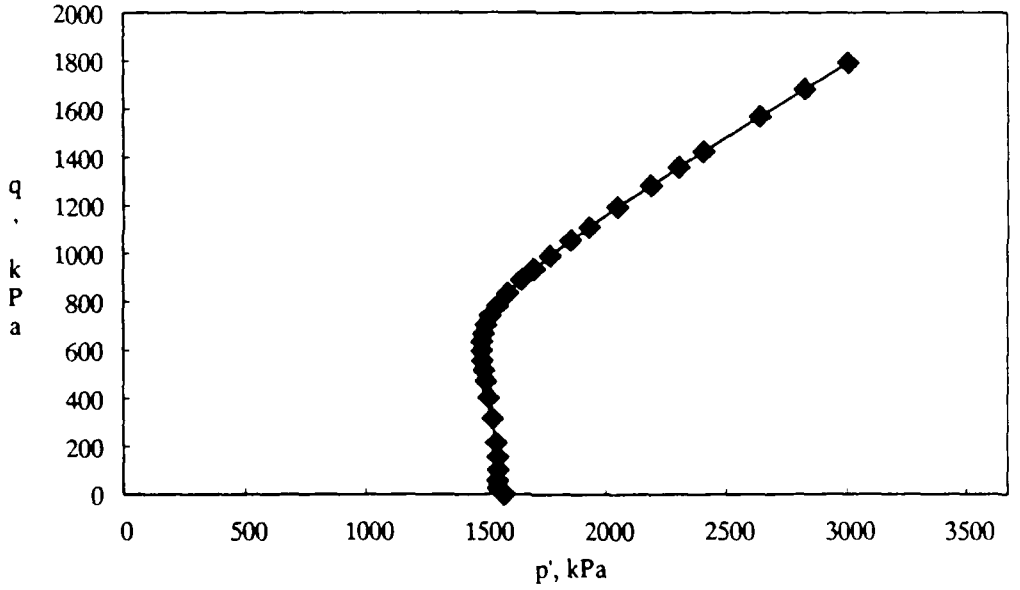


Figure B-5. CU Triaxial Test Results for 0% Kaolinite Mixture at a Standard Proctor Relative Compaction of 100% and an Effective Confining Pressure of 1572 kPa.

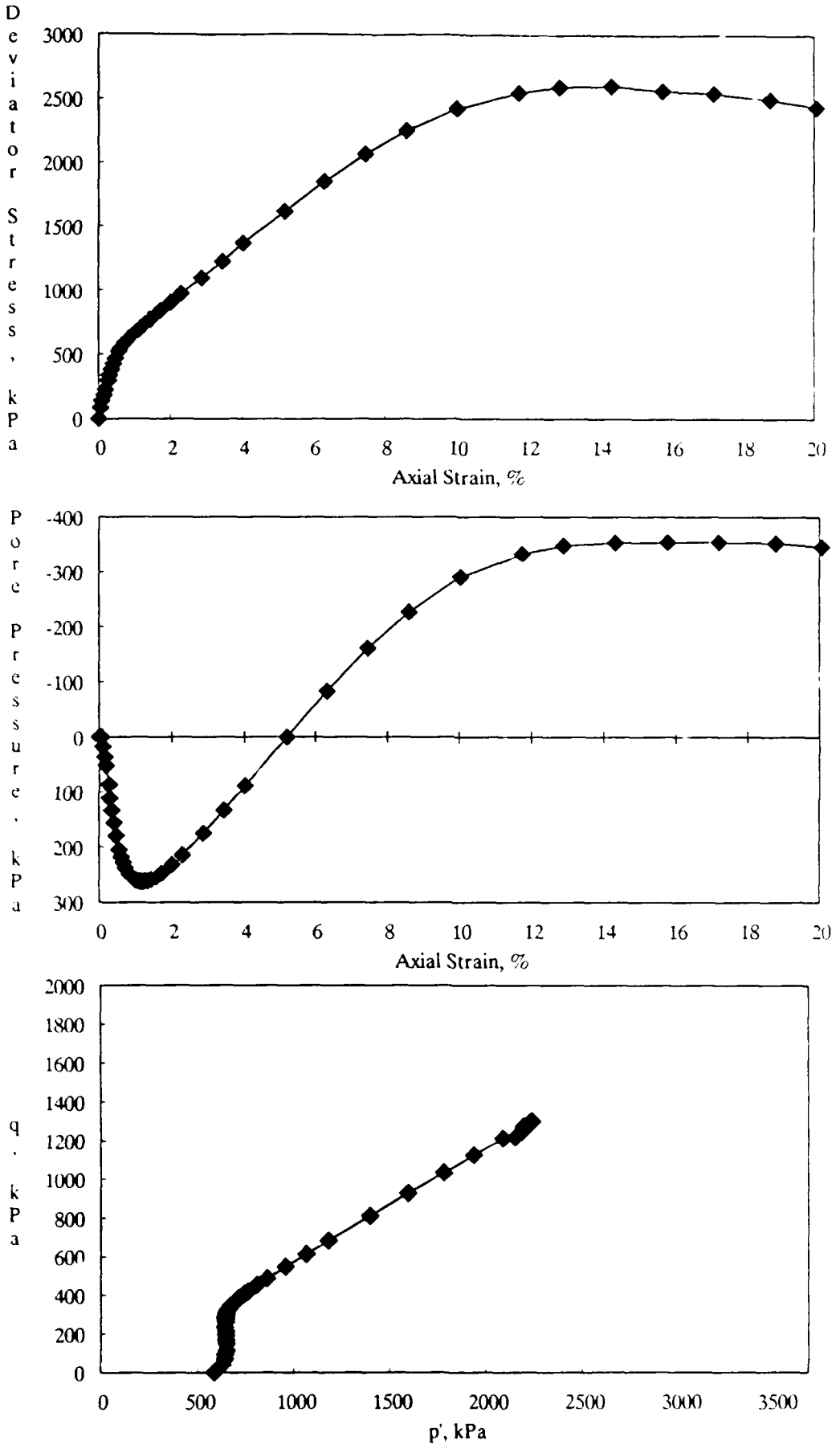


Figure B-6. **CU Triaxial Test Results for 0% Kaolinite Mixture at a Standard Proctor Relative Compaction of 95% and an Effective Confining Pressure of 583 kPa.**

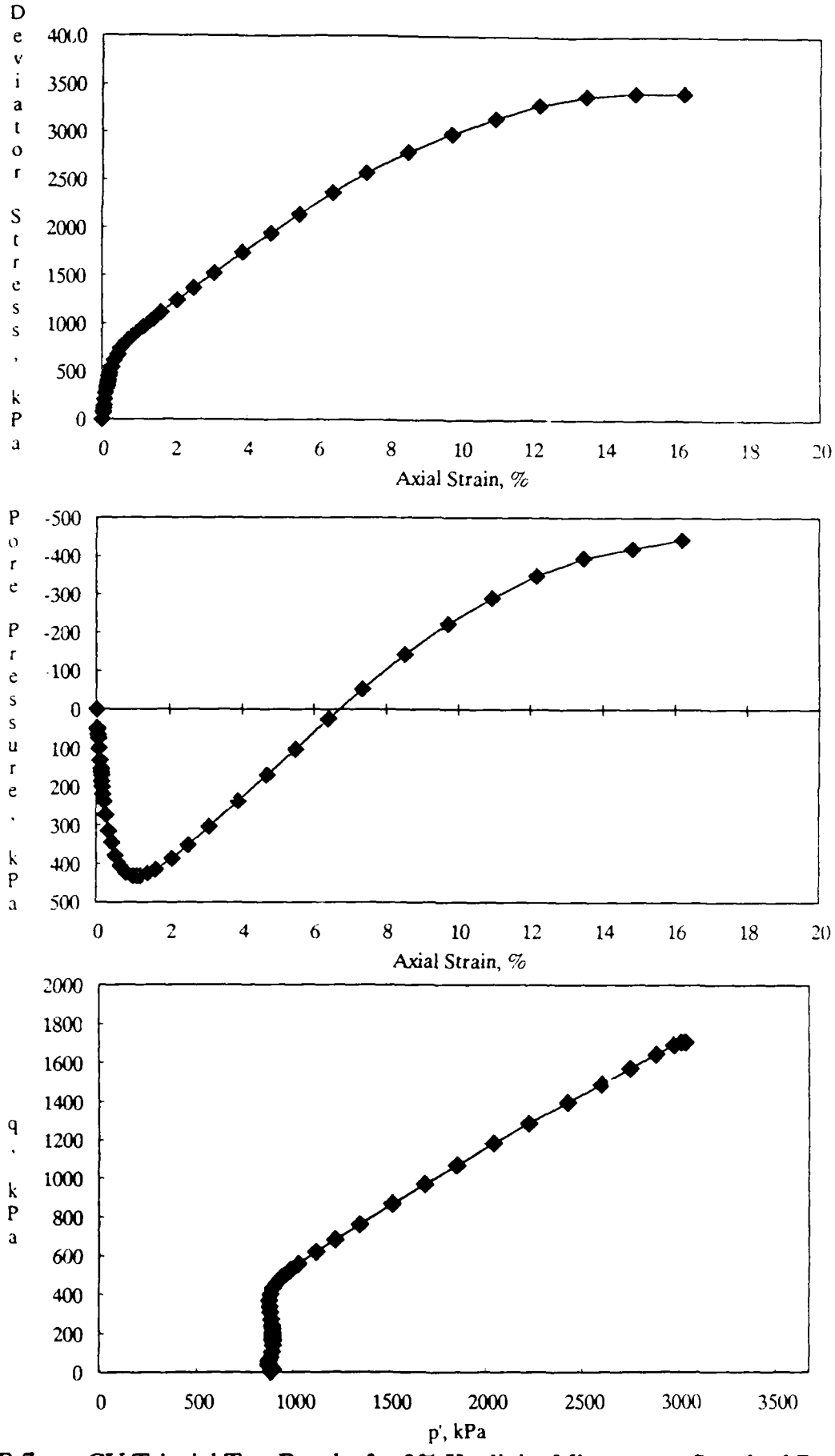


Figure B-7. **CU Triaxial Test Results for 0% Kaolinite Mixture at a Standard Proctor Relative Compaction of 95% and an Effective Confining Pressure of 882 kPa.**

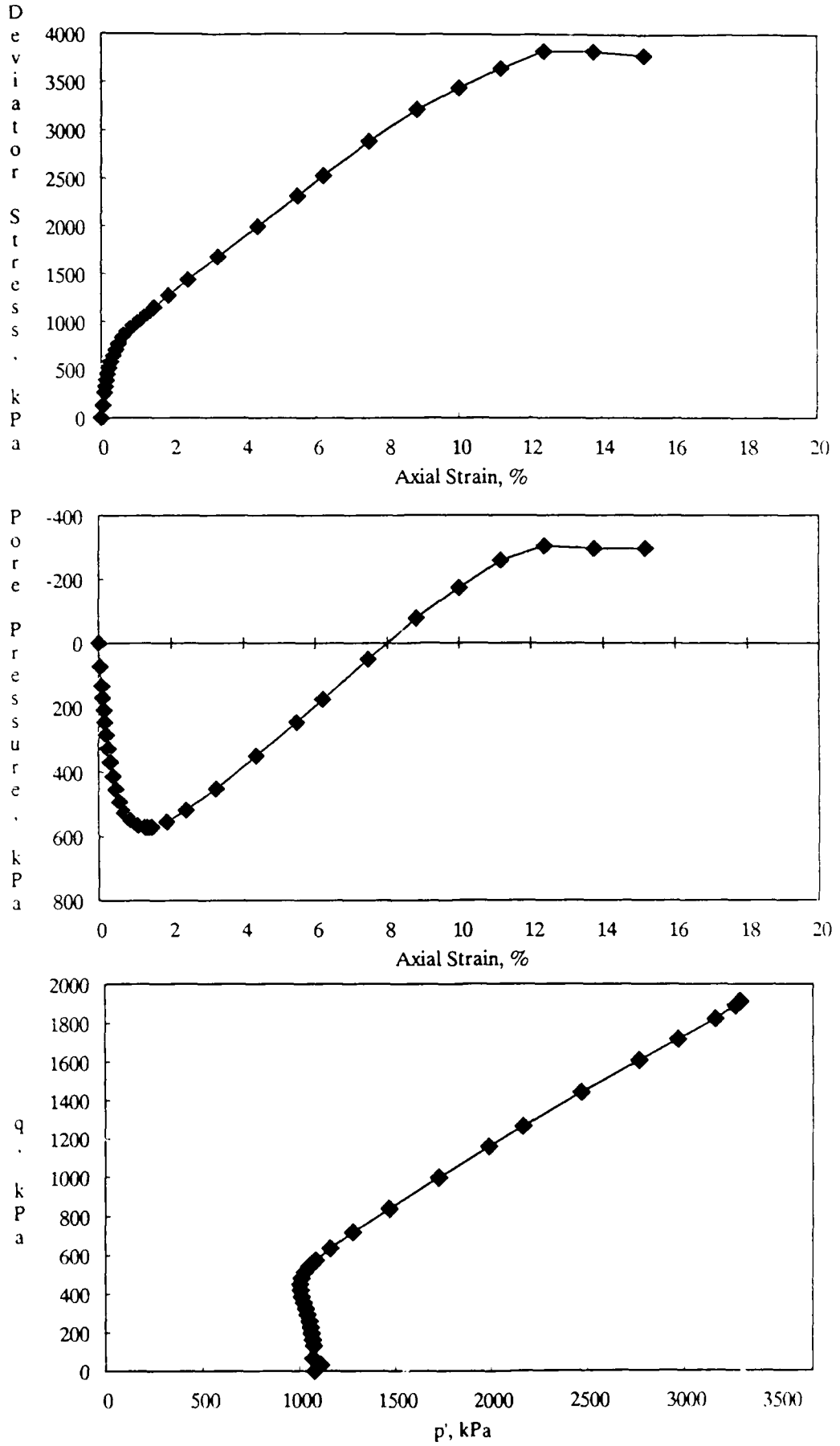


Figure B-8. CU Triaxial Test Results for 0% Kaolinite Mixture at a Standard Proctor Relative Compaction of 95% and an Effective Confining Pressure of 1079 kPa.

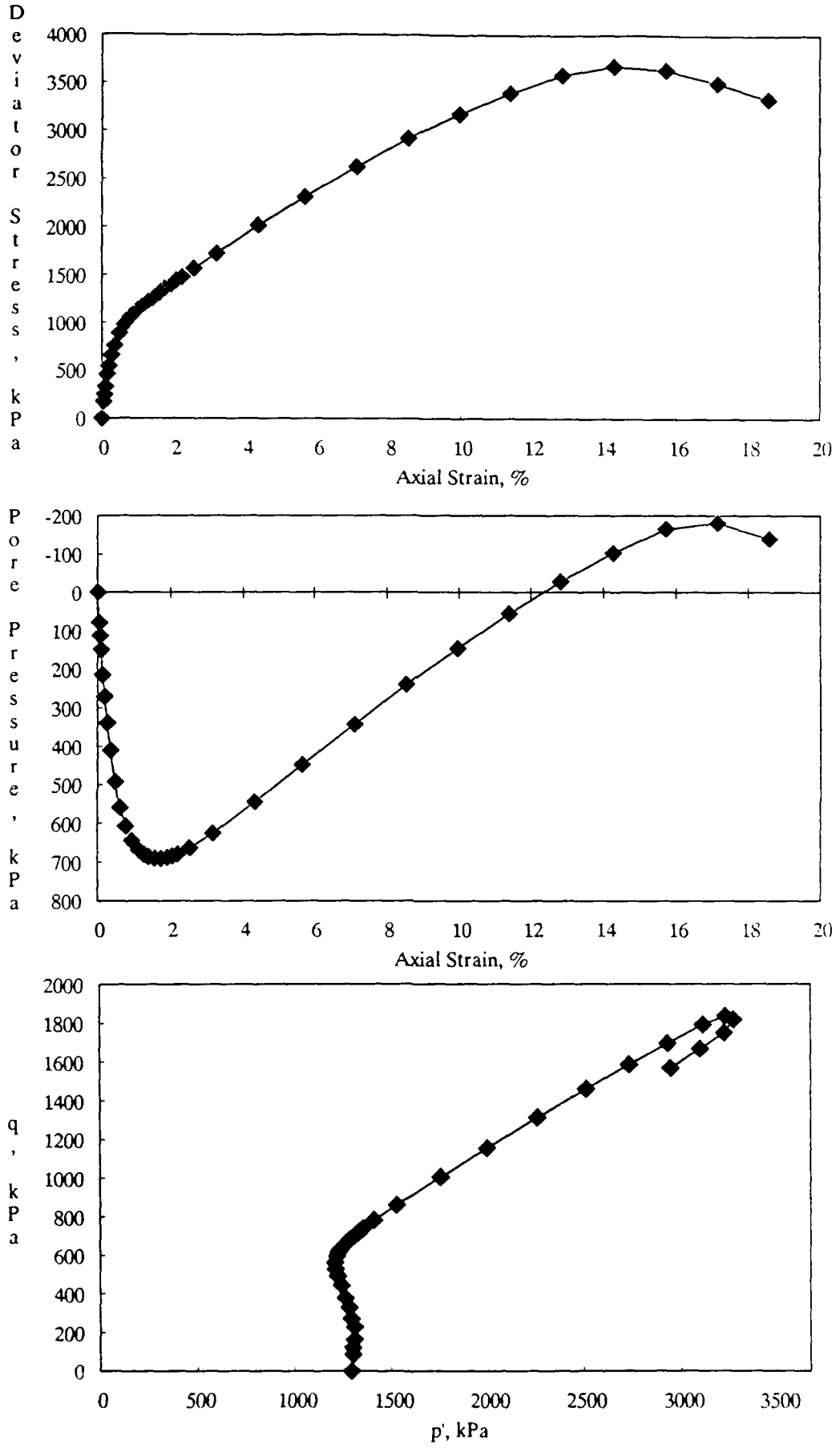


Figure B-9. CU Triaxial Test Results for 0% Kaolinite Mixture at a Standard Proctor Relative Compaction of 95% and an Effective Confining Pressure of 1292 kPa.

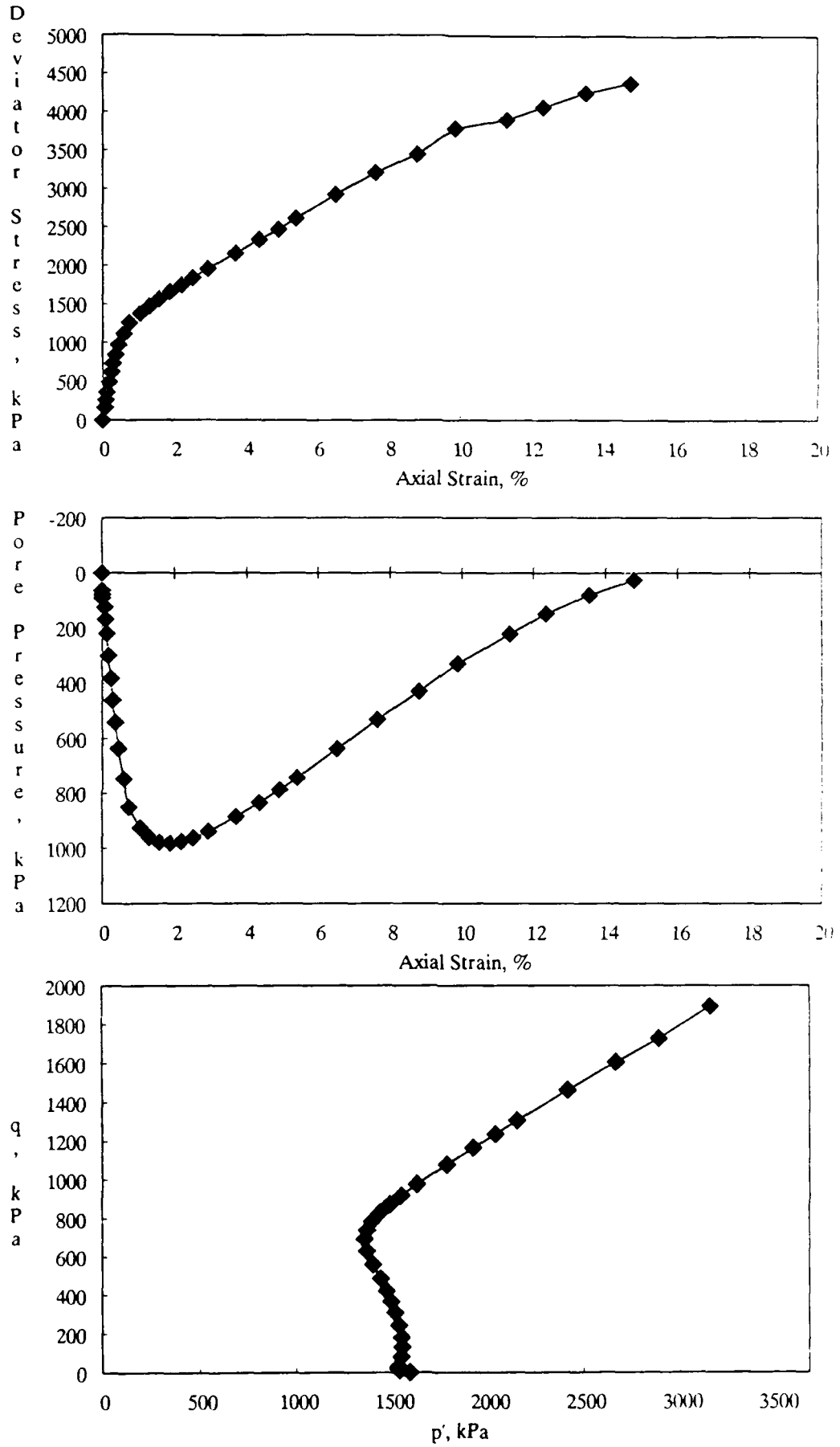


Figure B-10. CU Triaxial Test Results for 0% Kaolinite Mixture at a Standard Proctor Relative Compaction of 95% and an Effective Confining Pressure of 1590 kPa.

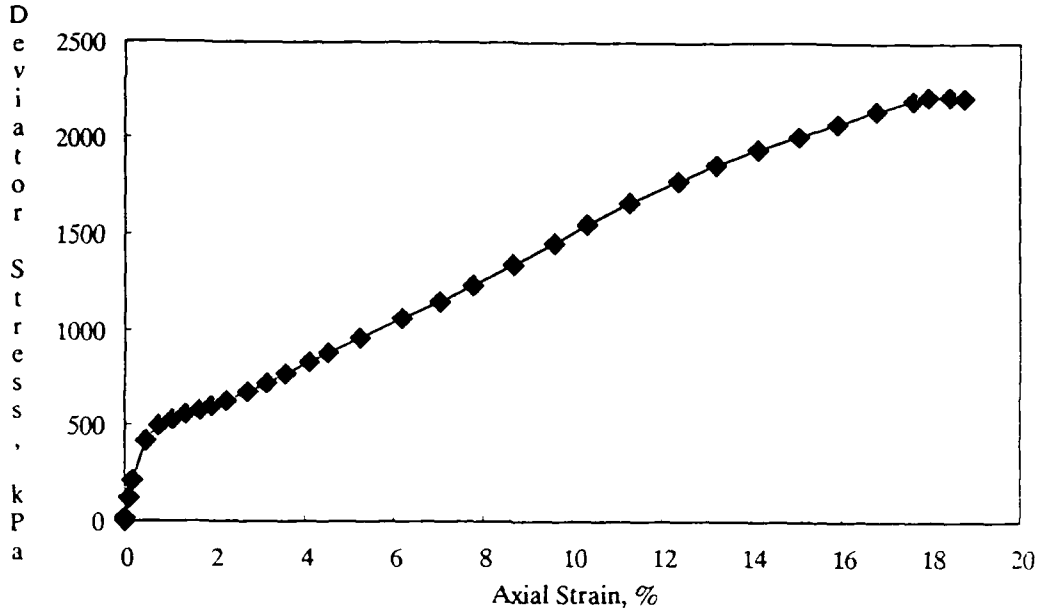


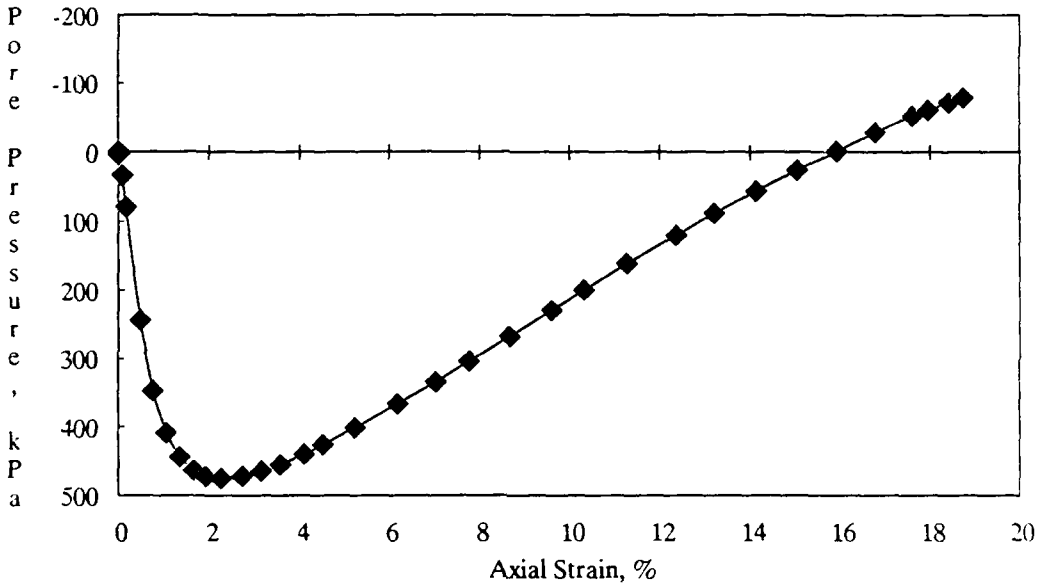


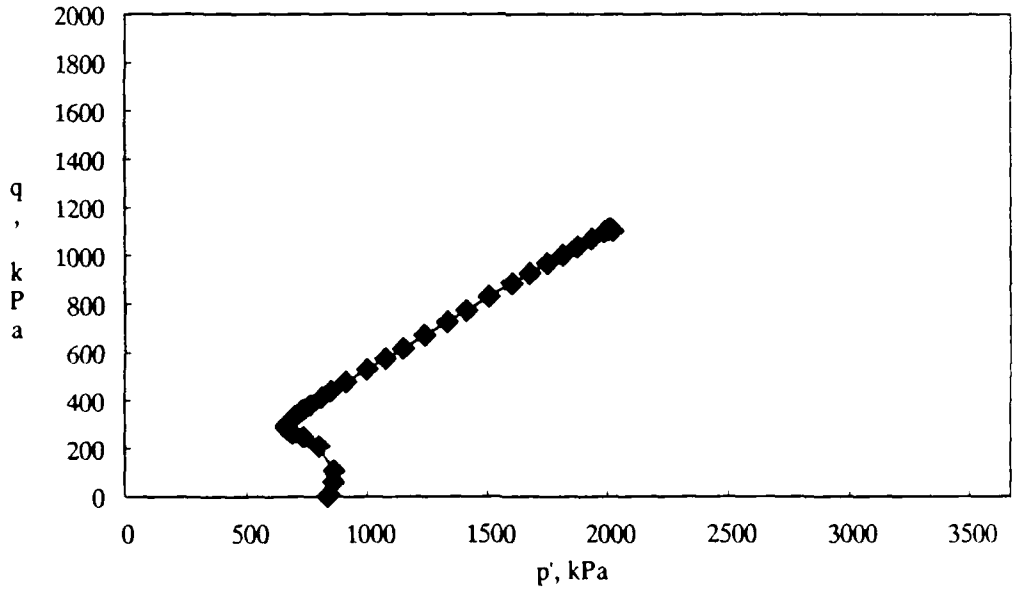


Figure B-11. CU Triaxial Test Results for 0% Kaolinite Mixture at a Standard Proctor Relative Compaction of 90% and an Effective Confining Pressure of 834 kPa.

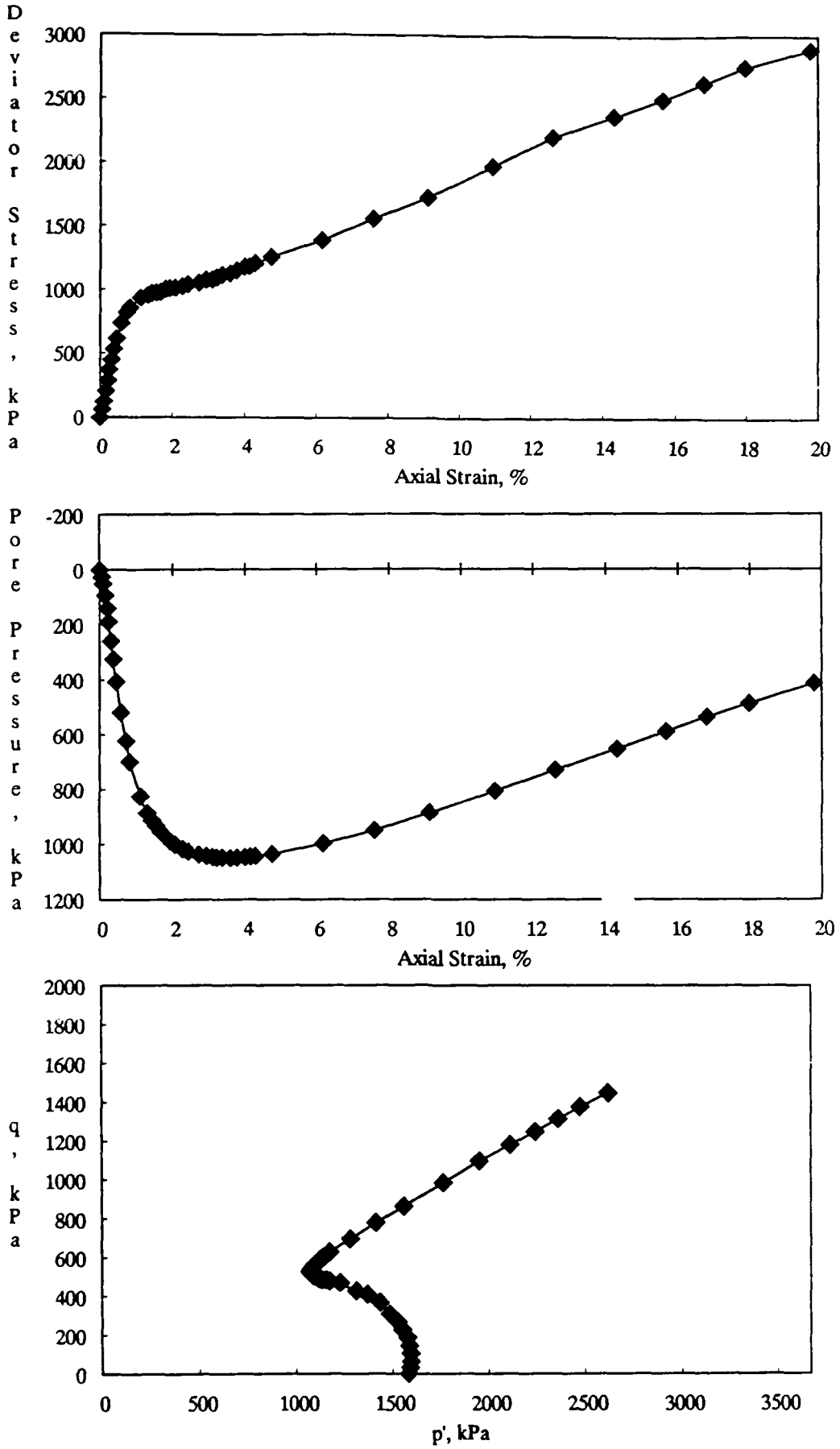


Figure B-12. CU Triaxial Test Results for 0% Kaolinite Mixture at a Standard Proctor Relative Compaction of 90% and an Effective Confining Pressure of 1583 kPa.

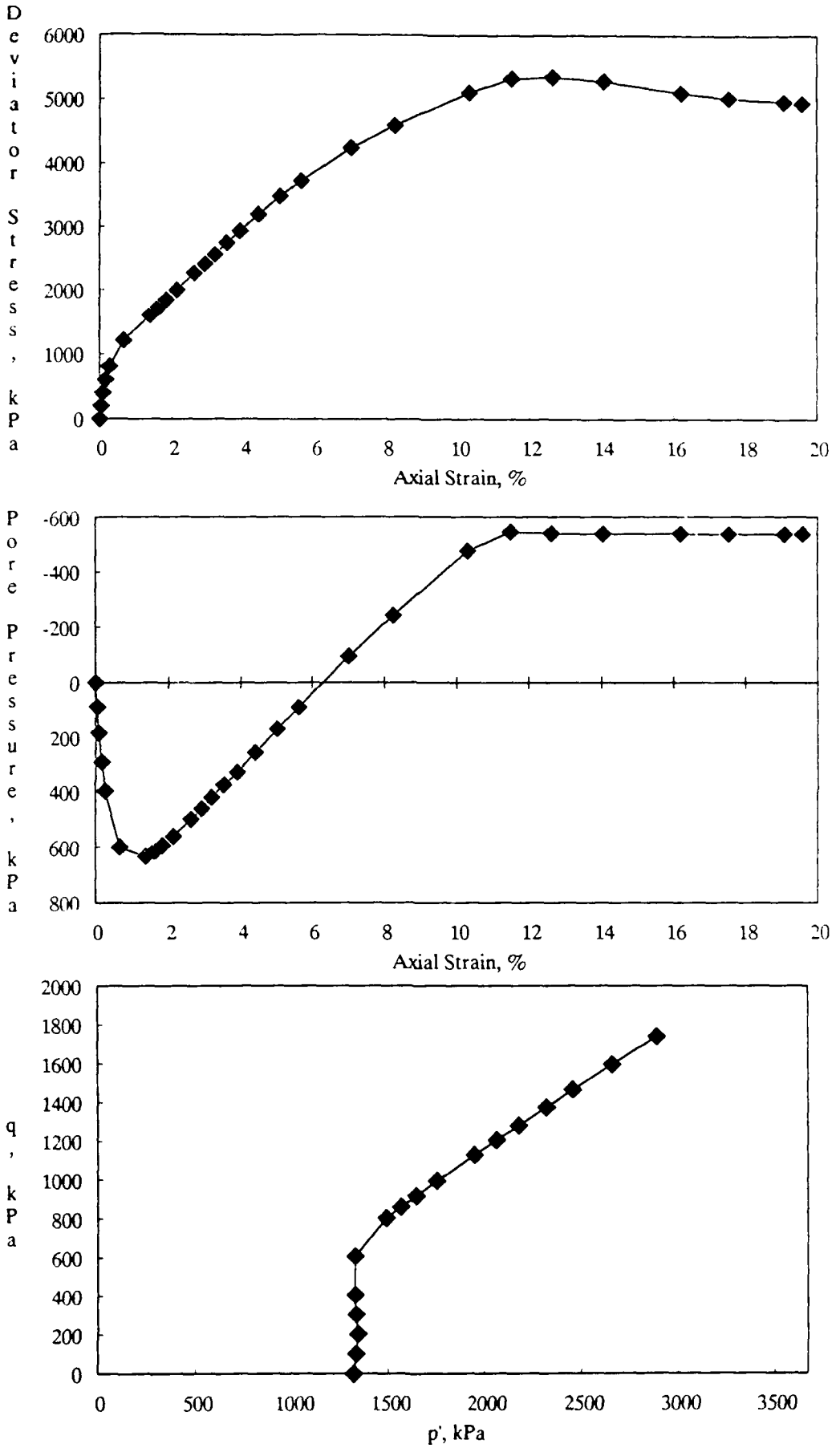


Figure B-13. CU Triaxial Test Results for 10% Kaolinite Mixture at a Standard Proctor Relative Compaction of 100% and an Effective Confining Pressure of 1318 kPa.

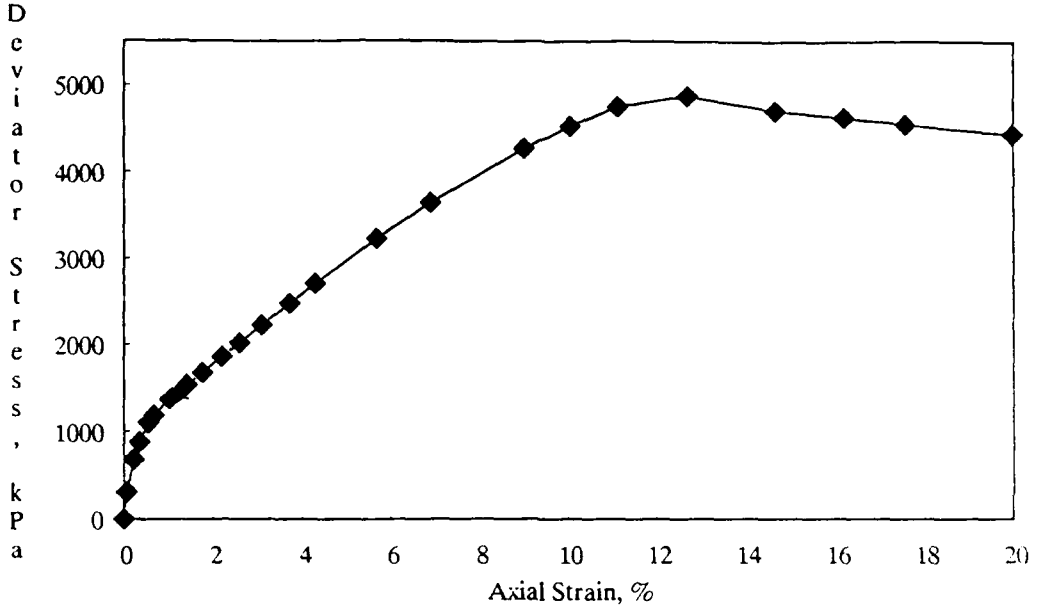


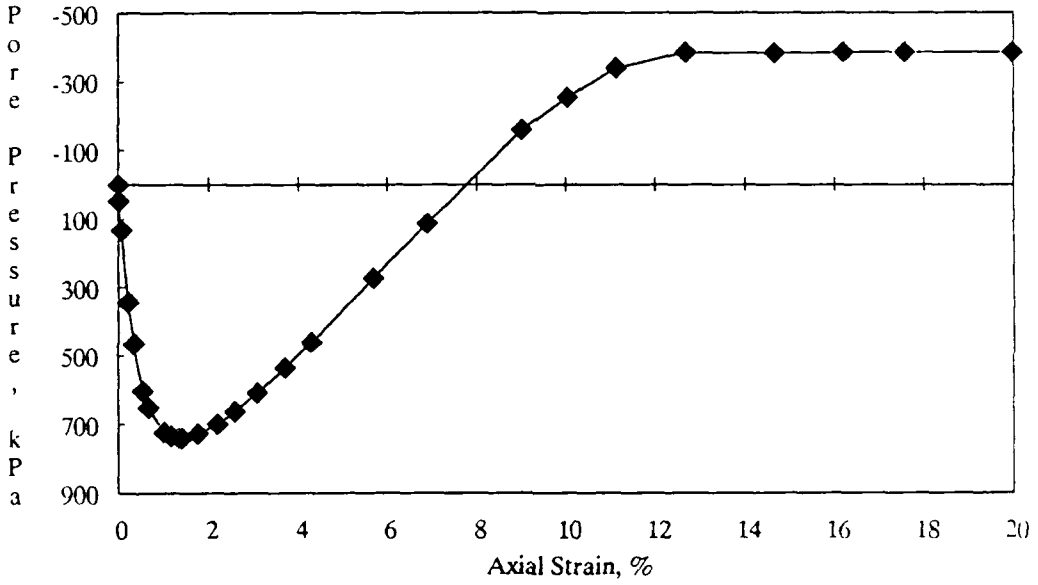


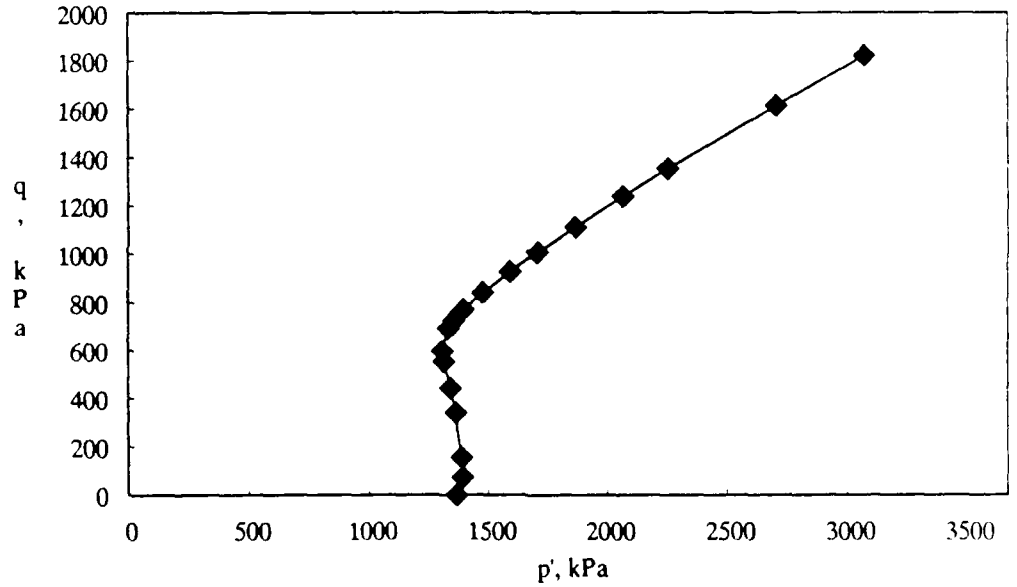


Figure B-14. CU Triaxial Test Results for 10% Kaolinite Mixture at a Standard Proctor Relative Compaction of 100% and an Effective Confining Pressure of 1363 kPa.

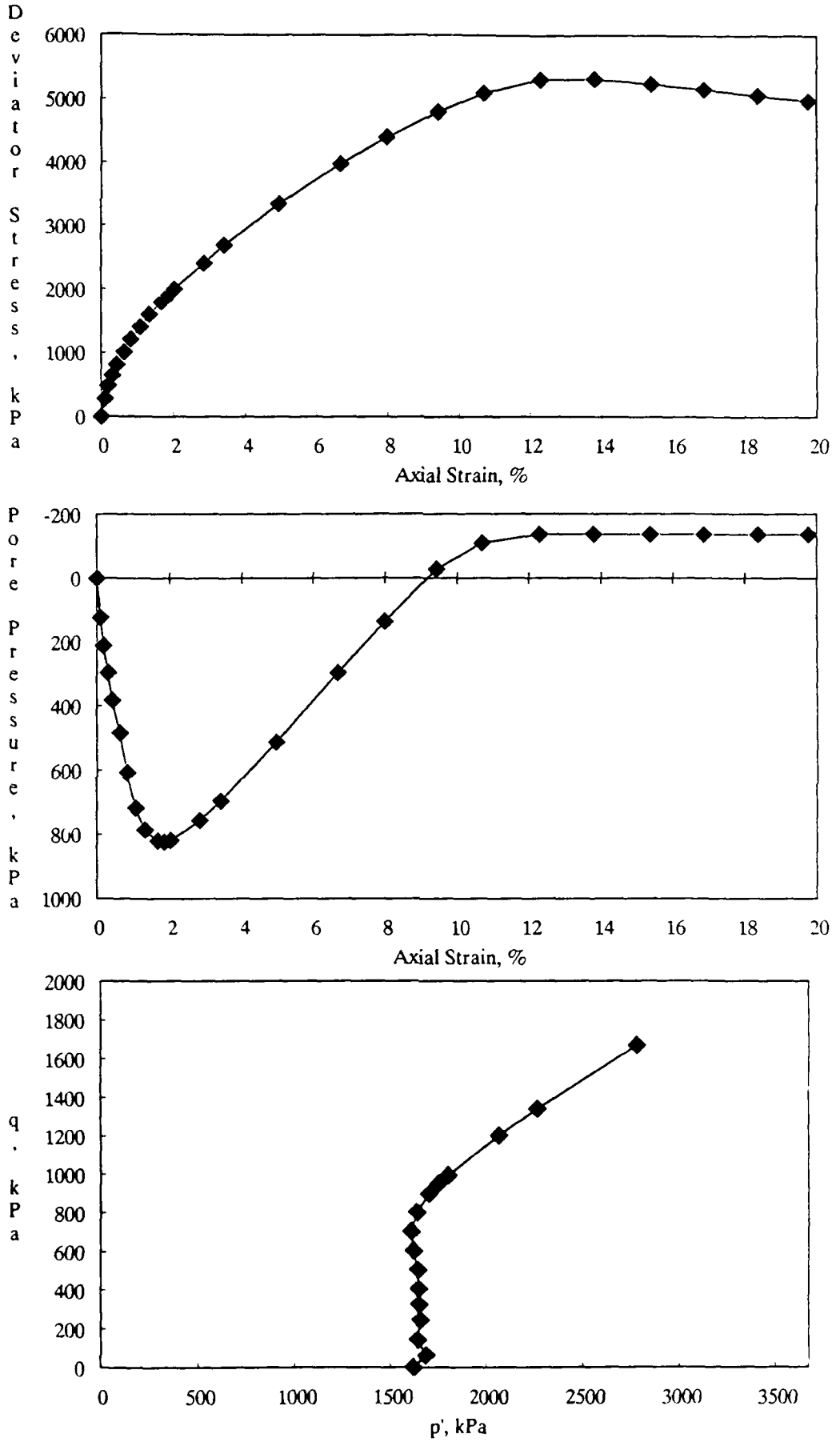


Figure B-15. CU Triaxial Test Results for 10% Kaolinite Mixture at a Standard Proctor Relative Compaction of 100% and an Effective Confining Pressure of 1618 kPa.

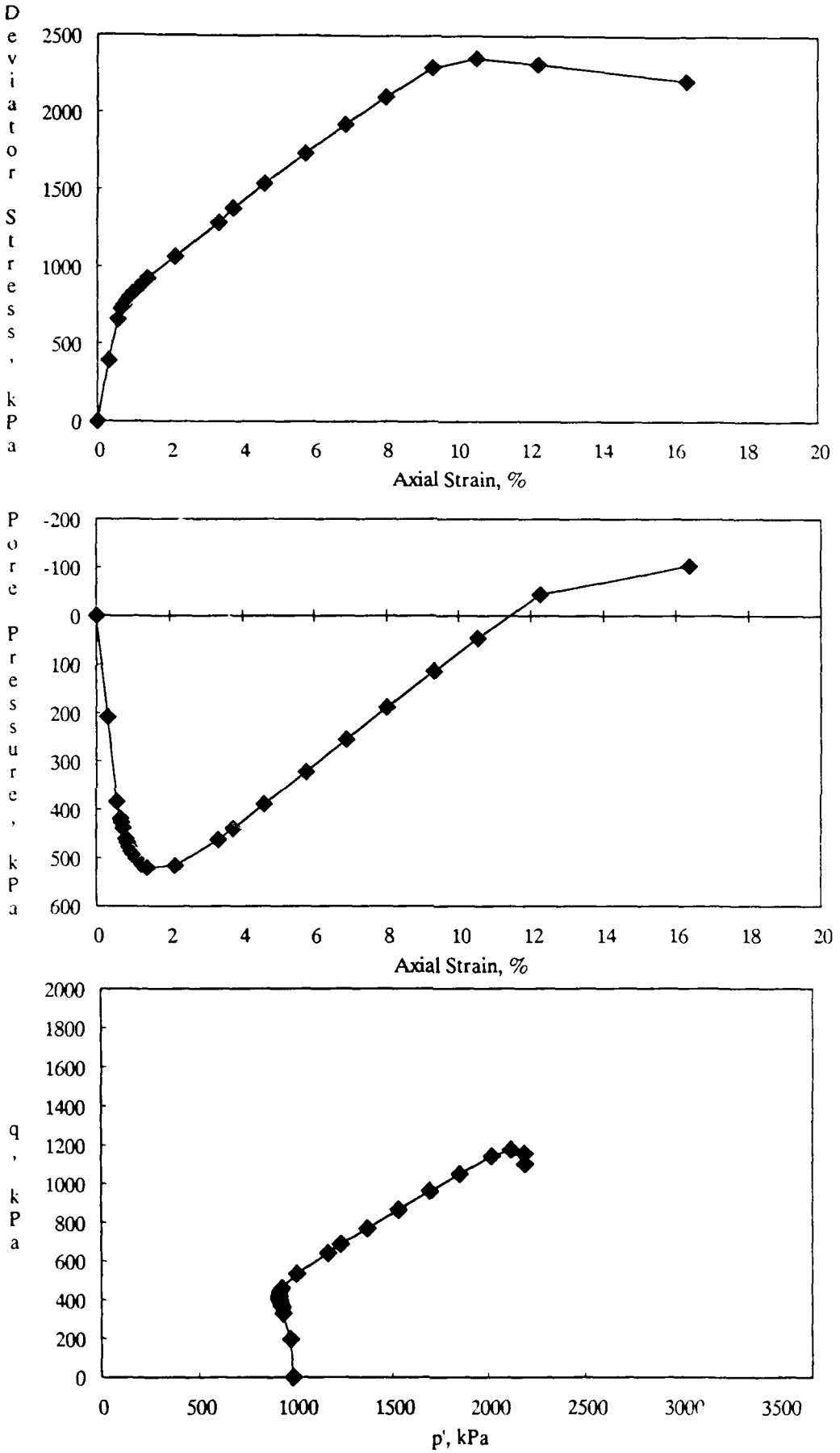


Figure B-16. CU Triaxial Test Results for 10% Kaolinite Mixture at a Standard Proctor Relative Compaction of 95% and an Effective Confining Pressure of 985 kPa.

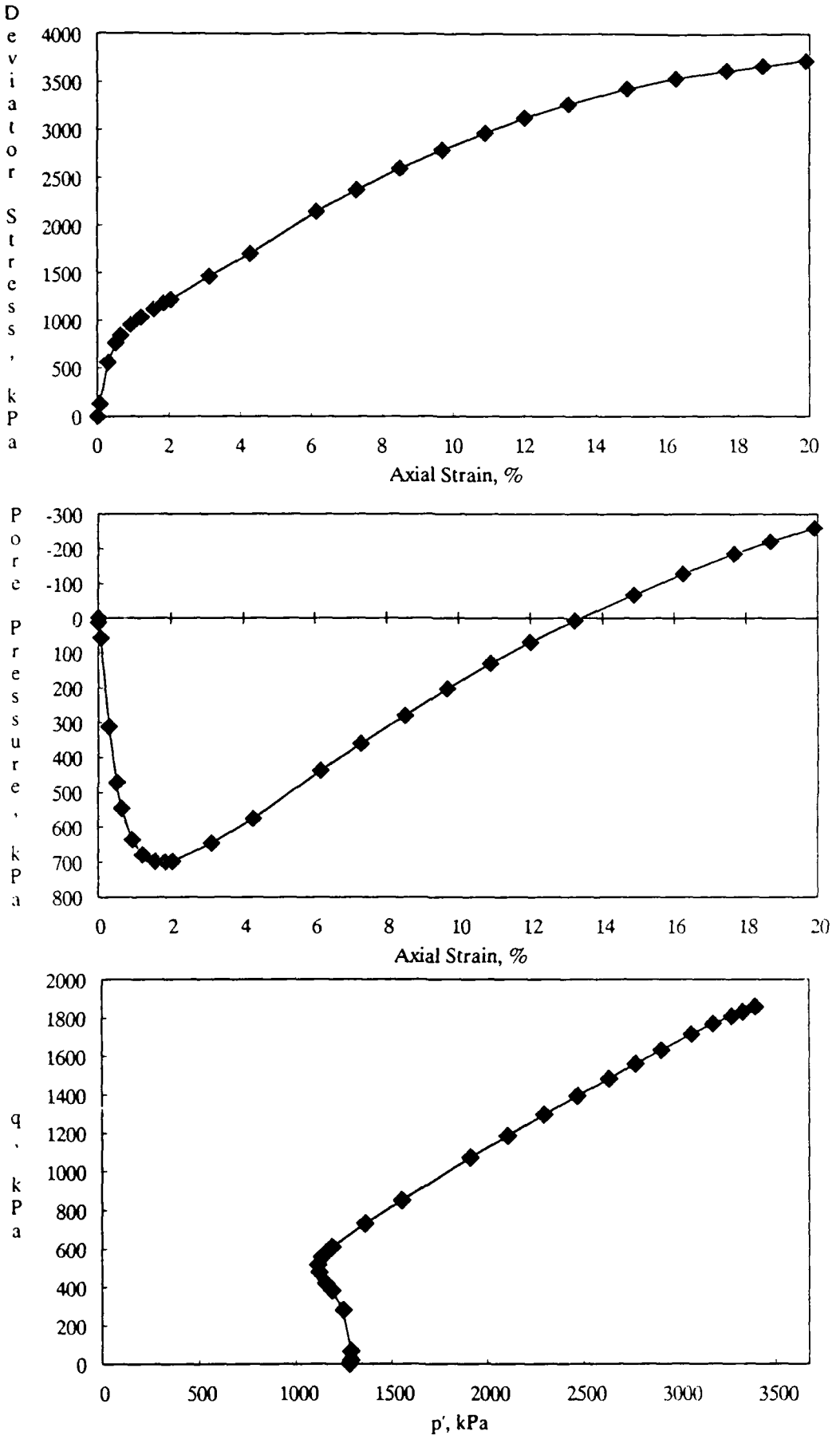


Figure B-17. CU Triaxial Test Results for 10% Kaolinite Mixture at a Standard Proctor Relative Compaction of 95% and an Effective Confining Pressure of 1275 kPa.

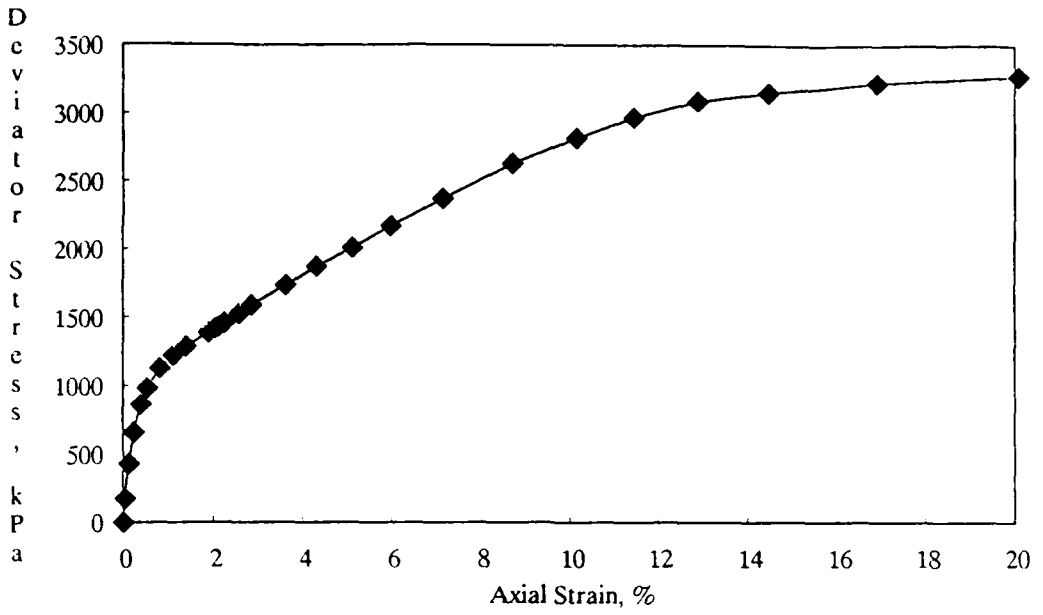


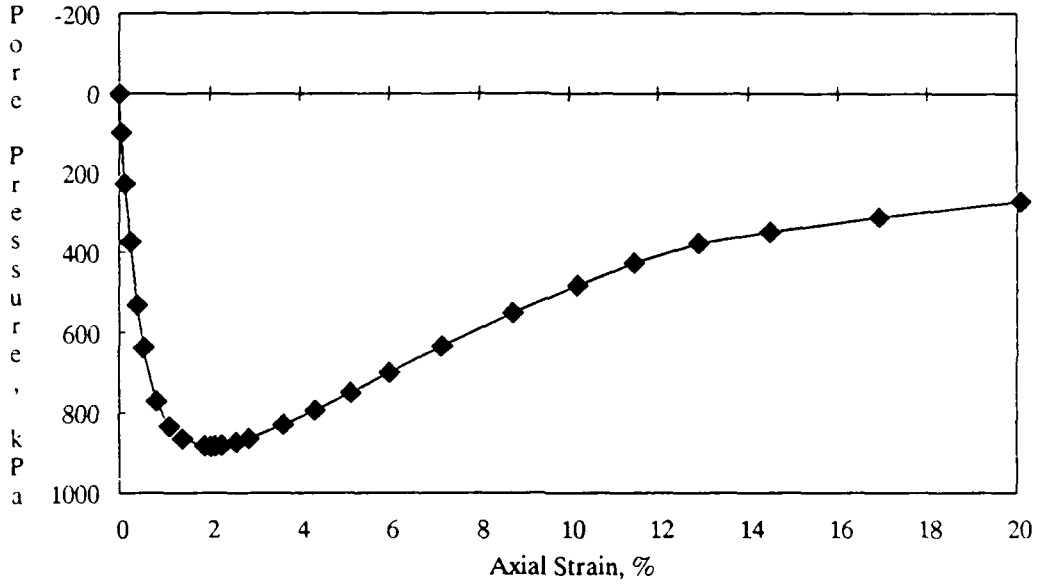


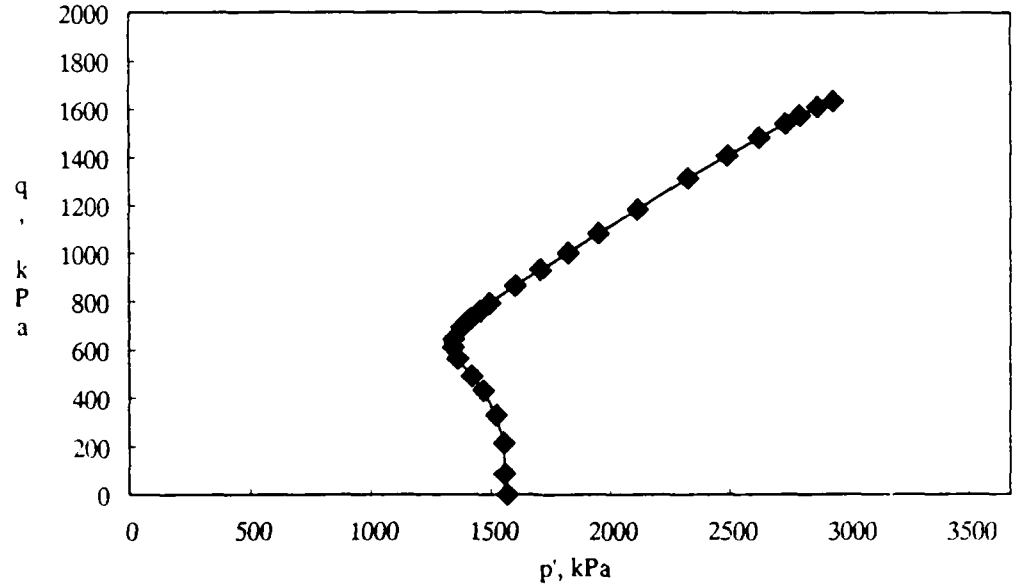


Figure B-18. CU Triaxial Test Results for 10% Kaolinite Mixture at a Standard Proctor Relative Compaction of 95% and an Effective Confining Pressure of 1565 kPa.

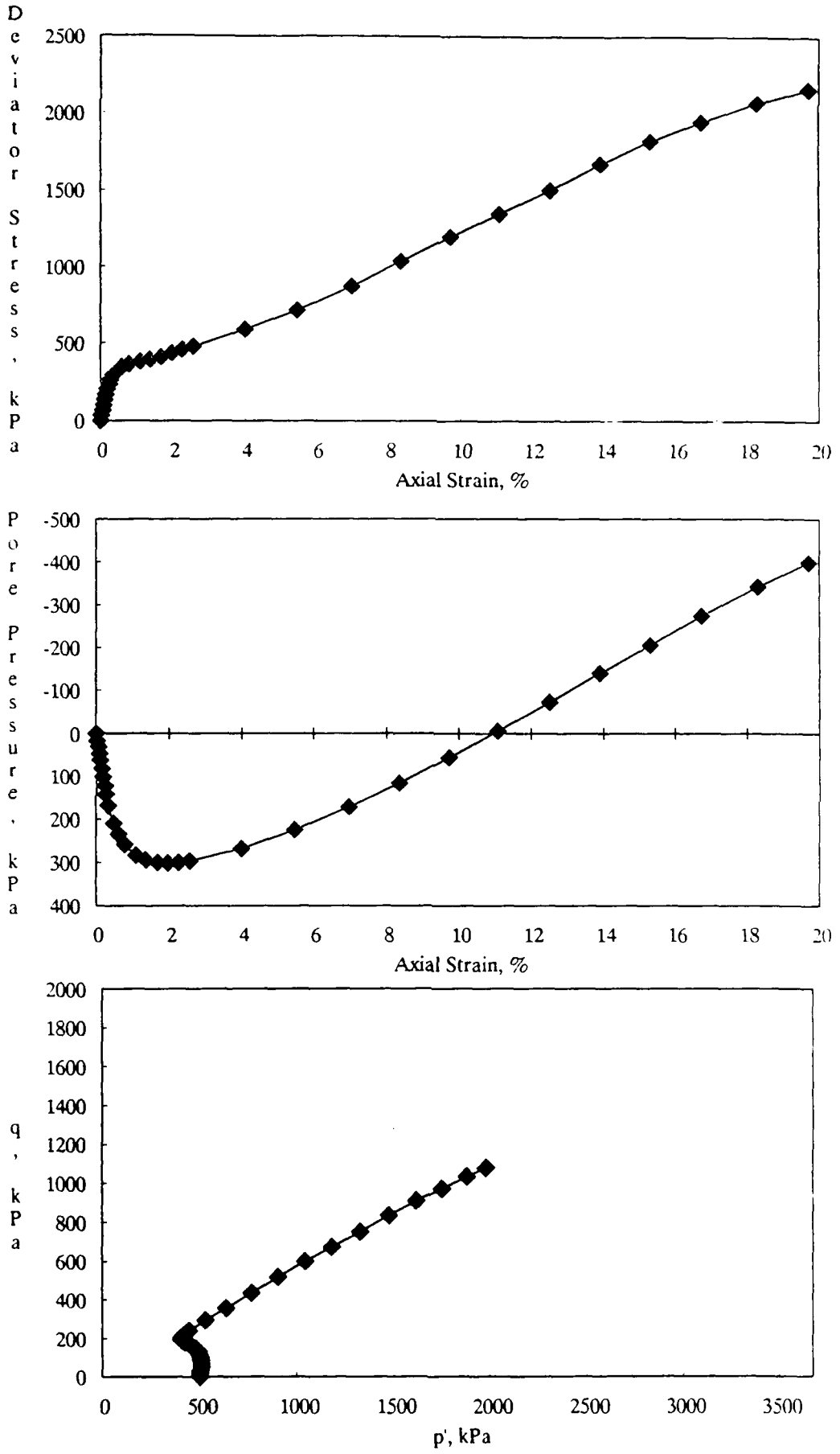


Figure B-19. **CU Triaxial Test Results for 10% Kaolinite Mixture at a Standard Proctor Relative Compaction of 90% and an Effective Confining Pressure of 500 kPa.**

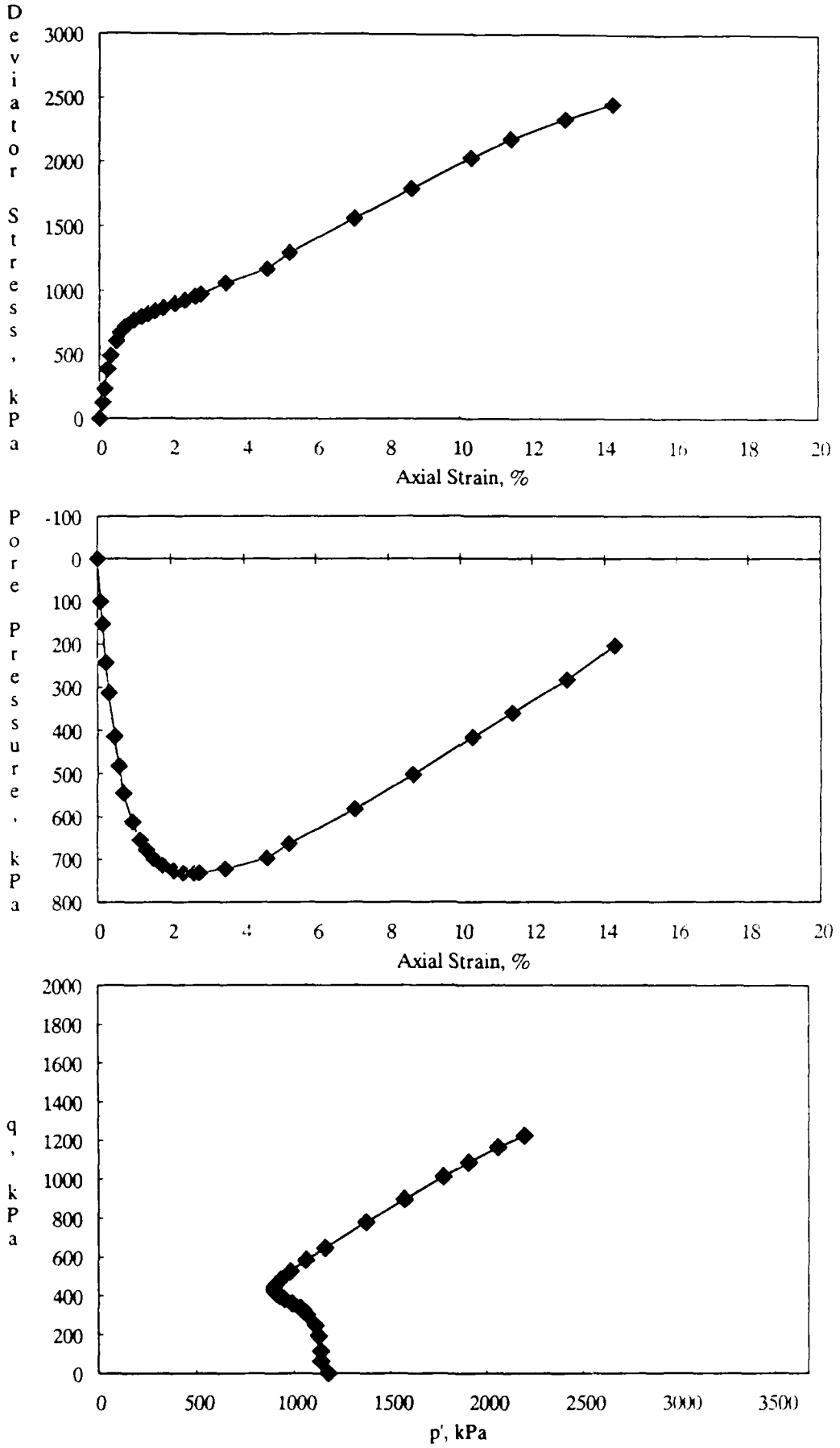


Figure B-20. CU Triaxial Test Results for 10% Kaolinite Mixture at a Standard Proctor Relative Compaction of 90% and an Effective Confining Pressure of 1177 kPa.

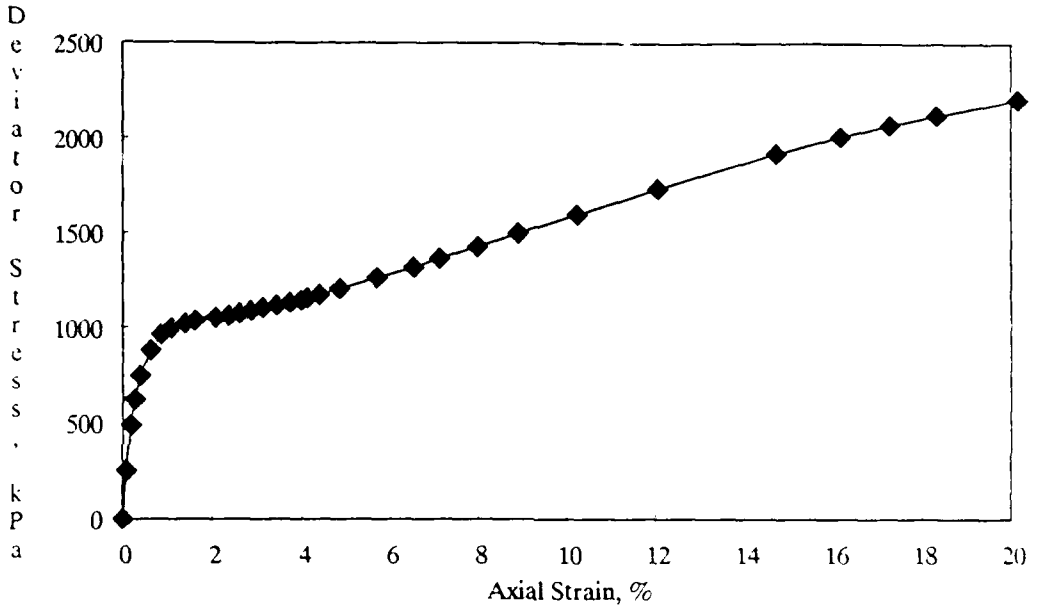


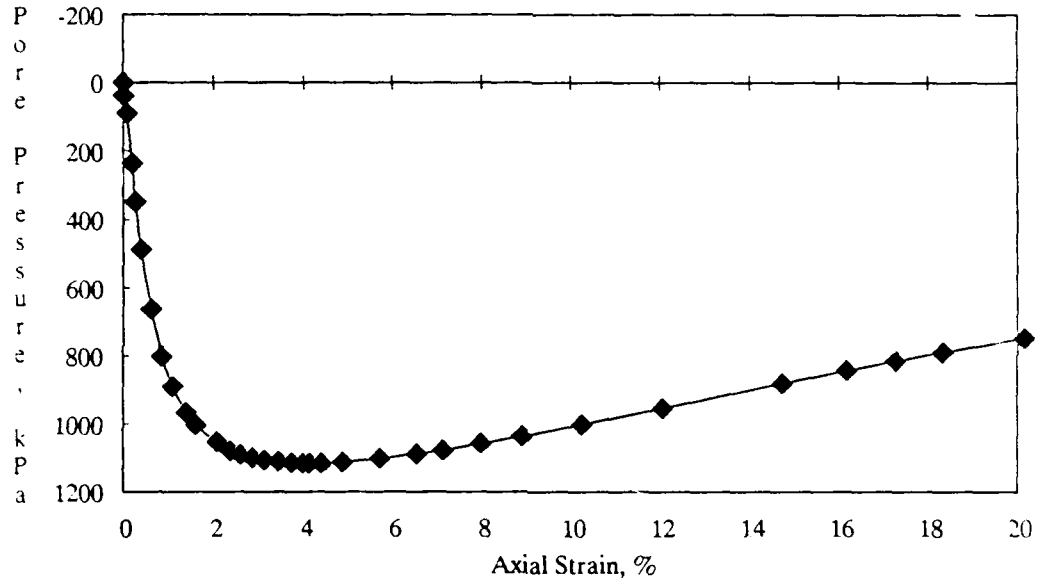


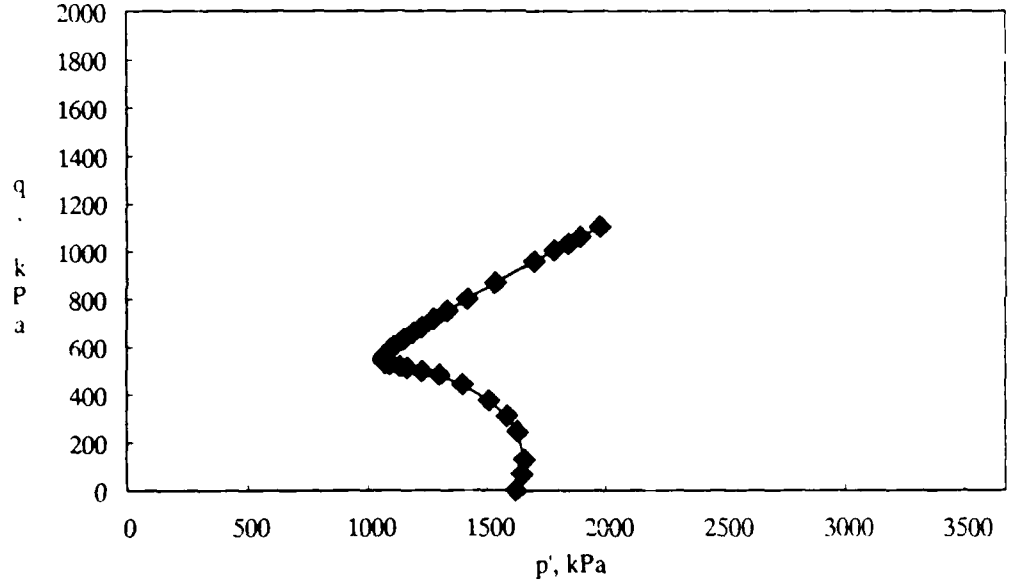


Figure B-21. CU Triaxial Test Results for 10% Kaolinite Mixture at a Standard Proctor Relative Compaction of 90% and an Effective Confining Pressure of 1619 kPa.

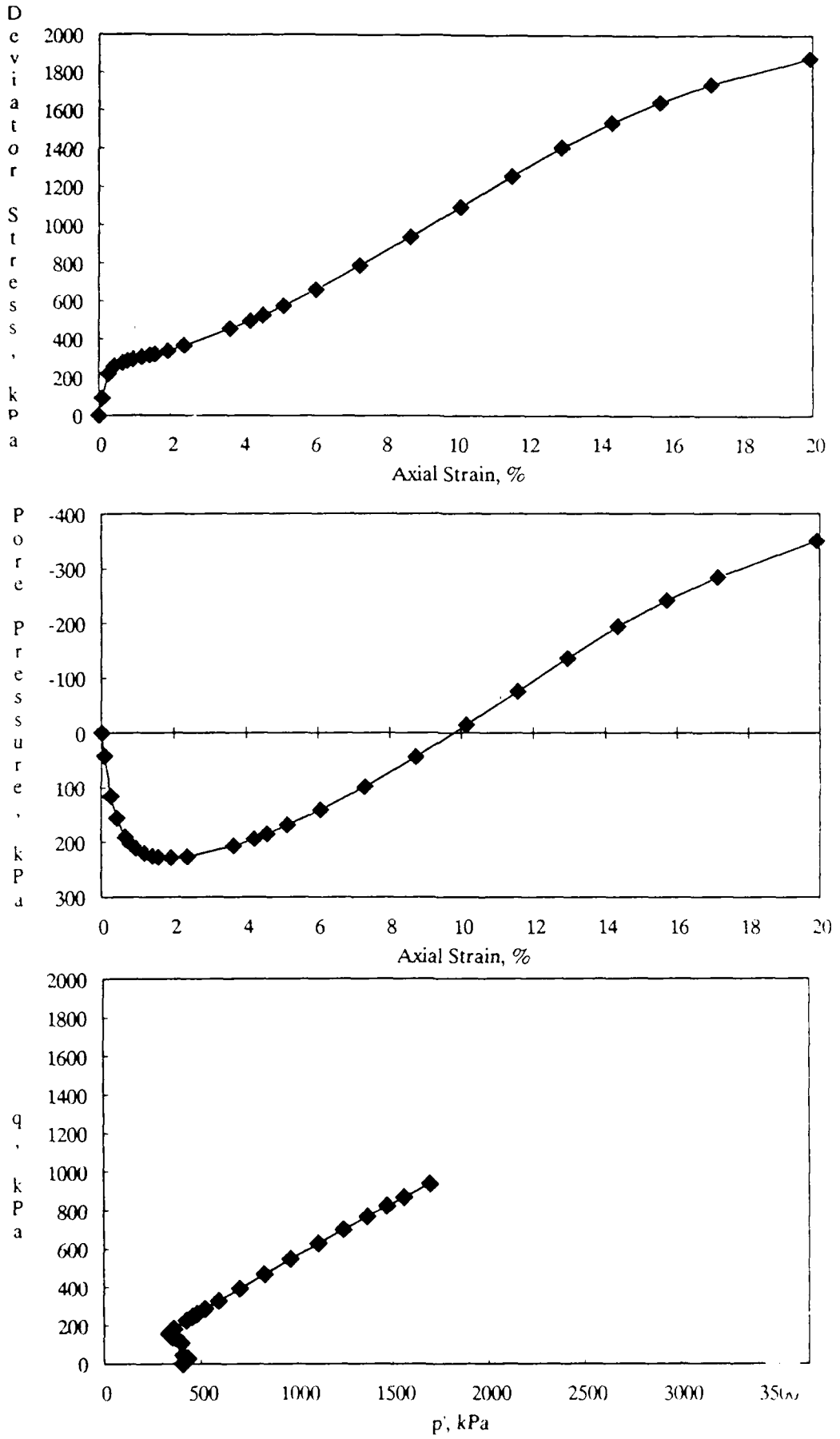


Figure B-22. CU Triaxial Test Results for 10% Kaolinite Mixture at a Standard Proctor Relative Compaction of 85% and an Effective Confining Pressure of 403 kPa.

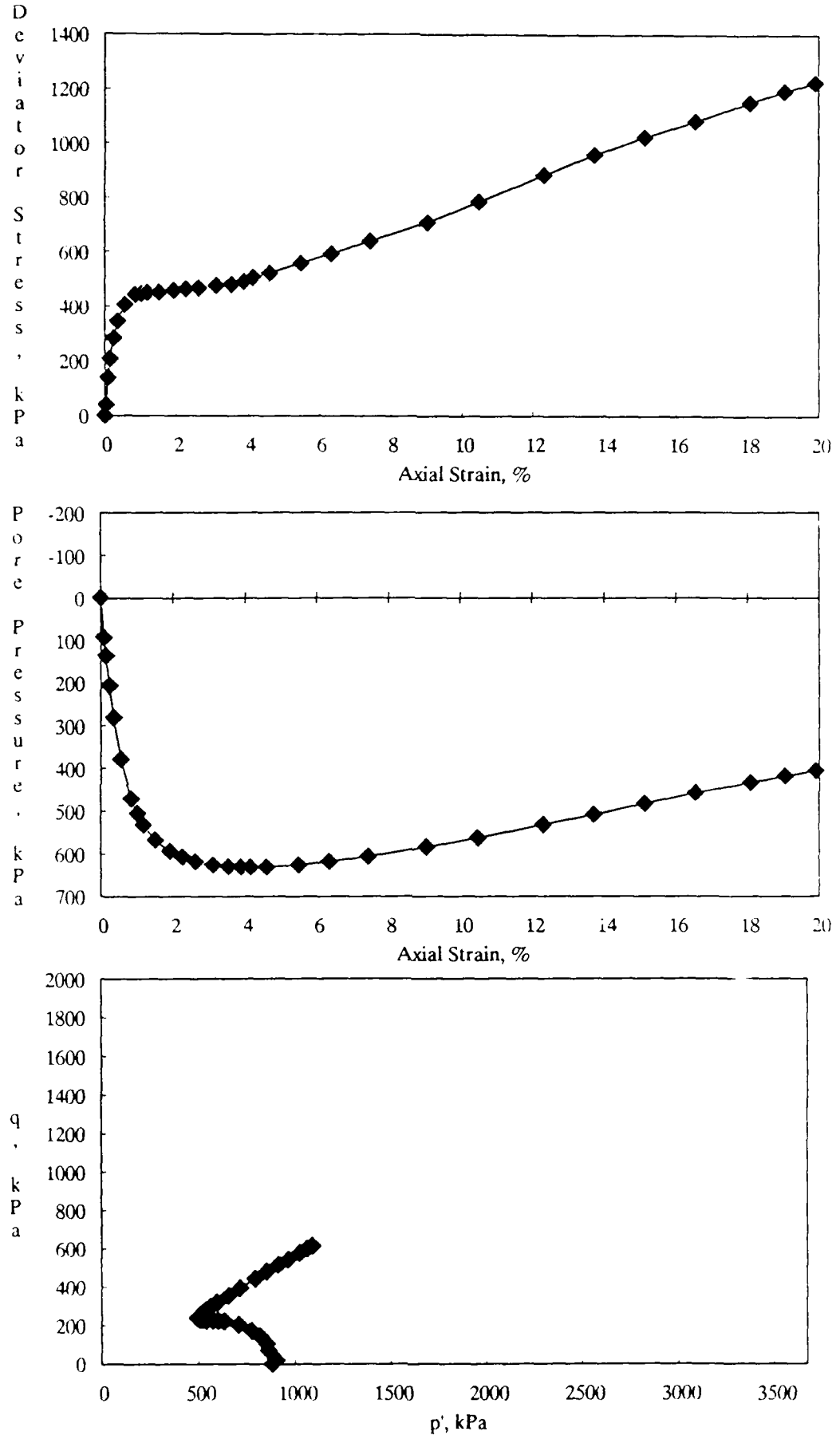


Figure B-23. CU Triaxial Test Results for 10% Kaolinite Mixture at a Standard Proctor Relative Compaction of 85% and an Effective Confining Pressure of 881 kPa.

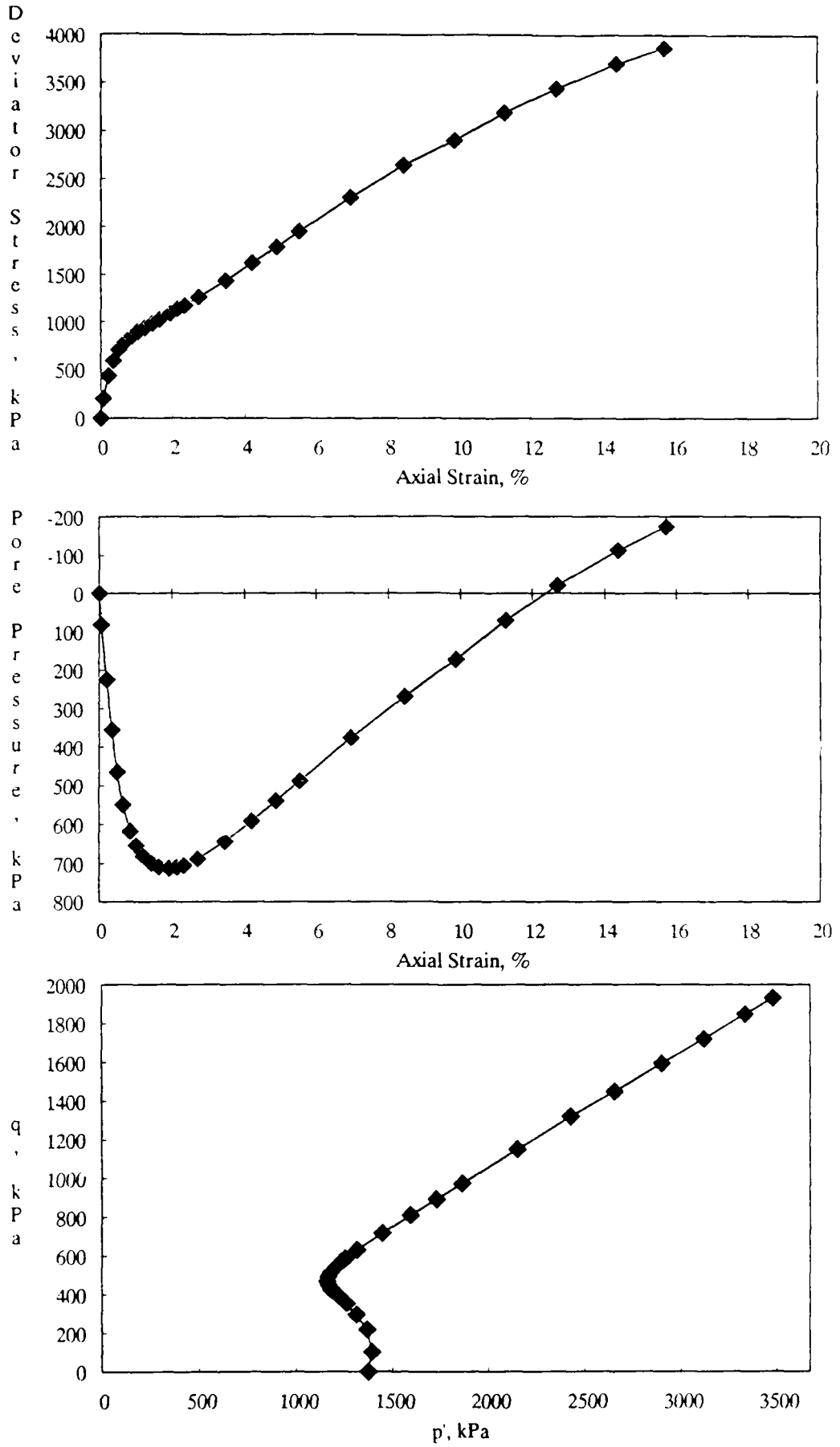


Figure B-24. CU Triaxial Test Results for 10% Kaolinite Mixture at a Standard Proctor Relative Compaction of 85% and an Effective Confining Pressure of 1373 kPa.

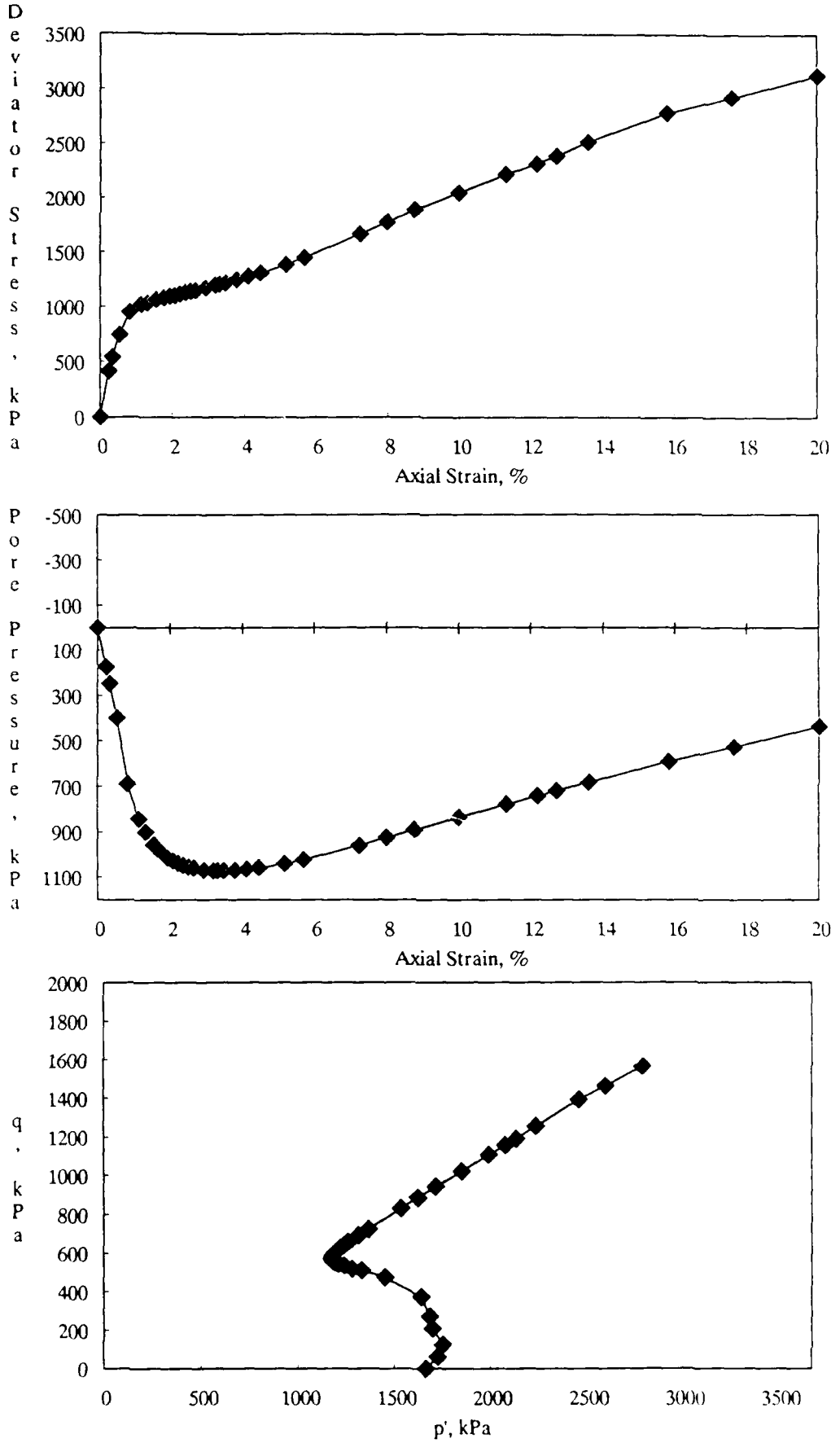


Figure B-25. CU Triaxial Test Results for 10% Kaolinite Mixture at a Standard Proctor Relative Compaction of 85% and an Effective Confining Pressure of 1661 kPa.

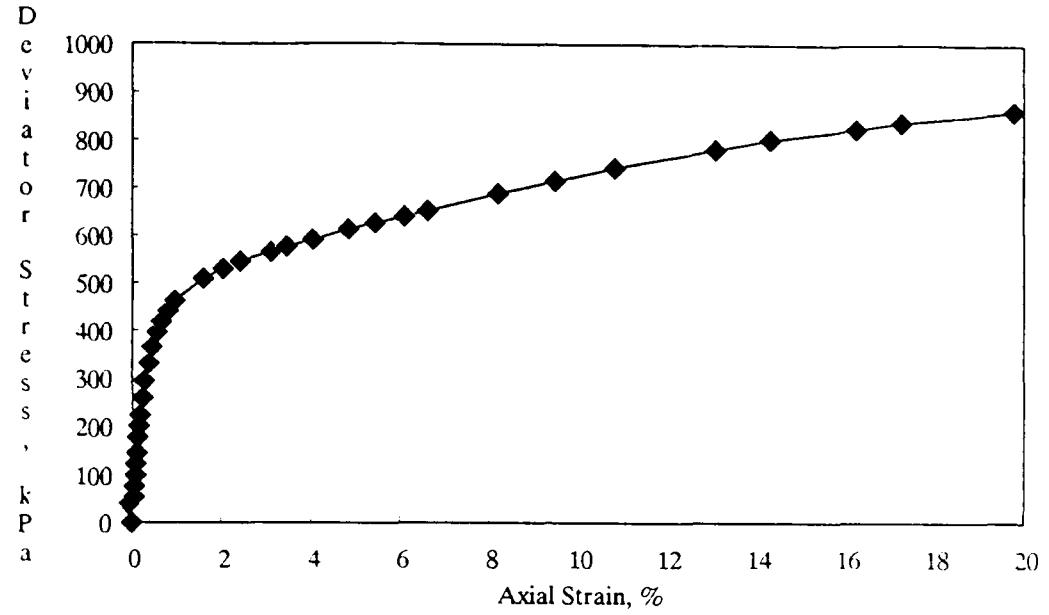


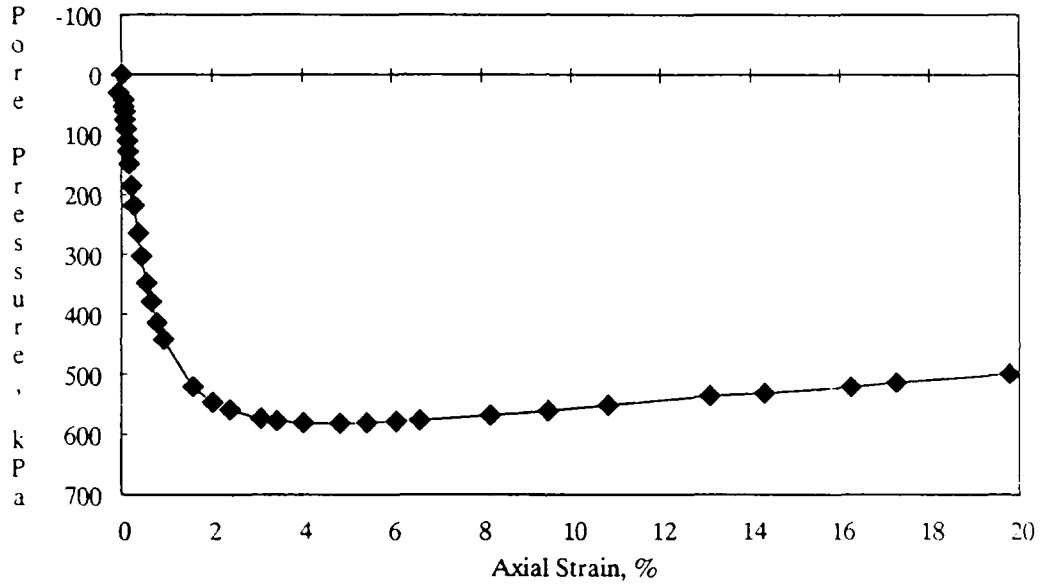


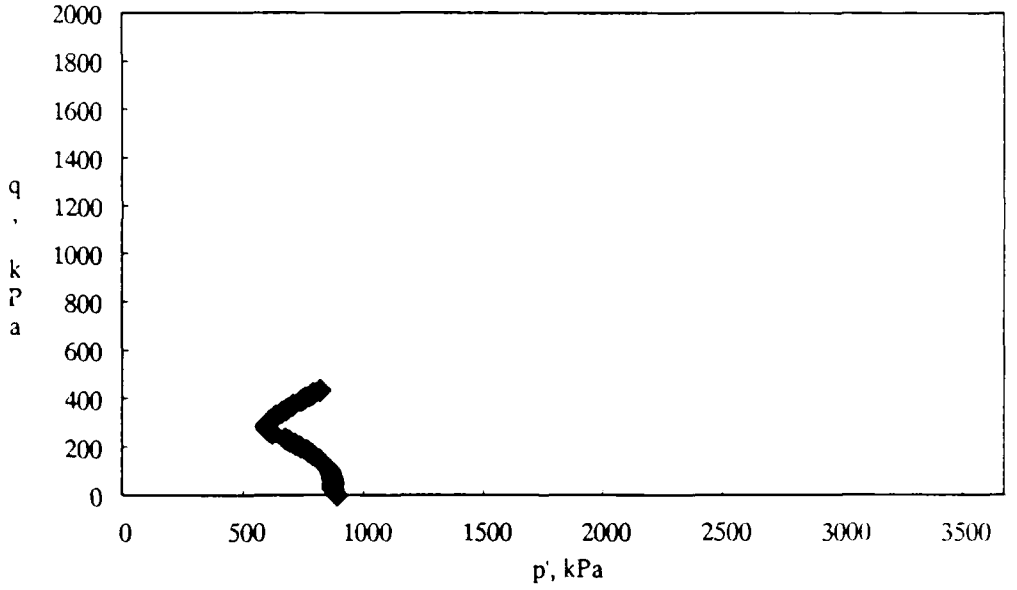


Figure B-26. CU Triaxial Test Results for 30% Kaolinite Mixture at a Standard Proctor Relative Compaction of 100% and an Effective Confining Pressure of 885 kPa.

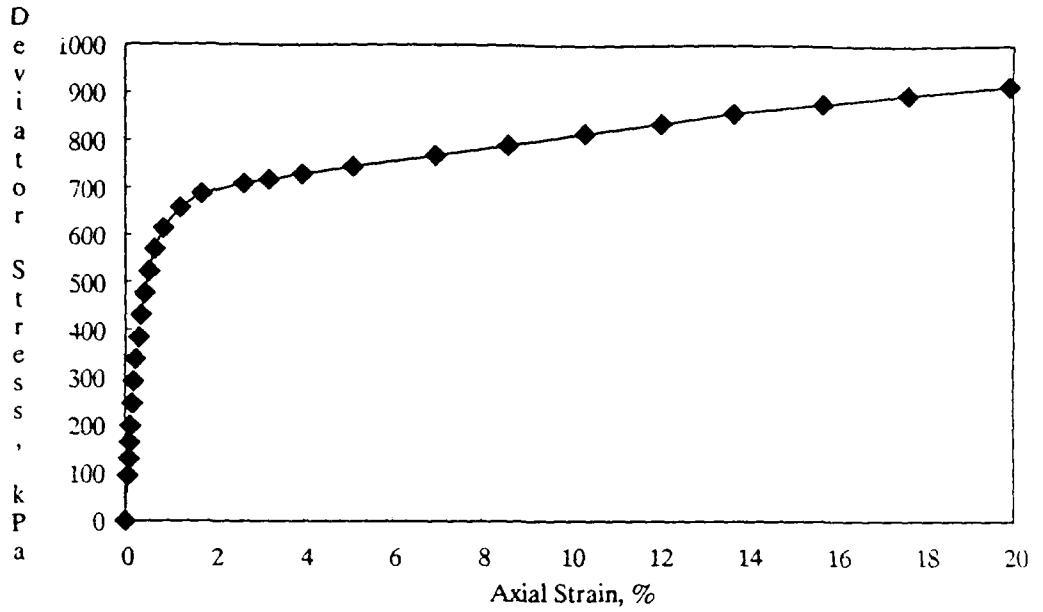


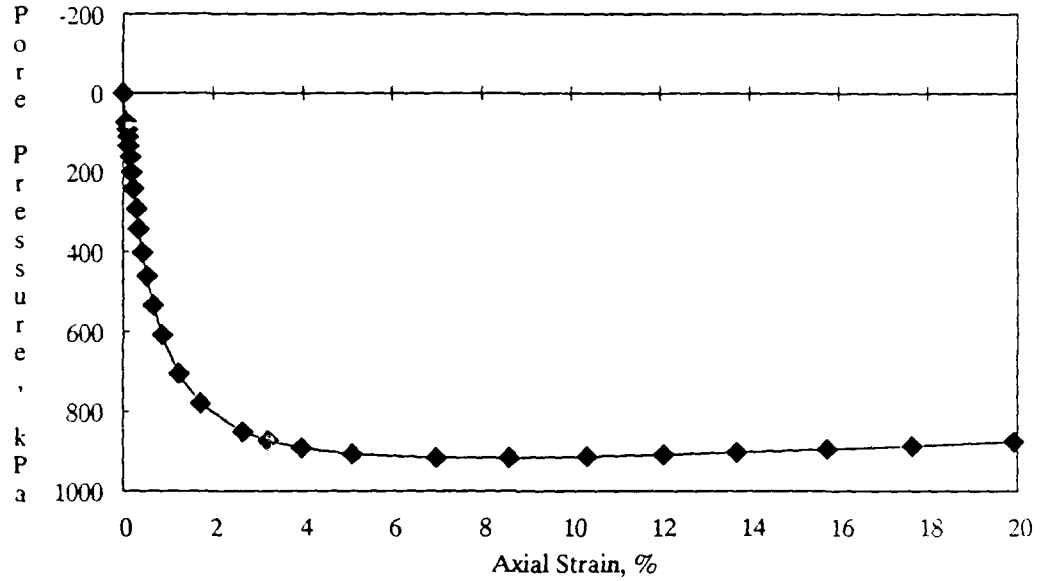


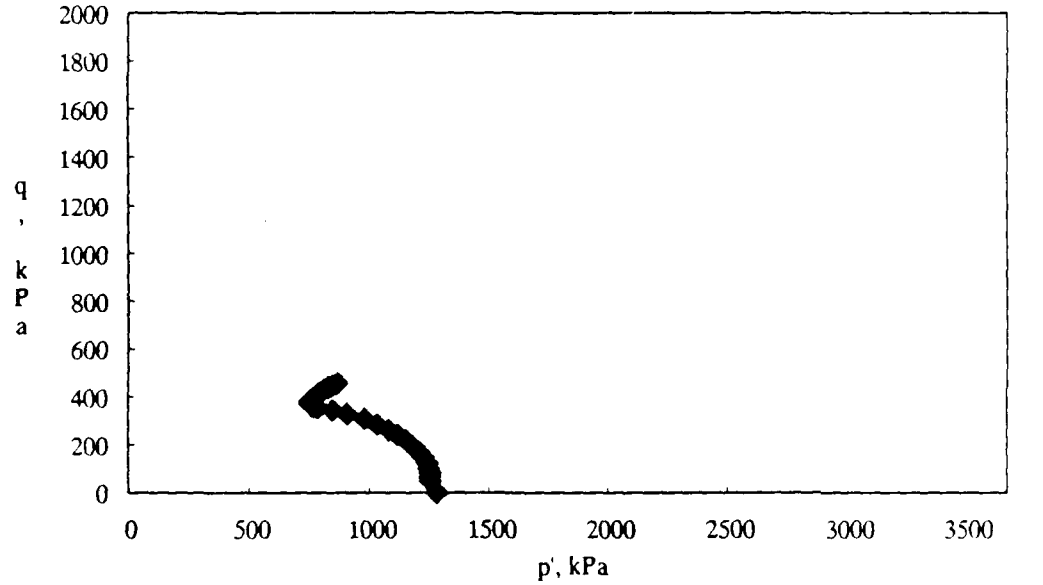


Figure B-27. CU Triaxial Test Results for 30% Kaolinite Mixture at a Standard Proctor Relative Compaction of 100% and an Effective Confining Pressure of 1282 kPa.

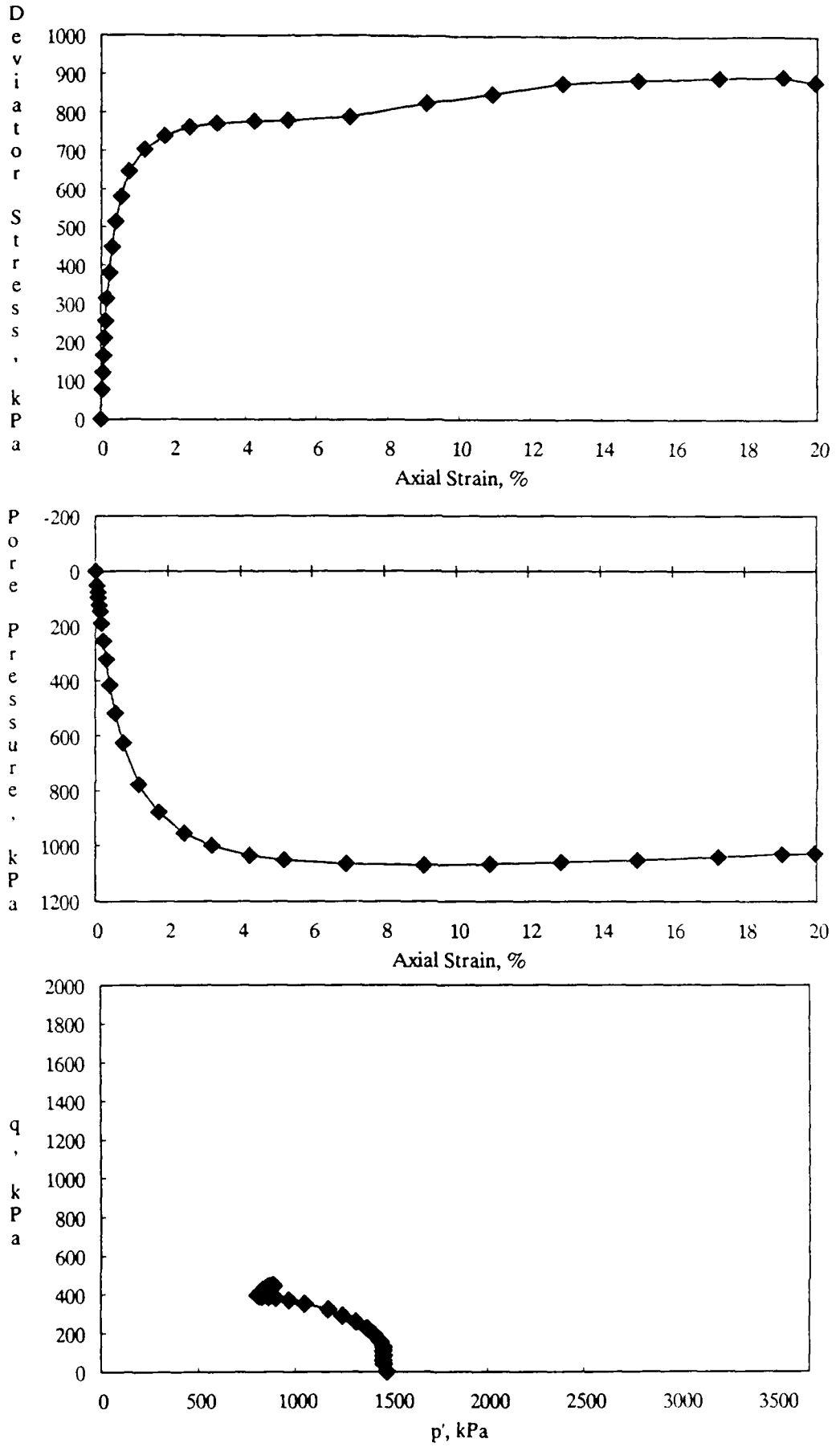


Figure B-28. CU Triaxial Test Results for 30% Kaolinite Mixture at a Standard Proctor Relative Compaction of 100% and an Effective Confining Pressure of 1472 kPa.

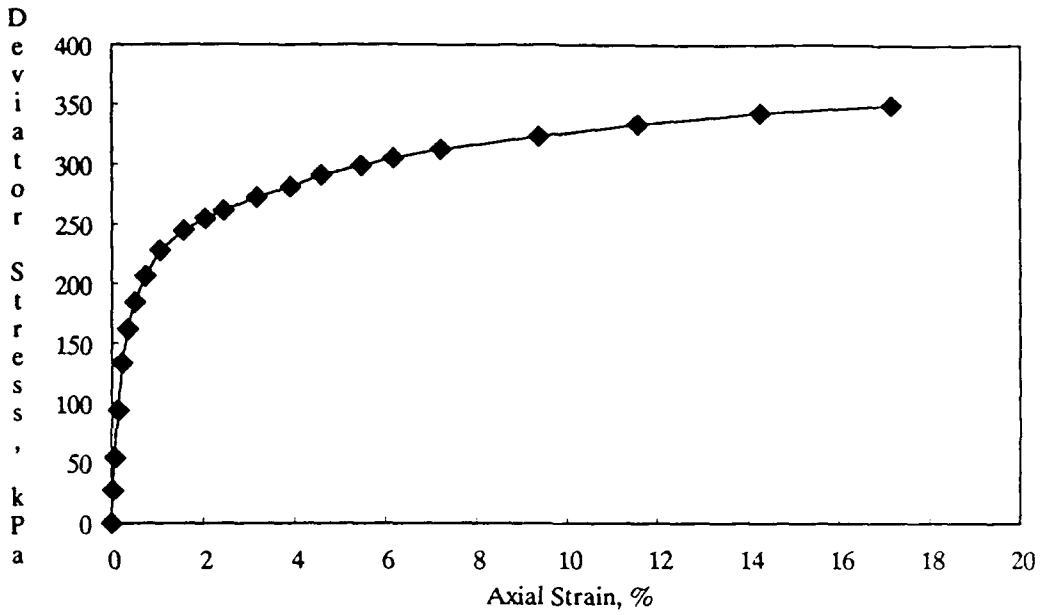


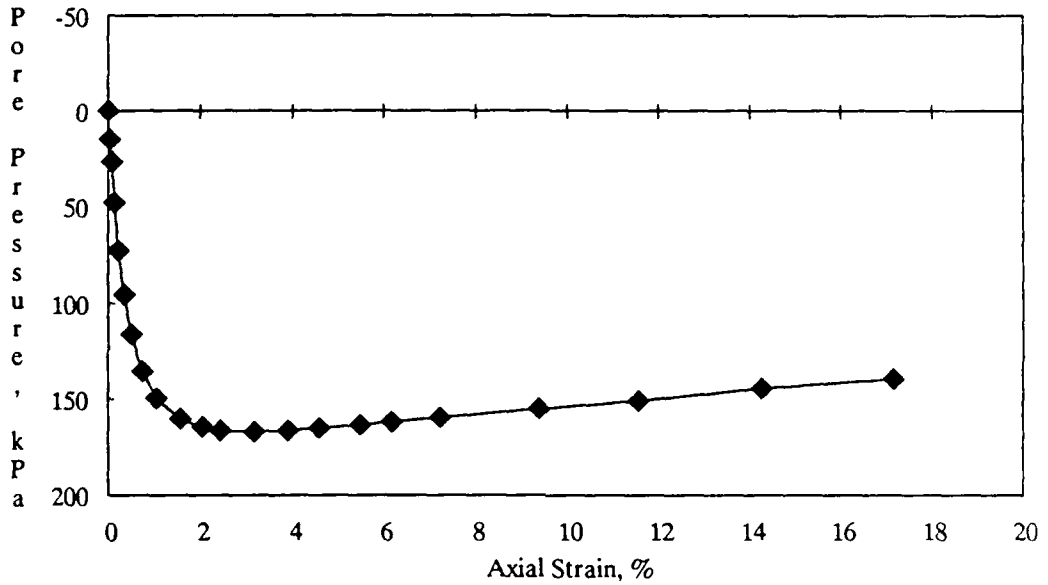


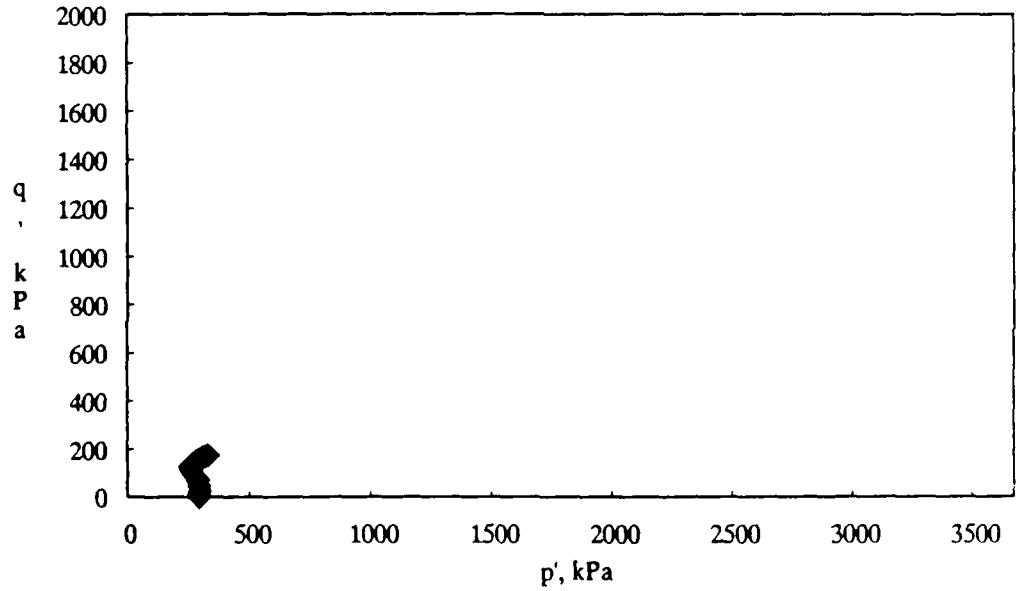


Figure B-29. CU Triaxial Test Results for 30% Kaolinite Mixture at a Standard Proctor Relative Compaction of 95% and an Effective Confining Pressure of 294 kPa.

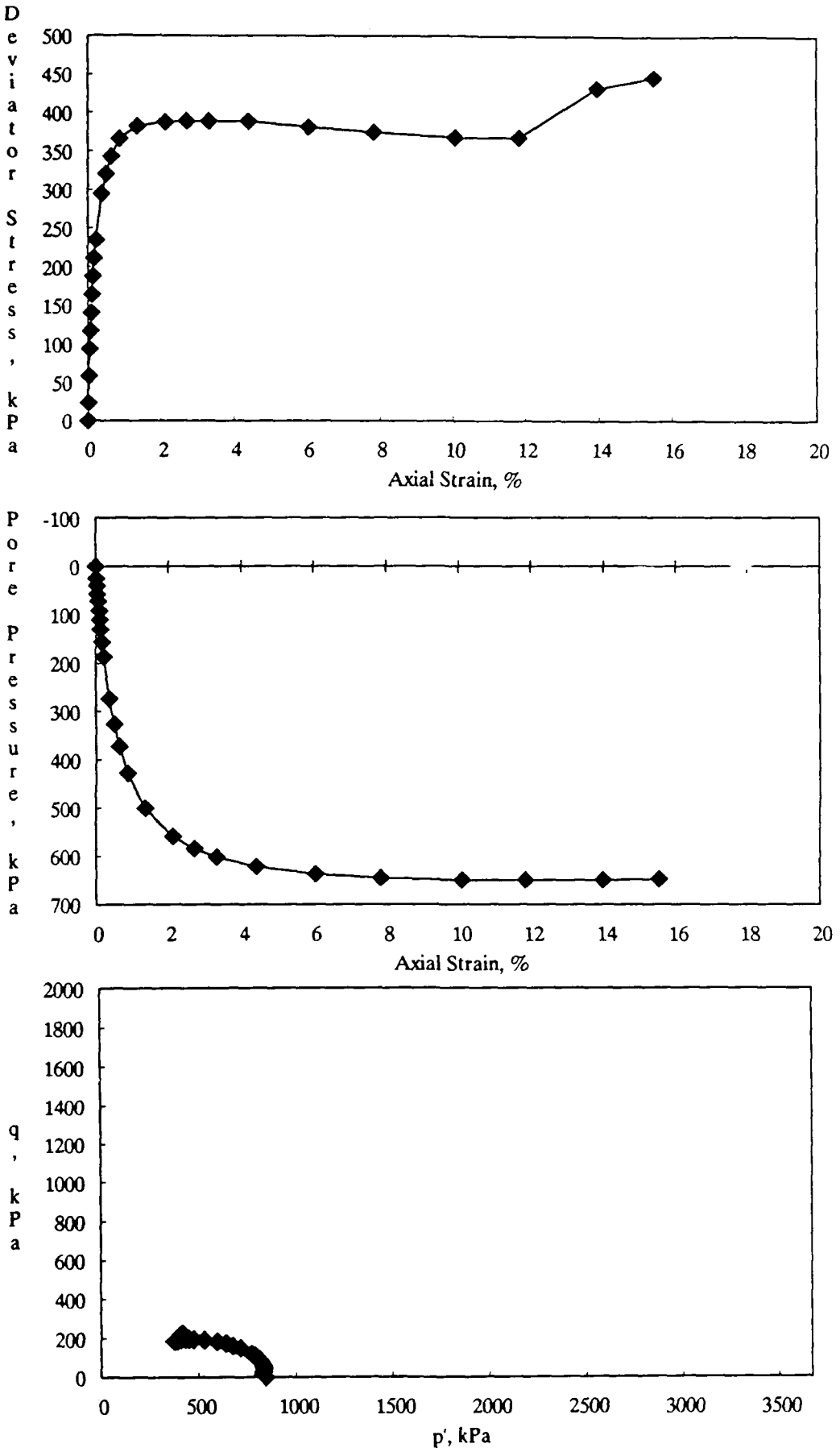


Figure B-30. CU Triaxial Test Results for 30% Kaolinite Mixture at a Standard Proctor Relative Compaction of 95% and an Effective Confining Pressure of 840 kPa.

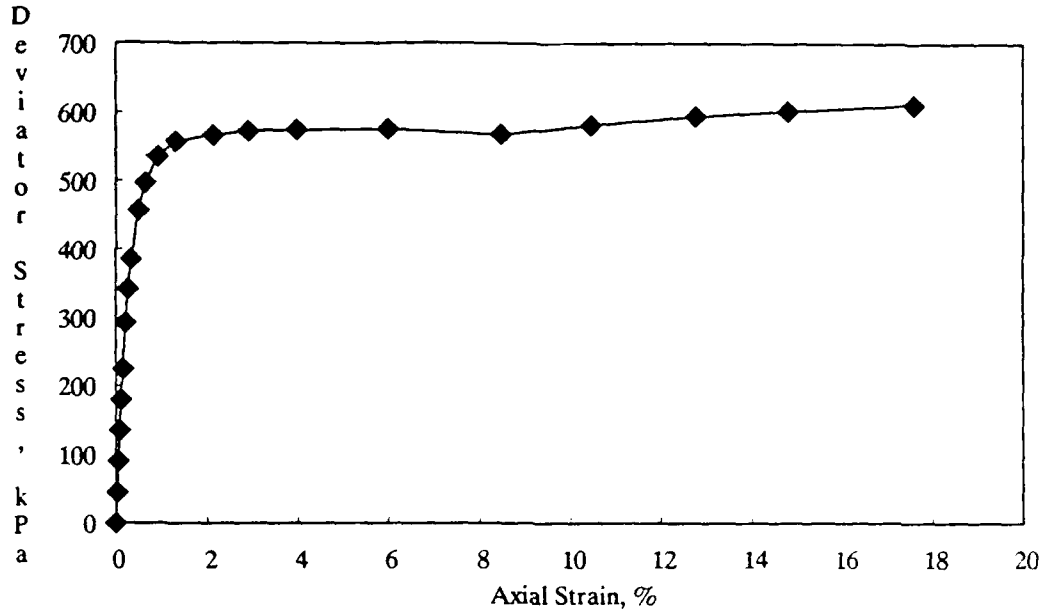


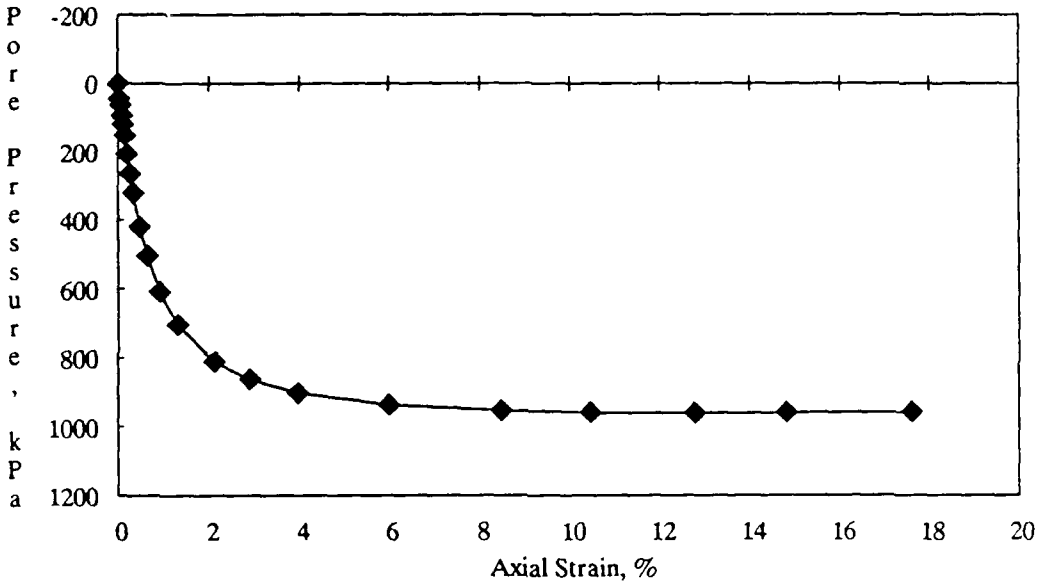


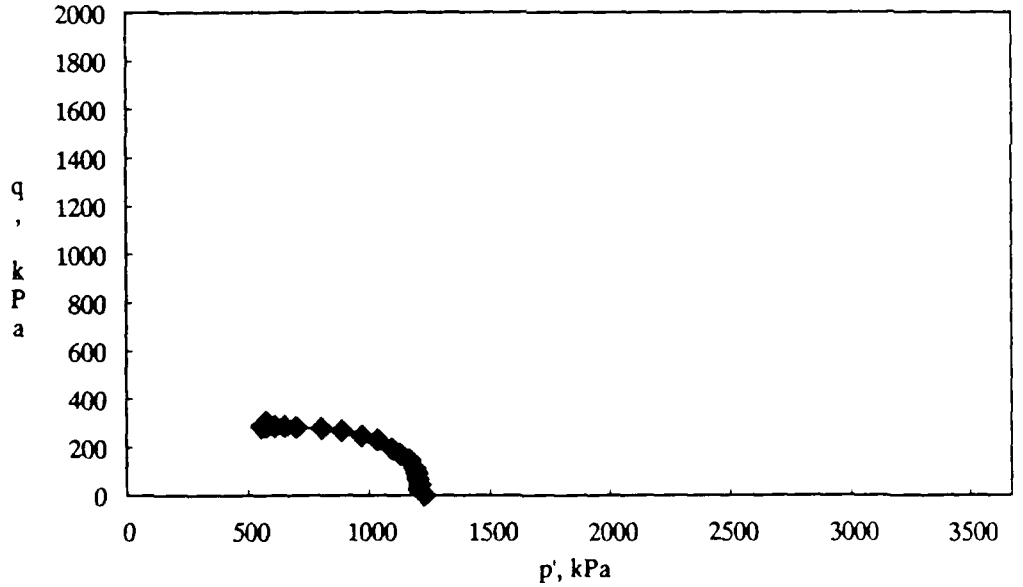


Figure B-31. CU Triaxial Test Results for 30% Kaolinite Mixture at a Standard Proctor Relative Compaction of 95% and an Effective Confining Pressure of 1226 kPa.

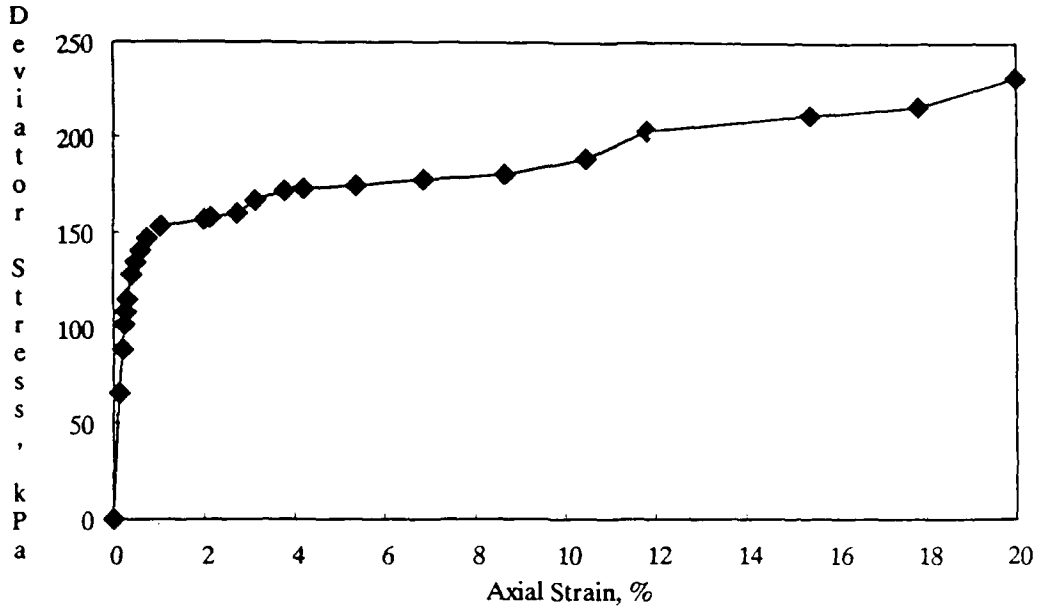


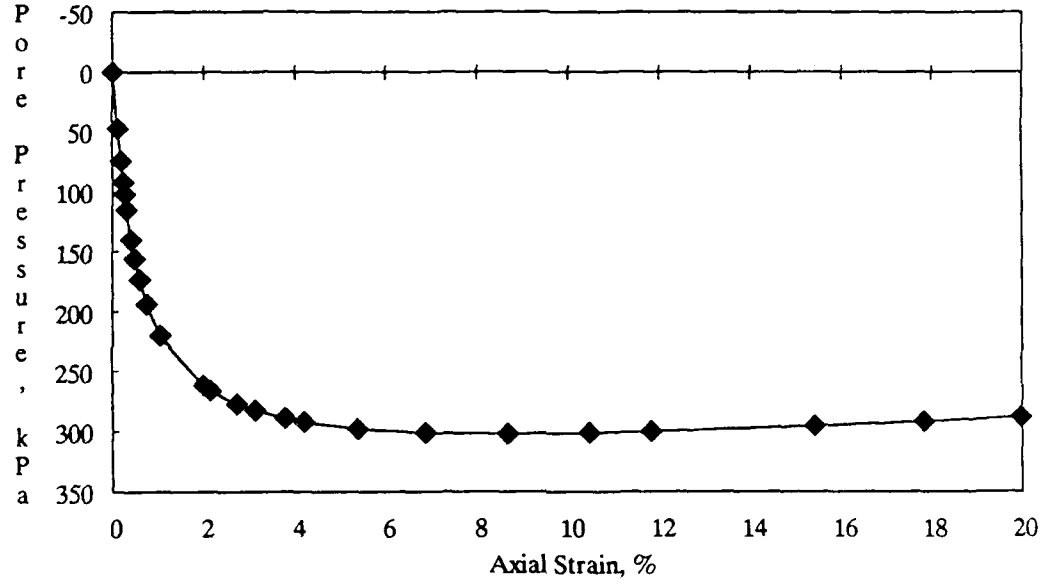


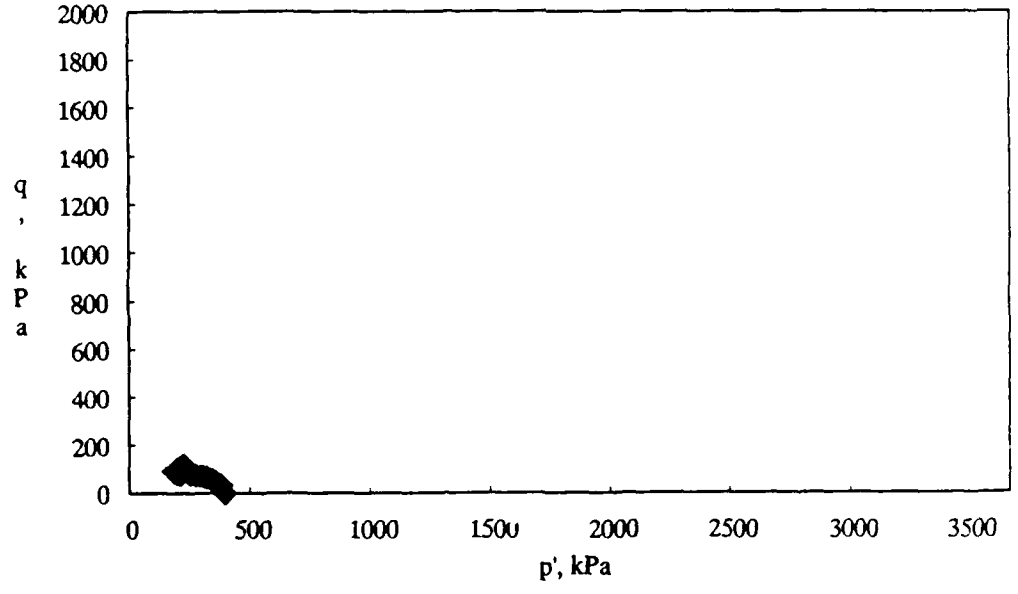


Figure B-32. CU Triaxial Test Results for 30% Kaolinite Mixture at a Standard Proctor Relative Compaction of 90% and an Effective Confining Pressure of 395 kPa.

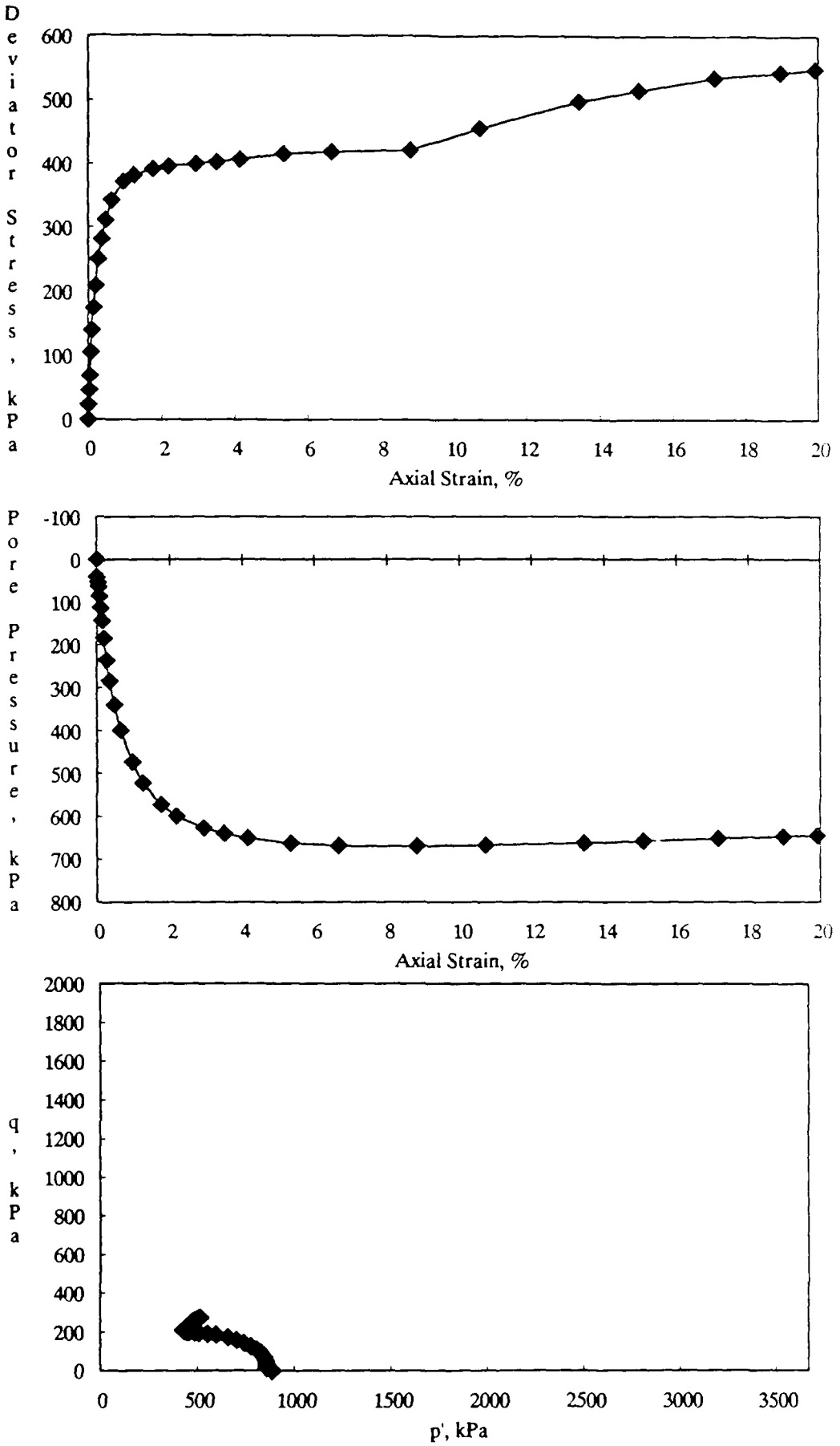


Figure B-33. CU Triaxial Test Results for 30% Kaolinite Mixture at a Standard Proctor Relative Compaction of 90% and an Effective Confining Pressure of 885 kPa.

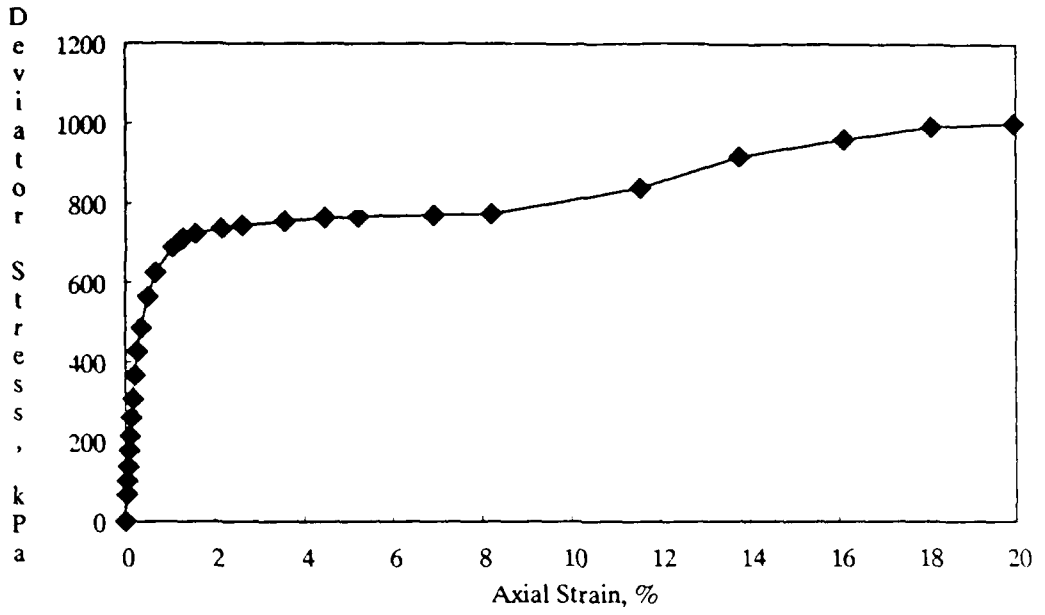


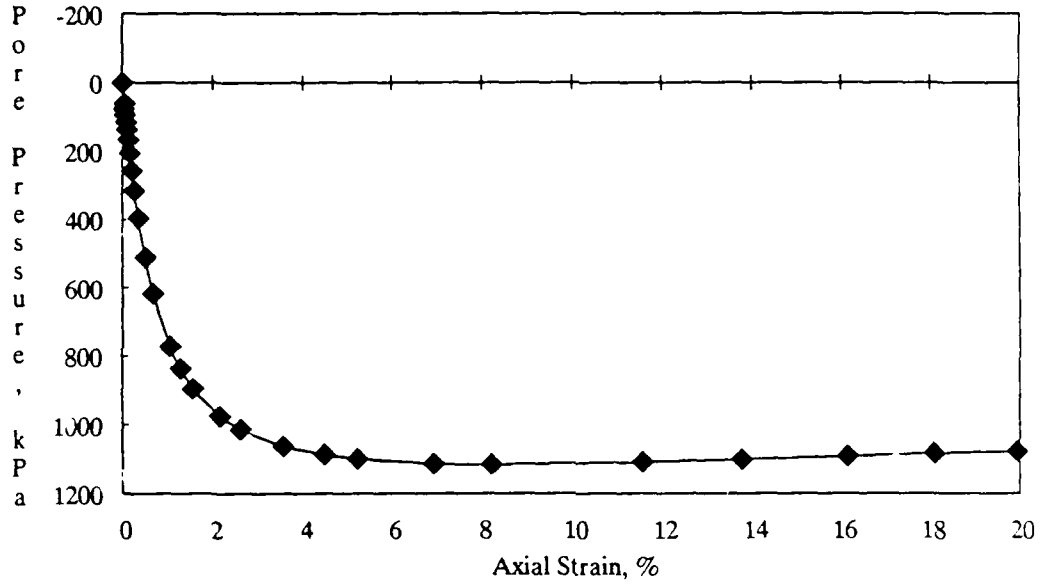


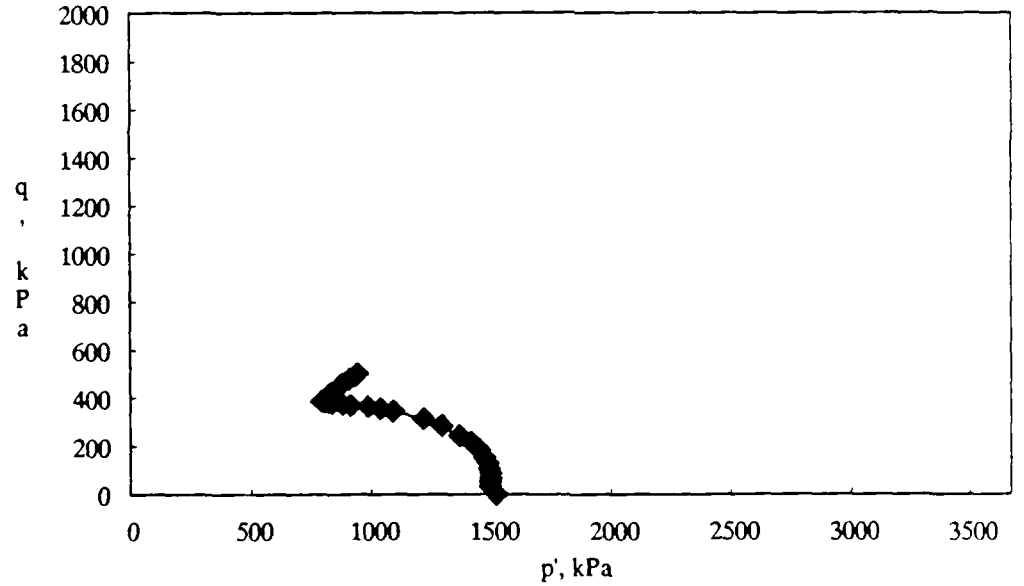


Figure B-34. CU Triaxial Test Results for 30% Kaolinite Mixture at a Standard Proctor Relative Compaction of 90% and an Effective Confining Pressure of 1519 kPa.

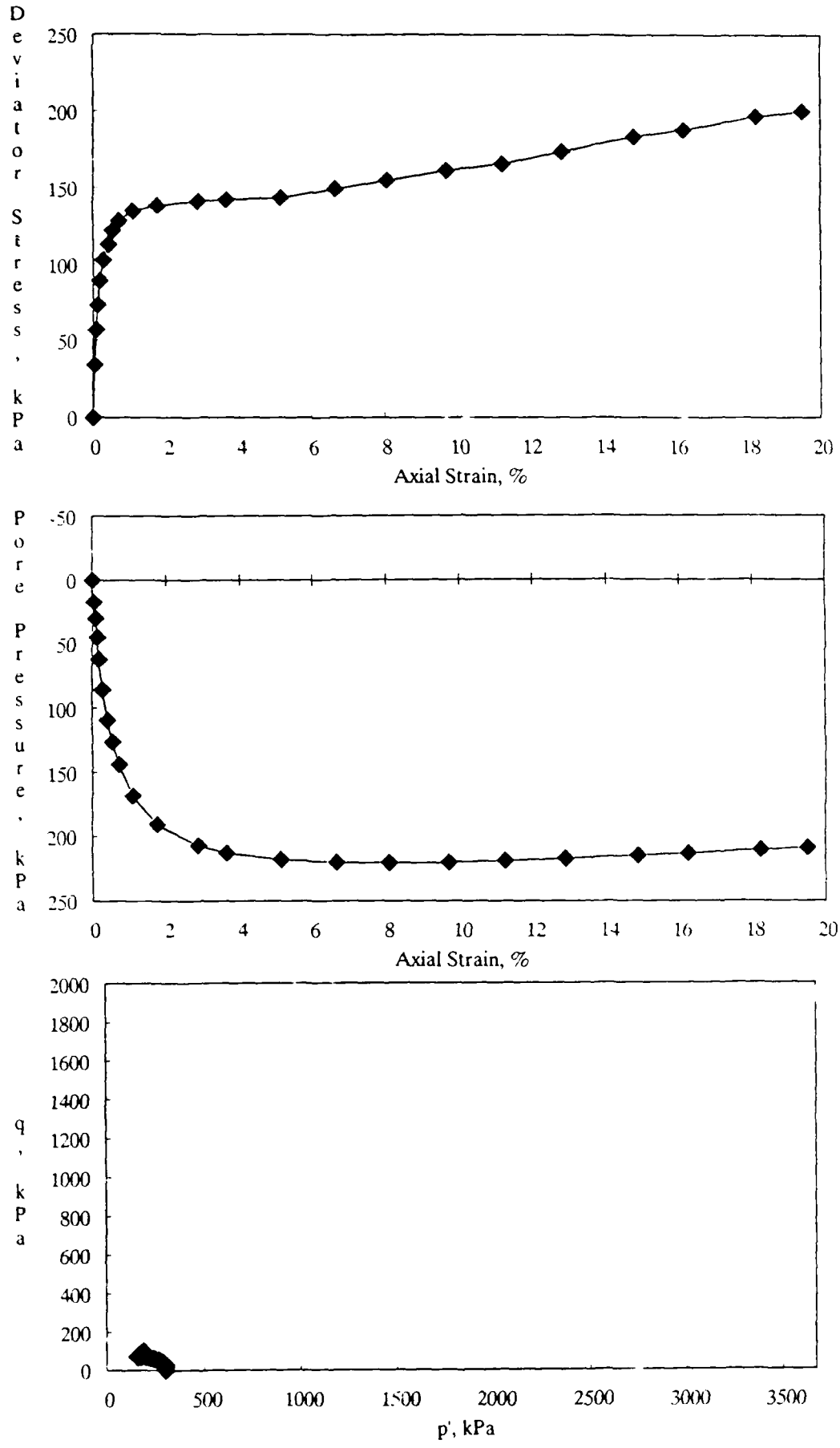


Figure B-35. CU Triaxial Test Results for 30% Kaolinite Mixture at a Standard Proctor Relative Compaction of 85% and an Effective Confining Pressure of 301 kPa.

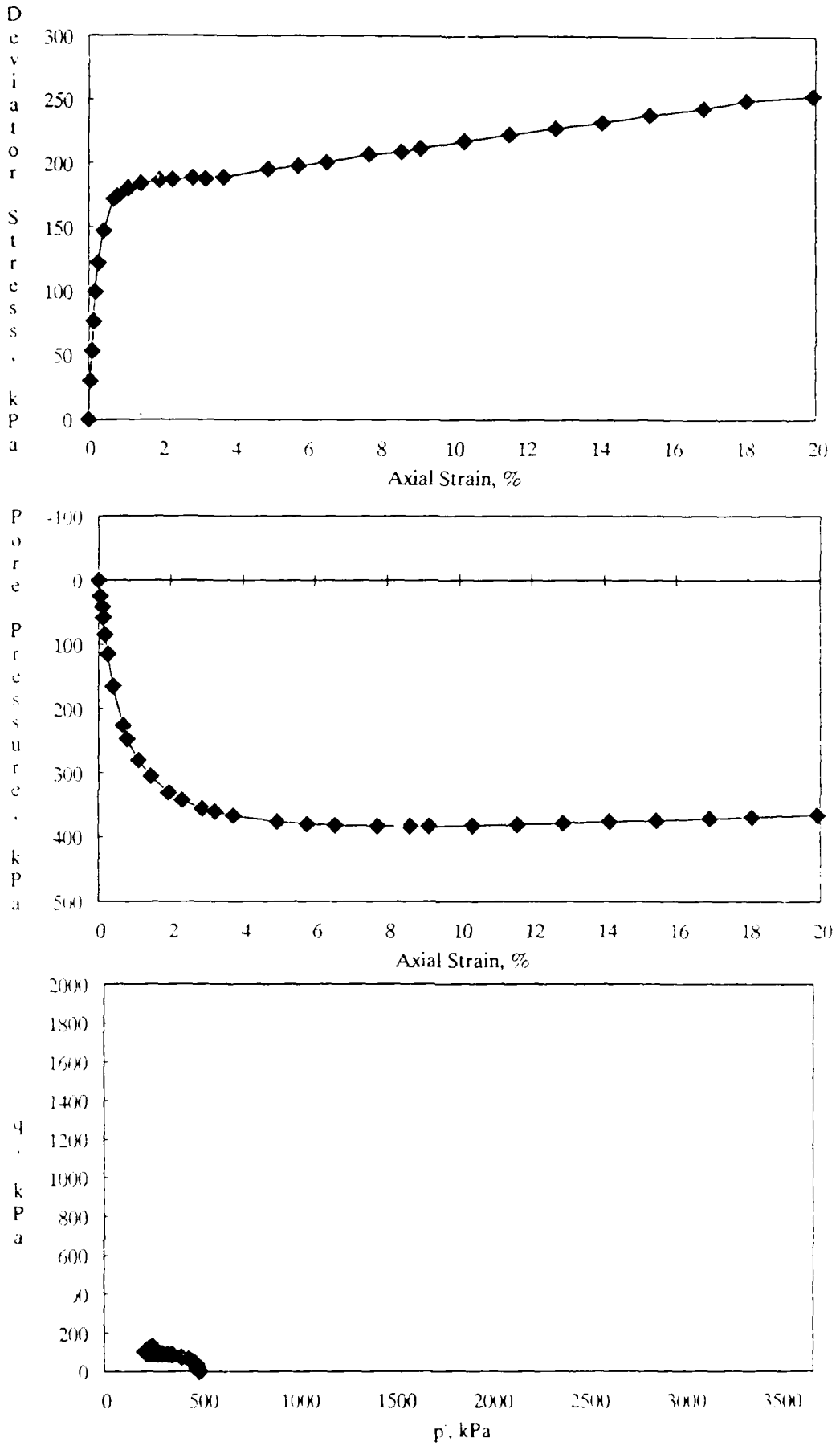


Figure B-36. CU Triaxial Test Results for 30% Kaolinite Mixture at a Standard Proctor Relative Compaction of 85% and an Effective Confining Pressure of 490 kPa.

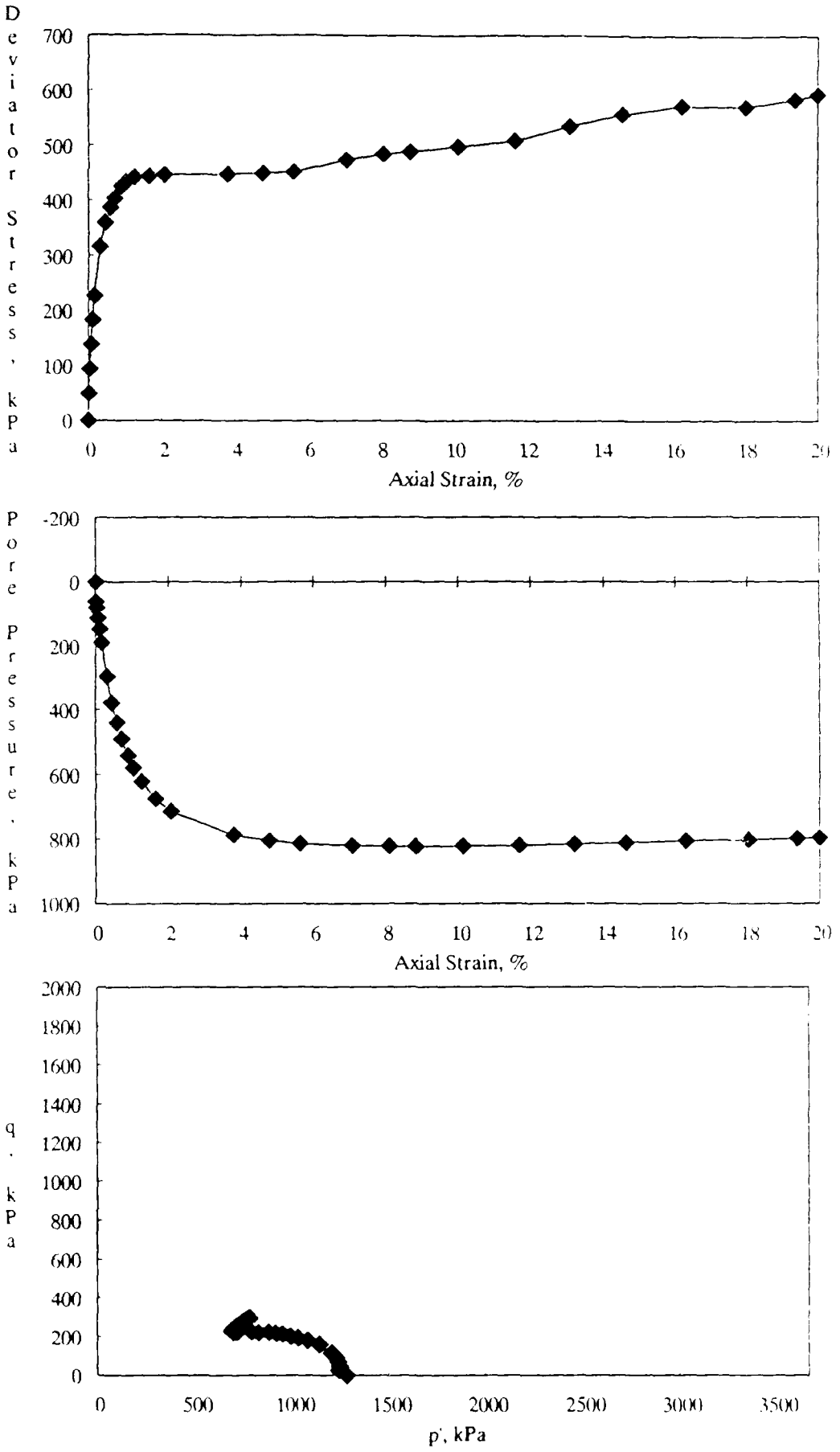


Figure B-37. CU Triaxial Test Results for 30% Kaolinite Mixture at a Standard Proctor Relative Compaction of 85% and an Effective Confining Pressure of 1081 kPa.

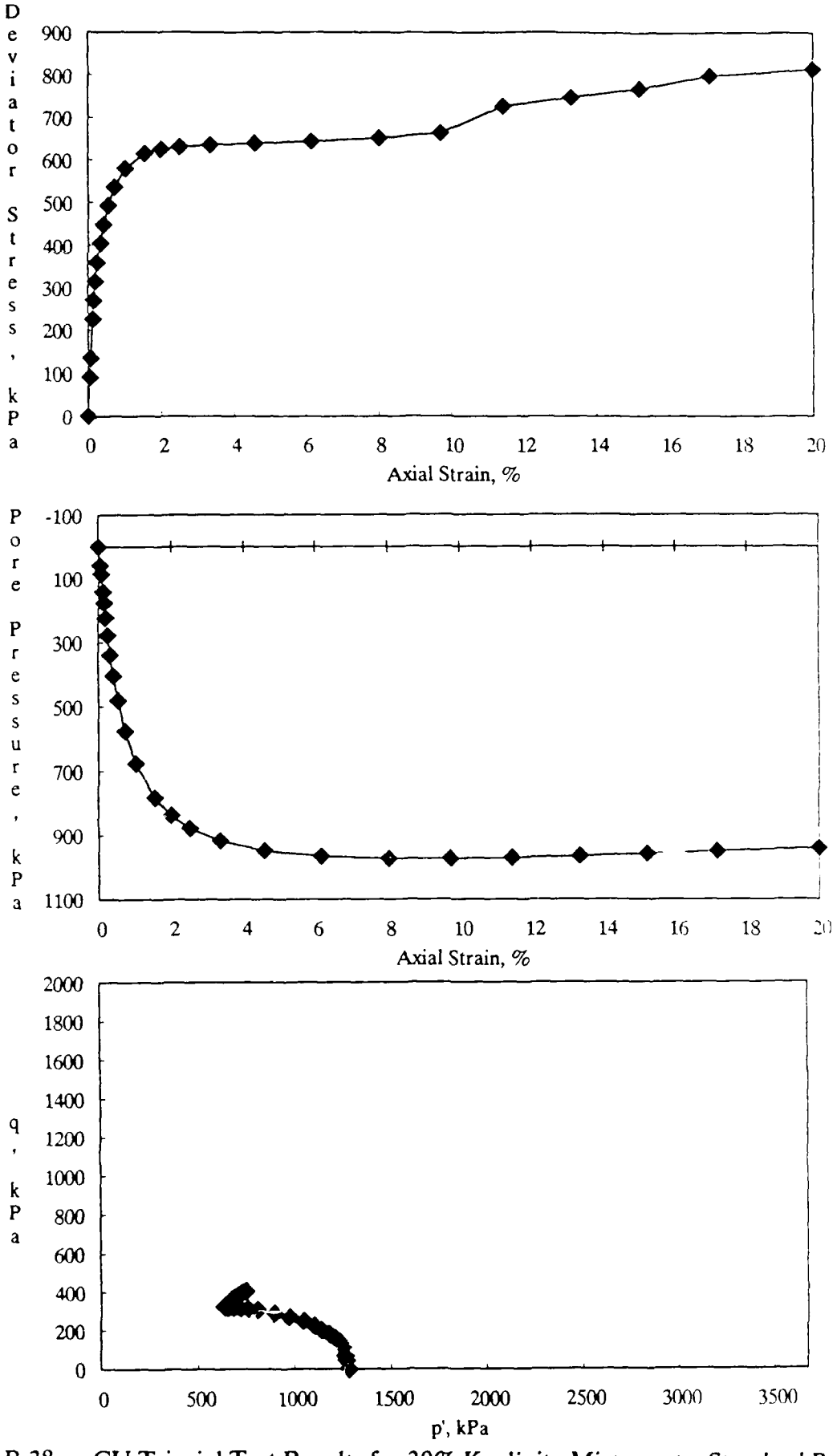


Figure B-38. CU Triaxial Test Results for 30% Kaolinite Mixture at a Standard Proctor Relative Compaction of 85% and an Effective Confining Pressure of 1278 kPa.

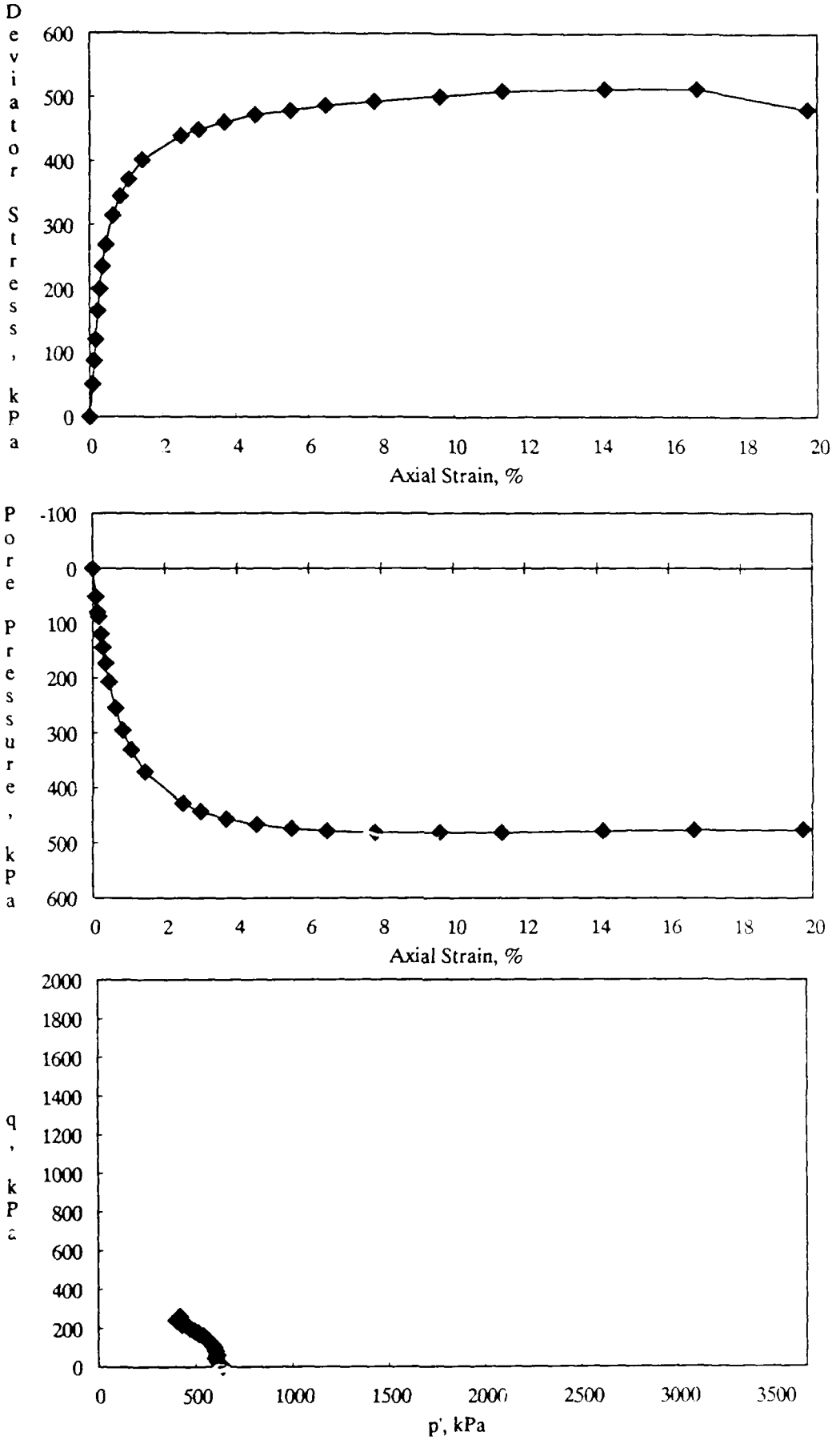


Figure B-39. CU Triaxial Test Results for 50% Kaolinite Mixture at a Standard Proctor Relative Compaction of 100% and an Effective Confining Pressure of 639 kPa.

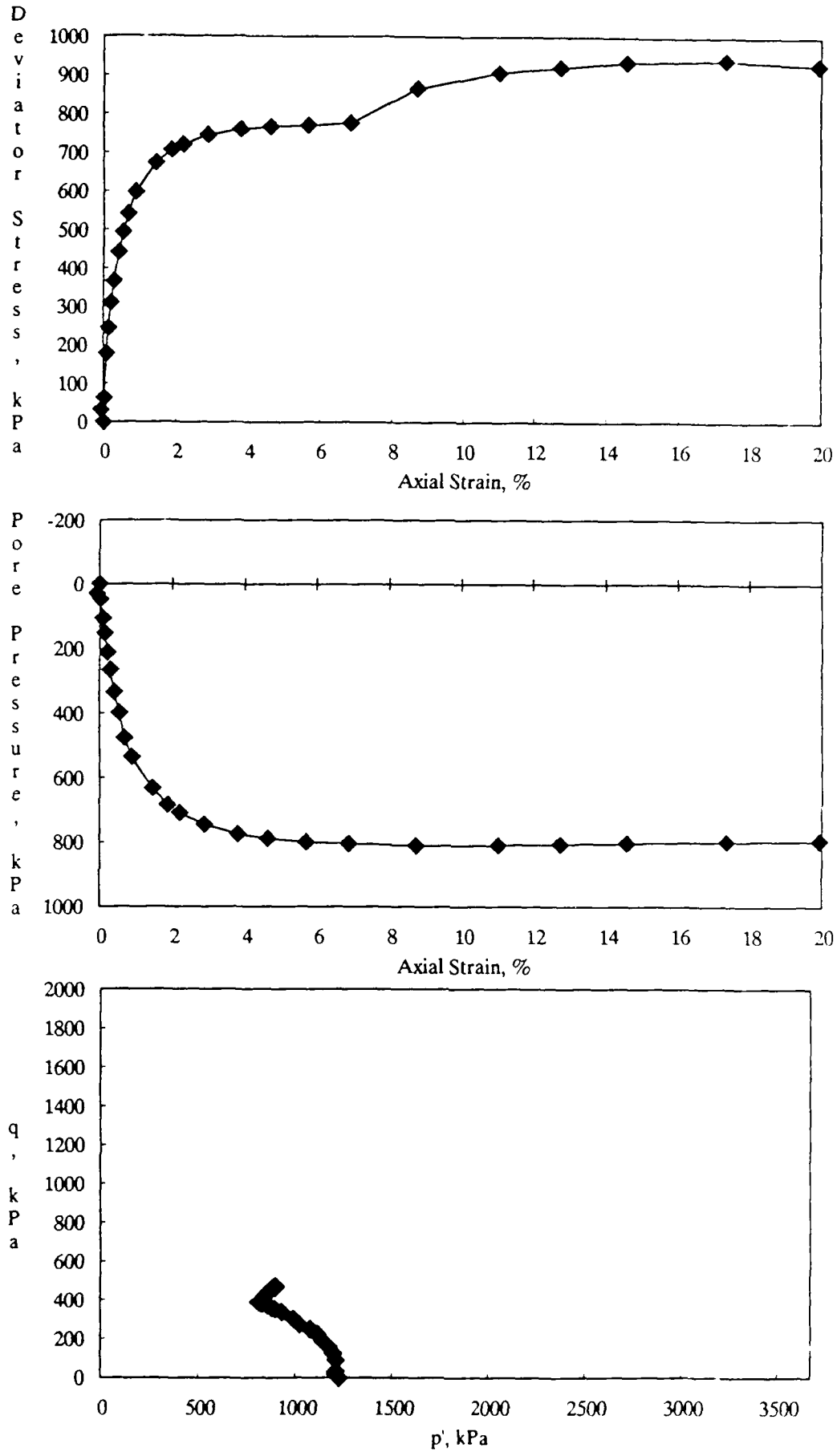


Figure B-40. CU Triaxial Test Results for 50% Kaolinite Mixture at a Standard Proctor Relative Compaction of 100% and an Effective Confining Pressure of 1227 kPa.

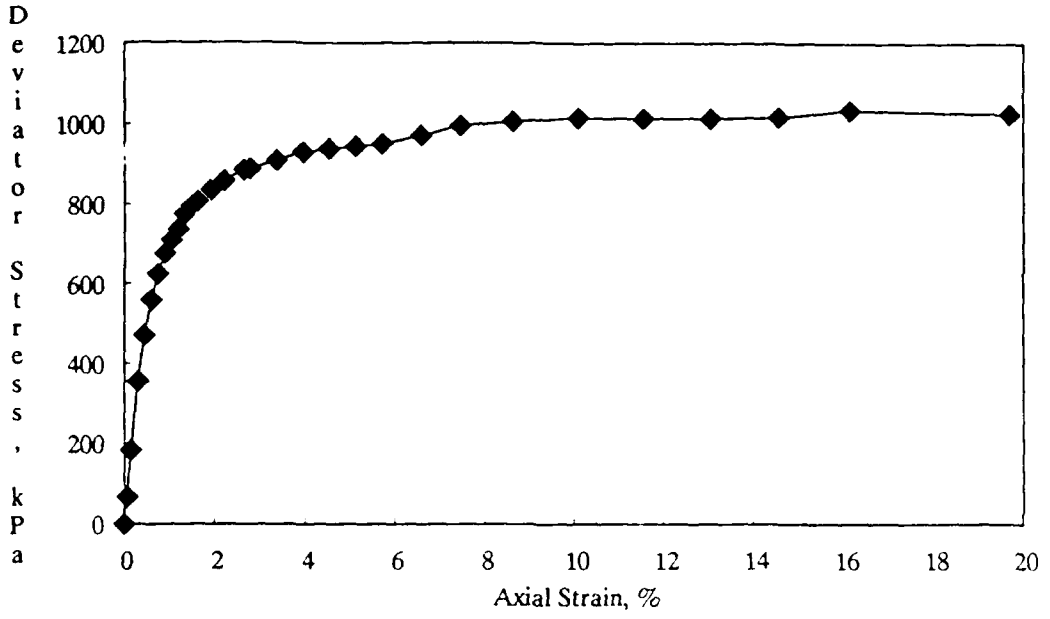


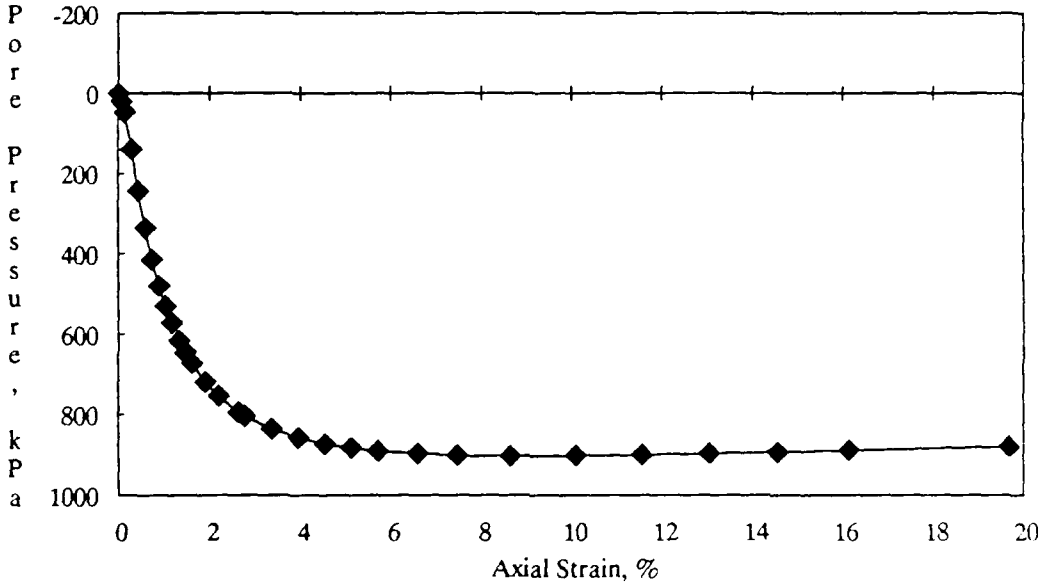


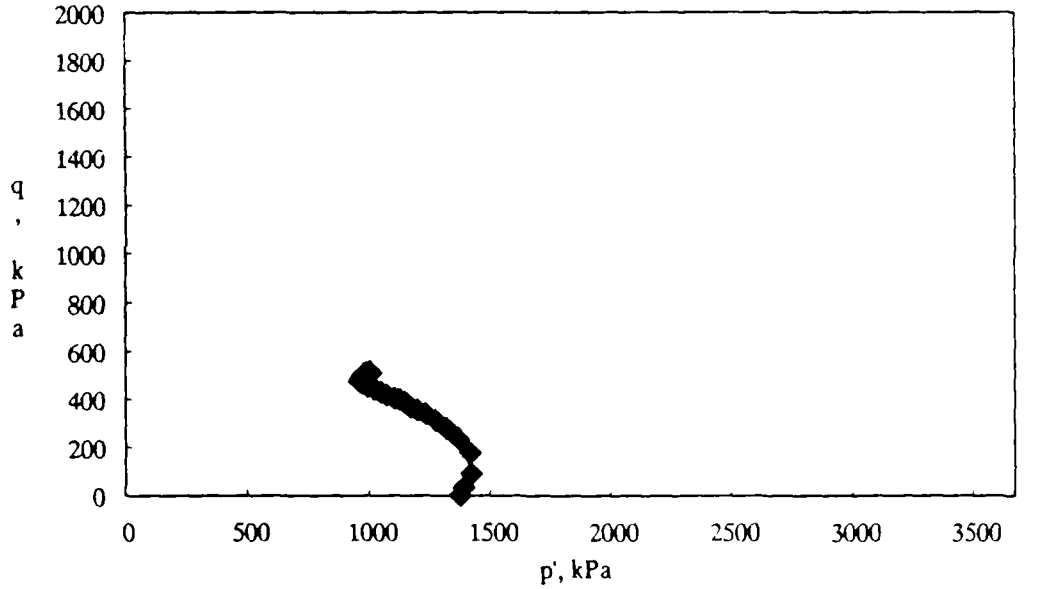


Figure B-41. CU Triaxial Test Results for 50% Kaolinite Mixture at a Standard Proctor Relative Compaction of 100% and an Effective Confining Pressure of 1373 kPa.

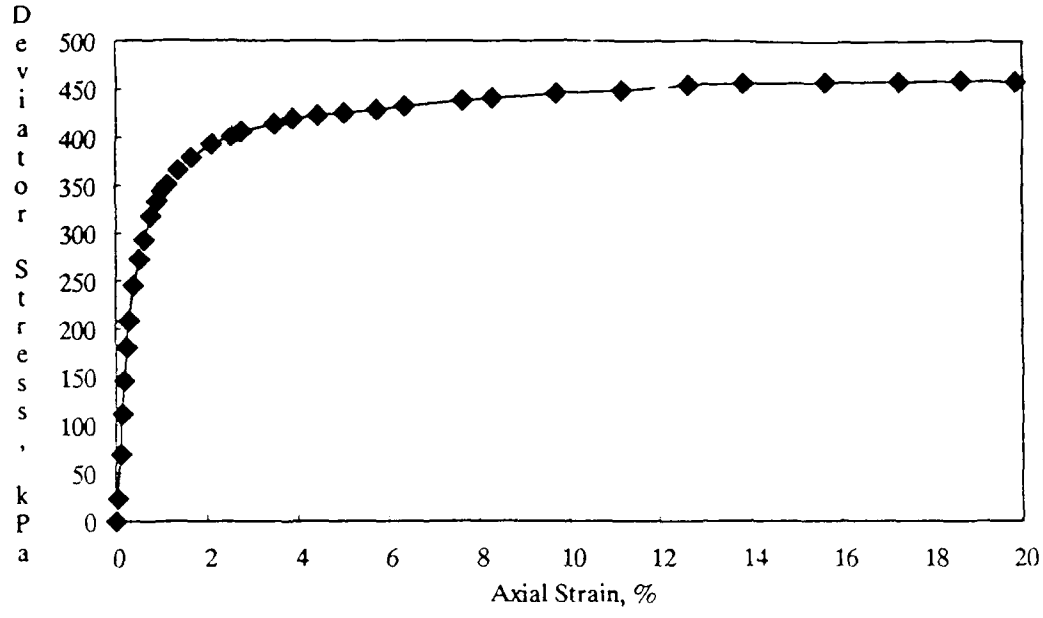


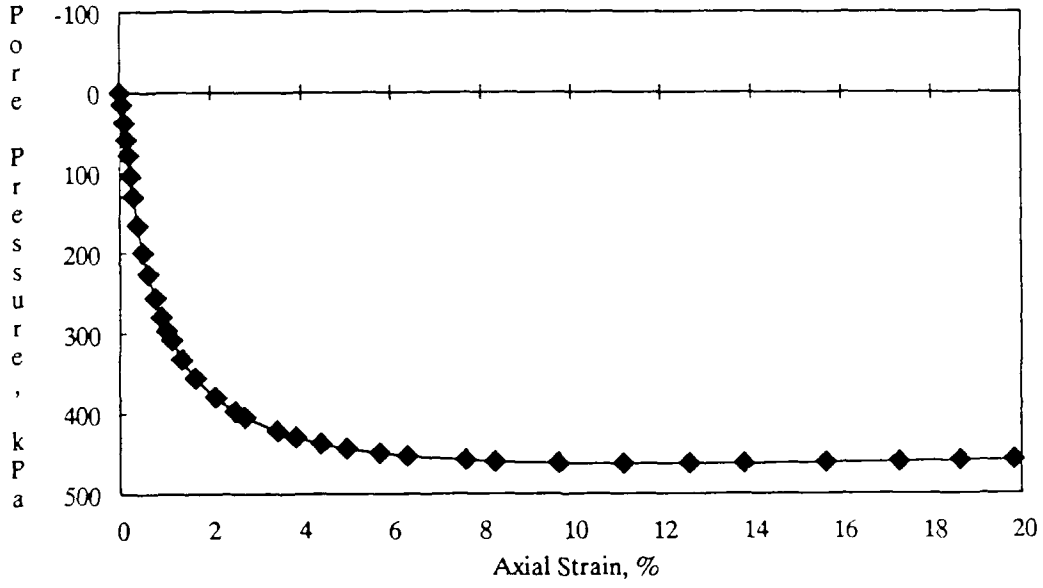


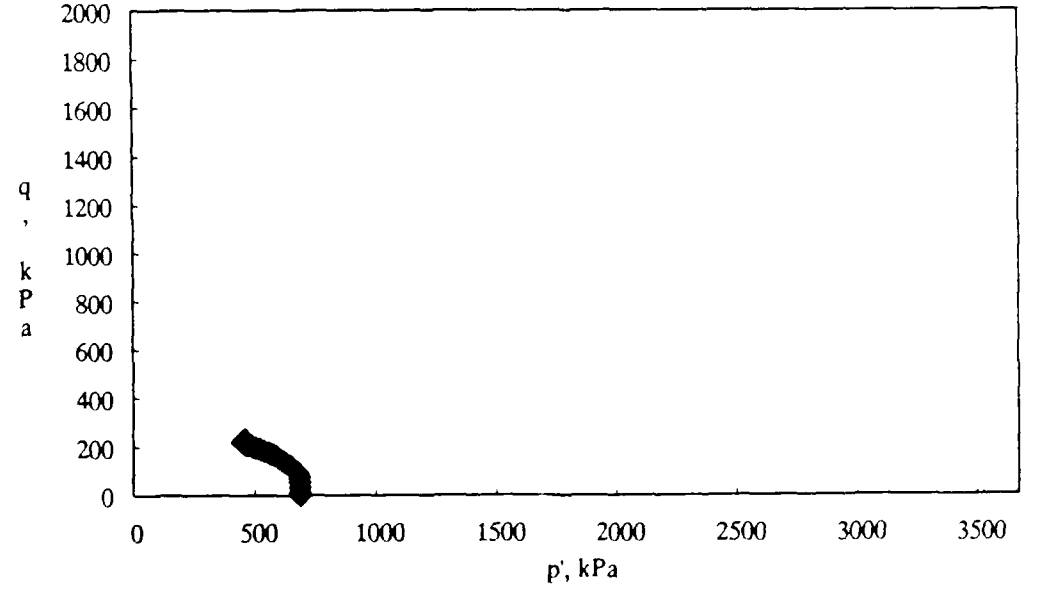


Figure B-42. CU Triaxial Test Results for 50% Kaolinite Mixture at a Standard Proctor Relative Compaction of 95% and an Effective Confining Pressure of 687 kPa.

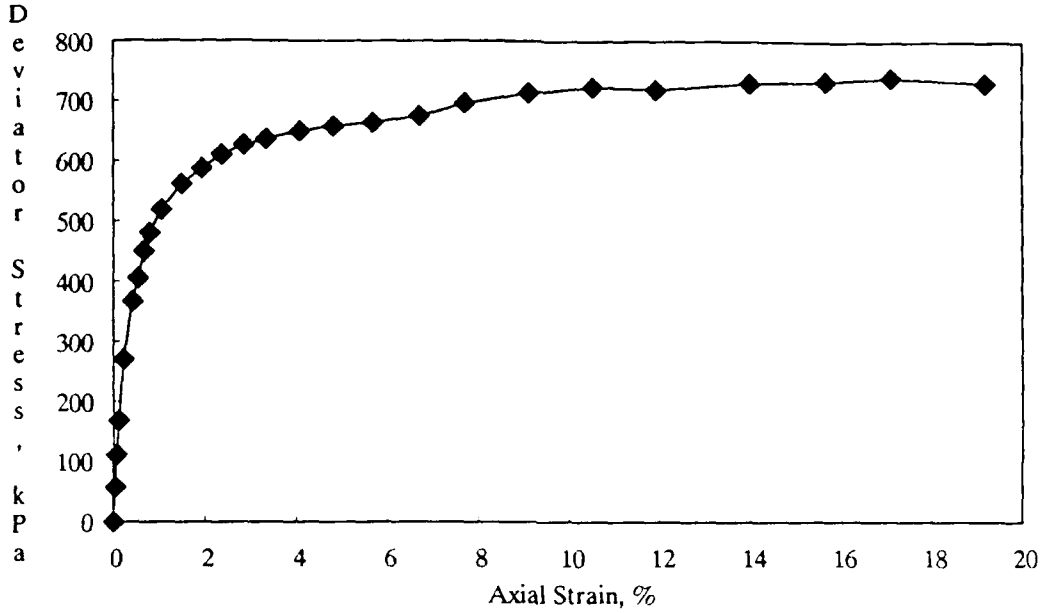


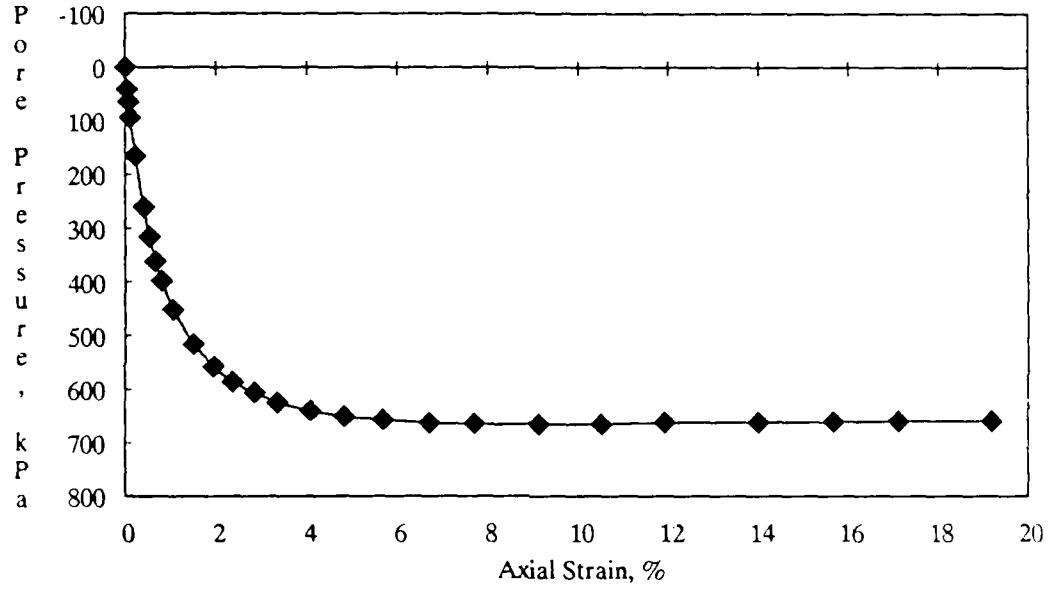


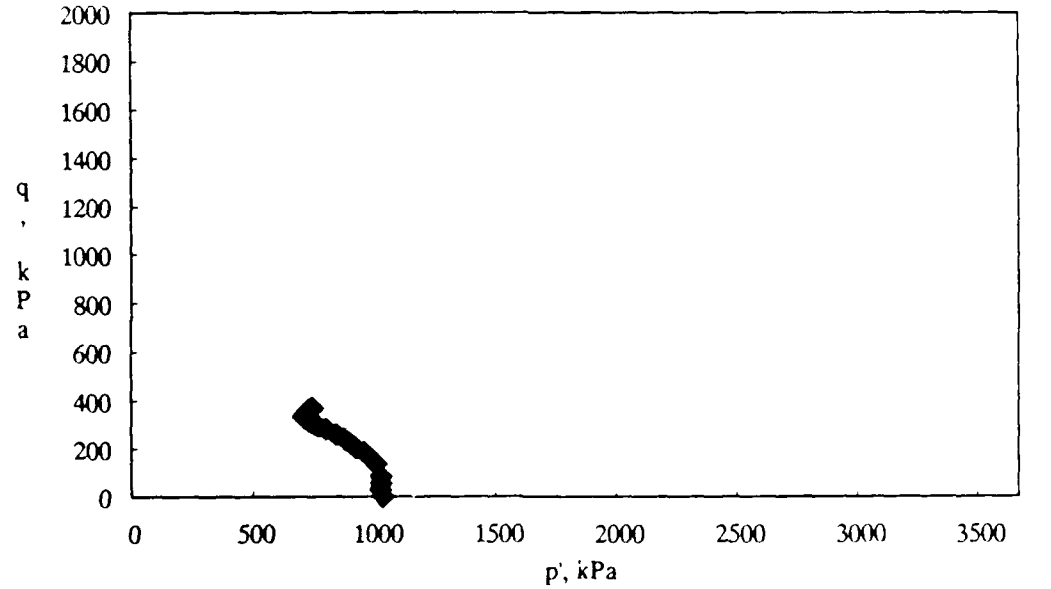


Figure B-43. CU Triaxial Test Results for 50% Kaolinite Mixture at a Standard Proctor Relative Compaction of 95% and an Effective Confining Pressure of 1033 kPa.

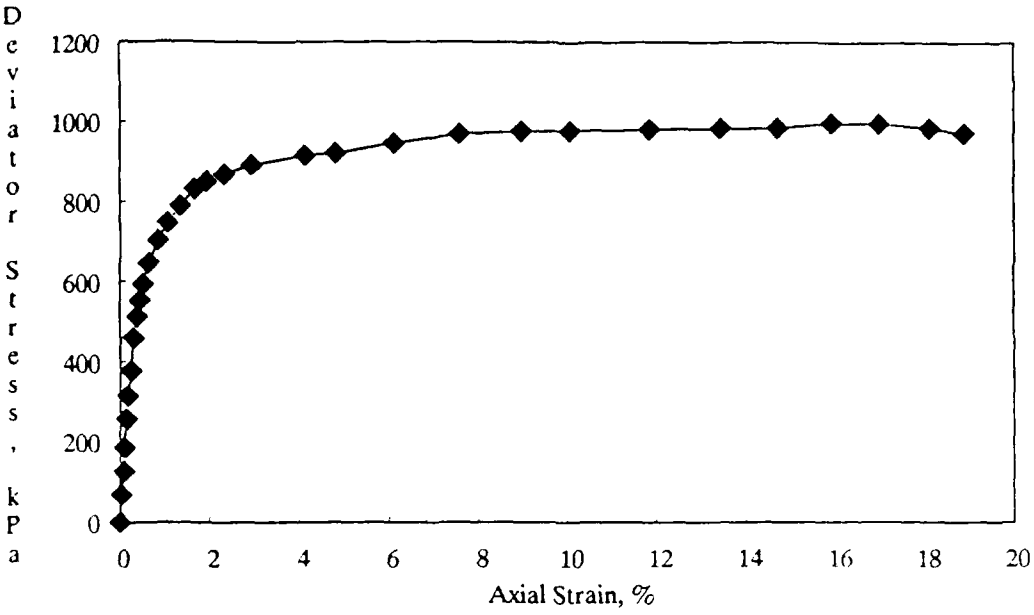


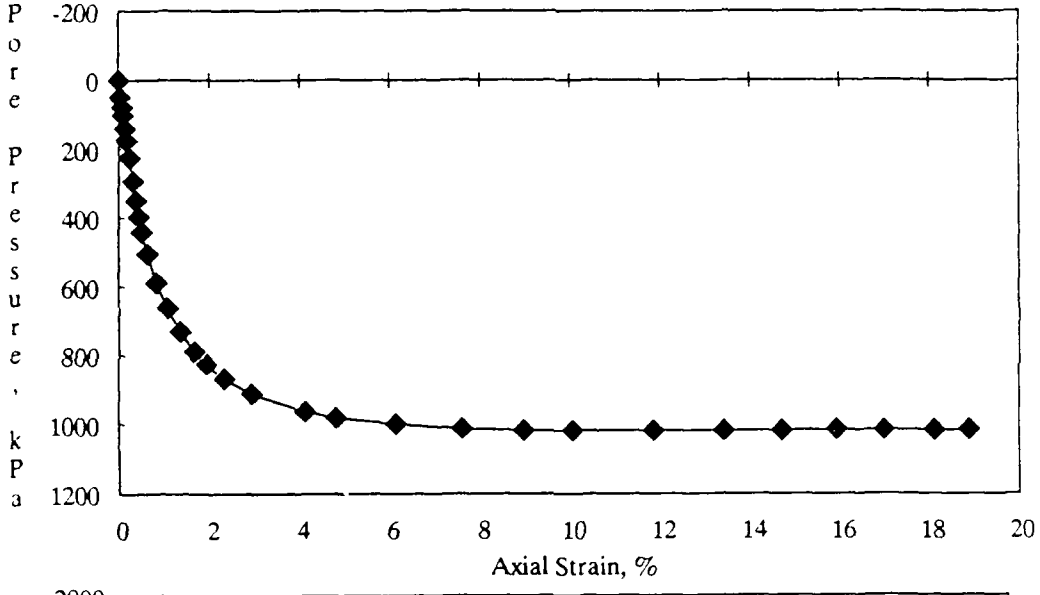


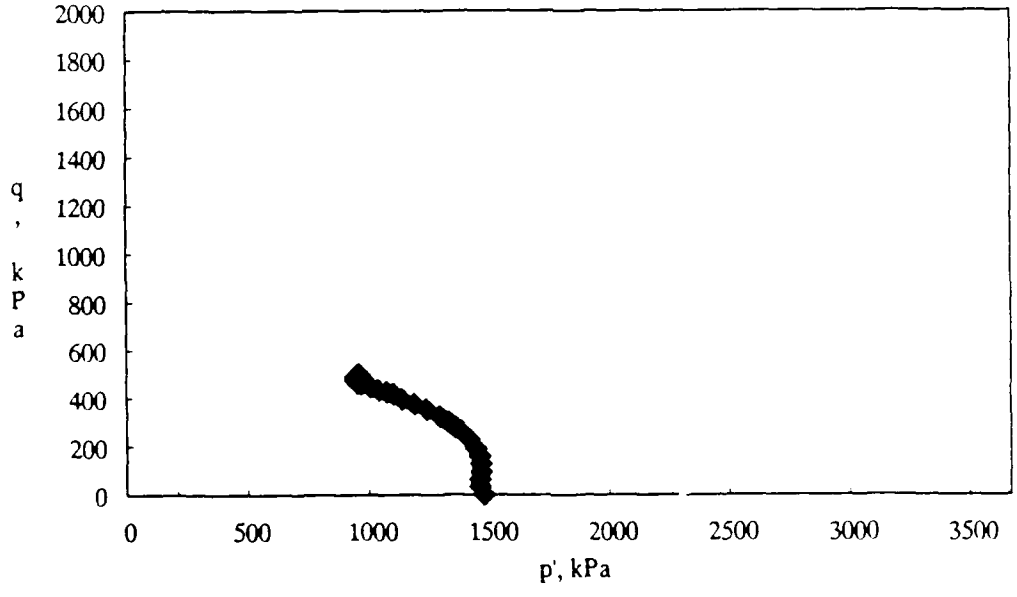


Figure B-44. CU Triaxial Test Results for 50% Kaolinite Mixture at a Standard Proctor Relative Compaction of 95% and an Effective Confining Pressure of 1473 kPa.

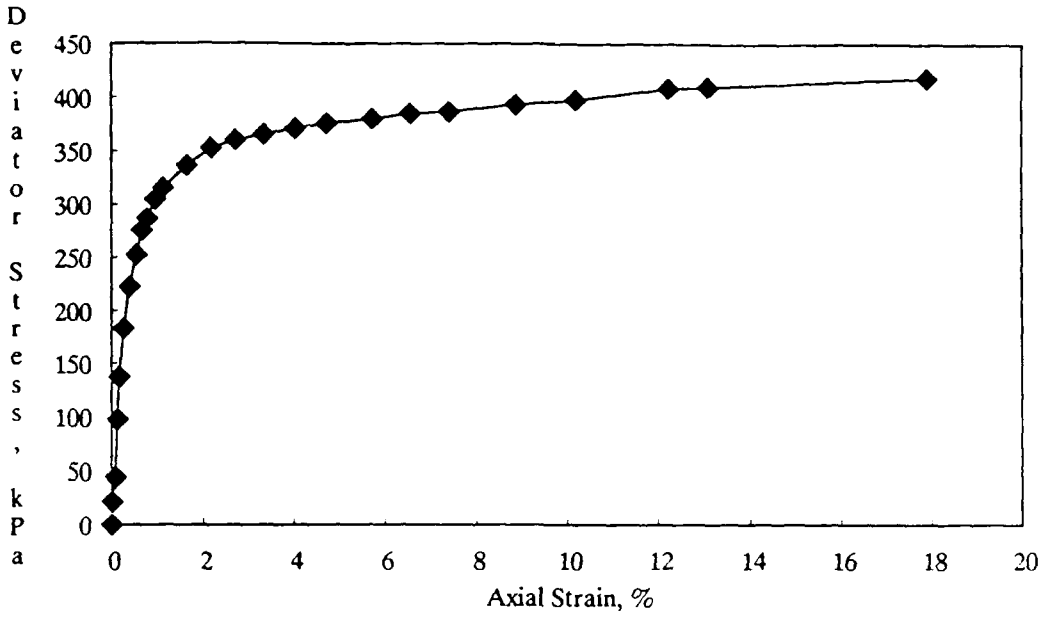


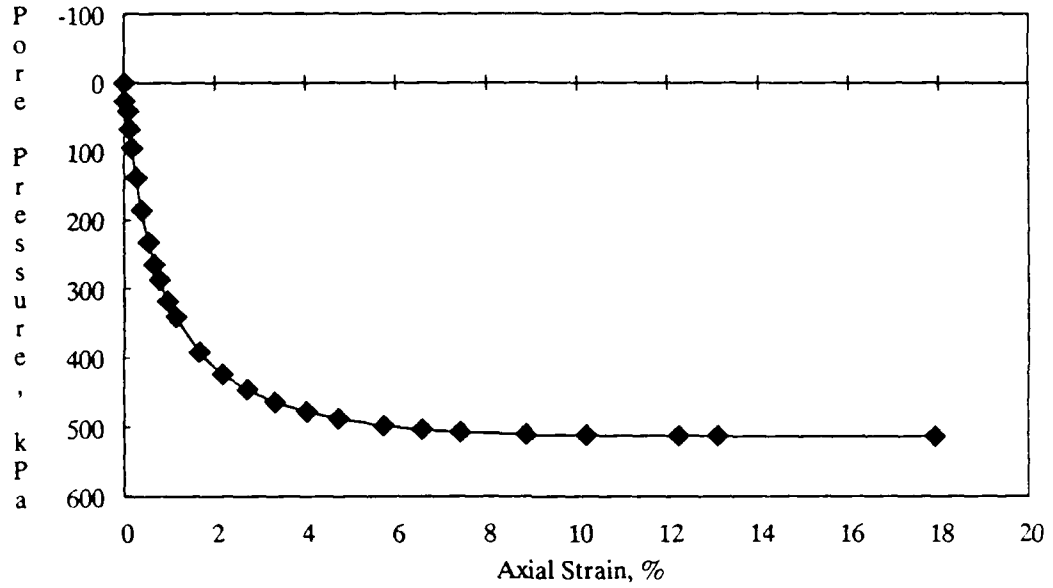


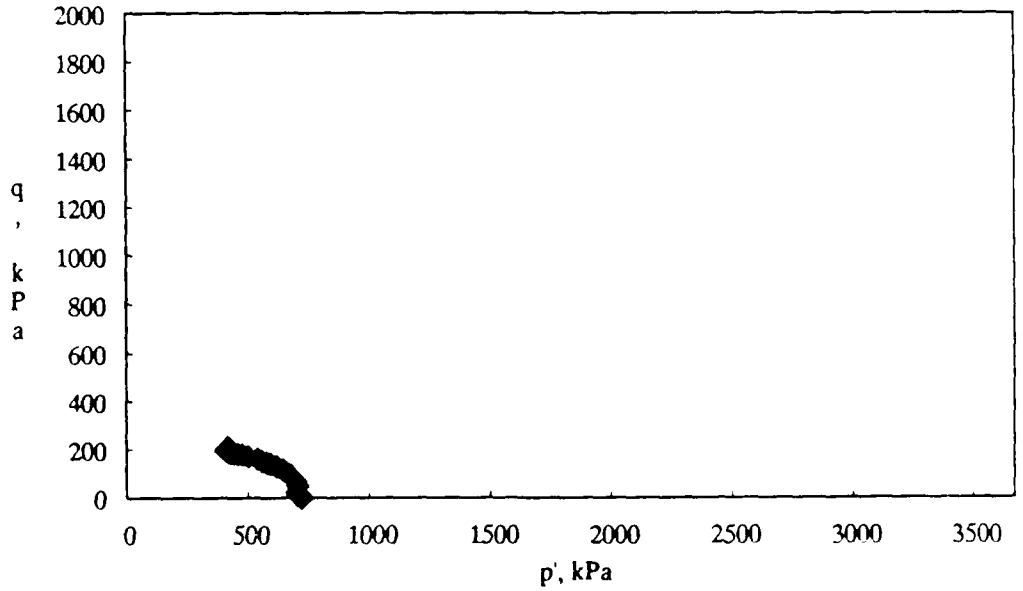


Figure B-45. CU Triaxial Test Results for 50% Kaolinite Mixture at a Standard Proctor Relative Compaction of 90% and an Effective Confining Pressure of 723 kPa.

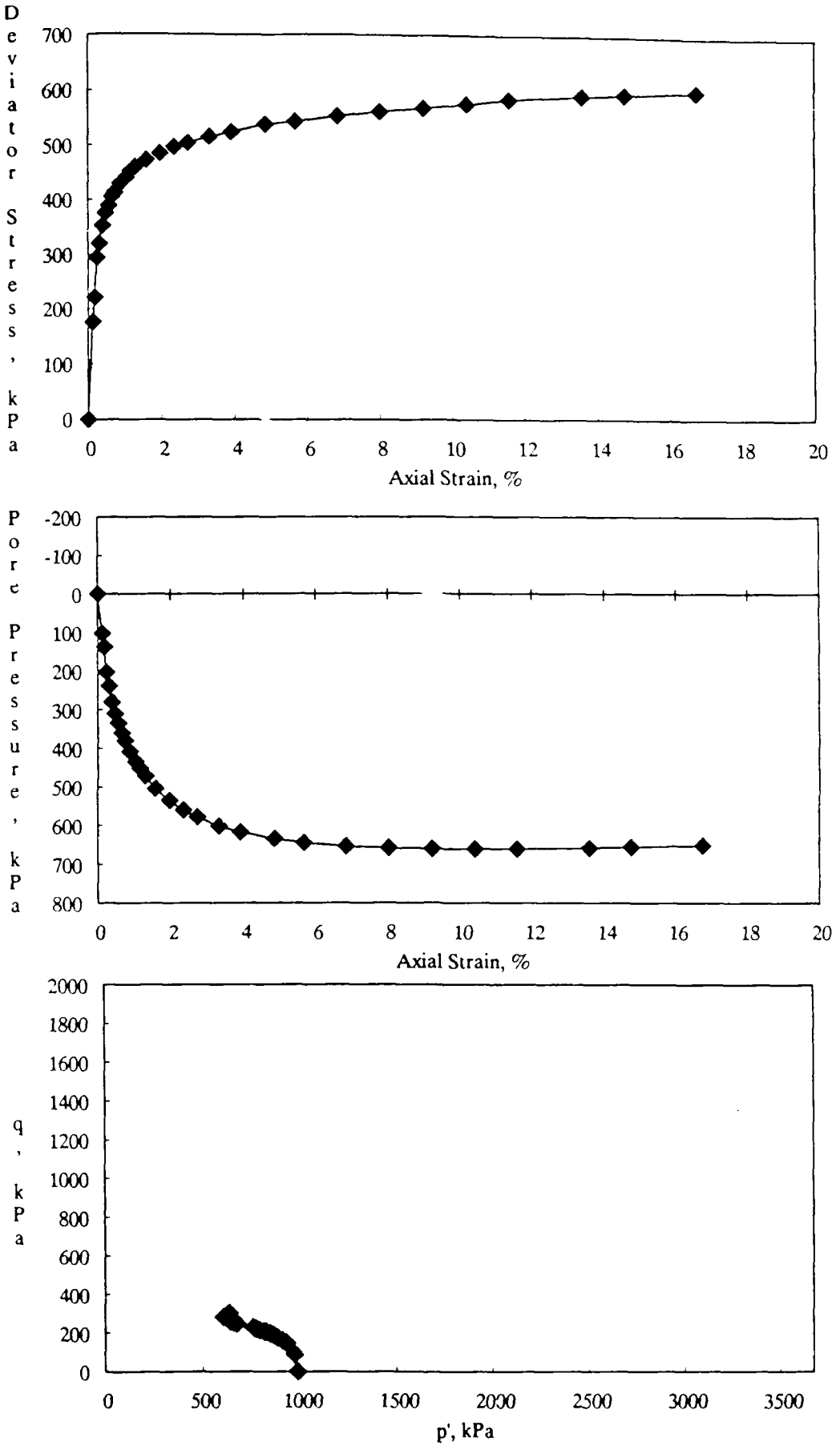


Figure B-46. CU Triaxial Test Results for 50% Kaolinite Mixture at a Standard Proctor Relative Compaction of 90% and an Effective Confining Pressure of 984 kPa.

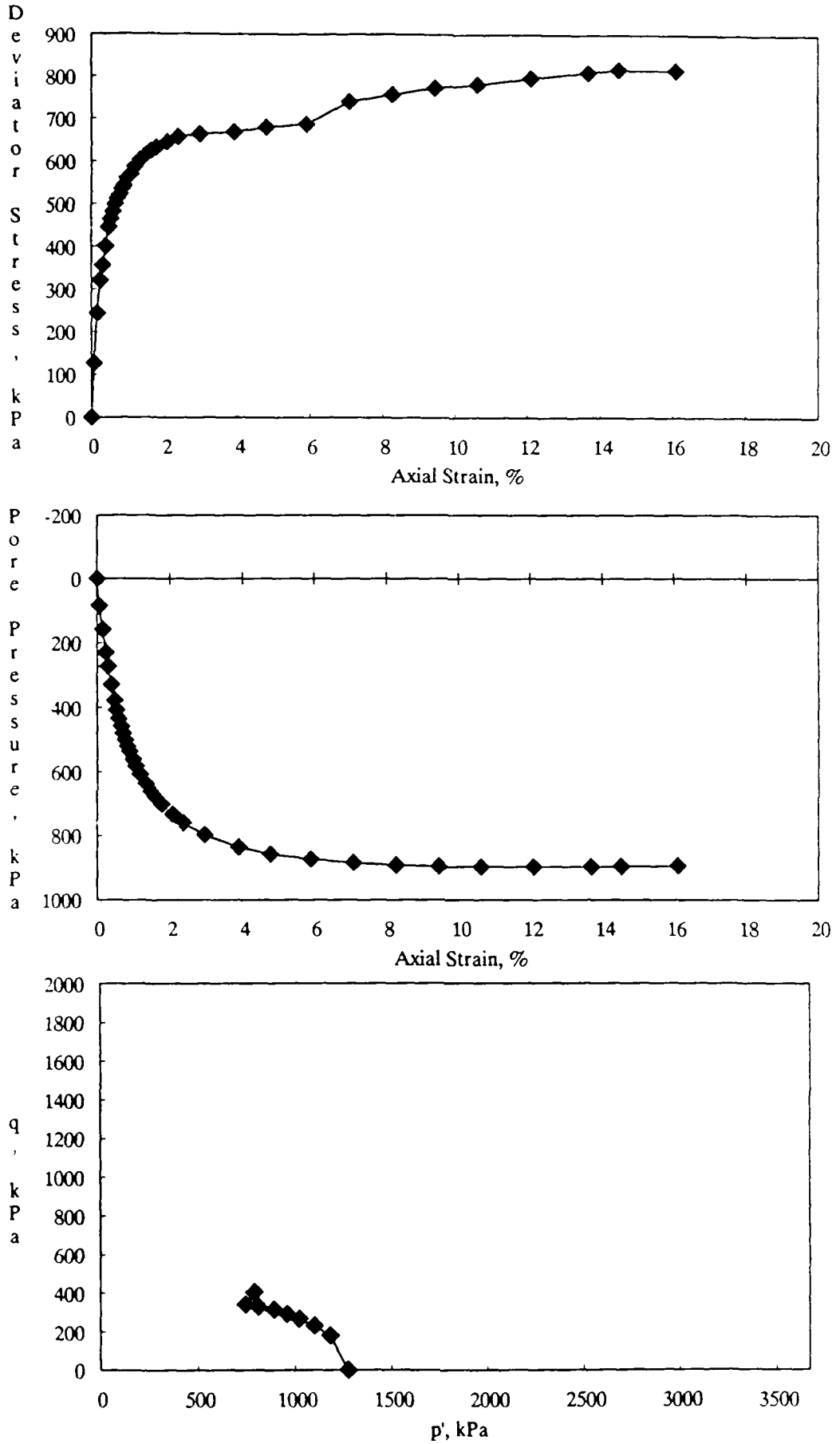


Figure B-47. CU Triaxial Test Results for 50% Kaolinite Mixture at a Standard Proctor Relative Compaction of 90% and an Effective Confining Pressure of 1274 kPa.

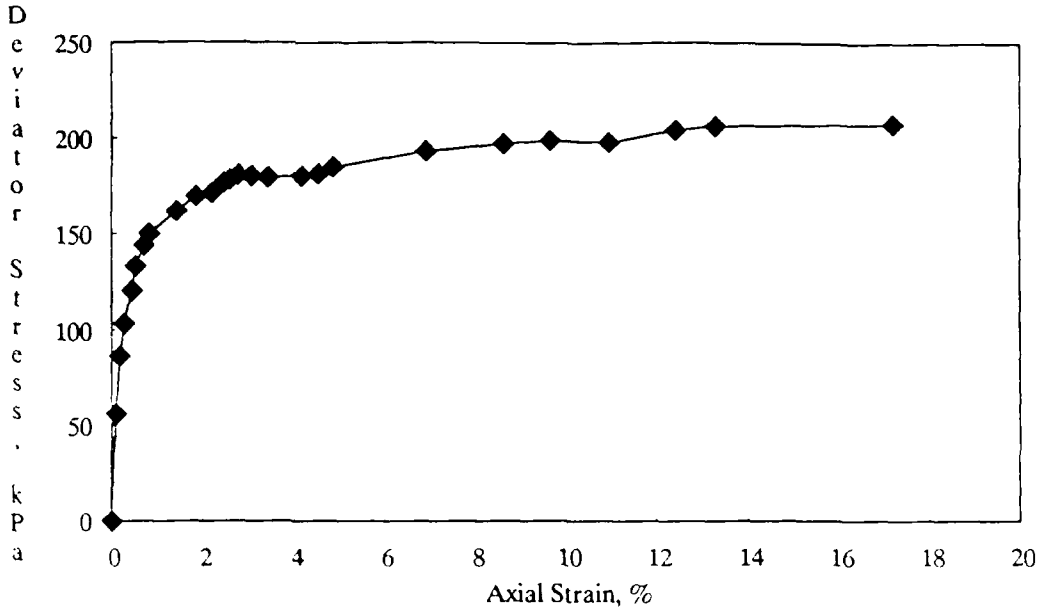


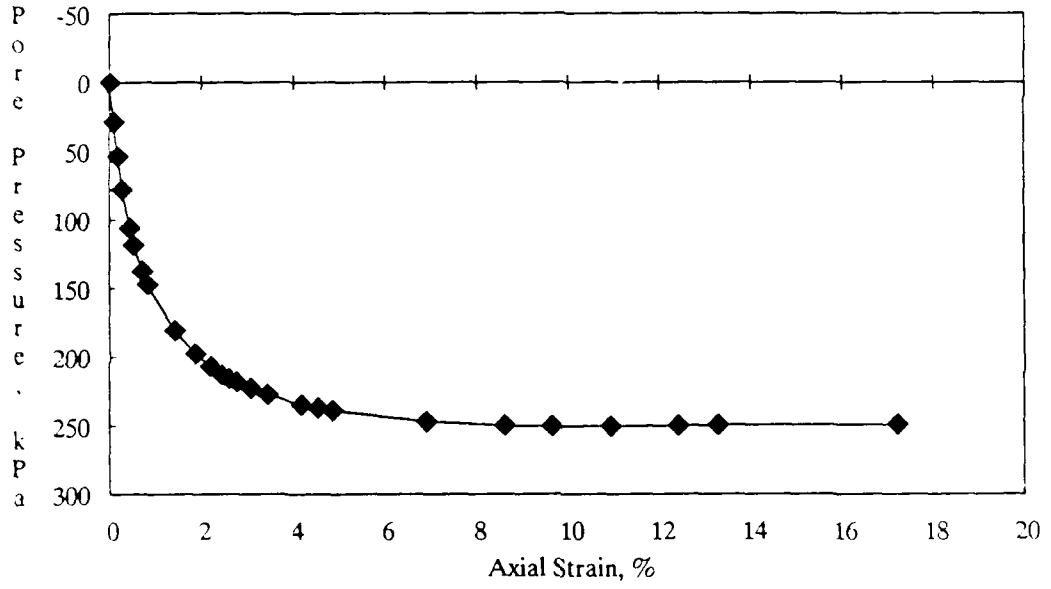


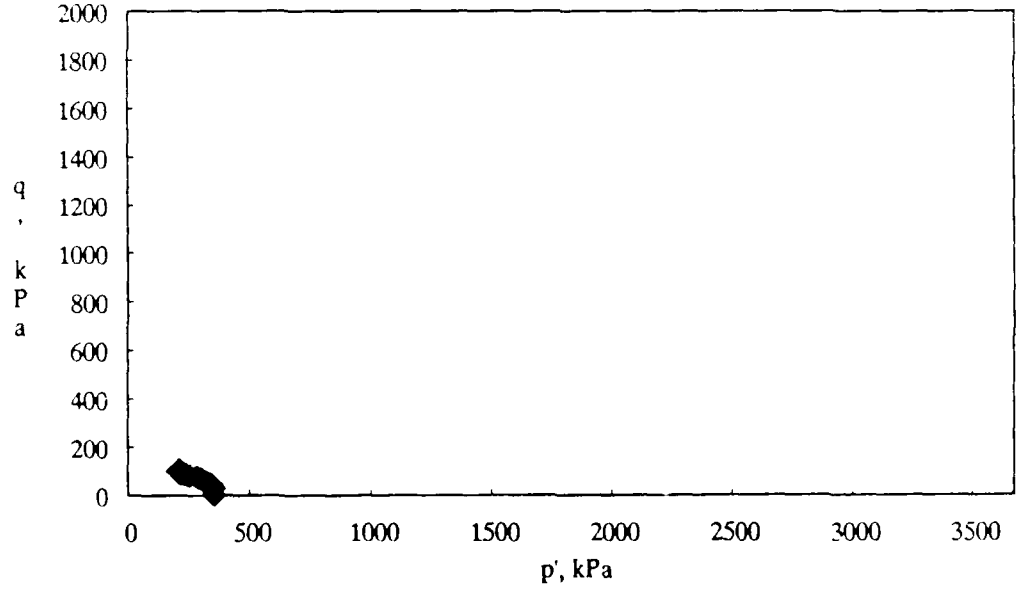


Figure B-48. CU Triaxial Test Results for 50% Kaolinite Mixture at a Standard Proctor Relative Compaction of 85% and an Effective Confining Pressure of 354 kPa.

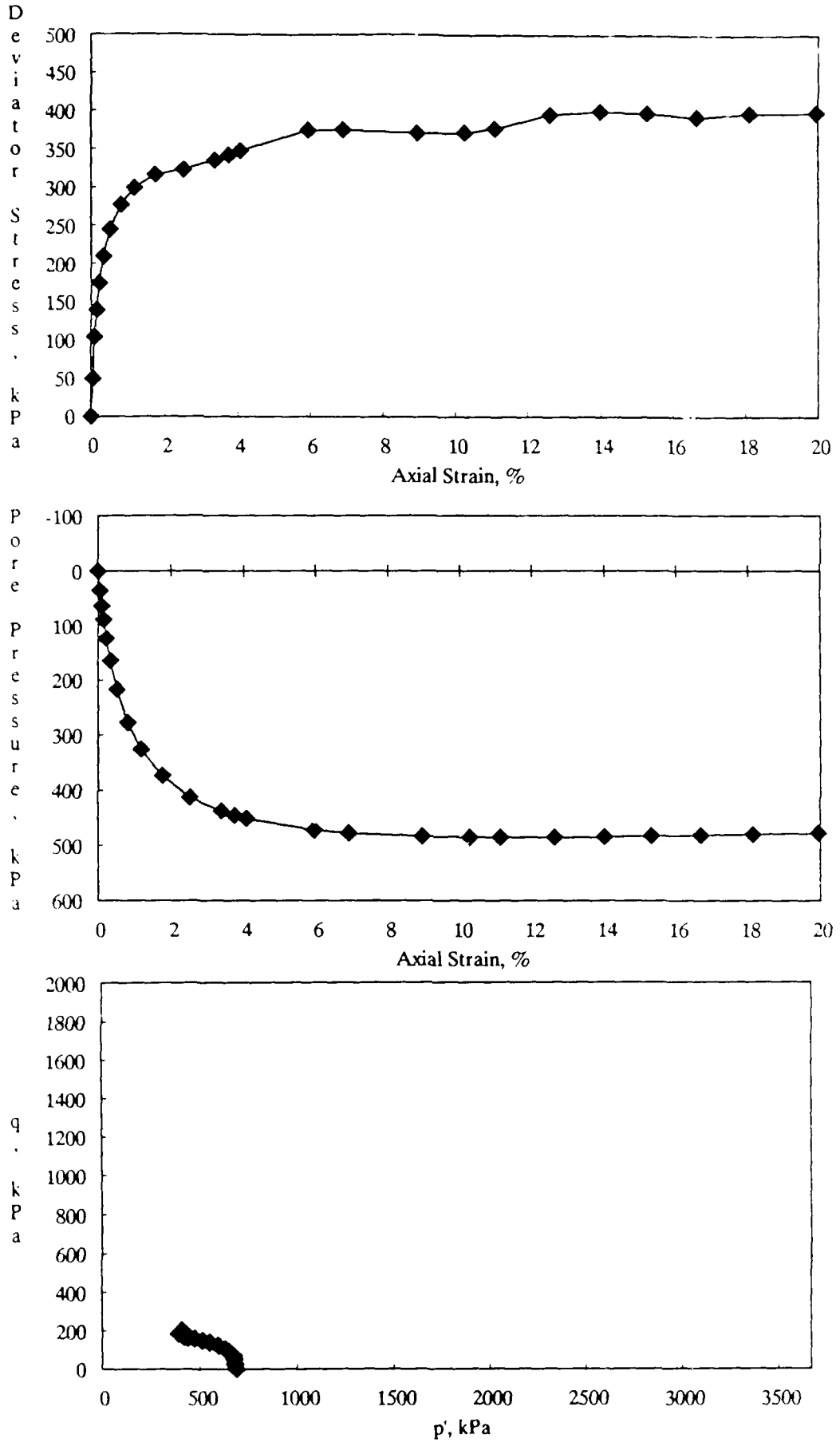


Figure B-49. CU Triaxial Test Results for 50% Kaolinite Mixture at a Standard Proctor Relative Compaction of 85% and an Effective Confining Pressure of 687 kPa.

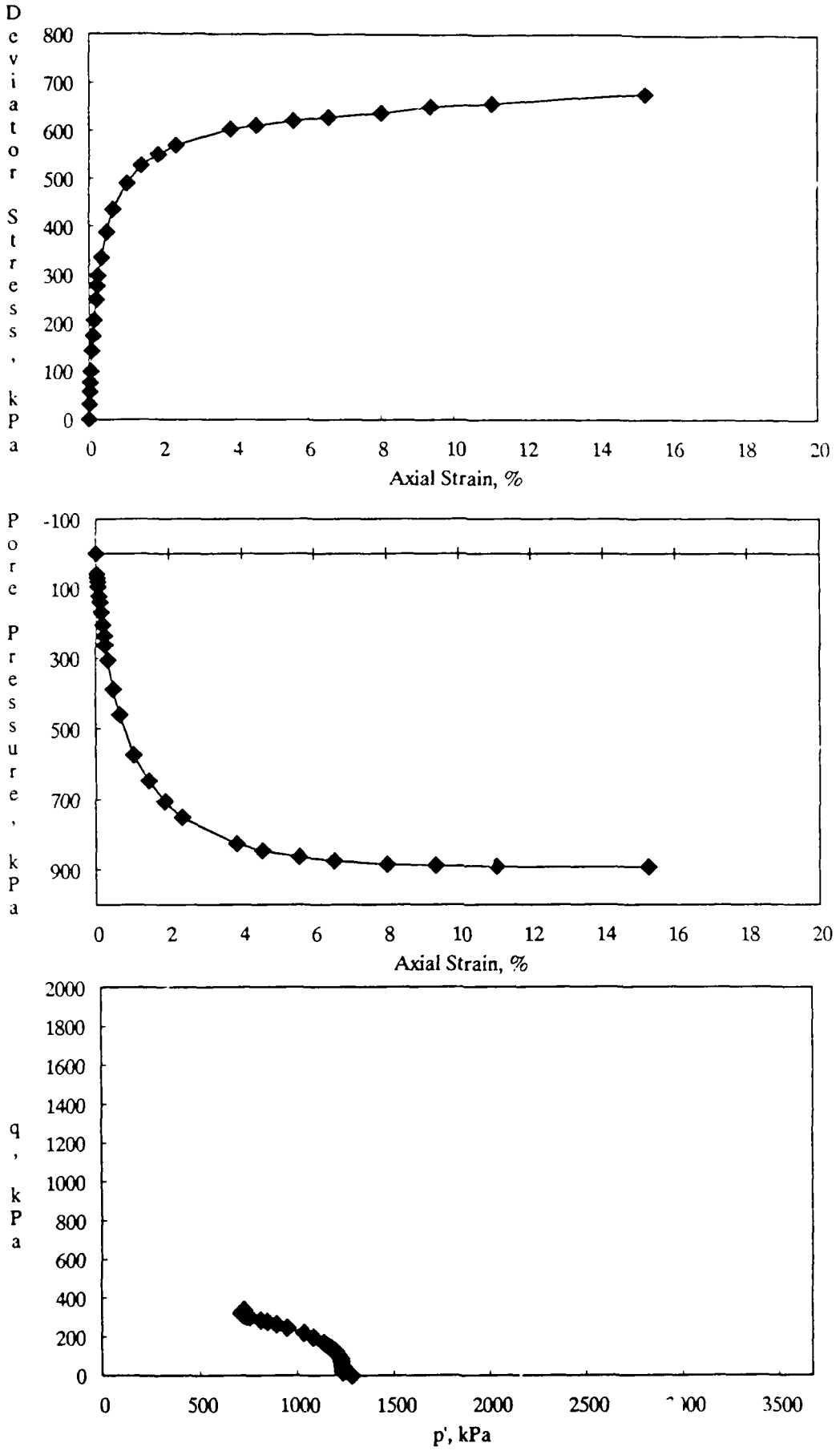


Figure B-50. CU Triaxial Test Results for 50% Kaolinite Mixture at a Standard Proctor Relative Compaction of 85% and an Effective Confining Pressure of 1278 kPa.

# APPENDIX C

## Isotropically Consolidated-Drained Triaxial Test Results on Montmorillonite-Silt Mixtures

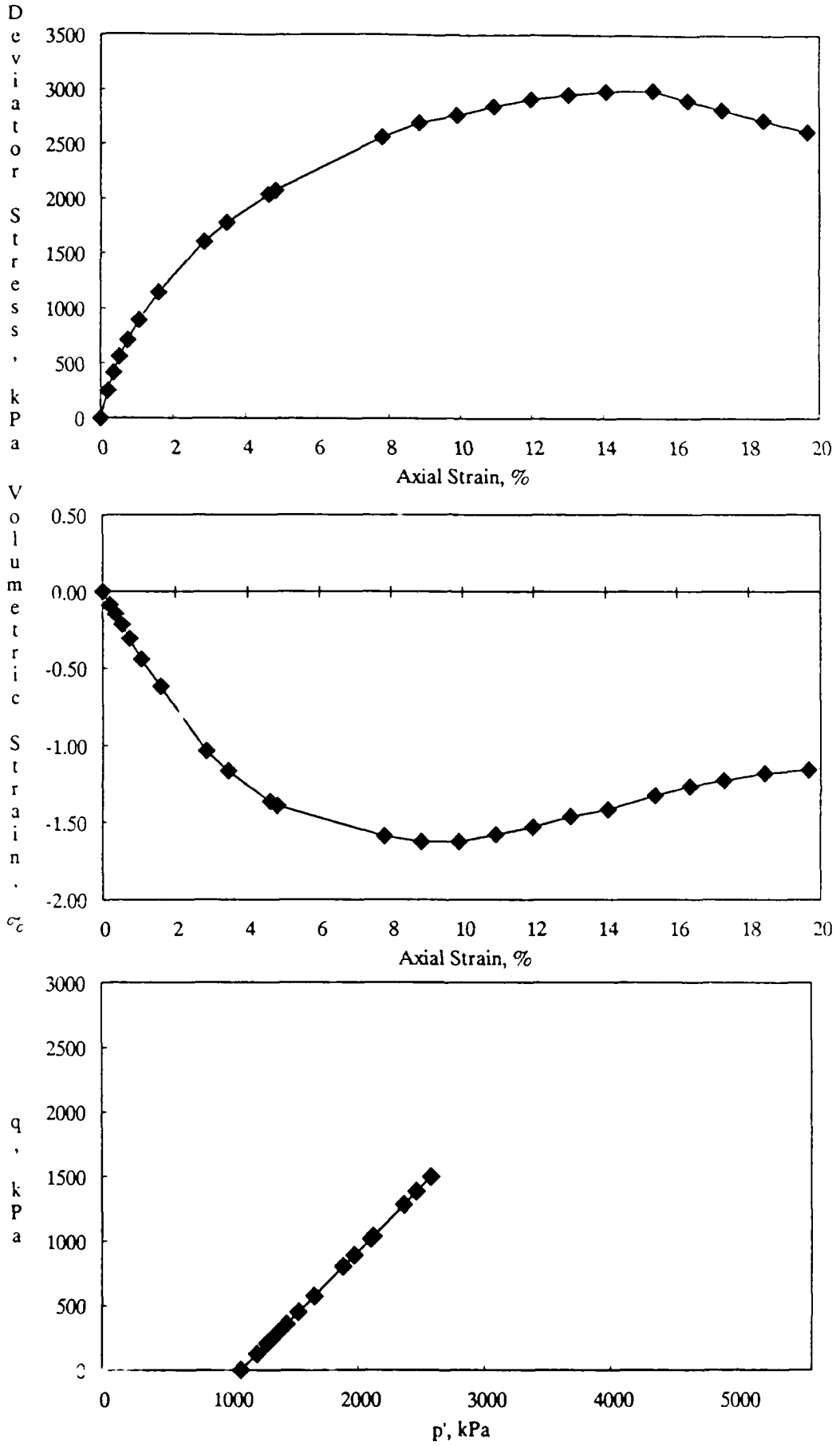


Figure C-1. **CD Triaxial Test Results for 10% Montmorillonite Mixture at a Standard Relative Compaction of 100% and an Effective Confining Pressure of 1080 kPa.**

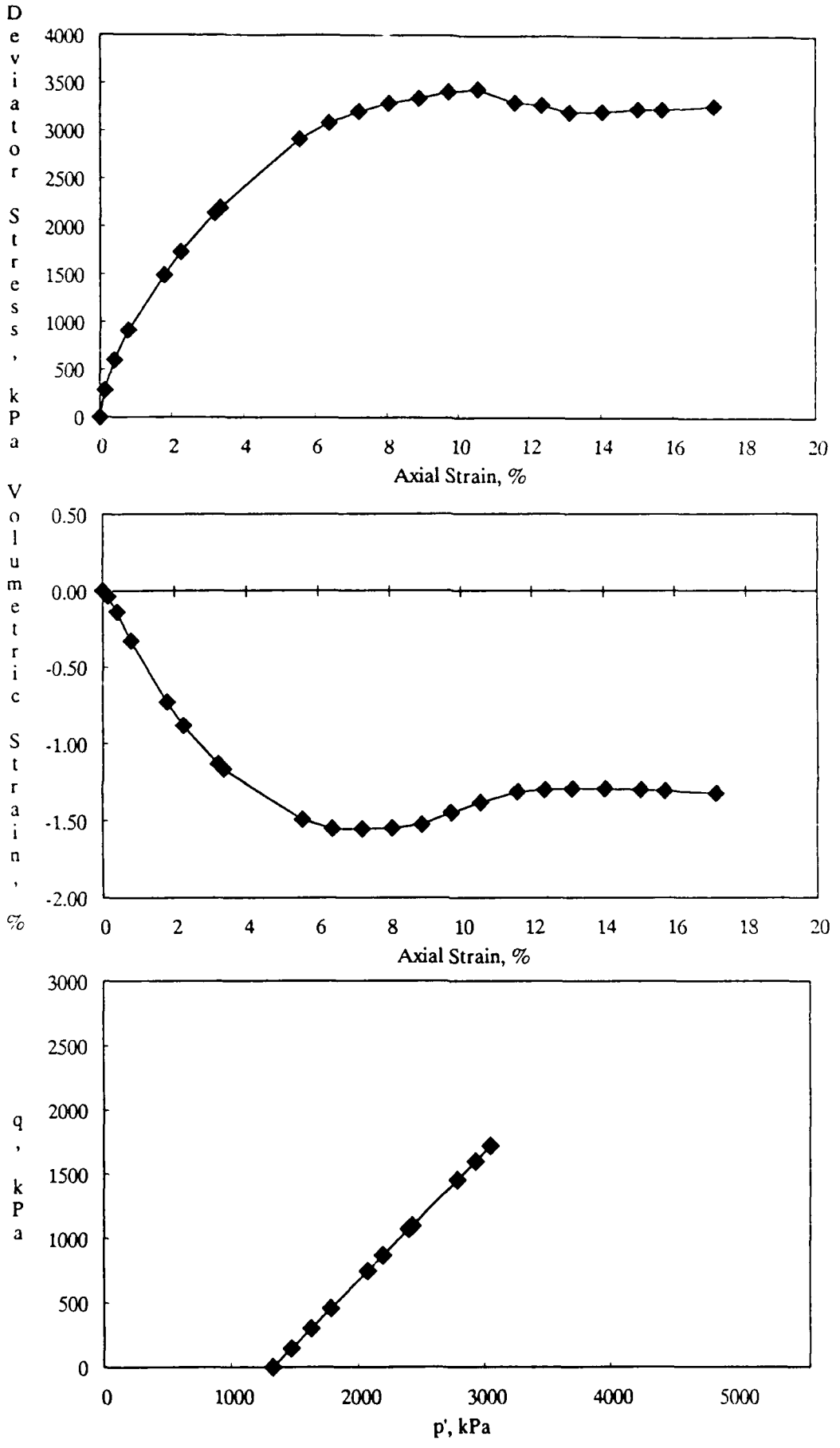


Figure C-2. **CD Triaxial Test Results for 10% Montmorillonite Mixture at a Standard Relative Compaction of 100% and an Effective Confining Pressure of 1325 kPa.**

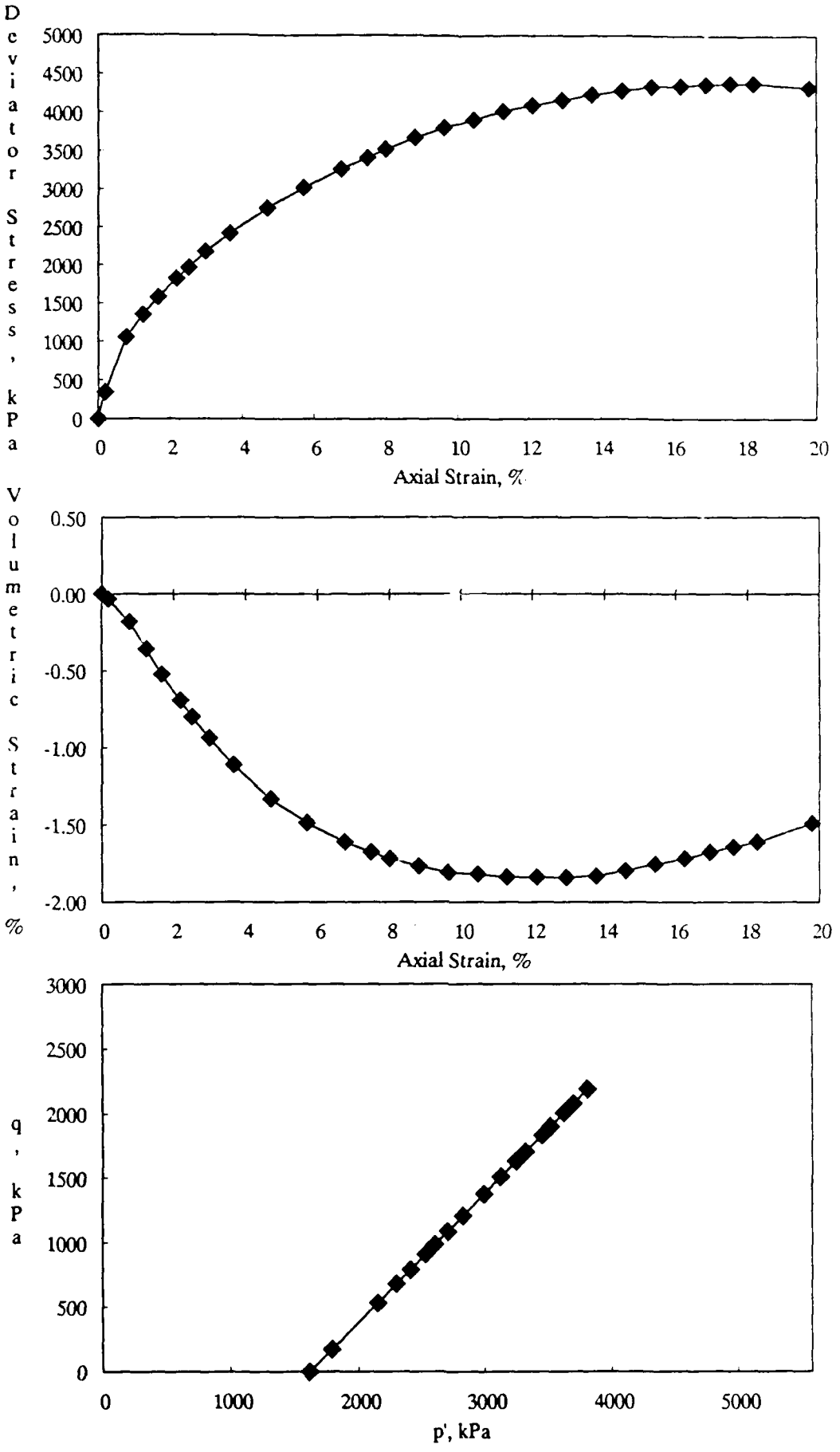


Figure C-3. CD Triaxial Test Results for 10% Montmorillonite Mixture at a Standard Relative Compaction of 100% and an Effective Confining Pressure of 1618 kPa.

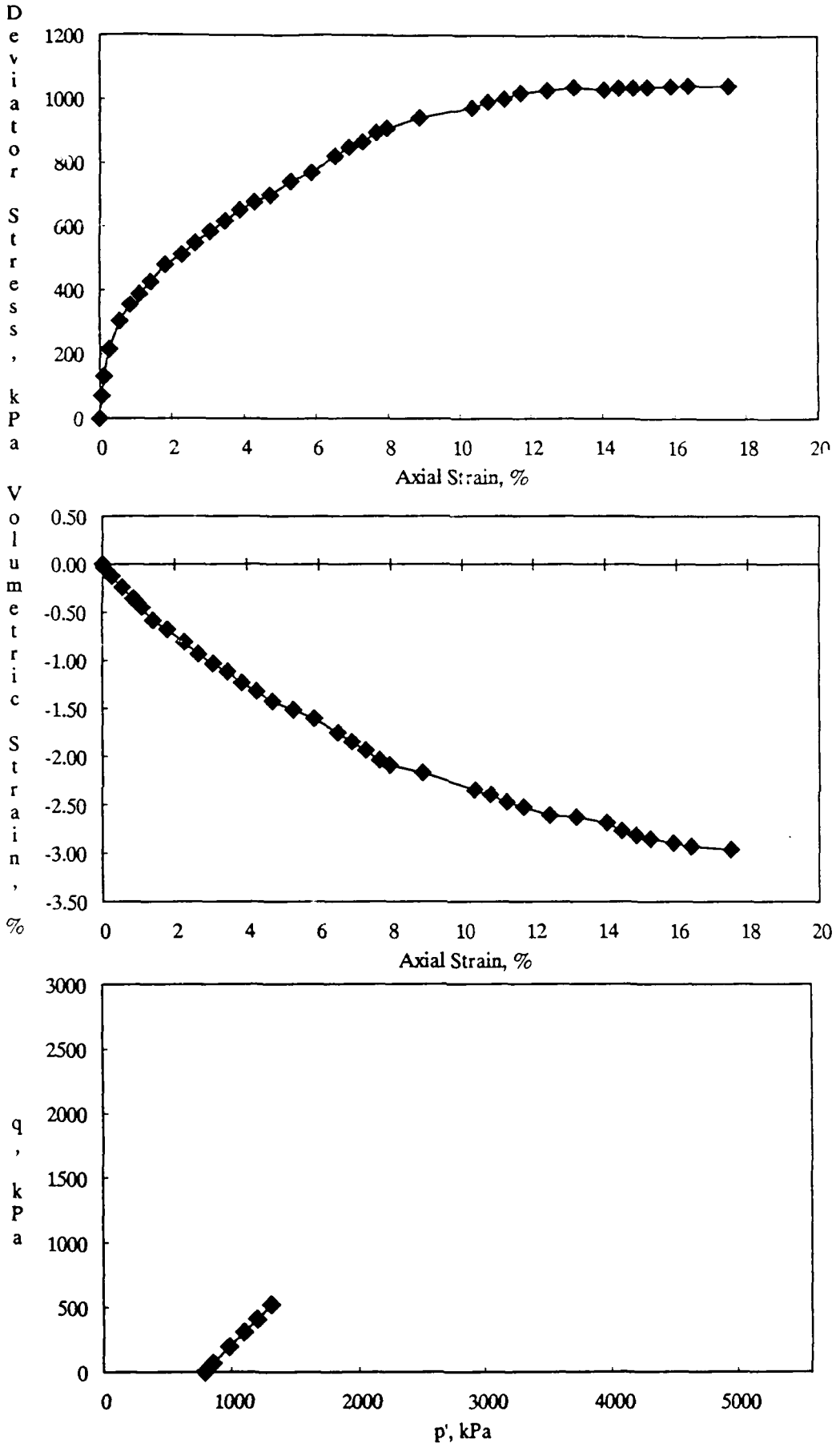


Figure C-4. CD Triaxial Test Results for 30% Montmorillonite Mixture at a Standard Relative Compaction of 100% and an Effective Confining Pressure of 787 kPa.

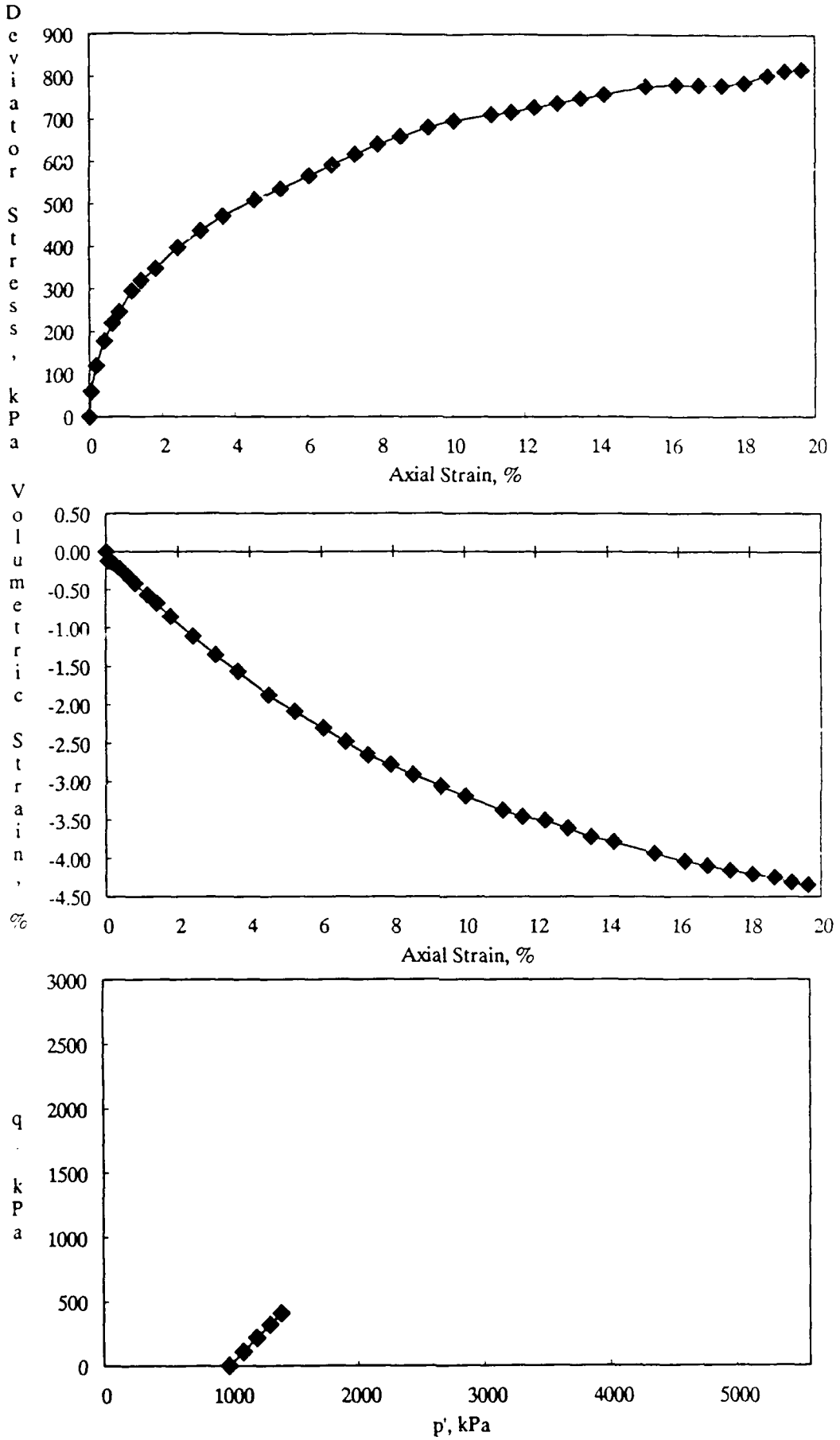


Figure C-5. **CD Triaxial Test Results for 30% Montmorillonite Mixture at a Standard Relative Compaction of 100% and an Effective Confining Pressure of 985 kPa.**

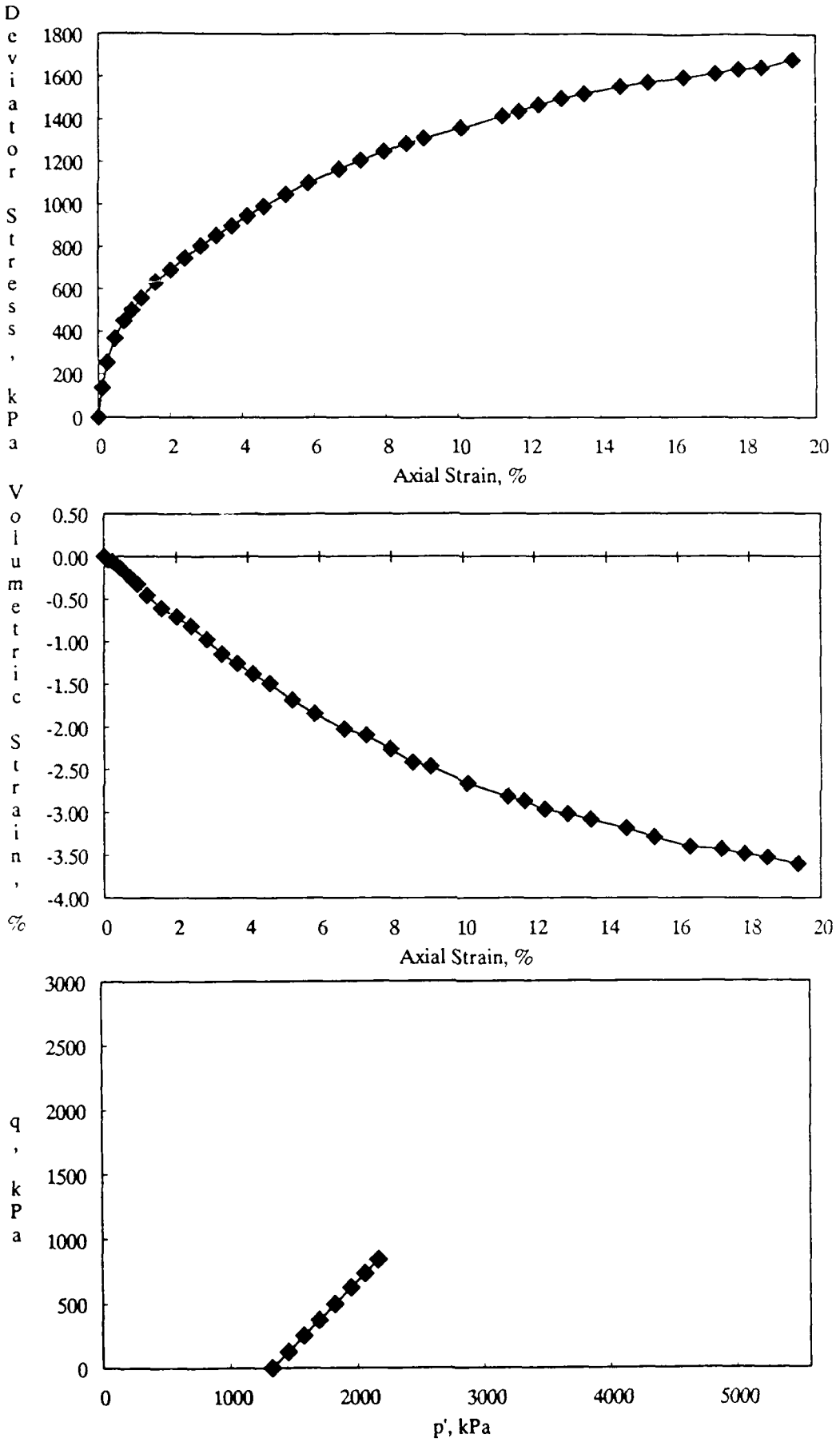


Figure C-6. CD Triaxial Test Resuits for 30% Montmorillonite Mixture at a Standard Relative Compaction of 100% and an Effective Confining Pressure of 1325 kPa.

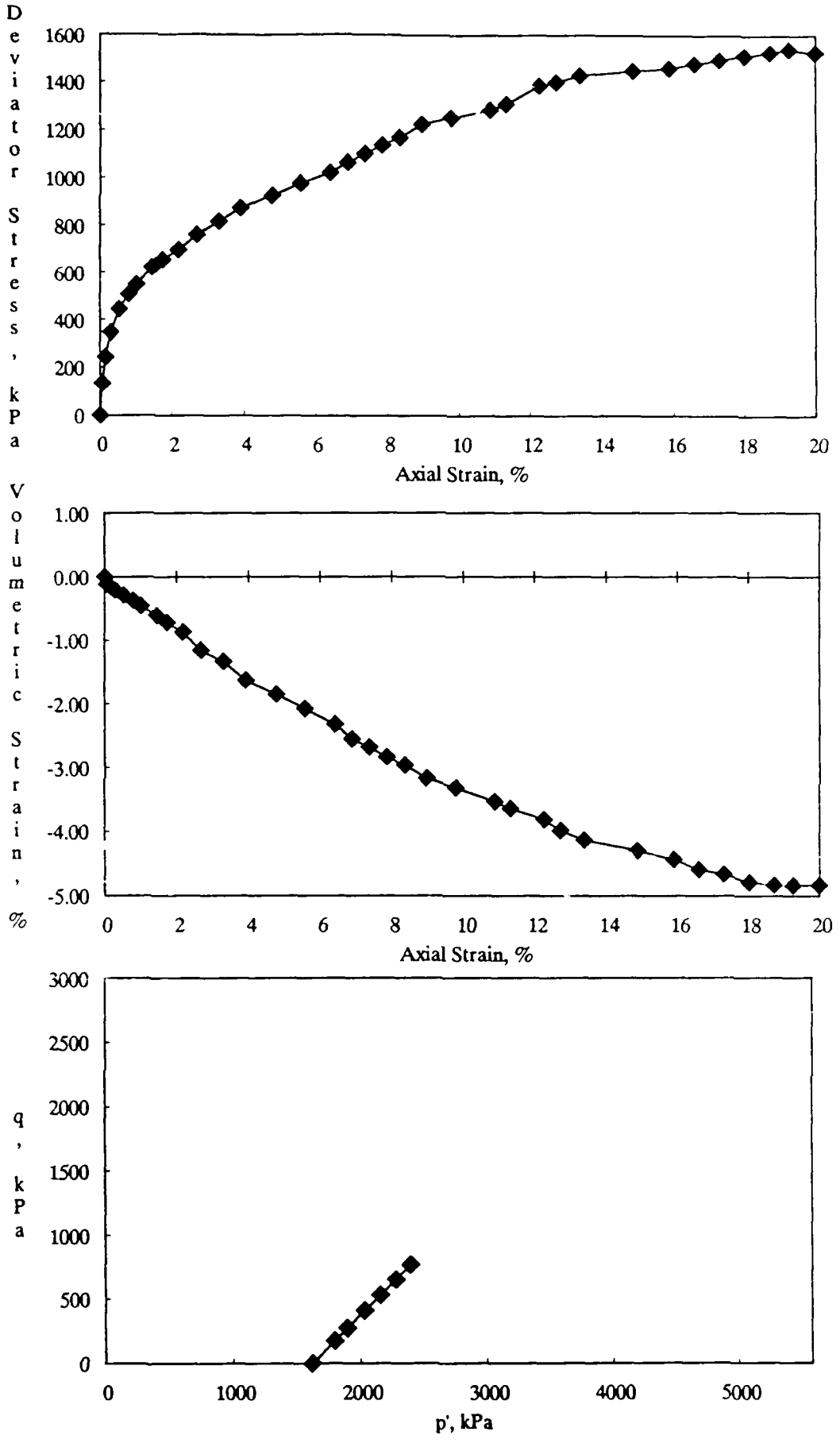


Figure C-7. CD Triaxial Test Results for 30% Montmorillonite Mixture at a Standard Relative Compaction of 100% and an Effective Confining Pressure of 1622 kPa.

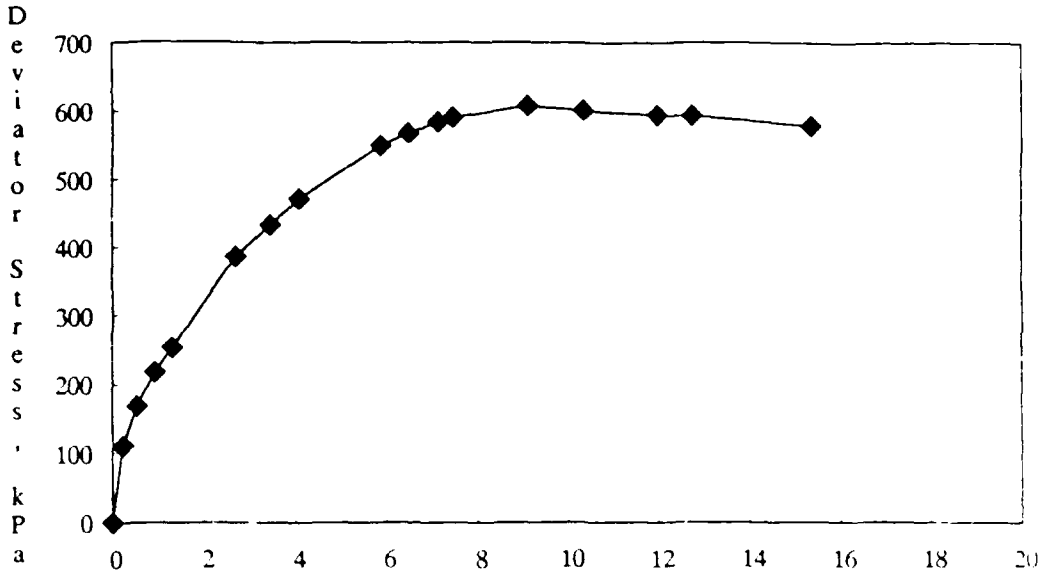


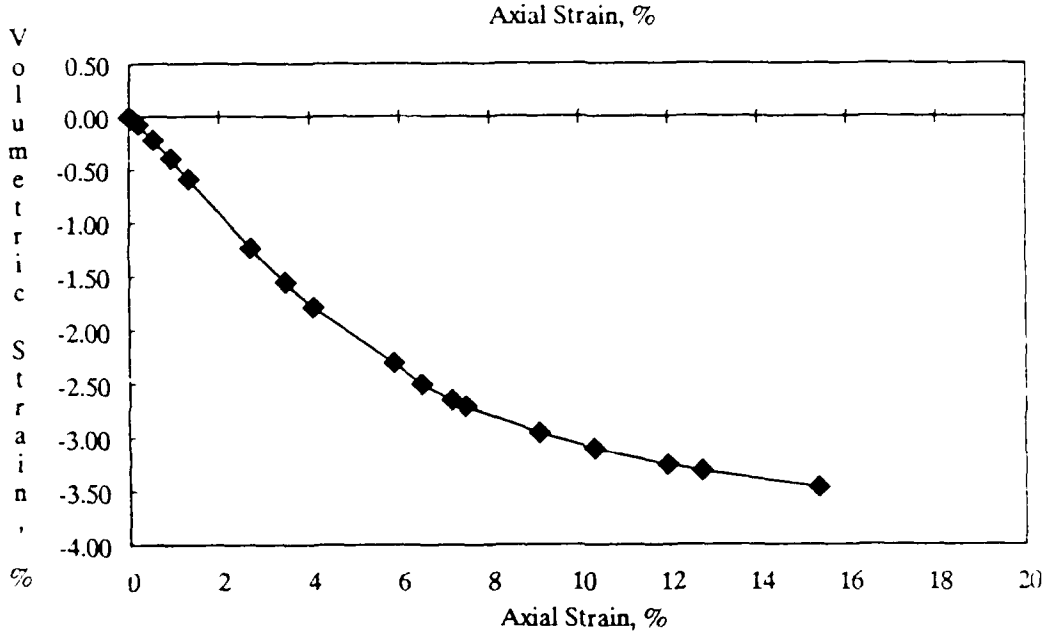


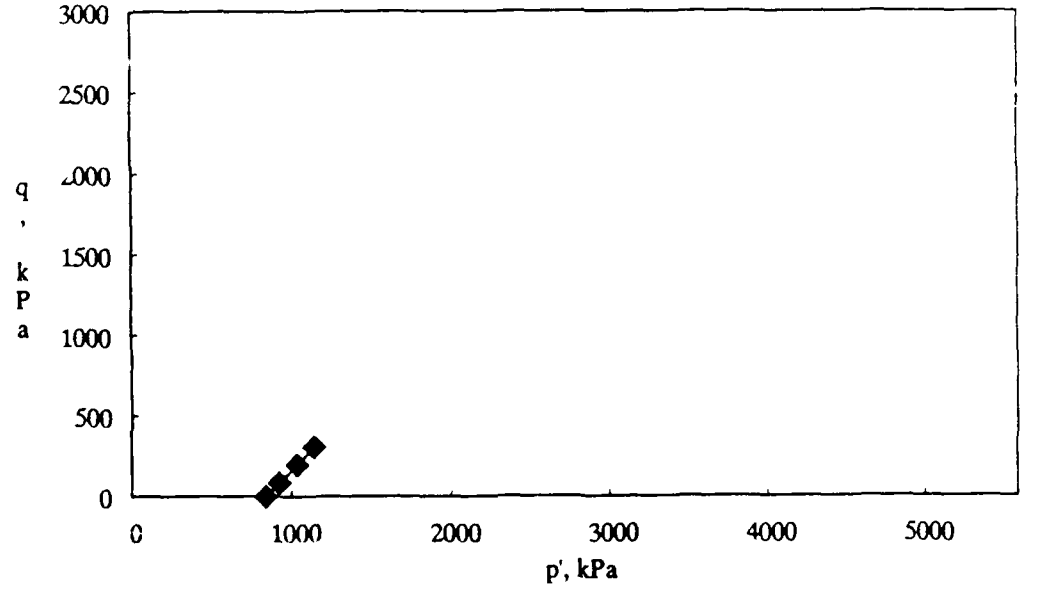


Figure C-8. CD Triaxial Test Results for 50% Montmorillonite Mixture at a Standard Relative Compaction of 100% and an Effective Confining Pressure of 837 kPa.

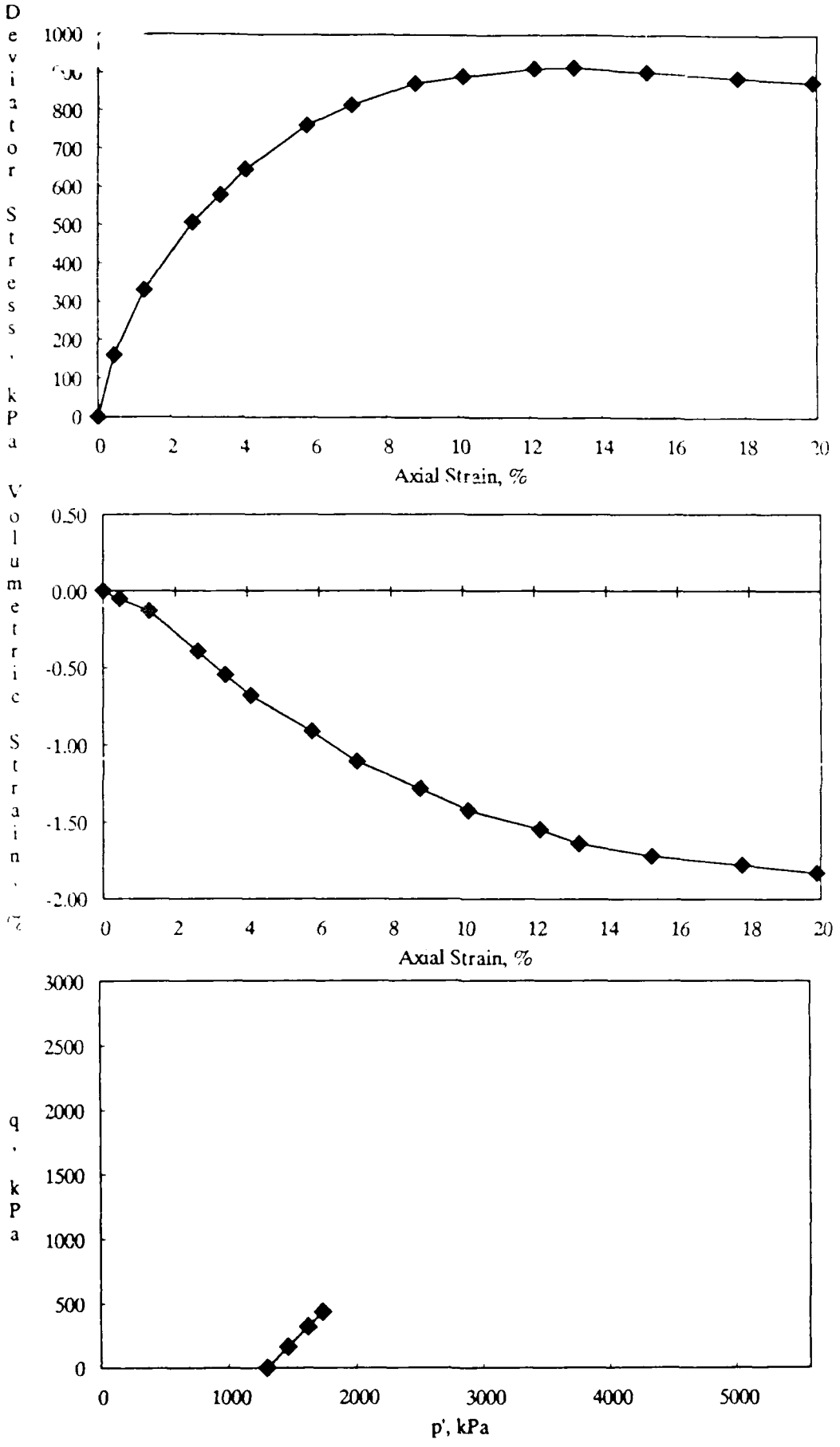


Figure C-9. CD Triaxial Test Results for 50% Montmorillonite Mixture at a Standard Relative Compaction of 100% and an Effective Confining Pressure of 1297 kPa.

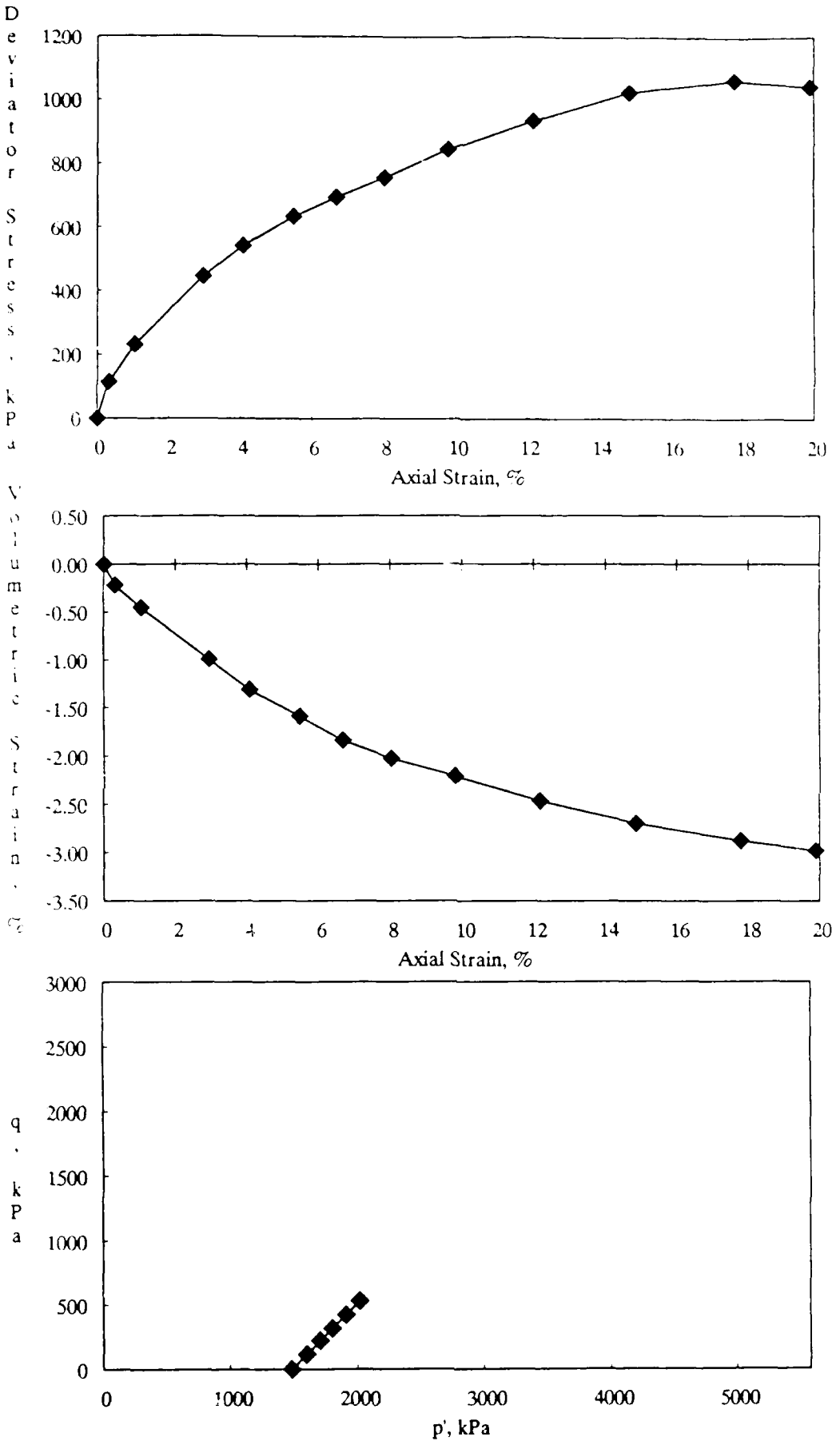


Figure C-10. CD Triaxial Test Results for 50% Montmorillonite Mixture at a Standard Relative Compaction of 100% and an Effective Confining Pressure of 1484 kPa.